Function of the laminin-derived protein LaNt α31 in corneal epithelium

Thesis submitted in accordance with the requirements of the University of Liverpool for the degree of Doctor in Philosophy

by

Valentina Iorio

October 2017

Index

List of Abbreviations 6
List of Figures 8
List of Tables 10
Acknowledgments 11
Abstract 12
INTRODUCTION 14
Section 1. The Basement Membrane 15
1.1.0 General Structure 15
1.1.1 Basement Membrane components 17
1.1.1.0 Collagens and Collagen type IV 18
1.1.1.1 Heparan sulfate proteoglycans 19
1.1.1.2 Nidogens 22
1.1.1.3 Fibulins 23
1.1.1.4 Fibronectin 23
1.1.1.5 Laminins 25
Section 2. Laminins 26
1.2.0 Nomenclature 26
1.2.1 Laminins in diseases 27
1.2.1.1 Laminin-related autoimmune diseases 28
1.2.1.2 Laminin-related genetic diseases 29
1.2.2 Laminin Structure 32
1.2.2.1 Laminin N-terminal domain 33
1.2.2.2 Laminin-type epidermal growth factor-like domains 38
1.2.2.3 Laminin G like domains 39
1.2.2.4 Laminin Coiled Coil domain 40
1.2.2.5 Laminin L4, LF and LFx domains 41
1.2.2.6 Laminin heterotrimer assembly 42
1.2.3 Laminin expression pattern in tissues 42
1.2.3.0 Laminin expression during mammalian organogenesis 42
1.2.3.1 Laminin expression in adult tissues 43
1.2.3.2 Laminins in wound repair 44
1.2.3.3 Laminin expression in corneal epithelium 44
1.2.3.4 LM332 47
Section 3. Cell to matrix adhesion devices 51

1.3.0 Hemidesmosomes 51
1.3.0.1 HD components 53
1.3.0.2 The cytoplasmic plaque proteins 53
1.3.0.3 The membrane proteins 55
1.3.0.4 Hemidesmosome assembly 59
1.3.0.5 Hemidesmosome disassembly 61
1.3.0.6 Hemidesmosomes in keratinocytes migration 63
1.3.1 Focal Adhesions 64
1.3.2 Focal Adhesions components 65
1.3.2.1 Talin 65
1.3.2.2 Vinculin 66
1.3.2.3 Paxillin 67
1.3.2.4 Focal Adhesion Kinase 68
1.3.2.5 Integrin $\alpha_3\beta_1$ 69
1.3.2.6 α-actinin 70
1.3.3 Focal adhesion assembly and disassembly 71
Section 4. Laminin N-terminus proteins (LaNts) 74
1.4.0 LaNt α31 alternative splicing mechanism 74
1.4.1 *LAMA3LN1* transcript localisation 75
1.4.2 LaNt α31 protein structure 76
1.4.2.1 Netrins 76
1.4.3 LaNt α31 functional data 80
Aim of the thesis 81
MATERIALS AND METHODS 82
2.1.0 Cell Culture 83
2.1.1 Antibodies and reagents 84
2.1.2 Bradford Assay 86
2.1.3 Adenovirus production and cell transduction 86
2.1.4 Short hairpin RNA (shRNA) and knockdown clone generation 87
2.1.5 Immunofluorescence microscopy 88
2.1.6 Tissue processing and immunohistochemistry 89
2.1.7 SDS PAGE and immunoblotting 90
2.1.8 Cell morphology analysis, low-density motility and 91
cross-matrix assays 91
2.1.9 Scratch closure assay 92
2.1.10 Attachment Assay 92

2.1.11 Polymerisation Assay 95
2.1.12 Immunoprecipitation 95
2.1.13 Live protein imaging 96
2.1.14 Proximity Ligation Assay (PLA) 96
2.1.15 Limbal Explants Culture 97
2.1.16 Statistical analysis 98
2.2.0 LaNt α31 mouse model preparation 99
2.2.0.1 Restriction Digests 99
2.2.0.2 Agarose gel electrophoresis 99
2.2.0.3 Plasmid Ligation, bacterial transformation and plasmid preparation 100
2.2.0.4 PCR amplification of the hK14 promoter 100
2.2.0.5 Cell transfection 102
2.2.1 LaNt α31 overexpressing mice generation and genotyping 102
2.2.1.1 DNA embryonic injection 102
2.2.1.2 Superovulation of egg donors 103
2.2.1.3 Pseudopregnant females' generation 103
2.2.1.4 Injection of fertilised eggs 104
2.2.1.5 DNA extraction 104
2.2.1.6 PCR 105
2.2.1.7 F1 generation 107
2.2.1.7a Tissue samples processing 107
2.2.1.7b E15.5 embryo analysis 108
In-Vitro RESULTS 109
Introduction 110
3.0 Anti-human LaNt α31 antibody generation 110
3.1 LaNt α31 distribution differs between the corneal, limbal and conjunctival epithelium 115
3.2 LaNt α31 knockdown does not affect corneal epithelial cell migration characteristics 117
3.3 LaNt α31 is not incorporated into the ECM deposited by hTCEpi cells 119
3.4 LaNt α31 overexpression leads to an extracellular protein deposition 121
3.5 Corneal epithelial cells overexpressing LaNt α31-GFP 123
display decreased motility and scratch wound closure rates 123
3.6 Cell-derived preformed ECM rescues the migration impairment in hTCEpi cells 127
3.7 LaNt α31 overexpressing cells show an increase in cell spread area 129
3.8 hTCEpi overexpressing LaNt α31 show a decreased attachment to LM111 132

3.9 Overexpressed LaNt α31 interacts with and modifies LM332 organisation in hTCEpi cells 134
3.10 LaNt α31 overexpressing cells display mislocalised focal contacts 136
3.11 LaNt α31 overexpressing cells display early HD maturation 138
3.12 LaNt α31 co-distributes with LM β3 during matrix deposition 140
3.13 Proximity Ligation Assay reports that LaNt α31 is spatially close to LM γ2 chain ... 145
3.14 LaNt α31 is also spatially close to actinin α4 148
3.15 LM β3 precipitates along with LaNt α31 150
3.16 LaNt α31 is observed in the LM111 polymer fraction in LM polymerisation assays 150
3.17 Exogenously added LaNt α31 influences the ability of hTCEpi to attach to LM111 153
3.18 Exogenously added netrin 1 or 4 do not affect hTCEpi attachment to LM111 155
3.19 LaNt α31 overexpression effects on pCEC cells behaviour mirror those observed in hTCEpi 157
DISCUSSION 162
3a.0 hTCEpi functional assays data summary 162
Interpretation 1. LaNt α31 influences LM network assembly 162
Interpretation 2. LaNt α31-cell surface receptor interactions affect matrix assembly ... 166
Interpretation 3. Cell phenotypes are dependent on LaNt α31 affecting FAs and HDs assembly 170
LaNt α31 indirect effect on HDs / FAs 170
LaNt α31 direct effect on HDs 171
LaNt α31 direct effect on FAs 173
LaNt α31 indirect effect on FAs and HDs via actinin α4 interaction 173
Interpretation 4. LaNt α31 overexpression induces GF release in the extracellular environment 175
My opinion 177
Open Questions 178
In-vivo RESULTS 180
Introduction 181
4.0 Construct features 181
4.0.1 Human keratin 14 and its promoter 181
4.0.2 Thosea asigna virus-derived 2A peptide sequence (T2A) 182
4.0.3 Murine Immonoglobulin (Ig) kappa (κ) chain secretory leader sequence (IgK leader sequence) 183
4.0.4 Myc and 6xHis tags 183
4.0.5 mCherry fluorophore 184
4.1.0 Cloning Step 1 187

4.1.1 Cloning Step 2 189
4.1.2 Cloning Step 3 191
4.1.3 *In-vitro* tests of construct 193
4.1.4 Litters genotyping shows that only few mice carry the transgene 195
4.1.5 LaNt α31 is not expressed in tissues isolated from transgenic mice 197
4.1.6 Early pregnancy interruption after transgenic mice timed-mating shows incredibly low offspring and absence of LaNt α31 overexpression 199
DISCUSSION 201
4a.0 LaNt α31 Overexpressing Animal Model data summary 201
Interpretation 1. The inserted DNA does not express 201
Interpretation 2. The exogenous DNA and/or the host genome is altered following microinjection 202
Interpretation 3. The injected DNA is not integrated into the host genome 203
Interpretation 4. The injected DNA is lethal during development 204
Final conclusions and future directions 207
Appendix 209

List of Abbreviations

Full name	Abbreviation
Actin-binding site	ABD
Ammonium hydroxide	NH_4OH
Atomic force microscopy	ATM
Basement membrane	BM
Basic fibroblast growth factor	FGF-2
Bone morphogenic protein 1	BMP-1
Bullous pemphigoid antigen	BP
Chinese hamster ovary cells	CHO
Collagen	Col
C-terminal globular non-collagenous domain	NC1
Deleted in colorectal cancer	DCC
Dulbecco's Modified Eagle Medium	DMEM
Endoplasmic Reticulum	ER
Engelbreth-Holm-Swarm tumour	EHS
Epidermal growth factor	EGF
Epidermal growth factor receptor	EGFR
Epidermolysis Bullosa Simplex associated with muscular dystrophy	EBS-MD
Ethylenediaminetetraacetic acid	EDTA
Extra-cellular matrix	ECM
Filamentous actin	F-actin
Fluorescence in situ hybridization	FISH
Fluorescence resonance energy transfer	FRET
Focal Adhesion	FA
Focal adhesion kinase	FAK
Focal adhesion targeting domain	FAT
Fubronectin	FN
Glycosaminoglycans	GAG
Growth Factor	GF
Hemidesmosome	HD
Heparan sulfate	HS
Heparan Sulfate proteoglycans	HSPGs
Human cytomegalovirus	CMV
Human Keratin 14	hK14
Human Retinal Pericyte cells	HRP
Human telomerase-immortalised limbal-derived corneal epithelial cell line	hTCEpi
Immunoprecipitation	IP
Intermediate filaments	IFs
Junctional epidermolysis bullosa	JEB
Junctional epidermolysis bullosa associated with pyloric atresia	JE-PA
Keratinocyte-Serum Free Medium	KSFM

Laminin	LM
Laminin coiled coil domain	LM LCC domain
Laminin G-like domain	LM G domain
Laminin N-terminal domain	LM LN domain
Laminin N-terminus α31	LaNt α31
Laminin-type epidermal growth factor-like domain	LE domain
Laminin β knob	Lβ
Laryngo-onycho-cutaneous syndrome	LOC
Mammalian tolloid	mTLD
Matrix metalloproteinase-2	MMP-2
Membrane type-1 matrix metalloproteinase	MT1-MMP
Merosin-deficient congenital muscular dystrophy	MDC1A
Monoclonal antibodies	mAbs
Mouse embrionic day	E
Murine Keratinocyte cells	KERA
Optimum cutting temperature formulation	O.C.T.
Pearson's Co-localisation Coefficient	PCC
Perlecan	PLC
Phenylmethysulfonyl floride	PMSF
Phosphatidylinositol (4,5) bis-phosphate	PI (4,5) P2
Phosphatidylinositol biphosphate	PIP-2
Phosphatidylinositol phosphate kinase type Iγ	PIPK1γ
Primary corneal epithelial cells	pCEC
Protein kinase C family	PKC
Proximity ligation assay	PLA
Pulsed-field gel electrophoresis	PFGE
Short hairpin RNA	shRNA
Sodium dodecyl sulfate	SDS
Spontaneously transformed human epidermal keratinocytes	HaCaT
Substrate adhesion molecules	SAMs
Sulfated glycolipids	SGLs
Surface plasmon resonance	SPR
Transmission Electron Microscopy	TEM
Vasodilator-stimulated phosphoprotein	VASP
Western immunoblotting	WB

List of Figures

Figure Number	Figure Title
1.1	BM simplified assembly process and structure.
1.2	LM structure representation.
1.3	LM ternary node.
1.4	LM truncated isoforms.
1.5	Human eye and cornea representation.
1.6	HD structure.
1.7	HD assembly.
1.8	FA structure.
1.9	LAMA3 alternative splicing; LaNt α31 and LM structure.
2.1	LM111, Col type IV and FN concentration test for plate-coating.
3.1	LaNt α31 mAb design and characterisation.
3.2	LaNt α31 knockdown clones.
3.3	LaNt α31 distribution in cells.
3.4	LaNt α31 protein is differentially distributed across ocular anterior segment epithelium.
3.5	LaNt α31 knockdown hTCEpi exhibit normal migration characteristics.
3.6	LaNt α31 is not deposited in hTCEpi ECM.
3.7	LaNt α31 overexpression leads to LaNt α31 deposition in the ECM.
3.8	LaNt α31 overexpression impairs hTCEpi migration.
3.9	LaNt α31 overexpression leads to a decrease in hTCEpi motility speed at times of new matrix formation.
3.10	Motility defects are rescued by a cell-derived preformed matrix.
3.11	LaNt α31 overexpressing hTCEpi display increased 2D area.
3.12	LaNt α31 overexpressing hTCEpi increased 2D area is rescued when cells are provided with a cell-derived ECM.
3.13	hTCEpi rapid attachment to LM111, but not to Col type IV or FN, is decreased when LaNt α31 is overexpressed.
3.14	Overexpressed LaNt α31 changes LM α3 organisation.
3.15	High levels of LaNt α31 induce mislocalisation of FAs.

3.16	High levels of LaNt α31 induce early maturation of HDs.
3.17	LaNt α31 gets deposited alongside LM β3 at cell peripheries.
3.18 3.19 3.20	LaNt α31 rapidly forms and disassembles clusters on top of LM β3.
3.21	PLA assay shows that LaNt α31 is spatially close to LM γ2 chain.
3.22	PLA assay shows that LaNt α31 is spatially close to actinin α4.
3.23	LM β3 is precipitated along with LaNt α31 and LaNt α31 is observed in the LM111 polymer fraction.
3.24	hTCEpi rapid attachment to LM111, but not to Col type IV, is decreased in the presence of exogenously added LaNt α31.
3.25	Exogenously added netrins 1 or 4 have no effects on hTCEpi rapid attachment to LM111.
3.26	LaNt α31 overexpressing pCECs display increased 2D area.
3.27	LaNt α31 overexpression leads to a decrease in pCEC cells motility speed.
3.28	Overexpressed LaNt α31 changes LM organisation in pCEC cells.
4.1	Flow diagram of the cloning steps to produce hK14 promoter-driven LaNt α31 overexpressing DNA construct.
4.2	Cloning Step 1: Insertion of LaNt α31 into pGEM®-5Zf(+) vector.
4.3	Cloning Step 2: Insertion of hK14 promoter into pUBCLoxP-TIMP3mCherry vector.
4.4	Cloning Step 3: Insertion of LaNt α31 into hK14 promoter-T2A-mCherry vector.
4.5	hK14 promoter drives the expression of LaNt α31 and mCherry *in-vitro*.
4.6	LaNt α31 transgenic mice genotyping.
4.7	LaNt α31 is not expressed in tissues collected from transgene-positive mice 4.1 and 6.3.
4.8	Early pregnancy interruption of LaNt α31 overexpressing DNA construct carrying mice.

Appendix - Figure Number	Title
1	Characterisation of telomerase-immortalised human corneal epithelial cells (hTCEpi).
2	RG13 mAb test for purity and functionality.
3	Rabbit polyclonal anti-LaNt α31 antibody characterisation in hTCEpi cell lysates.
4	Characterisation of corneal primary cells (pCEC).

List of Tables

Table number	Title
1	LM nomenclature.
2	Modified PCR primer sequences to amplify hK14 promoter.
3	Thermocycler programme for hK14 promoter amplification.
4	DNA primer sets, used for mice genotyping after DNA extraction from ear notches.
5	Thermocycler protocol applied to amplify DNA for mice genotyping.
6	Summary of the DNA cloning steps performed to prepare the hK14 promoter driven-LaNt α31 overexpressing construct.
7	DNA transfection set up to test the functionality of the hK14 promoter driven-LaNt α31 overexpressing construct *in-vitro*.

Acknowledgments

This thesis is only the final step to what has been a truly life-changing experience for me, handled and completed thanks to the help and encouragement I received from many people.

My very first, big, thank you goes to my primary supervisor Dr Kevin J. Hamill. Your wonderful enthusiasm, great guidance and constant support have been essential for me. Thanks for your trust, for reminding me that mistakes are okay, for pushing me to my limits and helping me break out of my shell.

Many thanks to Prof. George Bou-Gharios and Dr. Carl Sheridan, your valuable inputs and ideas have made my research project deeper and better.

I gratefully acknowledge the Institute of Ageing and Chronic Disease (University of Liverpool) for the funding received towards my PhD; without access to such resources, my experiments and, equally, my participation in many inspiring conferences would have not been feasible.

Thanks to Lee, Valentina, Aruni, Amu, Karen, Noelia, Alessandro and to all my colleagues for the laughs, coffees, gossip and for turning the lab into a playroom.

With all my heart, thanks to my parents Adriana and Roberto, to my brother Michele and to my husband Crescenzo; without you, I wouldn't have been the woman I am.

Abstract

Laminin N-terminus α31 (LaNt α31), a member of the relatively new LaNt protein family, is a product of alternative splicing from the laminin (LM) α3 encoding gene (LAMA3). Prior to these studies, very little was known about LaNt α31 biology; it had been shown to co-localise with LM α3β3γ2 (LM332) in the basement membrane (BM) of the skin and to play a role in adhesion and migration of epidermal cells. Still, no direct insight into the mechanism behind this effect has been described.

In this study, we performed the first analysis of LaNt α31 in the eye. Immunohistochemistry reveals that the protein is differentially distributed across the regions of the epithelium in the anterior surface of the eye. Specifically, LaNt α31 localises intracellularly through all layers of the corneal epithelium, but is restricted to the basal layers of the limbus and conjunctiva. Hence, we sought to investigate about LaNt α31 functional roles in corneal epithelial cells (hTCEpi) and its interplay with LM during corneal epithelial matrix assembly.

Our functional studies demonstrate that knockdown of intracellular LaNt α31 has no discernible effect on hTCEpi, in which LaNt α31 is not normally matrix-associated. However, when overexpressed by adenoviral delivery, LaNt α31 is deposited into the extracellular matrix (ECM) and causes a number of phenotypic effects including; impaired cell adhesion to LM111, changes to LM organisation, increased cell spreading, early recruitment of Collagen (Col) type XVII to β_4 integrin in hemidesmosome (HD) like-complexes and mislocalisation of focal adhesions (FAs). Increased LaNt α31 expression also leads to significantly decreased motility at times of new matrix synthesis, with this migration defect rescued when hTCEpi are provided with a cell-derived preformed ECM. Live imaging experiments indicate

that GFP-tagged LaNt α31 clusters at the periphery of cells, where it co-distributes and is deposited along with LM β3. As cells move across a preformed matrix, clusters of LaNt α31 rapidly form and dissociate intracellularly, alongside LM deposits.

To study the effects of overexpression *in-vivo*, we generated a human keratin 14 (hK14) promoter-driven LaNt α31 overexpressing mouse model by embryo microinjection. Using this construct, we obtained far fewer offspring than would normally be expected and were not able to detect expression of the protein product from the transgene in the animals carrying the construct. Based on these data, we hypothesise that, in this model system, LaNt α31 overexpression has induced lethality.

Together, these data demonstrate that LaNt α31 influences the assembly of LM matrix in hTCEpi affecting fundamental cell functions, and implicate the LaNt proteins as regulators of other LM dependent processes including wound repair, differentiation and tissue homeostasis.

Chapter 1

INTRODUCTION

The work described in this thesis represents the first study of LaNts outside the skin and provides a much deeper analysis of LaNt α31 function and interplay with laminins (LMs) in corneal matrix and cell adhesion devices. To put these findings into context, a fundamental appreciation of the different players and complexes involved is required. Therefore, this introduction will briefly describe the basement membrane (BM) main components and functions (section 1), the laminins with their domain architecture and known roles (section 2), the cell to LM adhesive devices that were investigated in this work, specifically the hemidesmosomes (HDs) and focal adhesions (FAs) (section 3) and, finally, what was known about the LaNt family of proteins prior to the initiation of these studies (section 4).

Section 1. The Basement Membrane

1.1.0 General Structure

BMs are thin, specialised forms of cell-associated ECM with a very wide distribution in the body; they are found beneath epithelial, mesothelial and endothelial cells and enclose muscle, fat and Schwann cells [1]. BM evolution started approximately 500 million years ago [2] and have been studied since the late 1970s as highly specialized substrates for cellular differentiation and gene expression.

BMs are known to play several fundamental roles. First, they are involved in the cell adhesion process by acting as anchoring devices between sheets of cells and connective tissue, via substrate-adhesion molecules (SAMs) [3]. Second, BMs are essential players in tissue and organ morphogenesis, as they support migration of cells during tissue remodelling; this also includes new cancer blood vessel growth, a process shown to be partially controlled by the BM beneath the tumour endothelium

[4]. Third, BMs are critical for maintaining mechanical barriers, preventing foreign bodies, bacteria or malignant cells from invading the underlying deeper tissues [5] and, under specific circumstances, BMs also have a role as diffusion barriers, e.g. in the lungs where they modulate O_2 and CO_2 diffusion between alveoli and capillaries [6], or as filters with selective permeability, e.g. in the kidney glomerulus [7]. Finally, BMs control cell differentiation by inducing tissue-specific gene expression [8] and can act as a reservoir for several types of growth factors (GFs) [9, 10].

High-power transmission electron microscopy (TEM)-based studies show that BM thickness is around 100 nm on average, with the exception of the lens capsule, where it is over 10 μm [2]. BMs are composed of approximately 50 types of proteins, organised in a complex structure that changes with age and is, therefore, dynamic [2]. Normally, BMs are visible in TEM as two distinct layers: an electron-lucent layer close to the plasma membrane, named as *lamina lucida*, and an electron dense layer or *lamina densa*. The *lamina lucida*, in epithelial tissue, is 20-40 nm thick and is traversed by anchoring filaments (5-7 nm in diameter) rich in LM332 and 311, and which interact with the extracellular domain of $\alpha_6\beta_4$ integrin [11]. The *lamina densa* has a thickness which varies with age (30-60 nm) and is mainly composed of collagen type IV, but contains also LM511 and 322, nidogens and heparan sulfate proteoglycans (HSPGs), such as perlecan (PLC) [11]. A third layer, known as *lamina fibroreticularis*, is only present in some tissues; it synthetized by fibroblasts and joins the BM to the underlying connective tissue [12].

From immunostaining studies [12], BM principal components are collagen type IV in different variants, HSPGs including PLC and agrin, nidogens, also referred to as entactins, fibulins, fibronectin (FN) and LMs [13](Fig. 1.1). It is now accepted that these proteins are the major contributors to the self-assembly of BMs on competent

cell surfaces [14], primarily via cellular receptors such as integrins and dystroglycan [2, 15]. Mutations negatively influencing the folding and functions of the BM structural proteins have been shown to lead to either problems during development [16] or life-threatening diseases involving abnormal functions of muscles, nerves, brain, eyes, skin, vasculature and kidneys, highlighting the importance of BMs to the function of many tissues [8].

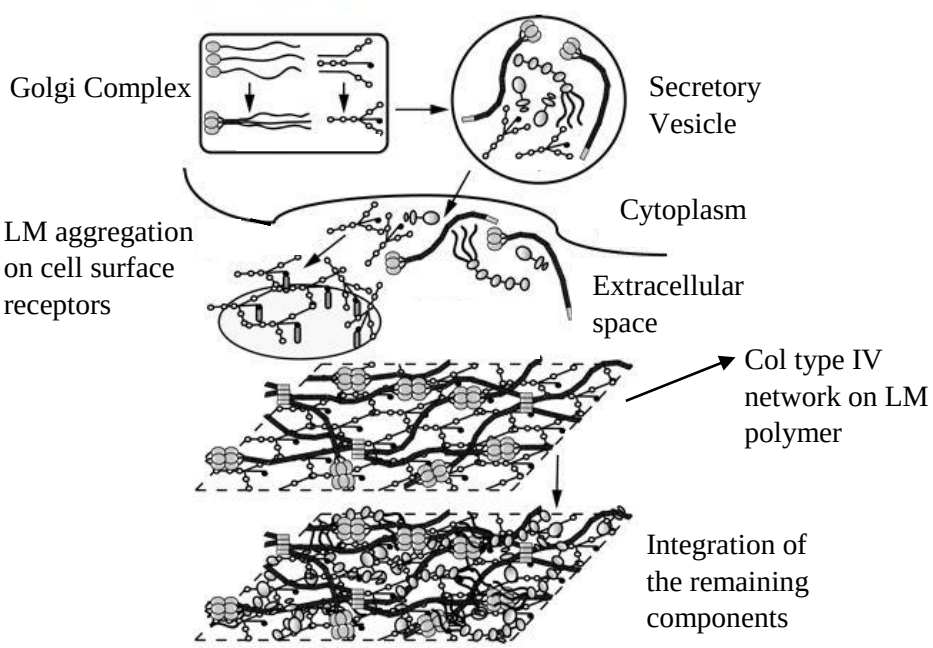

Fig. 1.1: BM simplified assembly process and structure.

Schematic diagram of the BM assembly phases, adapted from LeBleu, MacDonald et al. 2007.

1.1.1 Basement Membrane components

The research described in this thesis is primarily related to LaNt α31, a LM related protein. LMs are not the only molecules present in the BM and, as LMs interact at different levels with the rest of the BM components, it is important to have a brief

vision of all the BM elements to fully understand their implications in the wider context of tissue functions.

1.1.1.0 Collagens and Collagen type IV

Collagens are the most abundant structural proteins in mammals [17], with 28 types identified and analysed [18]. The building blocks of collagen structure, termed tropocollagen, are right-handed triple helixes stabilized by many hydrogen bonds, made up by three parallel polypeptide strands twisted together with a left-handed helical conformation and a very specific amino acids arrangement. Tropocollagen is typically formed by two identical chains termed α1, and a third chain termed α2, which is slightly different in its chemical composition [19]. The binding of several tropocollagen molecules leads to the formation of a fibril, which interdigitates with neighbouring fibrils to form a fibre [20].

Collagen type IV is the primary type of collagen found ubiquitously in all the BMs. Six individual chains have been identified, named as α1(IV) to α6(IV), each one consisting of three domains: an N-terminal 7S domain, a middle triple-helical domain and a C-terminal globular non-collagenous (NC1) domain [21]. The six α-chains have been shown to self-assemble and form sets of triple-helical molecules that associate via their NC1 domains and their middle triple-helical regions to form spider web-like scaffolds [4]. This high order architecture forms an insoluble structure which is used by other BM components to interact and form the final BM scaffold [7].

With regards to the affinity and interplay between LM and Col type IV, it is known that their interaction plays an important role in defining the organisation and heterogeneity of the BM structure in tissues [22, 23]. It has been shown that LM/collagen type IV binding is enhanced by the presence of zinc [24] and can either be direct [25] or facilitated by nidogens [26, 27].

1.1.1.1 Heparan sulfate proteoglycans

HSPGs are ubiquitous glycoproteins found in the BM, named after the presence of one or more covalently attached heparan sulfate (HS) chains, a type of glycosaminoglycan (GAG), in their molecular structure [28].

In cells, HSPGs can be found either on the cell membrane, such as syndecans and glycosylphosphatidylinositol-anchored proteoglycans (glypicans), or in the secreted ECM, and this is the case of agrin, PLC and Col type XVIII [29]. HSPGs' small size (40-160 nm) allows them to arrange self-assembling macromolecular structures and to play several different roles. These proteins have a crucial function in regulating key developmental signalling pathways [30], can regulate the formation of ligand-receptor complexes by acting as co-receptors [31], can be involved in cell attachment and endocytosis [32], are used as indirect factors in ECM modulation of cell migration [33], show a protective barrier function [34] and control many of the signalling molecules involved in stem cell maintenance [35].

1.1.1.1a Perlecan

PLC or heparan sulfate proteoglycan 2 (HSPG2) is a protein encoded by the HSPG2 gene [36]. It has a high molecular weight (~ 470 kDa), is formed by five domains, termed I-V, and is synthesized by numerous cell types including vascular endothelial and smooth muscle cells, and corneal, limbal and skin epithelial cells [37, 38]. PLC has been demonstrated to be a strong inhibitor of smooth muscle cell proliferation and, on the other hand, a stimulator of endothelial growth and regeneration [39]; it is also involved in cell adhesion, GF binding and modulation of apoptosis [40].

Once assembled, PLC is secreted into the ECM, where it cross-links many ECM components and cell-surface molecules [41]. Among all the structural domains, the C-terminal Domain V, which has homology to the G domain of the long arm of LM, is responsible for PLC self-assembly and, therefore, for BM formation in vivo [42].

PLC, via its domain IV [43], has been shown to bind to the LN-domain of LM α1 chain [44], and a recent study demonstrated a strong correlation between PLC and the intact structure of corneal epithelium, as PLC-deficient mice are characterised by altered corneal epithelium architecture [45].

1.1.1.1b Agrin

Agrin is a ~ 200 kDa, ~ 95nm long molecule produced by the growing end of motoneuron axons, named after its involvement in the aggregation of acetylcholine receptors during synaptogenesis [46]. In humans, agrin is encoded by the AGRN gene [47]. This protein is composed of a highly conserved N-terminal basal membrane-binding domain, nine follistatin-like repeats, and two laminin-B-like

modules, followed by three LG domains at the C terminus [48]. Agrin function can be post-translationally regulated, a process which allows this protein to have roles in different tissues of the body. Agrin is known to exert a key role in the formation, maintenance, and regeneration of the neuromuscular junction [49] as well as a regulator of postsynaptic differentiation and a modulator in the T-cell immunologic synapse [50]. In the skin, agrin and PLC show an anti-apoptotic function in dermal-epidermal junctions [51] and downregulation of both these proteins by UV irradiation [52] can induce a higher level of apoptosis in keratinocytes. Agrin is also highly expressed in the eye, where it is found in the inner limiting membrane, the BM that separates the retina from the vitreous cavity [2], in the corneal epithelium [53] and in the stroma [54].This abundant expression, together with ocular phenotypes in mice and fish with mutated agrin protein [55, 56], suggest a function for agrin during eye development.

Agrin is deposited from *Xenopus Laevis* cells cultured on LM containing-substrates [57] and it uses its N-terminal portion to bind to different LM isoforms, association which may play a role in the BM stabilization [58, 59]. The agrin-binding site has first been characterised in LM111 and it resides in a 20-residue long region of the γ1 chain, in the LM LCC domain [60]. Agrin binds to LM211 and 221 too, with the link being strongest for LM221 [61]. Differential tissue distributions of LMs may regulate agrin binding [62] and it is, therefore, possible to speculate that the interaction between agrin and LMs drives the correct integration of agrin into the ECM scaffold.

1.1.1.2 Nidogens

Nidogens, also known as entactins, are ubiquitous ECM components and belong to the sulfated monomeric glycoproteins family. To date, two nidogens have been described in humans: nidogen-1, of about 150 kDa and encoded by NID1 gene, and nidogen-2, of about 200 kDa and encoded by NID2 gene [63]. Each isoform is organised into three structural domains, an N-terminal globule linked to a smaller C-terminal globule by a rigid stalk largely consisting of cysteine-rich EGF-like homology repeats and a cysteine-rich thyroglobulin homology repeat [63]. Structural analysis revealed that nidogen-1 is formed by a single 1200-residue polypeptide chain [22]; it contains binding sites for perlecan and collagen type IV at approximately 80 nm from its carboxyl non-collagenous end [64] and, most relevant for our studies, it can also bind to the LE repeats of LM γ1 and γ3 chains [65, 66]. By simultaneously binding different components, the nidogens act as bridging molecules in basement membranes.

Nidogen-1-deficient mice show a mild deficit in nervous system function [56] and, interestingly, mouse animal models lacking either nidogen-1 or nidogen-2 show only minor effects [67, 68] pointing to a redundancy of function between the two isoforms. This is supported by the early lethality resulting from the deficiency of both isoforms, which affected integrity of lung and cardiac tissues because of modifications in the BM [69, 70]. Nidogens are able to bind calcium ions and support cell adhesion and are also known to be very sensitive to proteases, suggesting that they may be a target for proteolytic activity during tissue remodelling, metastasis and other events requiring the turnover of the BM [71].

1.1.1.3 Fibulins

A recent addition, in terms of discovery, to the ECM proteins is represented by the fibulin family, composed of six isoforms sharing calcium-binding consensus sequences with a broad range of interaction potentials [72]. Fibulins are composed by several epidermal growth factor (EGF)-like modules followed by a carboxy-terminal fibulin-type module; they can vary in size (367-1196 residues) and can undergo alternative splicing modifications [73].

Fibulins are involved in elastic matrix fibre assembly [74, 75], they are highly expressed in blood vessels during development [76] and play a fundamental role in several types of eye disorders. For instance, the macular dystrophy named as Malattia Leventinese has been linked to a mutation (Arg345Trp) in the fibulin 3 gene, and fibulins 1 and 4 have been indicated as candidate genes for retinopathies [77]. The expression of fibulins 3 and 1 is also elevated in a murine retinopathy model that primarily involves degeneration of rod photoreceptors [78].

Fibulins can bind several protein ligands; with regards to this project, they bind to the LN-domain of LM γ2 chain and to the LE domains of LM α1 chain [79]. In addition, fibulin 2 has been reported to bridge LM111 and LM332 with other BM components, providing a linkage between the cell surface and the basement membrane [73, 79].

1.1.1.4 Fibronectin

Fibronectin (FN) is a high-molecular weight (~440 kDa) adhesive glycoprotein present in the ECM, widely expressed by several cell types and fundamental during development, as demonstrated by the early embryonic lethality of knock-out mice

[80]. This protein is found as a dimer, formed by two nearly identical subunits with a molecular weight of 230-250 kDa, consisting of rod-like regions connected by disulfide bonds [81]; it is encoded by a single gene but, in humans, is present in almost 20 variants resulting from alternative splicing [82, 83].

Fibronectin modules are arranged into several functional and protein-binding domains, allowing the protein to associate with other FN molecules [84]. Among the different domains, fundamental are the I1-5 domain, shown to be the "assembly domain" required for the initiation of FN matrix assembly, the III9 domain, known as the "cell-binding domain" and the III10 domain, site of cell attachment, via $\alpha_5\beta_1$ and $\alpha V\beta_3$ integrins, to the cell surface [84].

Fibronectin is involved in numerous biological processes, such as cell adhesion, growth, migration, and differentiation [85]. It also plays a crucial role in wound healing [86] and embryogenesis [80]. Interestingly, fibronectin is present in the oral cavity, where it helps preventing the colonization by potentially pathogenic bacteria [87]. Related to our study is the FN-integrin binding, in particular the binding with $\alpha_5\beta_1$ integrin receptor. In skin, the latter is involved in the re-epithelialisation process, when cells need to adapt their integrin receptors to be able to use the provisional FN-rich matrix, adhering and moving on top of it to close the wound [88]. LM332 is the ECM protein required for cell adhesion and, therefore, the one involved in the binding with integrins. Any change in the laminin conformation, assembly and/or interactions within the ECM may, therefore, affect fundamental processes like wound healing.

1.1.1.5 Laminins

Among all the BM components, laminins are the first type of glycoproteins to be detected during embryogenesis, i.e. before collagen type IV, PLC, nidogens, etc. [13]. LMs are heterotrimeric proteins of high molecular weight (~400 to ~900 kDa), cross or T-shaped with three short arms and one long arm. Each LM consists of three chains; a α-chain, a β-chain, and a γ-chain, encoded in mouse and humans by five α (LAMA1-5), three β (LAMB1-3), and three γ (LAMC1-3) encoding genes respectively [88, 89]. Additionally, via an alternate promoter, LAMA3 gene encodes for two isoforms, a short α3a form and a longer α3b form [90-92], therefore increasing the number of α chains to 6. Although this means that, potentially, the laminin chains could combine into more than 50 αβγ trimers, due to interaction forces and/or differential tissue distribution patterns, only 16 isoforms have been shown to exist *in-vivo* [93]. However, the structural and functional diversity between the different laminin heterotrimers means that differences between specific laminins within a BM have dramatic effects on cellular responses to that BM.

As the LMs are the primary focus of this thesis, a deeper description of this protein family is presented in section 2.

Section 2. Laminins

1.2.0 Nomenclature

The chains of the first isolated laminin from Engelbreth-Holm-Swarm (EHS) tumour cells were named as A, B1 and B2 [94]. Following the discovery of related but non-identical laminins from other cells and tissues, the three constitutive chains were renamed with the Greek letters α, β and γ. In 1994, the first unified LM family nomenclature was introduced, based on the use of one Arabic number per chain according to the order in which they were discovered, with no relationship to chain numbers [95]. For instance, LM5 is α3β3γ2. Given the high number of laminin isoforms discovered over time, the nomenclature has undergone a simplification in 2005 [93]. According to the new system, each laminin trimer is named to describe which chains are present in each isoform; LM5 is now known as LM332. Table 1 summarises the old and the new nomenclature. Throughout this thesis, the 2005 nomenclature will be used.

Subunits	New naming system, 2005	Old naming system, 1994
α1β1γ1	LM111	1
α2β1γ1	LM211	2
α1β2γ1	LM121	3
α2β2γ1	LM221	4
α3Aβ3γ2	LM332, or LM3A32	5, or 5A
α3Bβ3γ2	LM3B32	5B
α3Aβ1γ1	LM311, or LM3A11	6, or 6A
α3Aβ2γ1	LM321, or LM3A21	7, or 7A
α4β1γ1	LM411	8
α4β2γ1	LM421	9
α5β1γ1	LM511	10
α5β2γ1	LM521	11
α2β1γ3	LM213	12
α4β2γ3	LM423	14
α5β2γ2	LM522	–
α5β2γ3	LM523	15

Table 1: LM nomenclature.

1.2.1 Laminins in diseases

LMs are very widely expressed in tissues, where they tightly connect the BM to the adjacent cell layer. As is now well known, the basement membrane provides stabilisation for cellular structures and serves as a physical barrier. Metastasizing solid tumours, for instance, must pass through basement membranes to reach the

vascular system, and various microbes and viruses enter the cells through direct interaction with BMs [96]. Due to the importance of LMs in basement membrane's roles, dysfunctional LMs lead to many different types of diseases [97].

1.2.1.1 Laminin-related autoimmune diseases

Although published data reported the presence of antibodies against LMs in healthy individuals [98], several more recent studies revealed that different LM isoforms can act as antigens in autoimmune diseases [99-102]. Experimental models showed that tissue damage is due to antibody-mediated disruption of ligand-binding function of LMs, with a consequent activation of inflammatory pathways [99, 103]. Mucous membrane pemphigoid, caused by autoimmunity against LM332, is characterised by blisters and erosions of the mucous membranes [104] and has been shown to associate with solid cancers [105]. Furthermore, lupus erythematosus, graft-versus-host disease, kidney rejection and linear IgA bullous dermatosis have been associated with reactivity against LM332 chains [106-110].

Experimentally, the pathogenic potential of antibodies targeting LM332 has been characterised in mice and rabbits in which they have been passively transferred, leading to blistering [111, 112]. Furthermore, other studies indicate the presence of autoimmune diseases linked to antibodies against LM111, such as ANCA-associated vasculitis [113], systemic sclerosis, Raynaud phenomena, infertility and renal disorders [114-116].

1.2.1.2 Laminin-related genetic diseases

There are numerous examples of LM-related genetic diseases, three of which are specifically related to this research project; the junctional epidermolysis bullosa (JEB), the Pierson syndrome and the merosin-deficient congenital muscular dystrophy (MDC1A). Some, but not all, of the mutations causing the mentioned pathologic conditions reside in the LN domain of the involved laminin chain, which is the structural domain involved in the laminin polymerisation process, as described afterwards.

JEB is a skin blistering disease due to defects in any of the subunits of LM332 [117, 118] and is characterised by blisters and skin erosions forming in response to minor injuries or frictions, such as rubbing or scratching. JEB is classified into two main types, both inherited in an autosomal recessive manner [119]; a severe form called Herlitz JEB, which causes death during the first year of life [120, 121], and a milder form named non-Herlitz JEB, typically associated with a normal lifespan [122, 123]. Patients affected by Herlitz JEB present large skin regions with the presence of severe patches of granulation tissue, usually around nose, mouth, ears, tips of the fingers, toes and the back of the head. The condition becomes life-threatening as patients undergo extensive loss of blood, fluids and proteins, making the body susceptible to electrolyte imbalance and infections [124, 125]. In some cases, the granulation tissue may appear in the respiratory tract, leading to compression and obstruction of the airway [126], or in the urinary tract, leading to dysplastic or multicystic kidney, acute renal tubular necrosis, obstructive uropathy or duplicated renal collecting system [127, 128]. Non-Herlitz JEB, on the other hand, appears with a milder phenotype characterised by skin blistering usually confined to hands, feet, knees and elbows [129].

Analysis of skin biopsies by TEM revealed altered basement membrane in the epidermis, specifically the splitting of the *lamina lucida*, with hypoplastic and reduced in number hemidesmosomes and decreased or completely absent anchoring filaments [125, 130, 131]. Immunofluorescence staining of cells isolated from JEB patients highlighted the abnormal or absent staining of LM332 [132], resulting from pathogenic variants in LAMA3, LAMB3, or LAMC2 genes [133]. There is a strong genotype/phenotype correlation; mutations leading to loss of expression of any subunit give rise to more severe form, whereas most missense mutations give milder phenotypes [123].

Specifically relating to the studies described here is a relatively common LAMB3 mutation leading to non-Herlitz JEB, which causes Glu210Lys substitution within a highly conserved region in the N-terminal domain of LM β3 [134], although it should be noted the mutation is near a splice site and could therefore have a broader effect on exon usage. Subsequently, knock-in mice were generated with this mutation and, whereas heterozygous mice were phenotypically normal, homozygous knock-in animals displayed blisters and died within 3 days of birth [135]. Moreover, staining for LM α3 and LM β3, but not Col type VII was diminished in skin sections of these animals. Together, these data suggest that the LM β3 N-terminal domain is functionally important in establishing an epithelial BM.

The Pierson syndrome, a congenital syndrome caused by mutations in the LAMB2 gene, gives a second example of laminin-related genetic disease [136-138]. Pierson syndrome is characterised by kidney failure and ocular abnormalities, symptoms leading to death in the first months of life [136]. Most affected infants display abnormally small pupils, a condition known as microcoria, but patients can also show other ocular alterations including cataracts, glaucoma, retinal detachments and

blindness [138]. Renal problems usually start just after birth and rapidly progress to end stage renal failure or, in the worst cases, are already noticeable in utero [136].

As for LAMB3, mutations in the N-terminal domain of LAMB2 have specifically been demonstrated to lead to Pierson syndrome [139]. Moreover, *in-vitro* functional studies have been performed, demonstrating how missense mutations within this region affect folding and interactions [140]. These will be described in the laminin polymerisation section.

In addition to these pathologic conditions, LAMA2 mutations cause MDC1A [141]. LM α2 chain deficiency is characterised by congenital hypotonia, delayed or arrested motor abilities and feeding difficulties. Moreover, patients show respiratory insufficiency, orthopaedic complications, usually represented by joint contractures and spinal rigidity, ophthalmoplegia and brain signalling alterations [136, 142]. The MDC1A phenotype is related to the binding properties of LM α2, also called merosin [143]. LM α2 is a native ligand for dystroglycan and it is involved in the link between ECM and dystrophin, a basic component of the protein complex that connects the cytoskeleton of a muscle fibre to the surrounding ECM [141].

Both the autoimmune and genetic laminin-related diseases show the importance of laminins for a correct tissue function. In particular, the existence of missense mutations in laminins' LN domains points toward fundamental functional roles for the polymerisation process, as will be described afterwards.

1.2.2 Laminin Structure

Laminins are comprised of three polypeptide chains, named as α, β and γ chains, each of which is folded into different structural domains and ultimately arranged in a typical cross-like shape (Fig. 1.2). The short arms of the cross are formed by the separately folded N-terminal regions of each chain, while all three chains form the stem of the long arm through assembly of a triple helical coiled coil.

In the N-terminal short arms, the LM subunits contain three types of structural domains; a single N-terminal domain (LN), followed by tandem repeats of the LM-type epidermal growth factor-like domains (LE) interspersed with globular LM IV (L4 or LF) domains [93]. In the long arm the LM coiled-coil domain (LCC domain) is found [144]. Lastly, the C-terminus of the LM α chains contains a tandem repeat of five LM G domains [145].

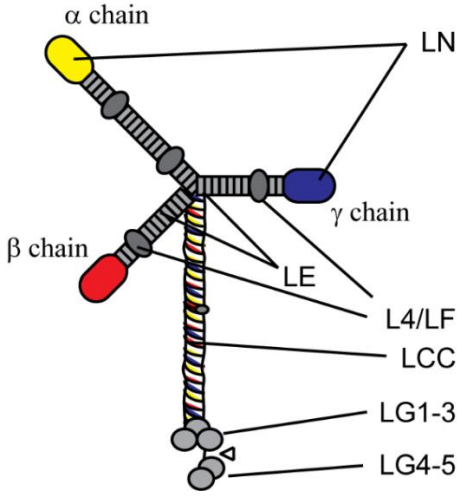

Fig. 1.2: LM structure representation.

Diagram showing the cross-like shape of LM, including the three chains and all the structural domains.

1.2.2.1 Laminin N-terminal domain

At the NH2 terminus of most LMs chains, excluding LM α3a, α4 and γ2 chains, there is a globular domain of 228-259 residues depending on the chain, known as the laminin N-terminal domain (LN domain). The published crystal structure of recombinant LN domain of the α5, β1 and γ1 chains shows that the respective polypeptides are similarly folded in a β-sandwich motif, with non-conserved elaborate loop regions [140, 146]. The LN domain is immediately followed by a stretch of LE repeats with the first LE repeat tightly associated with the LN domain itself, leading to a flower-like arrangement [147]. This association is important for laminin structural stability [148].

Numerous studies have demonstrated that LN domains play a fundamental role in LM self-polymerisation, a process required for the formation of LM scaffolding, and which contributes to overall BM assembly [148-151].

In addition, the LN domain has been shown to be involved in other functions not related to its LM-LM interaction role, such as cell adhesion and neurite outgrowth [148]. The LN domain interacts with several cell surface receptors; α1, α2 and α5 LN domains have been shown to bind to integrins $\alpha_1\beta_1$, $\alpha_2\beta_1$ and $\alpha_3\beta_1$, and some of the N-terminal globular domains have been reported to interact with sulfated glycolipids (SGLs) [8, 93]. *In-vitro* studies also reported LM111, 211 and 511 LN domains to interact with the HS-containing domains of PLC [148, 152].

Binding affinities for integrins and other receptors, analysis of conserved and chain-specific active sequences and polymerisation features of LM α1 and α2 chains LN domains were previously published [150, 153, 154], as well as for LM α3b and α5 chains LN-domains [148]. The alignment of the mouse sequences for α1, α2, α3b and

α5 LN domains revealed a 72% sequence identity between α1 and α2, 77% between α3b and α5 and 53-60% identity between both groups, with a strict conservation of 6 cysteine residues, but non-conserved N-glycosylation sites [148].

1.2.2.1a LN domain mediated polymerisation

Experiments like equilibration gel filtration assays, analytical ultracentrifugation, LM gelation inhibition studies and rotary shadowing of polymerised molecules have shown that LN domains are crucial for laminin network formation [151]. Laminins have been demonstrated to self- and co-polymerise; self-polymerisation involves the binding of LN domains at each end of three full length short arms, leading to the formation of a ternary node (Fig. 1.3).

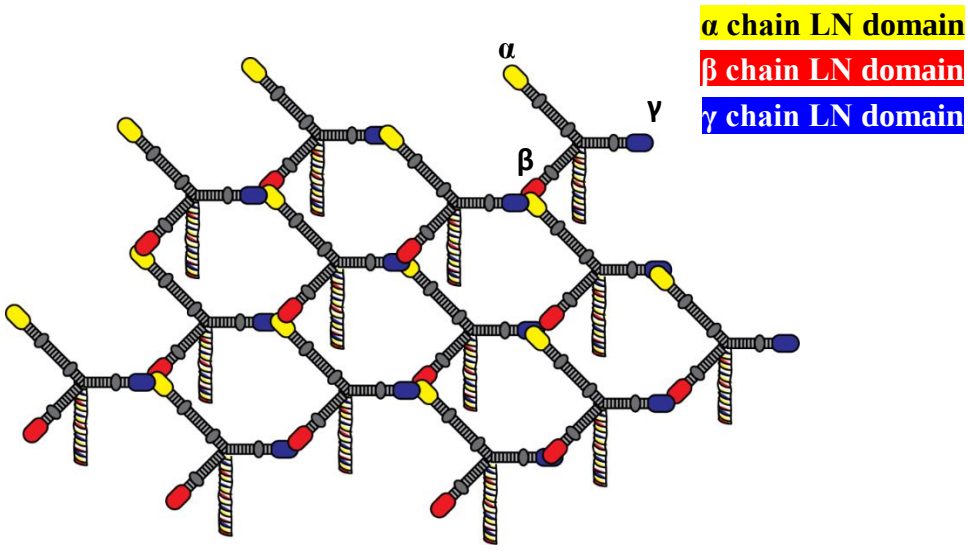

Fig. 1.3: LM ternary node.

Diagram showing a simplified LM ternary node assembly, with LM LN domains involved in the association colour-coded as indicated.

Co-polymerisation, instead, is defined as the process through which more than one laminin associate in a network [153, 155]. Self- and co-polymerisation of laminins are key processes for the assembly of functional basement membranes, and are both mediated by the LN domains located on the short arms of each trimer.

Co-polymerisation represents the first fundamental step for a correct basement membrane assembly [146, 156] and it occurs while the laminin molecule is bound to its receptors, such as integrins and dystroglycan, on the cell surface [157, 158]. Through co-polymerisation, laminins organise into complex polygonal arrays on the cell surface, an active process that requires remodelling of actin filaments and tyrosine kinase signalling and the reorganisation of LM receptors and elements of the cortical cytoskeleton, such as vinculin and dystrophin [158].

LN domain-dependent self-assembly is considered to be crucial for the integrity of BMs, and, as introduced above, the presence of mutations in such domain can lead to different types of pathological conditions. For example, in Pierson syndrome, missense mutations clearly clustered in the LM β2 LN domain [139]; in particular, Arg246Trp and the rarer Arg246Gln affect LM β2 chain secretion by inducing an alteration of the glycosylation site, which takes part in the protein folding [140]. Due to the misfolding, mutated LM β2 chain may be retained in the endoplasmic reticulum (ER) and, therefore, not being able to reach the correct destination [159]. Leu139Pro is an additional missense mutation in the LM β2 LN domain [139] which alters a conserved serine located at the top of the LN domain resulting in a dramatic LM β2 chain misfolding [140].

MDC1A has also been linked with different point mutations; a Gly to Ala substitution in a splice site consensus sequence of LAMA2 gene induces abnormal

splicing of the gene, with the consequent translation of a truncated LM α2 chain carrying a deletion in the LN domain [160]. In addition, MDC1A is related to a point mutation in the murine LAMA2 gene, resulting in a substitution of Arg with Cys in the LN domain [161].

Together, this evidence suggests that the naturally occurring assembly model can be considered as a complex event, highly dependent on the laminin isoforms present in the tissues.

1.2.2.1b Co-polymerisation conditions

Laminin co-polymerisation has been shown to be temperature, time and concentration dependent *in-vitro*, to occur in solution at a critical concentration of 70-140 nM and to be thermally reversible [153]. LM111 co-polymerisation is enhanced by calcium [13, 162], which induces conformational changes in the LN domains allowing them to interact [163]. The calcium-dependency has been confirmed by LM111 self-assembly blocking *in-vitro* using the chelating agent Ethylenediaminetetraacetic acid (EDTA) [148, 153, 163, 164].

1.2.2.1c Laminin self-polymerisation in isoforms lacking one or more LN domain

A study using purified EHS LM111 supported that laminin self-polymerisation requires the presence of all three short arms in an isoform, suggesting that only heterotrimers formed by three full-length subunits are able to self- and co-polymerise [164]. Nevertheless, the LM family consists of some truncated isoforms, which lack

the LN-domain, notably including two of the subunits of LM332, the major LM of most epithelial BMs (Fig. 1.4).

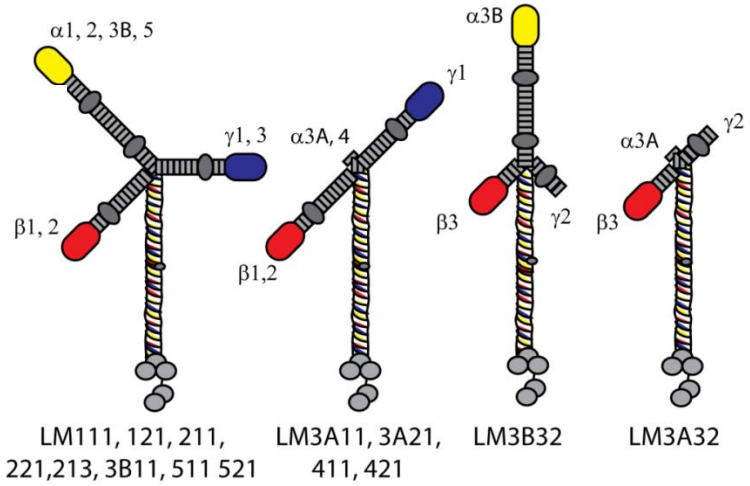

Fig. 1.4: LM truncated isoforms.

Schematic diagram showing the LM isoforms' different structure in terms of presence of the LN domain.

In 2004, Odenthal et al. used eight recombinant expressed LN and LE domains containing LM fragments, found in isoforms other than 111, to test homologous and heterologous interactions. The research demonstrated that α1, α2, α5, β2 and β3 LN domains are able to self-interact [151, 162], whereas the γ1 and γ3 LN domains showed affinity for β3 LN domain but a lower ability of self-binding [151]. The possibility of self-interaction between LN domains suggest that, probably, even the laminin isoforms lacking one or two LN modules could still self or co-polymerise [151]. Supporting the hypothesis of an association between truncated laminin isoforms to ensure a functional network assembly, LM332 has been isolated in a

complex together with LM311 and 321 from the human amnion basement membrane [165].

Interestingly, McKee et al. demonstrated that the inability to polymerise of mutated LM α1 subunits, lacking its LN domains, is rescued by the addition of a polypeptide containing the α1 LN-LE domains [166]. Therefore, an absent α LN domain could be replaced with a substitute protein resulting in the restoration of laminin self-assembly.

1.2.2.2 Laminin-type epidermal growth factor-like domains

The LM-type epidermal growth factor-like domains (LE domains) are found in tandem repeats, separated into stretches by globular domains. Each stretch is named in order from the N terminus as LEa, LEb and LEc, in the short arms of α, β and γ LM chains. LE repeats are also found in netrins, agrin and perlecan [167]. LE domains consist of 41 to 70 residues each, with the α3a, α4, α5, β1, β2 and γ2 chains also having an additional truncated LE domain each (15 to 35 residues) [168]. LE domains contain eight cysteine residues; disulfide bonds between these cysteine residues determine the formation of loops, like in EGF [169]. The tandem arrays of LE repeats in laminins have been demonstrated to adopt a linear, extended arrangement [170] with a highly variable number of copies in the different laminin isoforms; from 3 up to 22 copies have been found [169].

Concerning the functions in laminins, long consecutive arrays of LE domains form rod-like elements of limited flexibility, which determine the spacing in the formation of laminin networks in BMs [147]. LE domains can also bind to syndecans, which

regulates cell adhesion and motility [171, 172] and a high affinity-binding site for nidogens is located between residues 791 and 848 of the LE modules of LM γ1 chain [173]. The LE repeats, therefore, play a role in cross-linking the laminin network with collagen type IV network in basement membranes.

Following proteolytic cleavage, LE domains can be released from LM γ2 chain and these fragments can play different roles; the fragment containing LEa1-3 + L4 domains has been shown to promote cell adhesion via the syndecan-1 surface receptor, whereas the fragment containing LEa2-3 + L4 + LEb1-3 domains is involved in keratinocyte migration [174].

1.2.2.3 Laminin G like domains

The C-terminus of the LM α chains is 865-900 residues longer than that of the β and γ chains and forms the large LG domain at the end of the long arm. LG domains are also present in some collagens, cell surface receptors and anticoagulant and hormone-binding proteins [145, 170]. This domain is folded into five subunits, named as LG1 to LG5, in a range of 160 to 200 residues each [175]. The LG1 to LG3 trio is separated from the LG4-LG5 pair by a short stretch of amino acids and this region is subject to proteolytic cleavage [170].

From the crystal structure, is known that LG domains fold is based on 14 β-strands arranged in two curved sheets with an extensively hydrophobic core, including a calcium binding site[145], with a final diameter of approximately 3.5 nm [176]. Moreover, LG2 and LG3 contain between two and four cysteine molecules, which form disulphide bridges close to the C-terminus [177].

The LG domains contain the major binding sites for different cell surface receptors. Specifically, the LG1-LG3 domains can interact with $\alpha_3\beta_1$, $\alpha_6\beta_1$, $\alpha_6\beta_4$, $\alpha_7\beta_1$ and $\alpha_9\beta_1$ integrins [178, 179], however, each integrin displays different affinities for different laminins. Specifically, $\alpha_3\beta_1$ and $\alpha_6\beta_4$ integrin show the highest affinity for LM332, 511 and 521, whereas $\alpha_6\beta_1$ binds preferentially to LM111, 332, 511 and 521 [180]. Two $\alpha_7\beta_1$ integrin splice variants are also involved in LM binding; $\alpha_7X\beta_1$ does not bind to LM332, while $\alpha_7X\beta_2$ preferentially associates with LM111, 211 and 221 [180].

In addition to integrin binding, the LG 4–5 pair contains the binding sites for α-dystroglycan and syndecans, fundamental interactions required for BM assembly as well as muscle and nerve cell function [176]. LG4 also contains a major heparin-binding site [181] and binds to sulfatides [182], facilitating the laminin polymerisation into networks [183].

1.2.2.4 Laminin Coiled Coil domain

The LCC-domain is the long arm of the laminin and is formed by all the chains twisted with a α-helical motif, stabilised by hydrophobic interactions and electrostatic interactions [147]. The LCC domain is composed of 90 heptads [170] and, in the β chain, is interrupted by a stretch of amino acids termed the LM β knob (Lβ) [147]. The LCC-domain is important during the laminin heterotrimer assembly, where it is required for the formation of βγ dimers [184] and for the orientation of the LG domain [185]. Via binding to different proteins, such as integrins or syndecans, the LCC domain also facilitates cell binding to laminins [145]. Supporting this idea, data show that LCC domain is needed for the interaction between LM332 and $\alpha_3\beta_1$

integrin [185], and that the central region of the coiled coil of LM111 contains a binding site for the N-terminal region of agrin, an interaction that is believed to be crucial for localisation of agrin to the basement membrane [186].

1.2.2.5 Laminin L4, LF and LFx domains

Within the EGF-like repeats of the laminin short arms, other additional domains named as L4, LF and LFx are embedded. In particular, the L4 domains are formed by ~250 amino acids and are found in central positions of the α1, α2, α3b, α5, γ1 and γ3 LM chains; in addition, three L4 domains are found in perlecan [187]. As demonstrated using recombinant expressed mouse α1 L4 domain is capable of autonomous folding and of fibulin 1 binding [188]. Moreover, the LM α2 L4 domain appears to have a functional role in humans; it has been showed that a congenital muscular dystrophy is linked with an in-frame deletion within this domain [189].

Regarding the LF and the LFx domains, almost no data are available; their structures have not been determined, nor have they yet been assigned functions. One interesting study reported that the amino acid sequences of these domains are highly conserved, indicating that the domains have been maintained for physical or functional purposes throughout evolution [190]. Potentially, they could provide additional sources of binding and signalling activities.

1.2.2.6 Laminin heterotrimer assembly

Laminins are structurally organised as heterotrimers, the assembly of which happens inside the cell. The first step of this process is the formation of disulphide linked βγ dimers [184]. Studies revealed that the β chain is also able to homodimerise whereas the γ chain is not but, when both chains are expressed, βγ dimers formation happens preferentially [184]. A 10-amino-acid region located in the LCC domain joins the β and γ chains together and stabilises the disulfide bonds between them [147, 191, 192]. The laminin trimerisation process can be completed, and the protein secreted in the extracellular environment, only when the α-chain is incorporated in the structure [193]. Interestingly, however, it has been shown that the α chain can also be secreted independently as a monomer even if it is still unclear if this happens *in-vivo* [184, 194].

1.2.3 Laminin expression pattern in tissues

1.2.3.0 Laminin expression during mammalian organogenesis

LM expression starts at the very beginning of the pregnancy, when the uterus has to morphologically change; this process, and therefore the gestation progress, depends on the laminins for support [194]. After successful mating, the decidual cells of the blastocyst start to synthesize LM111, the first laminin deposited in the endometrial ECM [195]. Gradually, the laminin isoforms expressed will vary according to the organ being formed.

The change in laminin isoforms expression during embryonic development has been characterised in several murine organs and tissues. For instance, during lung development, all LM α chains are present, except LM α4 [196],whereas a basement

membrane primarily formed by LM111 and LM411 is found during the mesenchyme-epithelium transition in kidney formation, as demonstrated by blocking antibody-based experiments targeting LM α1, which stopped such transition [197]. When kidneys are completely formed, a developmental transition in α and β chains deposition leads to the LM111 replacement with LM521 [198]. LM421/521 are found in peripheral nerves, whereas individual axons within the nerve are surrounded by myelinating Schwann cells synthesizing LM211 [199]. Studies of the placental BM revealed that it contains LM111, LM221, LM411 and LM521 [200], in addition to a truncated form of LM213, first purified from human placental chorionic villi [201]. A very interesting study, using laminin gene trap mice, showed no evidence of a laminin accumulation in the brain [202]. However, netrins, which are structurally very similar to LaNts as described ahead, have been shown to be expressed in the brain [203, 204].

1.2.3.1 Laminin expression in adult tissues

In adult tissues, LM α1 chain expression is generally characteristic of newly forming epithelial cells, whereas α2 chain is predominantly found in mesoderm derived cells. LM α4 chain, instead, is mainly expressed by endothelial cells, with LM411 being predominant in smaller and dermal vessels [205, 206]. LM α3 and α5 chains expression is restricted to epithelial cells [207], with the α5 chain being widely expressed in the dermal vasculature and in the interfollicular epidermis of adult tissues [208].

1.2.3.2 Laminins in wound repair

During the wound healing process, re-epithelialisation and angiogenesis involve laminins in different ways and with different roles. During re-epithelialisation, the formation of new epithelial tissue as part of the restoration of structure and function of injured tissues, laminins are required to support epithelial keratinocyte migration [209, 210]. Laminins are deposited and provide a substrate over which the cells are able to move, leading to wound closure [211]. Indeed, LM332 deposition onto the wound bed appears to be one of the earliest events, occurring within hours of injury [92, 212]. Supporting these data, LM332 has been shown to be expressed at the leading edge of the motile keratinocytes and to be the only BM component deposited between the clot and the migrating tongue [211].

LMs are also key players in angiogenesis, defined as the new blood vessel growth and maturation; alterations in laminin deposition, particularly of LM511, result in delayed corneal epithelial wound closure associated with diabetes [213] and diabetic retinopathy [214]. In addition, *in-vivo* studies demonstrated the presence of vascular abnormalities and slightly altered vasculogenesis in LM α4 chain-deficient mice [215, 216], consistent with LM411 being the major component of capillary and larger vessel BMs [217].

1.2.3.3 Laminin expression in corneal epithelium

The cornea is the clear, dome shaped surface that covers the eye outermost layer, playing a fundamental role in focusing the vision; it accounts for approximately two-thirds of the eye's total optical power [218].

Although it may seem simple, the cornea is characterised by a highly organised structure; human cornea is composed of three thicker basic layers with two thinner membranes between them; starting from the outer layer, there are the epithelium, the Bowman's membrane, the corneal stroma, the Descemet's membrane and the endothelium [219, 220] (Fig. 1.5). The central corneal thickness is approximately 520 µm, but increases towards the periphery, where it can reach 650 µm [221]. As opposed to conjunctiva, which is a highly vascularised and innervated mucous membrane, the cornea does not contain any blood vessels but rather receives nourishment and protection from infectious agents via a combination of tear film and aqueous humor [222].

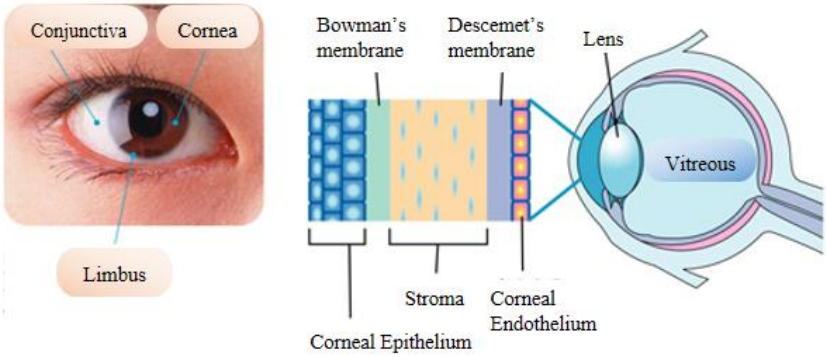

Fig. 1.5: Human eye and cornea representation.

Schematic diagram of the structures of the human eye and the cornea, including all the corneal layers. Figure adapted from J-TEC company website (www.jpte.co.jp).

The cornea, which is the portion of the eye we focused on during this project, is composed by keratocytes, endothelial and epithelial cells; corneal integrity is maintained by stem cells located within the basal layer of the limbus, the border separating the cornea from the conjunctiva and the sclera [223]. The limbus ensures a

cyclic corneal cell shedding and replacement, during either normal cell turnover or following injuries [224, 225].

Human corneal epithelial basement membranes significantly change in terms of components between the infant and adult phases [226]. In infants, stem cells are present in the central cornea, while in adults they are localised mainly in the limbus [227]. In addition, LM α2 and β2 chains are absent from the infant basement membrane, whereas they are both found in the adult's limbal and conjunctival basement membrane. Nidogen-1, -2 and netrin 4 are found in stromal and endothelial sides of the Descemet's Membrane in infants, but they remain only on the endothelial side of such membrane in adults [226].

Corneal epithelial cells are of fundamental importance for protecting the eye against foreign material and bacteria, and for providing a smooth surface to absorb O_2 and nutrients from tears, which are then distributed to the other layers of the cornea [228]. The majority of our *in-vitro* functional work has been based on the use of hTCEpi, immortalised limbal-derived corneal epithelial cells [229]. These cells display the same characteristics as their *in-vivo* counterparts, the cells that form the corneal epithelium.

Immunoprecipitation (IP) data revealed that cultured corneal epithelial cells produce a LM332-rich BM, found *in-vitro* as small plaques beneath the adhering cells first, and widely spread in co-localisation with β_4 integrin subunit thereafter [230]. As LM332 and LM311/321 have the same α chain [95], it has been proposed that corneal epithelial cells also contain small amounts of these laminin isoforms [231]. Published studies on all these laminins have demonstrated their involvement in

regulating keratinocyte motile behaviour [89, 232, 233] and in contributing to wound repair [209, 212].

1.2.3.4 LM332

LM332 has a central role in the maintenance of epithelial-mesenchymal adherence in tissues exposed to external forces, in cell migration, in tissue development, in wound healing and in tumorigenesis [234, 235]. It is also the major laminin produced by corneal epithelial cells and, therefore, a major focus of the studies described in this thesis. As such, a deeper introduction to this specific laminin is required.

1.2.3.4a LM332 processing

Two of the LM332 chains, α3a and γ2, undergo extracellular proteolytic processing events to smaller forms [236]. LM332 is first synthesised as a precursor protein of 460 kDa that is subsequently processed to a 440 kDa form, in low calcium concentrations, or to a 400 kDa form in high calcium concentrations [236]. These size changes are due to removal of the α3 chain C-terminal LG 4-5 domains, converting the 190kDa form to a 165 kDa mature form [237, 238], and to the cleavage of the N-terminal region of the γ2 chain, converting the 155 kDa form to a 105 kDa mature form [236, 239]. There is no evidence of processing events regarding the β3 chain, therefore LM332 containing the 165 kDa α3 and the 105 kDa γ2 processed chains is considered the mature form.

There are multiple *in-vitro* studies describing enzymes which are involved in LM332 processing. It has been shown that the α3 chain processing happens after treatment

with plasmin or via the tissue plasminogen proteolytic cascade [240]. Furthermore matrix metalloproteinase-2 (MMP-2), membrane type-1 matrix metalloproteinase (MT1-MMP) and the C-proteinase family of enzymes, in particular the mammalian tolloid (mTLD) and the bone morphogenic protein 1 (BMP-1), have been demonstrated to take part in LM332 proteolytic cleavage [237, 241]. N-terminal amino acid sequencing of human LG4-5, purified from the conditioned medium of human skin cells or human gastric adenocarcinoma cells STKM-1, revealed that the α3 chain is cleaved between the residues Q1337 and D1338, suggesting that the cleavage site matches the minimal consensus sequence LLQD [242, 243]. In addition, thrombin was shown to be able to cleave α3 LG4-5 specifically at R1343 and R1389, residues located in the LG3-4 linker sequence [244].

Mature LM332 is involved in different cell functions; among them, LM332 allows a non-HD forming matrix to become competent for HD assembly [237]. Supporting this, an *in-vivo* study using an mTLD/BMP1 deficient mouse revealed the skin γ2 processing to be dramatically reduced and the hemidesmosomes to be altered, suggesting a fundamental role of LM332 correct processing for a functional HD formation and integrity [245].

Interestingly, the proteolytically released LG4-5 module has been shown to support cell adhesion when coated onto plates, but not to bind to β_1 integrin [246]. Furthermore, purified LG4-5 was not able to stimulate cell scattering on rat liver epithelial cells until added to low concentration of LM332 [242]. LG4-5 has also been reported to bind to heparin [247] and to induce neurite outgrowth [247, 248], processes almost surely mediated by binding to syndecans 2 and 4 [247]. The proteolytic cleavage of the γ2 chain also leads to the release of a laminin fragment that increases cell migration [174, 245, 249].

LM α3a chain also undergoes a signal peptide cleavage, which has been shown to occur between Gly26 and Tyr27, located in the N-terminal region of the 200 kDa form [241]. Further cleavage has been reported to occur in the N-terminal LE region of the α3 chain, releasing the short arm which might be important for LM332 function [165, 241]. The importance of the N-terminal region in LM α3a chain is also demonstrated by the presence of a pathologic condition, named as Laryngo-onycho-cutaneous (LOC) syndrome, precisely linked to a LM α3a mutation. LOC is characterised by cutaneous erosions, nail dystrophy and chronic overproduction of granulation tissue in some epithelia, especially conjunctiva and larynx, and is caused by a frameshift mutation leading to the LM α3a N-terminus deletion [91].

LM α3b chain also undergoes proteolytic cleavage with processing resulting in the release of a 190 kDa NH2-terminal fragment [232]. This released fragment demonstrated as being active in promoting cellular adhesion, migration, and proliferation through its association with integrin $\alpha_3\beta_1$ [232]. Although this "fragment" is 3x larger than the LaNts, many of the domains are shared between it and the LaNt proteins (described below), which could suggest a similar role for LaNts too.

1.2.3.4b LM332 deposition

In-vitro studies have demonstrated that LM332 deposition depends on the LG domains and on the cleavage of the γ2 N-terminus [244]. Vector-driven expression of LM α3, with or without the LG domains, revealed a decreased secretion of recombinant α3 protein in the culture medium associated with the reduced numbers of LG domains [185], while the absence of the entire region prevents secretion

entirely [250]. Consistent with this, the presence of the α3 LG4-5 region was found to be necessary for keratinocytes isolated from a LM α3-/- mouse model, to bind and deposit soluble LM332 [244]. Moreover, γ2 chain processing has been shown to be required for the LM332 incorporation in the skin's basement membrane, possibly by facilitating collagen type VII interaction [251, 252].

Supporting the important role of γ2 chain proteolytic cleavage for LM332 deposition is the study of patients affected from cylindromatosis, a condition involving multiple skin tumours that develop from structures associated with the skin [253]. This rare inherited disease is characterised by an incomplete laminin processing which leads to ultrastructural alterations of the basement membrane and altered expression/distribution of integrin receptors [252, 254]. Together, these data highlight the importance of post-translational processing for a correct laminin deposition and network formation.

Section 3. Cell to matrix adhesion devices

Cell-matrix interactions are vital to enable cells to sense numerous extracellular signals and to regulate differentiation, cell cycle, migration and survival [255, 256]. These interactions are mediated by different proteins and adhesion receptors, leading to the formation of multi-component adhesive structures that link the actin cytoskeleton to the cell interior [257]. HDs and FAs complexes are the two main adhesive devices that connect the cells to the basement membrane and, in particular, to LM332.

1.3.0 Hemidesmosomes

Hemidesmosomes, originally called "bobbins" by Weiss and Ferris [258], can be defined as the major cell attachment site to the ECM and are known to be involved in tissue mechanical support and/or remodelling, cell differentiation, migration and wound healing[259-261]. The name "hemidesmosome" derives from their similarity to half a desmosome when observed under an electron microscope; however, the protein composition differs between the two structures although both play roles in intermediate filament association.

Hemidesmosomes appear as electron dense spots, of about 0.5 μm in diameter, located in the plasma membrane [259]. At the ultrastructural level, HDs are characterised by a tripartite cytoplasmic plaque anchored to bundles of intermediate filaments (IFs) [262]. A sub-basal dense plate and several anchoring filaments represent the connection between hemidesmosomes and the *lamina lucida* and *densa*

respectively [263-265]. At the protein level, the stable junctional structure known as the hemidesmosomal adhesion complex [266] is composed of the following proteins:

- The intracellular plaque proteins bullous pemphigoid antigen 230 (BP230, also known as BPAG1e) and plectin [267, 268];

- The transmembrane proteins CD151, collagen type XVII, also known as bullous pemphigoid antigen 180 or BPAG2, and $\alpha_6\beta_4$ integrin [262, 269, 270];

- LM332, found at the border between the *lamina densa* of hemidesmosomes and the *lamina lucida* at the base of anchoring filaments [271, 272].

This organisation is classed as a Type I HD (Fig. 1.6) and is present in basal keratinocytes of multi-layered squamous epithelia, including the cornea and the skin [262, 273]. Less mature hemidesmosomes, containing only $\alpha_6\beta_4$ integrin and plectin, have also been described and classified as Type II HDs; these are generally found in cylindrical epithelia [274, 275].

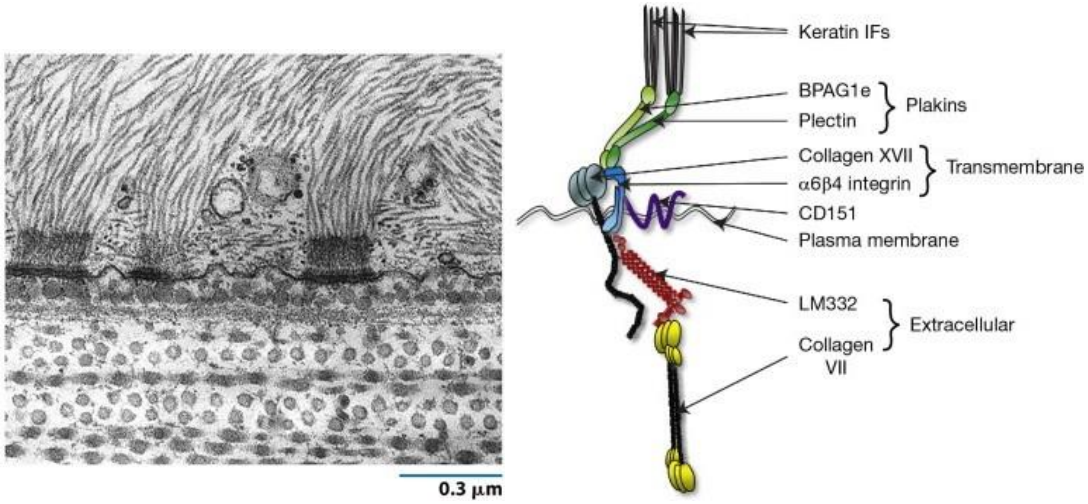

Fig. 1.6: **HD structure**.

Schematic outline of the HD structure, indicating all the components and their interactions in the hemidesmosomal adhesion complex. Electron micrograph adapted from "Cell and Molecular Biology"-Wiley & Sons, 2008.

1.3.0.1 HD components

To form a functional HD complex, several components have to be assembled together in a specific order and with a specific spatial localisation. LM332 has a crucial role in both the nucleation of hemidesmosome assembly and in the maintenance of the hemidesmosome structural integrity; any alteration in LM332 or any modification of one or more HD components may be reflected on hemidesmosomal activity. It is, therefore, helpful to describe some of the characteristics of the hemidesmosome's constituents.

1.3.0.2 The cytoplasmic plaque proteins

The cytoplasmic plaque of hemidesmosomes contains several proteins. The two major ones are plectin [276, 277] and BP230, named after being shown as a target antigen in the bullous pemphigoid, an autoimmune blistering disorder of the skin [278, 279]. In addition to these, the less studied protein P200 is also part of the cytoplasmic plaque.

1.3.0.2a Plectin

Plectin belongs to the plakin proteins family, involved in the organisation of the cytoskeleton [280]. Plectin acts as a multifunctional cytoskeletal linker [267] and undergoes alternative splicing to produce several isoforms [281]. These isoforms encode a protein of a 507-527 kDa size range, formed by a 200 nm central α-helical rod flanked by two large globular domains [267]. The major function of the different plectin isoforms has been associated with IFs network architecture [282].

Ligand binding analysis revealed that plectin-actin link occurs via an actin-binding site (ABD) located in the conserved N-terminal domain, which is also found in the actin binding proteins spectrin and dystrophin [273]; the same domain has been shown as able to bind to the cytoplasmic tail of integrin β_4 [283]. On the other hand, the COOH-terminal domain of plectin binds to keratins, neurofilaments, and vimentin *in-vitro* [273]. Plectin's interactions suggest it acts as a stabilising bridge between IFs and actin filaments and between IFs and HDs [267]. Supporting the latter role it has been demonstrated that loss of function mutations in the plectin encoding gene, *PLEC1*, are related to epidermolysis bullosa simplex associated with muscular dystrophy (EBS-MD), an autosomal recessive disorder [277, 284].

1.3.0.2b BP230

BP230, also known as BPAG1e, belongs to the same protein family as plectin and was the first autoantibody identified in patients with the autoimmune skin blistering disease bullous pemphigoid (BP)[285]. BP230 interacts with keratins and IFs via its globular C-terminus and uses the NH2-terminus to bind collagen type XVII in the cytoplasm [286]. Moreover, BP230 can associate with the protein erbin, involved in the Ras signalling pathway, and also, directly with β_4 integrin [287].

The BP230 encoding gene, DST, undergoes alternative splicing, giving rise to a neuromuscular isoform called BPAG1n or dystonin, and BPAG1a, related to the dystonia musculorum neurodegeneration syndrome in mice, as reviewed by[287]. Studies using a BP230 knockout mice showed that this protein is involved in IFs - cell surface anchorage, as HDs in the keratinocytes of these mice lack the inner

region of the hemidesmosomal plaque and exhibit very few associated intermediate filaments [288]. This evidence, therefore, suggests a similar role as plectin in linking the cytoskeleton to HDs, further supported by a recently identified form of EB caused by a homozygous nonsense mutation located in BPAG1e [289]. In contrast with the blistering affecting many patients who have autoantibodies against BP230, patients suffering from DST-e pathogenic mutations surprisingly show minor blistering, despite having the complete absence of the hemidesmosomal inner plaque [289].

1.3.0.2c P200

Very little is known about protein P200. From the available data, P200 is a 200 kDa protein recognised by the monoclonal antibody 6A5 and it is deposited at the epithelial-stromal interface [290]. P200 is likely to be involved in the linkage of intermediate filaments to the plasma membrane, also due to its localisation to the inner hemidesmosomal plaque [290].

1.3.0.3 The membrane proteins

Membrane proteins are responsible for several of the specific functions of membranes. This protein family includes integral membrane proteins, that are permanently anchored, or peripheral membrane proteins, that are only temporarily attached to the lipid bilayer or to other integral proteins. Accordingly, the amount and types of proteins in a membrane are highly variable. Hemidesmosome's membrane proteins are $\alpha_6\beta_4$ integrin and collagen type XVII.

1.3.0.3a Integrin $\alpha_6\beta_4$

Integrins are obligate heterodimeric matrix receptors, composed of non-covalently associated transmembrane glycoprotein subunits, named as α and β, which form bridges for cell-cell and cell-ECM interactions [291, 292]. Moreover, integrins can activate signal transduction pathways by triggering chemical pathways to the interior, playing a fundamental regulatory role in controlling the cell cycle, cell shape and/or motility [293]. Most integrins are connected to bundles of actin filaments [294], however the $\alpha_6\beta_4$ integrin found in hemidesmosomes is an exception, as it is connected primarily to intermediate filaments [295].

Structurally, α_6 integrin is initially synthetized by the ITGA6 gene as a 150-kDa polypeptide, and then cleaved into "heavy" and "light" chains that dimerise via disulfide bonds [296]. α_6 integrin (130 kDa) can pair with the β_1 subunit but the association with the β_4 subunit (250 kDa) has been shown to be happen preferentially [297]. Integrin β_4 subunit, instead, is characterised by an unusually long (for integrins) C-terminus; this tail contains approximately 1000 amino acids and two pairs of FN type III repeats, separated by a connecting segment comprising 142 amino acids [298]. It is within this tail region that the binding sites for plectin, BPAG1e and the intracellular site of collagen type XVII are located.

Intracellularly, β_4 interact with plectin and BP230, and therefore with the IF complex [299]. Extracellularly, the $\alpha_6\beta_4$ integrin complex associates with processed LM332 [273, 300]. The use of antibodies to block either subunits of $\alpha_6\beta_4$ integrin revealed the importance of this trans-membrane receptor for the nucleation of HDs formation; 804G cells with blocked $\alpha_6\beta_4$ integrin do not show formed hemidesmosomes at the ultrastructural level [290]. In a wound healing model, integrin α_6 blocking led to the

separation of the epithelial sheet from the underlying connective tissue, suggesting that α_6 is fundamental for cell attachment [301].

Further evidence on the major role of $\alpha_6\beta_4$ integrin are given by patients who suffer from junctional epidermolysis bullosa associated with pyloric atresia (PA-JEB); due to mutations in the genes for α_6 or β_4 integrin subunits, they form rudimentary hemidesmosomes [302-304]. In addition to these data, it has been reported that mice lacking the α_6 integrin chain die at birth, due to the HDs adhesion complexes not forming at all [305-307].

1.3.0.3b CD151

CD151 is a trans-membrane protein belonging to the tetraspanin superfamily. Structurally, CD151 contains two extracellular loops, one small and one large, and cytoplasmic COOH- and NH2-terminal domains [308]. Previous studies suggest that the large extracellular loop can bind to integrins $\alpha_3\beta_1$, $\alpha_6\beta_1$, $\alpha_6\beta_4$ and $\alpha_7\beta_1$ [309-312]. CD151 uses these interactions to take part in several cell biological processes, such as cell adhesion[313], motility [308, 310, 314] or the transport of integrins via vesicles [315].

Regarding the role of CD151 in cell adhesion, data from Sterk et al. revealed that CD151, recruited into HDs via the integrin α_6 subunit, is a major component of every pre-hemidesmosomal structure, with its expression decreasing on the basis of the HDs maturation stage [270]. The same group also showed that CD151 stabilises the HDs adhesion complex by facilitating the formation of a stable laminin-$\alpha_6\beta_4$ integrin interaction [270]. However, the use of animal models to analyse the role of CD151 in

HDs has given controversial results. CD151-null mice appeared to be healthy and with normal HDs formation in a study published from Wright et al, but were described as having serious renal pathologies in a study published in 2006 by Sacks et al [316] [317]. These incongruous results suggest CD151 is still a relatively unstudied component of hemidesmosomes, and future research should be done to address open questions on its function.

1.3.0.3c Collagen type XVII

Collagen type XVII, previously named as bullous pemphigoid antigen 180 (BP180) or BPAG2, is a transmembrane protein encoded by the gene COL17A1 [318]. It is a homotrimeric molecule formed by three α1 chains (180 kDa), each characterised by an intracellular N-terminal domain (466 amino acids), a transmembrane stretch (23 amino acids) and an extracellular C-terminal ectodomain of 1008 amino acids [319]. The C-terminal, in turn, contains 15 collagenous subdomains (COL1–COL15) flanked by 16 non-collagenous sequences (NC1–NC16A) [318]. The final structure is flexible, rod-like and triple-helical, with a significant thermal stability prevalently due to COL15, the largest collagenous subdomain of the C-terminal [320]. In its full-length form, the cytosolic N-terminus is present at the HD plaque level, whereas the extracellular domain is located in the BM. A soluble form, LAD-1, also known as ectodomain, is generated by proteolytic cleavage of the full-length form [321].

Collagen type XVII integrates into hemidesmosomes via α_6 and β_4 integrin chains binding, which occur respectively via amino acids 506-519 of the C-terminal ectodomain [269] and via the N-terminal region [322]. It can also interact with several other ligands, contributing to stabilise cell adhesion [322]. With regard to our

research, the ectodomain has been shown to co-localise with LM332 in the migration tracks of primary human keratinocytes, whereas LM332 deficient keratinocytes displayed a drastically reduced collagen type XVII deposition in the ECM [323].

Genetic and acquired diseases, caused by mutations in the COL17A1 gene, indirectly demonstrate this key role; the loss of function of collagen type XVII leads to diminished epidermal adhesion and skin blistering (JEB) or angiogenic pathologies, such as the bullous systemic lupus erythematosous [285, 324].

1.3.0.4 Hemidesmosome assembly

The first data describing HDs morphogenesis *in-vitro* were published by Krawczyk and Wilgram in 1973, who studied hemidesmosome's formation in a mouse epidermal wound-healing model [325]. The proposed model had four sequential ultra-structural phases. The first stage was the extension of fine filaments between the plasma membrane and the *lamina densa*. These extracellular filaments became increasingly dense until a narrow electron-dense line, parallel to plasma membrane and the *lamina densa*, developed within them. Thereafter, an intracellular electron-dense plate appeared in exact apposition to the extracellular filaments. The final stage was the insertion of intermediate filaments into the intracellular electron-dense plate [325].

The concept of mature and immature hemidesmosomes was firstly used in 1983, when Gipson et al. used viable sheets of adult rabbit corneal epithelium to study the time requirements for HD formation and the relationship between HD formation and anchoring fibrils [326]. They found that the 83% of new hemidesmosomes developed

within the first 6h of culture and mostly appeared over pre-existing anchoring fibrils [327]. It is now well known that the interaction of integrin β_4 with plectin is crucial for the formation of stable HDs [328, 329]. This is also supported by the defective assembly of HDs in patients affected by PA-JEB, caused by mutations in the ITGB4 gene (Arg1281Trp or Arg1225His) that prevent the β_4-plectin interaction [329] [330], and by plectin-deficient mice, which show dramatic epithelial detachment leading to death 2-3 days after birth [331].

HD assembly starts with CD151 and integrin $\alpha_3\beta_1$ forming the so called pre-hemidesmosomal clusters, hypothesised to serve as a 'nucleation site' for the process [270]. CD151 will, then, become a component of mature HDs, while $\alpha_3\beta_1$ is recruited into FAs after HDs have been assembled [332]. The first association happens between the plectin ABD domain and the integrin β_4, via the FNIII repeats and residues 1115-1355 of the β_4 tail [283, 328, 333]. This interaction is followed by a second link between the plectin N-terminus and the C-terminal domain of the β_4 integrin [333, 334]. Following the β_4-plectin association, collagen type XVII interacts with LM332 and with the plectin-$\alpha_6\beta_4$ integrin complex. Lastly, BP230 is recruited through associations with collagen type XVII and CD151 [268, 333, 335]. The entire process is summarised in Fig. 1.7.

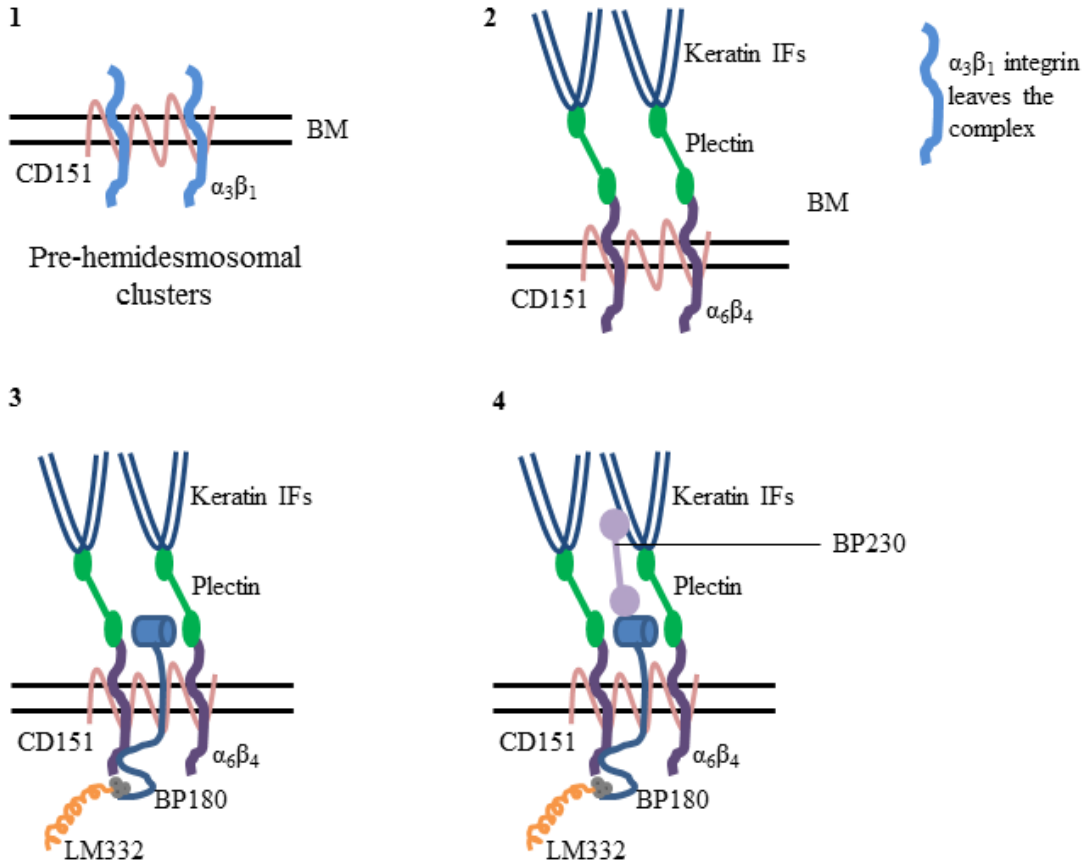

Fig. 1.7: HD assembly.

Schematic diagram showing the four steps of HD assembly. Plectin-$\alpha_6\beta_4$ integrin association triggers the binding of the other HD components and is facilitated by the presence of a pre-hemidesmosomal complex.

1.3.0.5 Hemidesmosome disassembly

HDs are highly dynamic structures that quickly disassemble during cell division, differentiation or migration [261]. When detachment from the basement membrane is needed, hemidesmosome's components diffuse over the plasma membrane or in the cytoplasm and are translocated to lamellipodia [290, 336]. Transient and permanent disassembly of HDs can be distinguished. A transient dissolution occurs, for

instance, when skin keratinocytes migrate to close a wound or during carcinoma invasion [337-339].

Due to the importance of the first of the HD assembly steps, it is believed that HD disassembly happens via disrupting the plectin-β_4 association [340]. HD transient disassembly is primarily triggered and regulated by post-translational changes, such as the phosphorylation of HDs components in response to GFs stimulation [340]. Although somewhat controversial, studies have revealed that EGF-induced tyrosine phosphorylation of Tyr1422 and Tyr1440 residues, located in the β_4 tail, mediates HD disassembly [341, 342]. In contrast with this, different reports shown that the redistribution of HD components during disassembly is mediated by the activation of members of the protein kinase C (PKC) family, suggesting that PKCs induces the phosphorylation of specific sites present in the β_4 tail and regulates HD disruption [343]. This was confirmed by other studies in carcinoma cells and normal keratinocytes, demonstrating the HDs undergo a disassembly process after the activation or the overexpression of PKC-family members [344-346].

Despite being still unclear, it is possible that HD transient disassembly is differentially regulated in different cell types; tyrosine phosphorylation pathways might be involved in the migration and invasiveness of tumour cells, while serine phosphorylation-mediated HDs disassembly could be more relevant under more "normal" cellular conditions [340] .

On the other hand, permanent dissolution of hemidesmosomes involves repression of gene transcription and proteolytic cleavage of the components [347]. Previously published data show that integrin $\alpha_6\beta_4$ expression in proliferating or differentiating keratinocytes is mostly controlled at transcriptional level, with integrin α_6 expression

repressed in presence of high levels of p63 [348, 349] and both integrin subunits expression repressed via the Notch signalling pathway, when cells undergo terminal differentiation [350, 351]. The involvement of the Notch pathway in the repression of integrin $\alpha_6\beta_4$ gene transcription and, therefore, in hemidesmosome disassembly, has also been shown by Ambler and Watt, who developed mice with hyperactivated Notch signalling in basal keratinocytes and observed a focal epidermal detachment [352].

1.3.0.6 Hemidesmosomes in keratinocytes migration

To move from one location to another, an essential process for normal development or tissue remodelling, cells must first disrupt, or at least loosen, their connection with the BM; HD components are highly involved in this mechanism.

There are data showing that keratinocytes derived from β_4 integrin-null mice display aberrant motility and do not move in linear tracks but in circles [307, 353, 354]. Interestingly, this defect can be rescued if the cells are plated onto a WT cell-derived matrix, where the migration goes back to linear fashion [353]. These data implicate integrin β_4 in regulating the deposition pattern of LM332, pointing to a regulatory role on cell motility for LM332 matrix organisation [353]. The same group indicated that $\alpha_6\beta_4$ integrin interacts with the Rac1 signalling pathway, a small G protein that regulates lamellipodia formation at the leading edge during migration and is required for an efficient establishment of cell front-rear polarity and processivity [353]. This interaction places Rac1 mediated pathways in the control of LM332 matrix organisation and in support of this idea, expression of dominant negative Rac1 leads to defective motility in keratinocytes [353]. In addition to $\alpha_6\beta_4$ integrin, Rac1

activity is also influenced by collagen type XVII; when the latter is absent, lamellipodial dynamics and keratinocytes migration are decreased [355].

When it comes to tissue remodelling in response to wounded epidermis, keratinocytes at the leading edge of the wound have to migrate to close it. This implies a so-called processive migration, during which skin cells are stably polarized and migrate linearly without a chemotactic gradient [356]. As described above, LM332 is known to be highly involved in cell motility. When containing an unprocessed α3 chain (190 kDa), LM332 supports keratinocyte motility [237]; instead, when α3 chain is cleaved within its G domain, LM332 induces HD assembly and a sequential decreased cell migration [209, 237, 357].

Moreover, in addition to the individual HD proteins roles, support for keratin-HD interaction being fundamental for cell-matrix adhesion and migration was generated by Seltmann et al, who recently showed that keratinocytes in which the entire keratin cytoskeleton was depleted are characterised by loss of plectin, dispersion of the HDs transmembrane core along the BM and faster adhesion/motility properties [358].

1.3.1 Focal Adhesions

Focal Adhesions (FAs) are defined as mechanical linkages between intracellular actin bundles and the ECM, acting as biochemical signalling hubs to direct and mediate the regulatory effects of a cell in response to ECM adhesion [359, 360]. FAs are the earliest and best-characterised cell-ECM adhesion structures; therefore, localisation to focal adhesions is often considered a good indication for the functionality of a protein in cell-ECM adhesion [360]. It is important to consider that

FAs are highly dynamic protein complexes, in a state of constant flux: proteins associate and dissociate with FAs continually as signals are transmitted to other parts of the cell. A large number of specific proteins are known to be present in FAs; these are usually structural and cytoskeletal proteins but many are also signalling molecules [361].

1.3.2 Focal Adhesions components

As part of adhesive devices, focal adhesion components are tightly modulated in terms of assembly, disassembly and, therefore, interactions with different ligands. Hundreds of proteins have been associated with focal adhesions in different contexts. Here, I will just deal with some of the main components that are either always present or are used to indicate different levels of FA maturity.

1.3.2.1 Talin

Talin is a high molecular weight (~270 kDa), elongated (approx. 60 nm) and flexible anti-parallel dimer, which appears as a series of "beads on a string" under the electron microscope [362]. Structurally, talin is characterised by a globular N-terminal domain followed by a flexible rod region [363]. The N-terminal head contains a FERM domain, named after its component proteins; 4.1, ezrin, radixin and moesin. The FERM domain is a widespread protein module, involved in localising proteins to the plasma membrane, which has binding sites for the cytoplasmic domains of β_1 and β_3 integrins and filamentous actin (F-actin) [364].

Via its N-terminus, talin also interacts with focal adhesion kinase (FAK), a crucial signalling molecule activated by numerous stimuli that takes part in controlling cell motility [365], with phosphatidylinositol phosphate kinase type Iγ (PIPK1γ), phosphatidylinositol (4,5) bis-phosphate (PI(4,5)P2) and with layilin, C-type lectin found in membrane ruffles [366]. In addition to such binding partners, the talin flexible rod contains further integrin-binding sites, two actin-binding sites and several binding sites for vinculin [367]. Finally, talin has a highly conserved, large C-terminal rod domain that contains bundles of α helices involved in actin-binding integrin-binding [368] and vinculin- binding [369].

Several studies have demonstrated that talin plays a key role in integrin-mediated adhesion; for instance, microinjection of talin antibodies in cultured cells disrupted FAs [370]. Moreover, FAs assembly and cell spreading decreased when talin expression was down-regulated using antisense RNA [371], as well as when the talin encoding gene TNL1 was silenced [372]. Further support to this concept is given by an *in-vivo* study, where mice with a targeted disruption of the talin gene survived only for 8.5-9.5 days post coitum, proving that talin is necessary for embryogenesis [373].

1.3.2.2 Vinculin

Vinculin is a 117 kDa cytoskeletal protein composed of 1066 amino acids. It contains an acidic N-terminal domain, which includes binding sites for talin and α-actinin as well as a tyrosine phosphorylation site, and a basic C-terminal tail region, containing binding sites for F-actin, paxillin and lipids [374]. These two domains are separated by a proline-rich middle segment. Vinculin is crucial for regulation of

cytoskeletal mechanics, cell spreading and lamellipodia formation [375]. Supporting this role, loss of vinculin prevents cell adhesion and spreading, leads to a decreased number of stress fibres and FAs, and stops lamellipodia extension [374], although vinculin overexpression studies demonstrated that these defects could be restored [376]. Moreover, a study using vinculin deficient mice showed that embryos are smaller than controls and die at embryonic day 10.5 (E10.5), due to major defects during brain and heart development [377].

When localising to focal adhesions, vinculin undergoes conformational changes [378] and, therefore, there is an intracellular equilibrium between vinculin's active and inactive state [379]. Such a conformational change allows vinculin to be accessible to its 19 binding partners [379] including; talin [380], α-actinin [381], VASP (VAsodilator-Stimulated Phosphoprotein) [382], Arp2/3 [383], paxillin [384], F-actin [385], synemin [386], calpain [387], polycystin-1 [388] and PIP2 [389]. Binding with vinculin can activate or link to other proteins, triggering different signalling cascades [390].

1.3.2.3 Paxillin

Paxillin is a phosphotyrosine-containing FA component of about 68-70 kDa [391]. Structural analysis revealed that the paxillin N-terminal region is characterised by a proline-rich portion, numerous tyrosine residues and, additionally, five copies of a peptide sequence, named as LD motif, which are now known to function as binding sites for other proteins [392]. Furthermore, paxillin is formed by a C-terminal domain, which comprises four LIM domains, zinc-binding structures named after their similarity to double zinc finger domain, which act as mediators for protein-

protein interactions [393]. The FA targeting sequence of paxillin is located in the C-terminal half of the protein, within the LIM domains 2 and 3 [394].

Several paxillin-associated proteins have been identified, among which there are vinculin, FAK enzyme and the cytoplasmic domain of the β_1, β_3 and β_4 integrins [395]. Regarding the latter, paxillin has been shown to regulate cell spreading and motility through its binding to the α_4 integrin subunit [395]. Giving further support to the importance of paxillin for fundamental cell behaviours, paxillin -/- mice die at E9.5, highlighting the key role that paxillin plays during embryonic development [396].

1.3.2.4 Focal Adhesion Kinase

Encoded by the PTK2 gene, Focal Adhesion Kinase (FAK) is 125 kDa cytoplasmic tyrosine kinase associated with FAs that participates in cell attachment, spreading and motility [397]. Structurally, four α helices arranged in a bundle form the C-terminal region, composed of 1059 amino acids, in which the FAK targeting domain (FAT), used for linking within the focal adhesions, is located [398]. The N-terminal domain has been demonstrated to interact with the integrin β_1 subunit *in-vitro* [399] and to directly bind the N-terminal domain of protein p53, leading to p53-mediated apoptosis suppression [400]. Moreover, FAK N-terminal domain interacts with the tumor suppressor protein neurofibromin, playing an important role in the intracellular signalling and carcinogenesis [401]. Between the N- and the C- regions lies the catalytic or regulatory domain, important for the kinase activation of FAK as it contains the so-called activation loop, involved in protein phosphorylation [402].

FAK displays different functions within FAs. It binds directly to talin and paxillin and is able to induce the activation of Rho-family GTPases by modulating various upstream regulators [403, 404]. Moreover, FAK is involved in the regulation of cell migration. In cultured cells, FAK deficiency negatively affects cell spreading on ECM proteins and cell movement in response to chemotactic and haptotactic signals [405, 406], defects rescued after the reconstitution of FAK-deficient cells with wild-type FAK [407]. FAK-deficient cells also appear to respond slowly to forces and to, therefore, have a decreased movement reorientation [408]. A study on FAK overexpression in Chinese hamster ovary (CHO) cells support this regulatory role in cell motility; FAK overexpressing CHO cells display an enhanced cell migration [409]. Not surprisingly, oncological studies on human tumour samples revealed elevated expression of FAK [410], which has been correlated with increased cancer cell motility, invasiveness and proliferation [410-412].

1.3.2.5 Integrin $\alpha_3\beta_1$

In FAs, $\alpha_3\beta_1$ integrin acts as a mediator for cell adhesion to the ECM, as shown in cultured human keratinocytes [413]. The intracellular tail of β_1 subunit binds to talin and FAK [414], whereas, extracellularly, integrin $\alpha_3\beta_1$ has been shown to mediate cell adhesion to LM332, 511 and 521 [415, 416]. In particular, the interaction between integrin $\alpha_3\beta_1$ and LM332 has been demonstrated to be fundamental for LM deposition, since α_3 and β_1 integrin subunits have been reported to co-localise with LM332 [417] and wound closure studies showed a decreased healing process after the treatment with antibodies against α_3 or β_1 integrin [209]. Supporting the interaction between LM332 and integrin $\alpha_3\beta_1$, *in-vitro* studies with α3 null mouse

skin cells showed that LM332 pattern changes from diffuse arcs to spikes and arrowhead, affecting the cell adhesion strength [417]. This suggests that α_3 integrin is crucial for a correct LM332 organisation in a similar but distinct way to that of $\alpha_6\beta_4$ integrin described above [353].

Further support to the role of $\alpha_3\beta_1$ integrin in cell-ECM interactions is given by *in-vivo* studies using $\alpha_3\beta_1$ integrin knockout mice; the α_3 integrin gene is expressed during the development of many epithelial organs, including kidneys [418], lungs [419] and skin [420], and homozygous offspring born from integrin $\alpha_3\beta_1$ mutant mice survived to birth, but died during the neonatal period due to BM defects [421].

$\alpha_3\beta_1$ integrin-LM332 interaction is also important in other circumstances. It has been demonstrated to be involved in gap junction communication, as keratinocytes cultured on LM332 promoted gap junction communication to a greater extent than when plated on collagen or fibronectin [422], indicating that, perhaps, gap junction formation is dependent on $\alpha_3\beta_1$ integrin-LM332 synergy. These data, considered together, highlight the central role of $\alpha_3\beta_1$ integrin in the adhesive interactions of epithelial cells with underlying basement membranes.

1.3.2.6 α-actinin

α-actinin is an actin filament crosslinking and bundling protein, part of the spectrin gene superfamily [423]. On the basis of its location, α-actinin plays different roles; in non-muscle cells, it is calcium sensitive and involved in binding actin to the cell membrane, whereas in skeletal, cardiac, and smooth muscle cells, α-actinin is calcium insensitive and helps in anchoring the myofibrillar actin filaments [424].

Four isoforms of α-actinin have been identified; α-actinin 1 is located primarily in FAs, 2 and 3 are muscle specific actin crosslinkers and 4 is present in membrane ruffles [425]. With regards to the structural features, α-actinin is composed of two identical anti-parallel peptides, with the actin binding domain close to the N-terminal region, followed by four spectrin-like repeats and two calcium binding motifs [426].

Studies of the α-actinin binding properties demonstrated that it is able to interact with vinculin [381, 427], syndecan-4 [428], collagen type XVII [429] and integrin β_1 cytoplasmic tail [430] [431], particularly important to maintain integrin-actin linkages at FAs [432]. As for many other actin-binding proteins, α-actinin function is regulated by polyphosphoinositides, particularly phosphatidylinositol 4,5 bis-phosphate (PIP2) [433]. Additionally, previous studies showed that actin binding to α-actinin protein can be modulated by FAK-dependent phosphorylation of the N-terminal domain [366].

1.3.3 Focal adhesion assembly and disassembly

Focal adhesion's components assemble and disassemble to maintain the balance of cell-ECM attachment, required for continuous migration. The assembly of FAs is a highly regulated mechanism, with protein recruitment occurring in a sequential manner. The first step of FAs assembly is an integrin clustering, the binding of adhesion receptors to ECM ligands, at the protruding edge of a cell [434]. In particular, β_1 integrin have been reported to act as a force-bearing molecule, due to its catch bond properties [435], the ability to create non-covalent bonds whose lifetime, instead of decreasing, increases when tensile force is applied [436].

At this point, several signal transduction cascades are activated, leading to the consequent recruitment of talin, which, in turn, binds the actin cytoskeleton and stabilizes the integrin-ECM linkage [437]. Then, the actin-talin-integrin cluster recruits, among the others, FAK [438] [439], and induces the contraction of myosin II, another f component. This contraction has been shown to stretch talin [440], revealing binding sites for vinculin [441]. After such a step, signal transduction molecules (e.g. Rap1 GTPase or VASP) are activated and α-actinin is recruited, to complete the FA maturation with the actin polymerisation and the recruitment of paxillin [442] plus several other components, such as zyxin or tensin[443]. Fig. 1.8 shows a schematic diagram of mature FA.

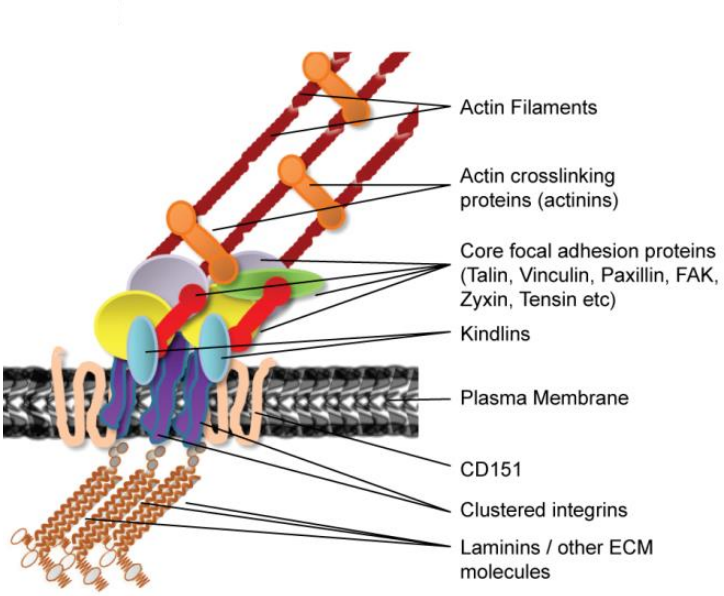

Fig. 1.8: FA structure.

Schematic outline of the mature FA structure, indicating the components and their interactions in the complex.

It is interesting to notice that, during growth and early maturation, the focal adhesion size correlates with traction stress [444], however, probably due to the altered chemical state of focal adhesion signalling components, upon maturation FAs effectively become passive anchorage devices, only involved in the maintenance of a spread cell morphology [445]. Normally, FAs disassembly occurs within 10-20 min from the maturation; this process is controlled by tyrosine phosphorylation events and changes in cytoskeletal tension [446], regulated, in turn, by molecules such as calpain or microtubules [447, 448]. At the rear of the cell, FAs protein aggregates leave the adhesion complex and disperse away from the adhesion site [449], moving centripetally; they, then, coalesce over 30 min before disintegrating [450]. Integrins are, instead, recycled for ligand binding [451].

The extracellular ligand for FAs also plays a role in their assembly and organisation. LM332 has been shown to play a role in regulating the activation of distinct sets of integrins and the induction of different molecular assemblies within the cell adhesion signalling complexes. In human skin fibroblasts, for example, integrin subunits, vinculin, talin and paxillin were recruited into thick and short aggregates at the end of actin stress fibres when cultured on LM111, while on LM332 they appeared as dots or streaks clustered on a long portion of actin microfilaments [452]. Using $\alpha_3\beta_1$ function-blocking antibodies on cells cultured on LM111, the same group demonstrated that focal adhesions have a similar distribution as if the substrate was LM332, pointing to a cross-talk between $\alpha_3\beta_1$ and $\alpha_6\beta_1$ integrin in FAs, resulting in the activation of $\alpha_6\beta_1$ integrin when $\alpha_3\beta_1$ is blocked [452].

Section 4. Laminin N-terminus proteins (LaNts)

The Laminin N-terminus proteins (LaNts) were identified in 2009 and they owe their name to their structural similarity with laminins, being products of alternative splicing from the 5' end of the LM α3 and α5 encoding genes, LAMA3 and LAMA5 [453]. To date, two LaNts transcripts generated from each gene have been identified and only one study has been published on their characteristics and possible roles in skin [453].

1.4.0 LaNt α31 alternative splicing mechanism

Alternative splicing in eukaryotic gene expression is a key process that increases the coding capacity of the human genome, resulting in a single gene coding for more than one protein; in humans, more than 95% of the genes undergo alternative splicing [454, 455]. ECM, due to its constant remodelling and context specific functional requirements, needs an appropriate balance between many different proteins and is, therefore, characterised by several alternative splicing events. With regards to the LM family, protein isoforms derived from alternative splicing have been identified in LAMA4 [456], LAMB3 [457], LAMA2 [458], LAMC2 [459] and LAMA5 [453], but LAMA3 gene is the one undergoing the most dramatic differential splicing.

LAMA3 gives rise to two major transcripts: *LAMA3A*, starting from a promoter within intron 38 and containing exons 39–76, which encodes for a N-terminally truncated protein named as LM α3a [90, 92], and *LAMA3B*, instead formed by exons 1–38 and 40–76, which generates the full-length LM α3b [91]. In addition to these

products, which are generated by use of different promoters, the LaNts are generated via a process of intron retention and alternative polyadenylation, a rarer form of splicing where an intronic region is retained in the final sequence [460].

LaNt α31 is generated from an mRNA termed *LAMA3LN1*, produced by read-through of the exon 9/intron 9 splice boundary and, therefore, carries an extension to the LAMA3 exon 9, known as exon 9e. This extended sequence contains a stop codon, a polyadenylation signal and the isolated expressed sequence tag (EST), through which it was initially identified to carry a polyA tail [461]. *LAMA3LN1*, therefore, is composed of exons 1-9 from LAMA3 gene +9e, and encodes for a protein of 488 amino acids. It is important to highlight that exon 9e encodes for 54 amino acids unique to the LaNt α31 protein generated [461], and this sequence was used to produce antibodies against LaNt α31 [461] (Fig. 1.9A).

1.4.1 *LAMA3LN1* transcript localisation

sqRT-PCR analysis of the *LAMA3LN1* expression pattern revealed a relatively strong expression in heart, placenta, prostate, testis, small intestine, leukocytes and keratinocytes, with lower expression levels in pancreas, brain, ovary and fibroblasts [461]. Studies using in site hybridisation on skin sections demonstrated that *LAMA3LN1* transcript is localised in the same tissues where LAMA3 gene has been shown to express, therefore epidermis and interfollicular epidermis, sebaceous glands, sweat glands and hair follicles, in which *LAMA3LN1* distribution is evident in the outer and inner root sheaths [461, 462].

1.4.2 LaNt α31 protein structure

The protein encoded by *LAMA3LN1* transcript has been named Laminin N-terminus α31 on the base of its structural characteristics [461]. LaNt α31 consists of LM globular LN domain, which is followed by a short stretch of LE repeats (Fig. 1.9B). Apart from the missing C-terminal domain, LaNts structure is highly similar to the structure of the netrin family of LM-related proteins (Fig. 1.9C) [156].

1.4.2.1 Netrins

All netrins are structurally composed of a LN domain followed by 2-3 LE repeats and a basic C-terminal domain. In terms of sequence similarity, netrins LN domains more closely resemble either LM γ chains (netrins 1, 3) or LM β chains (netrins 4, G1 and G2) and it is believed that these two subtypes of netrins evolved independently.

The netrins are best known for their roles as neuronal guidance cues [463]; however, they have been demonstrated to play significant roles in cell migration, cell-cell interactions and cell-ECM adhesion, processes that are important in wound repair [464]. The primary role of netrins in axonal guidance is based on modulating the activity of three groups of receptors; deleted in colorectal cancer (DCC), neogenin and UNC5A-D. The netrins' C-terminal-domain has capability to bind HS [465] and, in addition, a highly basic region of the netrin 1 C-terminus has been shown to contain a 25-amino acid region involved in the netrin 1 association with integrins $\alpha_3\beta_1$ and $\alpha_6\beta_4$, describing a role for netrin-integrin interactions in epithelial cell adhesion and migration [466].

The cellular responses to netrin exposure are determined both by the local netrin concentration and by the precise combinations of receptors expressed by the cell. Intriguingly, signalling via DCC and UNC5a in response to netrin has been demonstrated to induce dramatic rearrangement of the actin cytoskeleton, by modulating the activity of the small Rho GTPases Rac1 and Cdc42 [467, 468]. Netrin 4 is also involved in the regulation of glioblastoma multiforme cells' migration and proliferation, via interacting with β_4 integrin and triggering the downstream Akt and mTOR signalling [469].

In addition to direct binding of cell surface receptors, it has been suggested that netrins localise and multimerise in the ECM [465, 470]. Particularly interesting is a study showing that netrin 4 can be incorporated into the BM via interaction of its N-terminal domain with the LM LN domain [471]; this is supported by other studies showing that netrin 4 inhibits BM assembly by interfering with the LM polymerisation process [471-473]. Moreover, the high-resolution structure of netrin 4 has been elucidated, revealing unique behavioural characteristics belonging to netrin 4 only [474]. It has a high binding affinity for the LM γ1 chain LN domain, and has been shown to inhibit LM polymerisation process; very interesting is the ability of netrin 4 to also disrupt any pre-existing LM network, resulting in the alteration of the entire BM [474]. Netrin 4 binding to LM γ1 affects, in turn, processes like angiogenesis and vessel maturation, as it induces the collapse of the entire capillary network by disrupting the BM underlying the vasculature [474], an effect which may be helpful to reduce cancer progression. Netrin 4 association to LM γ1 chain is also important for the regulation of the mitogen-activated protein kinase pathway; this pathway occurs via ligating $\alpha_6\beta_1$ integrin, a process triggered by interaction with LM γ1 chain [475].

Specifically looking at the cornea, netrin 1 has been shown to reduce corneal inflammation and to suppress and reverse corneal neovascularization when topically applied in a corneal alkali burn rat model, a well-established severe ocular surface disease model [476]. Similarly, netrin 4 studied on the same animal model acts as an anti-angiogenic factor, leading to a decreased corneal neovascularization [477], increased wound healing and reduced inflammation when topically applied [477]. A very recent study supports netrin 4 anti-angiogenic functions in the cornea, showing that netrin 4 absence leads to increased corneal hemangiogenesis in suture-induced neovascularization mouse model [478].

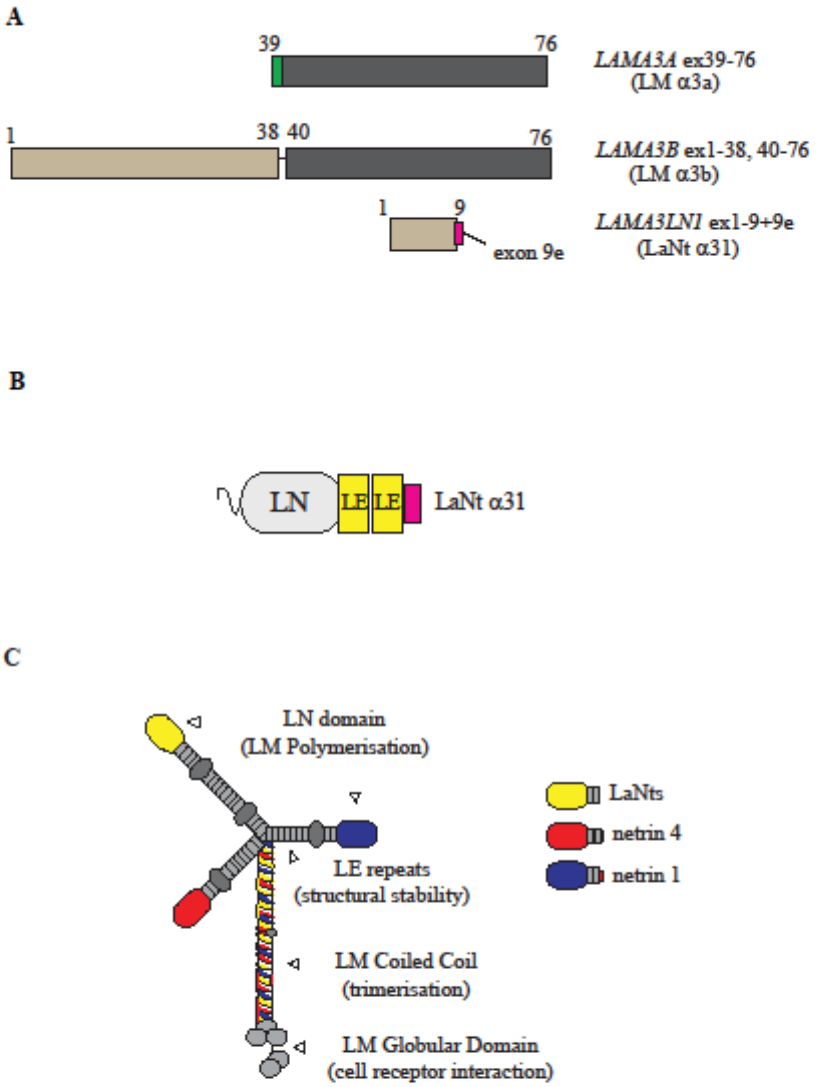

Fig. 1.9: LAMA3 alternative splicing; LaNt α31 and LM structure.
(A) Diagram showing transcripts generated from the LAMA3 gene. Green and magenta boxes represent exons specific to *LAMA3A* (encoding LM α3a) and *LAMA3LN1* (encoding LaNt α31) transcripts respectively. (B) Scheme of LaNt α31 protein domain architecture. LN= LM N-terminal domain, LE = laminin-type epidermal growth factor-like repeats. Magenta box represents unique C-terminus derived from exon 9e. Adapted from Hamill et al 2009. (C) Diagram showing the similarity between LaNt α31 and netrins, in comparison to LM structural domains.

1.4.3 LaNt α31 functional data

In the skin, LaNt α31 has been shown to partially co-distribute with LM332 in the BM. In cultured human keratinocytes, LaNt α31 is found beneath the edges of either individual or clustered cells, with a distinctive punctate pattern [461]. HaCaT cells do not retain the protein intracellularly though, but deposit it into the ECM and western blotting data indicate that upon secretion LaNt α31 possibly undergoes proteolytic cleavage [461].

LaNt α31 has been demonstrated to affect skin cell attachment, as keratinocytes in which LaNt α31 expression was knocked down, using siRNAs, displayed a decreased attachment rate [461]. However, the difference in adhesion rate between controls and knockdown cells was not significant anymore after 60 min, suggesting that the LaNt α31 knockdown primarily affects the initial stages of attachment [461].

LaNt α31 has also been implicated in playing a role in the wound healing process. In cultured epidermal keratinocytes, LaNt α31 expression increases following wounding, with the expression peak reached around 6h post-wounding [461]. Further support is given by the impairment in wound closure observed in LaNt α31 knockdown keratinocytes [461].

Aim of the thesis

The aim of my PhD project was to characterise, and then establish, the role of LaNt α31 protein in corneal epithelium. Specifically, we wanted to investigate LaNt α31 effects on hTCEpi cell behaviour in relation to ECM components. The study produced very interesting and novel results, highlighting a strong and specific interaction between LaNt α31 and LMs. The data collected from the *in-vitro* experiments inspired the creation of an animal model, the first one of this type, which gave preliminary yet extremely promising results.

Chapter 2

MATERIALS AND METHODS

2.1.0 Cell Culture

Telomerase-immortalised human corneal epithelial cells, hTCEpi cells [229], were cultured at 37°C with 5% CO_2 in Keratinocyte-Serum Free Medium (KSFM) supplemented with bovine pituitary extract (0.05 mg/ml), human recombinant Epidermal Growth Factor 1-53 (5 ng/ml) (Life Technologies, Carlsbad, CA) and 0.15 mM $CaCl_2$ (Sigma-Aldrich, St Louis, MO). hTCEpi cells were characterised using the corneal marker Keratin 12 (Appendix, Fig. 1).

HaCaTs, spontaneously transformed human epidermal keratinocytes [479], were cultured using Dulbecco's Modified Eagle Medium (DMEM, Sigma-Aldrich) supplemented with 10% Foetal Calf Serum (LabTech, East Sussex, UK) and 2 mM L-glutamine (Sigma-Aldrich).

KERA-308, Murine Keratinocyte cells [480], were purchased from CLS (Cell Lines Service GmbH, Eppelheim, Germany) and cultured in high glucose (4.5 g/L) DMEM (Sigma-Aldrich) supplemented with 10% Foetal Calf Serum (LabTech, East Sussex, UK) and 2 mM L-glutamine (Sigma-Aldrich).

Tenons fibroblasts [481] were isolated from the Tenon's capsule, beneath the conjunctiva, by Mrs Neeru Vallabh in the Department of Eye and Vision Science (University of Liverpool), and cultured in DMEM (Sigma-Aldrich) supplemented with 10 % foetal Calf Serum (Life Technologies), 100 units/mL penicillin (Sigma-Aldrich), and 100 μg/mL streptomycin (Sigma-Aldrich) at 37 °C with 5 % CO_2.

Human Retinal Pericyte Cells (HRP) were purchased from Cell Systems Corporation (Kirkland, WA) and cultured in DMEM supplemented with 5.5 mM D-glucose, 10%

Foetal Calf Serum, 1X Penicillin-streptomycin solution (Sigma-Aldrich) and 1X sodium pyruvate (Thermo Fisher Scientific, Waltham, Massachussets, USA).

2.1.1 Antibodies and reagents

Rabbit polyclonal antibodies against paxillin and lamin A/C, and mouse monoclonal antibodies against β_4 integrin (clone M126), GAPDH (clone 9484) and 6X-His Tag (clone HIS.H8) were purchased from Abcam (Cambridge, UK). Rabbit polyclonal antibodies against LM β3 and mouse monoclonal antibodies against GFP (a mixture of clones 7.1 and 13.1) were from Thermo Scientific (Loughborough, UK). J17, rabbit polyclonal antibodies against Col type XVII [482] was a kind gift from Professor Jonathan Jones, Washington State University, WA. Rabbit polyclonal antibodies against LAMA3exon9e were previously described [461].

Fluorescein isothiocyanate, rhodamine and Cy5 conjugated goat anti-mouse and goat anti-rabbit secondary antibodies were obtained from Jackson Immunoresearch (West Grove, PA). Goat anti-mouse and goat anti-rabbit IRDye 800CW and/or IRDye 680CW were obtained from LiCor BioSciences (Rugby, UK).

Mouse monoclonal antibody clone 3E11 was raised against the synthetic peptide VLPQRSHQANFGSV (GenWay Biotech, San Diego, CA), corresponding to human LaNt α31 residues 437-451, conjugated to keyhole limpet haemocyanin following the procedure described in [483], with help from the recombinant protein production core, Northwestern University, Chicago IL. Five days following the final boost, spleens were removed and isolated splenocytes were fused with the myeloma cell line Sp2 for the production of hybridomas using standard techniques [484].

Hybridoma cells producing antibodies against the LaNt α31-derived peptide were selected based on their ELISA reactivity to the unconjugated peptide and immunoblotting reactivity against HaCaTs' protein extract. Selected hybridoma cells were cloned twice by limited cell dilution.

RG13, mouse monoclonal antibodies against LM α3 [485] was purified in our lab starting from conditioned media, dialyzed for 24h at 4°C ,with constant shaking in PBS, using SnakeSkin® Dialysis Tubing (10K MWCO, 16mm DRY) sealed with the SnakeSkin® Dialysis Tubing Clips (Thermo Scientific, MA). IgG were purified using the NAb Protein G Spin Kit 1ml (Thermo Scientific). The IgG in PBS were diluted 1:1 in binding buffer (100 mM phosphate, 150 mM sodium chloride , pH 7.2) and applied to columns containing 1ml resin bed of protein G cross-linked 6% beaded agarose in 0.02% sodium azide. Columns were then washed using binding buffer and bound IgG eluted in 5x1ml fractions using elution buffer (2 M glycine), with pH 2.8. Eluted IgG were neutralised in 1M Tris-HCl (pH 8.5). The RG13 containing eluted solution was concentrated through ammonium sulphate precipitation. Eluted fractions were pooled and mixed with 100% saturated ammonium sulphate solution (Sigma-Aldrich) and precipitates allowed to form over a period of 4h at 4°C , with constant shaking. Precipitates were pelleted by 35 min centrifugation at 5850g; the pellet was washed twice with cold 33% saturated ammonium sulphate solution, dissolved in coupling buffer (0.1 M $NaHCO_3$ buffer containing 0.5 M NaCl, pH 8.3-8.5) and dialyzed in PBS for 48h at 4°C with constant shaking. Silver stain and indirect immunofluorescence staining of hTCEpi cells (Appendix fig. 2) tested RG13 mAb activity and purity; protein concentration was determined by Bradford assay.

2.1.2 Bradford Assay

RG13 mAb concentration was determined using a Bradford spectroscopic procedure, using the Quick Start Bradford kit from BioRad. Samples were mixed 1:1 with Bradford reagent, in a final volume of 200 µl in a 96 well-plate (NUNC™, NY). After 5 min incubation at room temperature, the absorbance was read at 595nm. A standard curve was generated using seven serial dilutions of commercially bought mouse IgG solution (Sigma-Aldrich) or bovine serum albumin supplied with the kit for proteins other than immunoglobulins, and the mAbs concentration (600 µg/ml) was extrapolated from the graph equation.

2.1.3 Adenovirus production and cell transduction

Full length *LAMA3LN1* was PCR amplified from cDNA generated from cultured human keratinocytes, cloned into pCR2.1 (Life Technologies) and sequence verified by DNA sequencing (DNA Sequencing and Services, University of Dundee). The native translational stop codon was converted to an *AgeI* restriction enzyme site by site-directed mutagenesis, following the manufacturer's directions of QuikChange II XL mutagenesis kit (Agilent, Santa Clara, CA). The mutated *LAMA3LN1* was then subcloned using *KpnI and AgeI* (New England Biolabs, Hitchin, UK) into pENTR4 (Life Technologies), with eGFP inserted into the *BglII* and *KpnI* sites of the multiple cloning site (a kind gift from Professor Jonathan Jones, Washington State University, WA).

LR recombination was used to transfer the *LAMA3LN1*-eGFP construct from pENTR to pAD-CMV/V5-DEST (Life Technologies) and adenoviral particles produced

following the standard gateway-adapted ViralPower adenoviral expression protocol (Life Technologies). Adenoviruses inducing CMV-driven expression of LM β3-mCherry [486] and eGFP were kind gifts from Professor Jonathan Jones, Washington State University, WA.

For cell transduction, $3x10^5$ hTCEpi cells were seeded in 60mm dishes (Greiner-BioOne) and transduced 24h after seeding with recombinant adenoviruses harbouring eGFP protein, LaNt α31-GFP protein and/or LM β3-mCherry protein, 10 µl each in 4ml of hTCEpi culture medium. All analyses of LaNt α31-GFP (+LaNt α31), LM β3-mCherry (+LMβ3), GFP (+GFP) or untreated cells were conducted 48-72h following transduction.

2.1.4 Short hairpin RNA (shRNA) and knockdown clone generation

shRNA sequences, targeting the unique portion of the *LAMA3LN1* transcript, were designed using the BROAD institute design algorithm (http://www.broadinstitute.org/rnai/public/seq/search). A gblock (Integrated DNA Technologies, Coraville, IA) containing the shRNA sequence (CCCTCTCTCTTCAGAGTATT*)* or validated non-silencing sequence (TCTCGCTTGGGCGAGAGTAAG), as well as stem loop sequence with *BamHI* and *XhoI* restriction enzyme compatible overhangs, was cloned into the miRNA adapted pGIPz plasmid (Open Biosystems, GE Healthcare Little Chalfont, Buckinghamshire, England). Lentiviral particles were generated as previously described [487] by the DNA/RNA Delivery Core, Northwestern University, Chicago, IL, using 293T packaging cells (Gene Hunter Corporation, Nashville, TN).

To generate stable clones, hTCEpi cells were seeded at $2x10^5$ cells/well in 6 well plates and transduced with lentiviral particles at final MOI of 0.5 with 8 μg/ml polybrene (Sigma-Aldrich). Transduced cells were selected in puromycin (10 μg/ml Gibco, LifeTech) for 7 days and resistant cells plated a 1 cell/well in 96 well plates. Clones were expanded and screened by western immunoblotting (WB).

2.1.5 Immunofluorescence microscopy

$1x10^5$ cells were seeded either for 5h or overnight on uncoated glass coverslips, then fixed and extracted in ice cold methanol or ethanol for 4 min. They were, then, air-dried or fixed in 3.7% formaldehyde (Sigma-Aldrich) for 5 min and extracted in 0.05% Triton X-100 in PBS for 7 min (Sigma-Aldrich).

For ECM analysis, cellular material was removed through exposure to 0.18% ammonium hydroxide (NH_4OH) for 5 min followed by extensive PBS washes [483] prior to fixation. Primary antibodies were diluted in PBS with 20% normal goat serum (Jackson Immunoresearch) and incubated at 37°C for 2h; coverslips were then washed extensively with PBS prior to probing for 1h at 37°C with FITC, Rhodamine or Cy5 conjugated secondary antibodies diluted in PBS. After being washed in PBS, coverslips were mounted with polyvinyl alcohol mounting medium with DABCO (Sigma-Aldrich).

Images were obtained using Zeiss LSM510 confocal microscope or Zeiss ApoTome.2 fluorescence microscope (Zeiss, Cambridge, UK).

LM α3 staining area was measured for 50 regions of staining per cell treatment, using the freehand selection tool on Fiji32-ImageJ software (National Institutes of

Health, Bethesda, MA). Pearson's correlation coefficients were calculated using the Coloc-2 plugin on Fiji32-ImageJ software (NIH) for all pixels above channel thresholds in both acquired channels.

2.1.6 Tissue processing and immunohistochemistry

Human donor eyes, obtained from the Liverpool Research Eye Bank (Liverpool, UK) were fixed in formalin, embedded in paraffin wax and processed as previous described [488]. The study was approved by local Research Ethics Committees and was performed in accordance with the Declaration of Helsinki.

Eyes were sectioned anteroposteriorly through the pupil and the anterior segment analysed separately. 4 μm sections were cut using a rotary microtome RM2235 (Leica, Wokingham, UK), adhered to coated microscope slides (Dako, Cambridge, UK) and allowed to dry overnight at 37°C. Sections were then de-waxed and rehydrated through a series of decreasing ethanol concentrations. Antigen retrieval was performed by microwaving sections in preheated 0.01M citrate buffer (pH6, Sigma-Aldrich) for 5 min at 95-100°C. Endogenous peroxidases and non-specific binding were blocked by treatment with 0.3% v/v hydrogen peroxide (15 min; Dako) and 20% v/v goat serum (Sigma-Aldrich) respectively. Sections were then incubated with anti-LaNt α31 antibodies at a final concentration of 7.2 μg/ml, in 5% v/v goat serum, or isotype matched controls overnight at 4°C.

Immunostaining was performed using the EnVisionTM+ System-HRP (Dako) kit following manufacturers' recommendations. Sections were counterstained with haematoxylin, dehydrated and mounted in pertex mounting media (HistoLab,

Gothenburg, Sweden). Images were captured with an Olympus BX60 system microscope equipped with an Olympus DP71 digital camera and cell imaging software (Olympus, Southend-on-Sea,UK).

2.1.7 SDS PAGE and immunoblotting

Cells were plated at $1x10^6$ in 100mm dishes (Greiner-BioOne, Stonehouse, Gloucestershire, UK) and lysed after 24h using Urea/SDS buffer (10 mM Tris-HCl pH=6.8, 6.7 M Urea, 35 mM SDS, 10% Glycerol and 7.4 μM bromophenol blue) containing 50 μM PMSF and 50 μM N-methylmaleimide.

Prior to use, lysates were sonicated and 15% β-mercaptoethanol (final volume, Sigma-Aldrich) added. Proteins were separated by SDS PAGE using a 10% polyacrylamide gel (Biorad, Hercules, CA), transferred to a nitrocellulose membrane using a Biorad TurboBlot system (Biorad) and blocked at room temperature in Odyssey®TBS-Blocking Buffer (Li-Cor BioSciences, Nebraska, USA) for 1h. The blocked membranes were probed for 2h at 37°C with primary antibodies diluted in blocking buffer, washed 3 x 5 min in TBS/0.1% Tween and probed for 2h at 37°C with IRDye® 800CW and/or IRDye® 680CW conjugated secondary antibodies (Li-Cor) diluted in blocking buffer (1:13.000). Membranes were then washed for 3 x 5 min in TBS/0.1% Tween and imaged using an Odyssey® CLx 9120 Infrared Imaging System.

2.1.8 Cell morphology analysis, low-density motility and cross-matrix assays

For cell morphology analyses and low-density migration assays, cells were seeded at $2.5x10^4$ cells/well onto uncoated 24 well plates (Greiner-BioOne). Where cell-derived preformed matrixes were required, non-transduced hTCEpi or +LaNt α31 hTCEpi were plated at $1.8x10^5$/well overnight on a 24 well plate, after which cellular material was removed through exposure to NH_4OH, as previously described. Fresh untreated or +LaNt α31 hTCEpi were then seeded on top of the prepared matrixes for 2h prior to analysis.

For morphology, 20X phase contrast images were acquired on a Nikon TiE epifluorescence microscope (Nikon, Surrey, UK). Images of individual cells were analysed using Fiji32 software (NIH). Cell perimeters were manually traced to define cell area; cell length was measured as the longest linear axis, with width measured at widest point at right angles to length measurement. Aspect ratio was defined as the ratio of width to length.

For low-density migration assays, cells were imaged every 2 min over a 2h period of time, using a 20X objective on a Nikon TiE fluorescent microscope, then individual cells tracked using the MTrackJ plugin of the Fiji32-ImageJ software (NIH). Speed (total distance travelled/time) and processivity (total distance/linear distance) were calculated for each cell.

2.1.9 Scratch closure assay

For scratch closure assays, hTCEpi, scrambled shRNA or LaNt α31 shRNA clones were seeded at $2x10^5$ cells/well in a 24 well plate (Greiner-BioOne). For overexpression studies, 16h after seeding hTCEpi were adenovirally transduced. 24h later a scratch was introduced into the confluent monolayers using a 200 µl tip. Cell debris was removed with several PBS washes. Scratch closure was imaged using a Nikon TiE epifluorescence microscope with a 4X objective for 16h. Scratch closure rates were determined by measuring scratch area after 0, 4, 8, 12 and 16h using the freehand image tool in Fiji32-ImageJ software (NIH).

2.1.10 Attachment Assay

Coatings were prepared using LM111 from EHS, Col type IV or FN (Sigma-Aldrich). Each protein was initially tested at the following range of concentrations; LM111 1, 2 3 or 4 µg/ml, Col type IV 0.025, 0.05, 0.1, 0.25 µg/ml, FN 0.1, 0.25, 0.5, 1 µg/ml. This range was selected to allow us to identify a mid-point of attachment rate so that we would be able to detect increases or decreases induced by LaNt α31 overexpression or exogenous addition. Based on the obtained attachment rate (Fig. 2.1), an appropriate starting concentration was chosen for each protein: LM111 was used at 2 µg/ml, Col type IV at 0.1 µg/ml and FN at 1 µg/ml.

ECM proteins were mixed with either 0.02 µg/ml or 0.1 µg/ml LaNt α31 (produced by Northwestern University protein production core) and TBS (50 mM Tris and 150 mM NaCl, pH 7.6, Sigma-Aldrich), or 0.02 µg/ml or 0.1 µg/ml netrin 1 or 4 (R&D Systems, Minneapolis, MN) and TBS. LM111 coating solutions also included 1 mM

$CaCl_2$ or 1 mM EDTA (Sigma-Aldrich). Coatings were prepared in a 96 well plate (Greiner-BioOne) with each well coated with 100 µl of solution for 2h at 37°C, followed by blocking of unoccupied binding sites with 100 µl of 1% Bovine Serum Albumin (Sigma-Aldrich) in PBS (phosphate buffered saline Tablets, Oxoid-Thermo Scientific) for 1h at 37°C.

$1x10^5$ cells in a final volume of 100 µl were plated in each coated well and incubated at 37°C for 1h. Attached cells were fixed with 100 µl of 3.7% formaldehyde (Sigma-Aldrich) in PBS for 15 min at room temperature. Fixed cells were washed three times with PBS and stained with 100 µl per well of 20% Crystal Violet solution (Sigma-Aldrich) in methanol (Chemistry Department, University of Liverpool) for 15 min at room temperature. Excess staining was removed with ddH_20. To permeabilise the cells, 100 µl of 1% SDS (Sigma-Aldrich) in PBS were added to each well and the plate was shaken at room temperature for 1h. The absorbance was measured at 570 nm, using the microplate reader LUMIstar Omega (BMG labtech). To evaluate hTCEpi cell attachment in different cell treatments or coating conditions, absorbance readings were normalized to the value obtained from FN 10 µg/ml coated well.

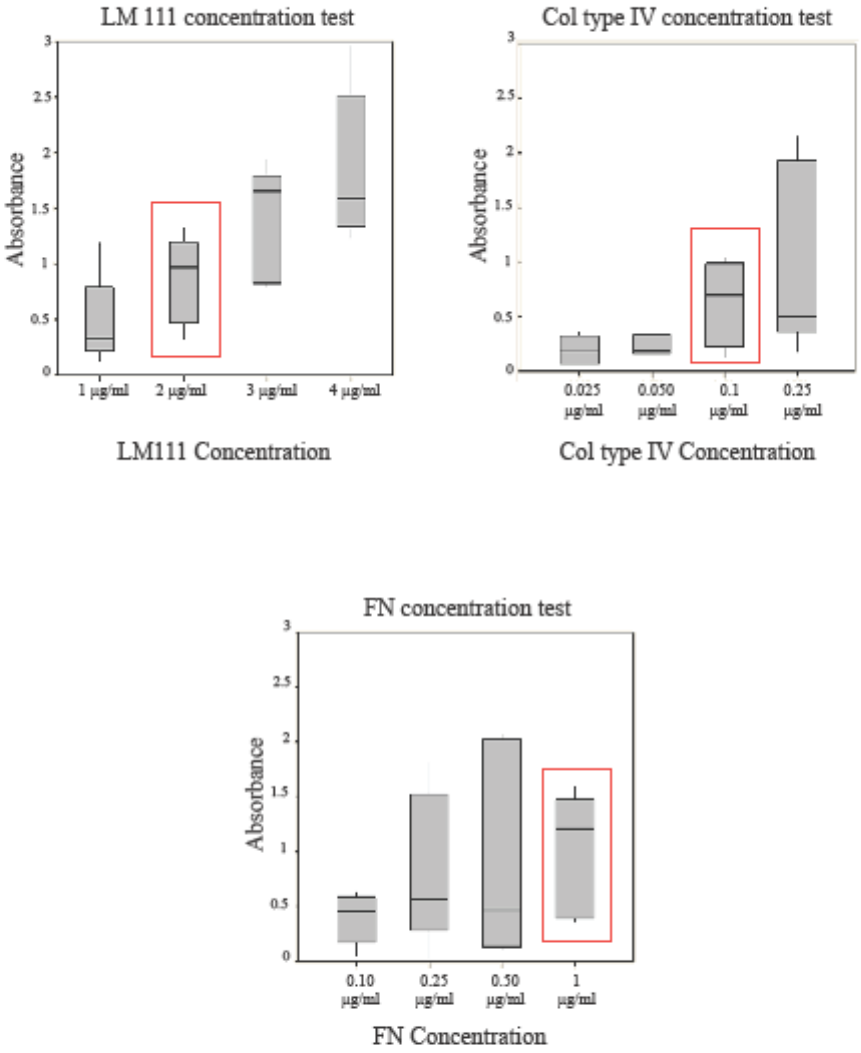

Fig. 2.1: LM111, Col type IV and FN concentration test for plate-coating.
Wells were coated with indicated protein concentrations for 2h at 37°C. After blocking with BSA, hTCEpi were plated onto the prepared substrates and incubated at 37°C for 1h; attached cells were fixed, stained with crystal violet and absorbance read at 570 nm. Boxplots show cell absorbance values at different protein concentrations. Orange boxes highlight the final concentration chosen for each protein.

2.1.11 Polymerisation Assay

25 µl of LM111 from EHS (1 mg/ml, Sigma-Aldrich) were mixed with 75 µl of a 0.01% Triton X-100/1X TBS solution to a final concentration of 0.25 mg/ml and centrifuged for 15 min at 11,000 rpm. Supernatants were transferred into two fresh tubes, 50 µl each, and mixed with 1 mM $CaCl_2$ or 10 mM EDTA [164]. 15 µl of LaNt α31 solution, either cloned into pSecTag plasmid (pSec) or V5 plasmid (V5), and purified by affinity chromatography (AC) or gel filtration (GF), were also added to some of the samples, with a final pure LaNt α31 mass of 0.4 µg. Prepared samples were incubated at 37°C for 3h and then centrifuged for 15 min at 11,000 rpm; supernatants were transferred to fresh tubes and pellets incubated overnight at 4°C with 1 mM EDTA (50 µl final volume). After 24h, supernatant and pellet from both the samples were separated via SDS PAGE on a 7.5% polyacrylamide gel, for 3h at 200 V. Silver stain (Pierce™ Silver Stain Kit, Thermo Fisher Scientific) was performed according to manufacturer's instructions.

2.1.12 Immunoprecipitation

hTCEpi cells were plated at $1x10^6$/plate in 100 mm plates and 24h later transduced with GFP or LaNt α31-GFP adenovirus. 48h later cells were extracted in 0.1% SDS, 0.5% sodium deoxycholate, 1% Nonidet P-40, 150 mM NaCl, 1 mM $CaCl_2$ in 50 mM Tris-HCl, pH 7.5 containing a mixture of protease and phosphatase inhibitors (Sigma-Aldrich). Cell extracts were clarified by centrifugation and 50% slurry of sepharose beads covalently conjugated with rabbit anti-GFP polyclonal antibodies (Abcam) was added to the supernatant. The bead/supernatant mixture was incubated

overnight at 4°C; the beads were then washed in lysis buffer, collected by centrifugation and boiled in SDS-PAGE sample buffer prior to immunoblotting.

2.1.13 Live protein imaging

$1x10^5$ hTCEpi cells, doubly transduced with LaNt α31-GFP and LM β3-mCherry adenoviruses, were seeded either directly or within a cloning ring on a 35 mm glass bottomed dish (MatTek Corporation, Ashland, MA). For preformed matrix studies, $5x10^5$ singly transduced LM β3-mCherry hTCEpi were seeded for 24h, then ECM extracts prepared as above, fresh LaNt α31-GFP expressing cells were then plated onto the preformed matrix for 2h prior to imaging.

Dishes were placed in the holder of a Zeiss 510 Multiphoton 2 confocal microscope at 37°C for 1h, to stabilise. Images were acquired at 63X objective every 20 min over 16h. Images were processed using Fiji32-ImageJ (NIH).

2.1.14 Proximity Ligation Assay (PLA)

$8x10^4$ hTCEpi cells were seeded onto glass coverslips. Cells were fixed after 24h, as described in the immunofluorescence microscopy section, and non-specific binding blocked for 30 min at room temperature using 5% normal goat serum in PBS (Sigma-Aldrich). Primary antibodies against LM γ2, LaNt α31, integrin β_4 and actinin α4 were diluted 1:100 in the Odyssey®TBS-Blocking Buffer blocking solution (LiCor BioSciences) to a final volume of 30 μl and each probed coverslip was incubated at 37°C for 2h. After 3x5 min washes with PBS, coverslips were incubated at 37°C for 1h with Duolink® Orange secondary probes (emission at 579

nm), 1:5 diluted in the Odyssey®TBS-Blocking Buffer to a final volume of 30 µl, following PLA® Technology kit instructions (Sigma-Aldrich). Secondary probes were removed with 2x5 min washes in 1X Wash Buffer A (Duolink® using PLA® Technology kit), under gentle agitation; ligation was performed for 30 min at 37°C probing the samples with the supplied ligation mix and ligase enzyme, respectively 1:5 and 1:40 diluted in ddH_2O. Coverslips were washed 3x5 min in TBS + 0.5% Tween-20 before being incubated, for 100 min at 37°C, with the supplied amplification mix and the polymerase enzyme (Sigma-Aldrich), 1:5 and 1:80 respectively diluted in ddH_2O . Final coverslips washes were performed 2x10 min in 1X TBS; Duolink® In Situ Mounting Medium with DAPI was used to mount the samples on slides and signal was detected using a Zeiss ApoTome.2 fluorescence microscope (Zeiss).

2.1.15 Limbal Explants Culture

Human rims were received as a waste product from St Pauls 'eye theatre and stored in organ culture media. Track record of the identification numbers was taken.

Limbal rims were put into a 100 mm petri dish (Greiner-BioOne), with some of the storage medium to prevent dryness. The endothelium was gently rubbed off using sterile forceps and some of the sclera was cut out, leaving a ring of about 3 mm in diameter. Every ring was put into PBS mixed with 2.5 µg/ml Amphotericin B (Fungizone) and 2% Penicillin/Streptomycin solution (Sigma-Aldrich) to prevent contamination, and chopped into 12 portions. After 15 min, each explant portion was placed in the centre of a 12 well plate (Greiner-BioOne) in 500 µl of limbal media consisting of; 3 parts DMEM low glucose medium (1000 mg/l) containing pyruvate

and GlutaMAX (Sigma-Aldrich), 1 part DMEM Ham/F12 (Sigma-Aldrich), 10% foetal calf serum (Labtech), 1% penicillin/streptomycin solution (Sigma-Aldrich), 1% Amphotericin B (Sigma-Aldrich), 20 mM HEPES (Thermo Fisher Scientific), 26 mM $NaHCO_3$ (Sigma-Aldrich).

Aliquots of 50 ml of media were made, and supplemented with 5 μg/ml Transferrin, 5 μg/ml Insulin, 1.4 ng/ml Triiodothyronine, 12 μg/ml Adenine, 0.4 μg/ml Hydrocortisone and 10 ng/ml EGF (Sigma-Aldrich). To prevent dryness, plates were placed into a larger box with a 60 ml pot of ddH_2O. Explants were fed three times a week, leaving 150 μl of old medium behind to maintain secreted components.

Primary corneal epithelial cells (pCEC) grew after 10-14 days in culture, and were detached from the tissue culture plastic using TrypLE™ Express Enzyme, 1X without phenol red (Thermo Fisher Scientific).

2.1.16 Statistical analysis

Quantification of experiments was derived from a minimum of 3 biological replicates. One-way ANOVA and Tukey's post hoc analysis were used to analyse and interpret the data generated from cell morphology, LM cluster area, adhesion and scratch assays. Instead, one-way ANOVA and Bonferroni post hoc analysis were used to analyse and interpret the cell motility assay data. All the statistical analyses were performed using SPSS software (IBM, Hampshire, UK); differences were deemed significant where $p<0.05$.

2.2.0 LaNt α31 mouse model preparation

2.2.0.1 Restriction Digests

Unless otherwise stated, restriction digests were set up with 1 µg of plasmid DNA, 20 U of each enzyme (New England Biolabs) and CutSmart buffer (50 mM Potassium Acetate, 20 mM Tris-acetate, 10 mM Magnesium Acetate, 100 µg/ml BSA) and incubated at 37°C for 2h. Where necessary, digested DNA products were treated with 5 U of the DNA Polymerase I, Large (Klenow) Fragment (New England Biolabs) [489] and 33 µM dNTPs mix (Qiagen, Hilden, Germany) at 37°C for 30 min, to create blunt ends by filling in of 5´overhangs [490]. To prevent cloning vector recirculation, the removal of the 5´ phosphates in linearised DNA was achieved by treatment with 5 U of the Antarctic Phosphatase enzyme (New England Biolabs) and 1X of reaction buffer (50 mM Bis-Tris-Propane-HCl, 1 mM $MgCl_2$, 0.1 mM $ZnCl_2$, New England Biolabs) at 37°C for 30 min. Enzymatic activity was subsequently inactivated by a 10 min incubation period at 65°C. Digested products were gel-purified using the QIAquick gel extraction kit (Qiagen), following manufacturer's instructions, and successful purification confirmed by gel electrophoresis.

2.2.0.2 Agarose gel electrophoresis

Agarose gels were prepared by dissolving 1% agarose powder (Sigma-Aldrich) and 35 µg Ethidium Bromide solution (Sigma-Aldrich) in 1X TAE buffer (40 mM Tris pH 7.6, 20 mM acetic acid, 1 mM EDTA). A voltage of 85V was applied for 95 min and the DNA products were visualised using the UV transilluminator ChemiDoc™ MP System (BioRad).

2.2.0.3 Plasmid Ligation, bacterial transformation and plasmid preparation

Purified inserts were ligated overnight into cloning vector at 3:1 molar ratios, chosen as a mass of insert to backbone ratio, using 400 U of the T4 DNA ligase (New England Biolabs) and 1X reaction buffer (50 mM Tris-HCl,10 mM $MgCl_2$,1 mM ATP,10 mM DTT, New England Biolabs) at 16°C. Ligated DNA was heat shock transformed into One-Shot TOP10 Chemically Competent E.Coli cells (Life Technologies), following the procedural steps suggested by the manufacturer, and plated onto ampicillin (100 µg/ml, Sigma-Aldrich) LB plates.

Amplified DNA from selected bacterial colonies was purified using the GenElute™ Plasmid Miniprep Kit (Sigma-Aldrich). For maxiprep DNA, DNA from verified bacterial colonies was expanded in 300 ml LB Broth (Sigma-Aldrich) with ampicillin (100 µg/ml, Sigma-Aldrich) and purified using the Qiagen Plasmid Maxi Kit (Qiagen).

2.2.0.4 PCR amplification of the hK14 promoter

Modified primers to amplify the hK14 promoter (table 2) were designed using the NCBI Primer Blast designing tool, on the base of the published DNA sequence (GenBank accession No. Ul1076) [491]. 5’ end of the forward primer was modified with *MluI* restriction enzyme site; Reverse Primer 3’ end with *NdeI*, *NsiI* and *KpnI* restriction sites.

OLIGO	Tm°	GC%	SEQUENCE 5'- 3'
hK14 promoter 213F+ *MluI*	66.4 °C	47.8	TATACGCGTGGAGGAAGGAGTTTCTTTTGGGT
hK14 promoter 256R+ *NdeI* *NsiI* *KpnI*	66.6 °C	57.1	ATGGTACCATGCATCATATGTATACTCATGGGTAGGGGGCG

Table 2: Modified PCR primer sequences to amplify hK14 promoter.

The hK14 promoter was amplified by PCR in a reaction containing 1 µg of human genomic DNA template (1 µg/µl, Bioline, London, UK), 2.5 µM forward and reverse primers, 1 mM $MgCl_2$, 1X reaction buffer, 2.50 U Taq polymerase, 400 µM dNTPs and the thermocycler T100™ Thermal Cycler (BioRad) set as follows:

	STEP	TIME	TEMPERATURE
	Initial activation step	3 minutes	95°C
x 30 cycles	**Denaturation**	30 seconds	95°C
	Annealing	1 second	60°C
	Extension	3 minutes	72°C
	End of PCR cycling	Indefinite	4°C

Table 3: Thermocycler programme for hK14 promoter amplification.

The samples were separated by gel electrophoresis technique and amplified DNA bands gel-purified using the QIAquick gel extraction kit (Qiagen).

2.2.0.5 Cell transfection

$1x10^6$ KERA-308 or HaCaT cells were seeded in 6 well plates (Greiner-BioOne) the day before transfection. Lipofectamine® 2000 Reagent and OptiMEM® Medium (Life Technologies) were used to set up the transfection, following the procedural steps suggested by the manufacturer, with a 3:1 (µl:µg) Lipofectamine to DNA ratio for KERA-308 cells, and 0.8:2 (µl:µg) Lipofectamine to DNA ratio for HaCaT cells. One well was left untransfected as a negative control. Transfected cells were visualised with 10X and 40X objectives 24h post transfection, using a Nikon TiE epifluorescence microscope. LaNt α31 protein expression levels were analysed by WB.

2.2.1 LaNt α31 overexpressing mice generation and genotyping

All animal procedures were approved by local ethical review and licensed by the UK Home Office under the Animal (Scientific Procedures) Act 1986, project licence number (PPL) 70/7288.

2.2.1.1 DNA embryonic injection

To generate the transgenic model, Dr. Ke Liu (Prof. George Bou-Gharios' laboratory, University of Liverpool) injected DNA in the mouse oocyte [492]. The

DNA was diluted to 2 ng/μL in embryo water (Sigma-Aldrich) and filter-purified using Durapore®-PVDF 0.22 μM centrifuge filters (Merck Millipore LtD).

2.2.1.2 Superovulation of egg donors

Superovulation was performed on F1 females aged between 4-6 weeks. 5 IU of follicle stimulating hormone was injected intraperitoneally, followed by 5 IU of luteinising hormone 46h later. Treated females were mated with F1 males overnight. Mated females, identified via copulation plugs checking, were anaesthetised and oviducts removed and dissected in M2 media (Millipore, Specialty Media, EmbryoMax®). Eggs were transferred to clean media via mouth pipetting. Cumulus cells were removed by hyaluronidase (300 μg/mL) treatment in M2 media with gentle shaking until visibly detached from the egg surface. Eggs were then rinsed and transferred to M16 media (Millipore, Specialty Media, EmbryoMax®) ready for injection.

2.2.1.3 Pseudopregnant females' generation

Pseudopregnant females were generated by mating vasectomised F1 males overnight. Copulation plugs were checked and females were used 1 day post-coitum. Females were anaesthetised with 50 μL hypnorm and 50 μL hypnoval by intraperitoneal injection.

2.2.1.4 Injection of fertilised eggs

Injection pipettes were used to pierce the outer layers of the oocyte, avoiding the nucleus, and to inject DNA. Undamaged eggs were transferred to clean M16 media and incubated until transfer into pseudopregnant F1 females. Eggs were microinjected at the 1 cell stage and transferred to the oviducts using the infundibulum. In the first session (November 2015), 90 embryos were collected from 8 F1 females and 60 of them were injected. 50 embryos survived after the injection and were transferred into 2 recipient mothers. In the second session (December 2015), 110 embryos were collected from 8 F1 females and 100 of them were injected. 90 embryos survived after the injection and were transferred into 3 recipient mothers. Surprisingly, the number of offspring obtained was very low, compared to what normally expected [493]; two pregnancies were aborted, one pregnant female gave birth to a litter of five animals and the remaining two gave birth to one animal each.

2.2.1.5 DNA extraction

4 weeks after birth, ear punches from the few born mice were collected from the Technical Staff of the Biomedical Services Unit (BSU, University of Liverpool). Ear tissue was digested using 100 µl of lysis buffer (50 mM Tris-HCL pH 8, 0.1 M NaCl, 1% SDS, 20 mM EDTA) and 10 µl of proteinase K (10 mg/ml) overnight, at 55°C. The day after, samples were allowed to cool down at room temperature and vortexed until tissues were disintegrated. Solutions were incubated with 3.75 M NH_4OAc on ice for 5 min and centrifuged at 14,000 rpm for 10 min. 100 µl of absolute Chloroform were added and samples spun again. Once centrifugation was completed,

supernatants were transferred to new tubes, mixed with 500 µl absolute Ethanol and incubated at -20°C for 2h. Samples were centrifuged at 14,000 rpm for 10 min and Ethanol removed. Equal volumes of cold (-20°C) 70% Ethanol were used to wash the pellets, which were then allowed to air dry for 10 min and reconstituted in 100 µl of TE buffer.

2.2.1.6 PCR

100 ng of the extracted DNA were mixed with 12.5 µl of REDtaq ® ReadyMix PCR Reaction Mix (20 mM Tris-HCl pH 8.3,100 mM KCl, 3 mM $MgCl_2$, 0.002 % gelatin, 0.4 mM dNTP mix, 0.06 unit/mL of Taq DNA Polymerase, Sigma-Aldrich) and 0.5 µM of each primer; volume was then brought up to 25 µl with PCR-grade H_2O (Sigma-Aldrich). Each sample was amplified using two sets of DNA primers, as summarised in table 4.

OLIGO	Tm°	SEQUENCE 5'- 3'
MUS LaNtα31 For3428 into mCherry	69.5 °C	CAGATGTTGAGCGGCAGCAG
MUS mCherry Rev4426 into LaNt α31	70.3°C	CGAAGTTCATCACGCGCTCC
llc016 mCherry F	65°C	ATGGTGAGCAAGGGCGAGGAGGATAAC
llc017 mCherry R	65°C	CTTGTACAGCTCGTCCATGCCGCC

Table 4: DNA primer sets, used for mice genotyping after DNA extraction from ear notches.

PCRs were run according to the following protocol (table 5) and the samples separated by gel electrophoresis technique and imaged using BioRad Gel Doc™ XR+ System.

	STEP	TIME	TEMPERATURE
	Initial activation step	5 minutes	95°C
x 30 cycles	**Denaturation**	30 seconds	94°C
	Annealing	30 second	61°C
	Extension	1 minutes	72°C
	End of PCR cycling	Indefinite	4°C

Table 5: thermocycler protocol applied to amplify DNA for mice genotyping.

2.2.1.7 F1 generation

Transgene-positive males 1.2 and 1.3 were time-mated with two and three females respectively, to produce the first filial generation (F1). Mouse 1.2 mating generated two litters composed of 5 newborn each, whereas mouse 1.3 generated three litters composed of 4, 3 and 4 newborns each. F1 genotyping was performed as previously described.

2.2.1.7a Tissue samples processing

Transgene-positive mice 4.1 and 6.3, respectively born from males 1.2 and 1.3, were sacrificed and skin and kidneys collected. Both the organs were positioned on labeled cork pieces and covered in optimum cutting temperature (O.C.T.) formulation (Tissue-Tek; Sakura Finetek, USA) for few minutes. Without fully submerge them, samples were snap-frozen in isopentane (Merck Millipore, Darmstadt, Germany) and

then covered in aluminium foil to be stored at -80°C. Part of the frozen samples were cut in 10 μm sections, using the CM1850 Cryostat (Leica, Wetzlar, Germany), whereas the remaining specimens were homogenised in preparation for WB.

Tissues were grinded into powder in liquid nitrogen, dissolved in UREA/SDS lysis buffer (10 mM Tris-HCl pH=6.8, 6.7 M Urea, 35 mM SDS, 10% Glycerol and 7.4 μM bromophenol blue) containing 50 μM PMSF and 50 μM N-methylmaleimide, and incubated with agitation for 1h at 4°C. Samples were then clarified by centrifugation at 13,000 rpm for 10 min and supernatant transferred to fresh Eppendorf tubes. 1:200 diluted tissue solutions were used for WB and probed with antibodies against 6X-His tag (Abcam).

2.2.1.7b E15.5 embryo analysis

Transgene-positive males 1.2 and 1.3 were time-mated for a second time, to start pregnancies planned to be prematurely stopped in order to collect embryos and analyse LaNt α31 and mCherry expression during development. The two pregnant females were sacrificed at E15.5; notably, as for the previous pregnancies, offspring number was very low; only one foetus was collected from mouse 1.2 timed-mating and genotyped as described before.

Chapter 3

In-Vitro RESULTS

LANT α31 DISPLAYS DIFFERENTIAL DISTRIBUTION ACCROSS THE ANTERIOR SURFACE EPITHELIUM, AND IT REGULATES CELL MIGRATION VIA MODIFYING CELL-LM INTERACTIONS DURING MATRIX ASSEMBLY

Introduction

To date, there has been only one study looking at LaNt α31 biology and that was restricted to the skin [461]. As previously established, LaNt α31 encoding gene LAMA3 is also expressed in the anterior segment; we decided, therefore, to further analyse LaNt α31 distribution and functions in the eye, and, on the base of the differential localisation in the anterior segment layers, specifically in the corneal epithelium.

This chapter includes the data obtained from *in-vitro* studies, using LaNt α31 overexpressing hTCEpi cells. Starting from the LaNt α31 protein expression in the anterior segment and in hTCEpi cells, the results will describe the effects of LaNt α31 overexpression on the main cell behaviours, such as cell adhesion, migration, wound closure and protein deposition.

3.0 Anti-human LaNt α31 antibody generation

Human LaNt α31 shares the majority of its sequence with the amino terminus of LM α3b; however, the final 54 amino acids, encoded by exon 9e, are unique to LaNt α31 (Fig. 3.1A). Mouse monoclonal antibodies were raised against the 14-mer peptide VLPQRSHQANFGSV within this unique region. Clones were screened by ELISA against the unconjugated peptide and then by WB against protein extracts from HaCaT cells, which have previously been shown to express LaNt α31 protein toward the edge of either single or clustered cells, partially co-distributing with LM332 [461]. We also probed hTCEpi cells extracts and confirmed that a similarly sized protein product (~58 kDa) is recognised by the antibodies in both HaCaT and hTCEpi cells (Fig. 3.1B).

To confirm the specificity of our antibodies, we used lentiviral transduction of shRNAs targeting the *LAMA3LN1* sequence to generate stable knockdown clones in hTCEpi cells, followed by WB of whole cell extracts from knockdown clones relative to non-transduced hTCEpi or hTCEpi cells expressing a non-silencing shRNA (scrambled shRNA) (Fig. 3.2).

Processing hTCEpi and HaCaT cells for indirect immunofluorescence microscopy with the mouse anti-LaNt α31 antibodies revealed diffuse staining throughout the cell body, with clustered puncta or short stretches of linear staining toward cell peripheries in both cell types (Fig. 3.3A). A similar protein distribution was observed in hTCEpi when probed with the previously characterised rabbit polyclonal anti-LaNt α31 antibodies (Appendix Fig. 3); staining confirmed the presence of discrete intracellular puncta, with protein enrichment at the cell peripheries. Consistent with knockdown, fewer and less extensive regions of organised staining were observed in LaNt α31 knockdown clones compared to scrambled shRNA cells (Fig. 3.3B).

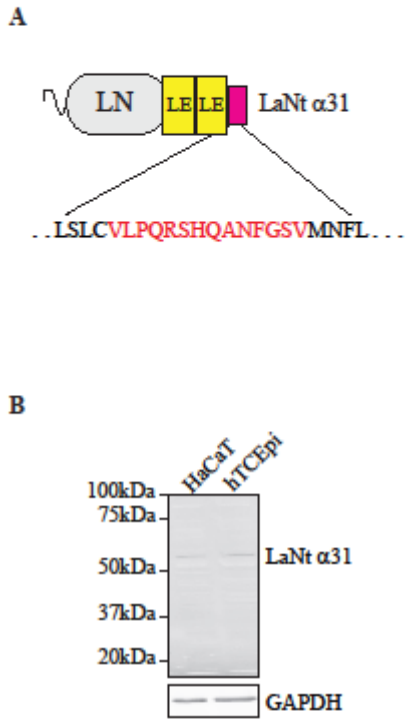

Fig. 3.1: LaNt α31 mAb design and characterisation.
(A) LaNt α31 diagram indicating location and sequence (in red) of peptide used to generate a novel mouse monoclonal antibody. (B) WB of total protein extracts from HaCaT and hTCEpi cells, probed with antibodies against LaNt α31 and GAPDH.
Sizes of molecular weight markers are indicated.

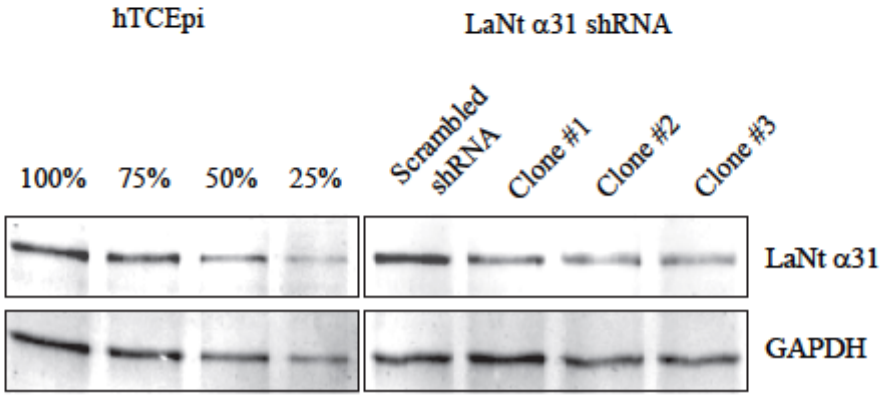

Fig. 3.2: LaNt α31 knockdown clones.
hTCEpi cells were stably transduced with a lentiviral particles delivering shRNA against *LAMA3LN1* transcript or a non-coding (scrambled) shRNA. hTCEpi lysates loaded at 100, 75, 50 and 25% and total protein extracts from scrambled shRNA and LaNt α31 knockdown clones 1, 2 and 3 probed with antibodies against LaNt α31 and GAPDH. *Knockdown studies courtesy of Mr. Lee David Troughton.*

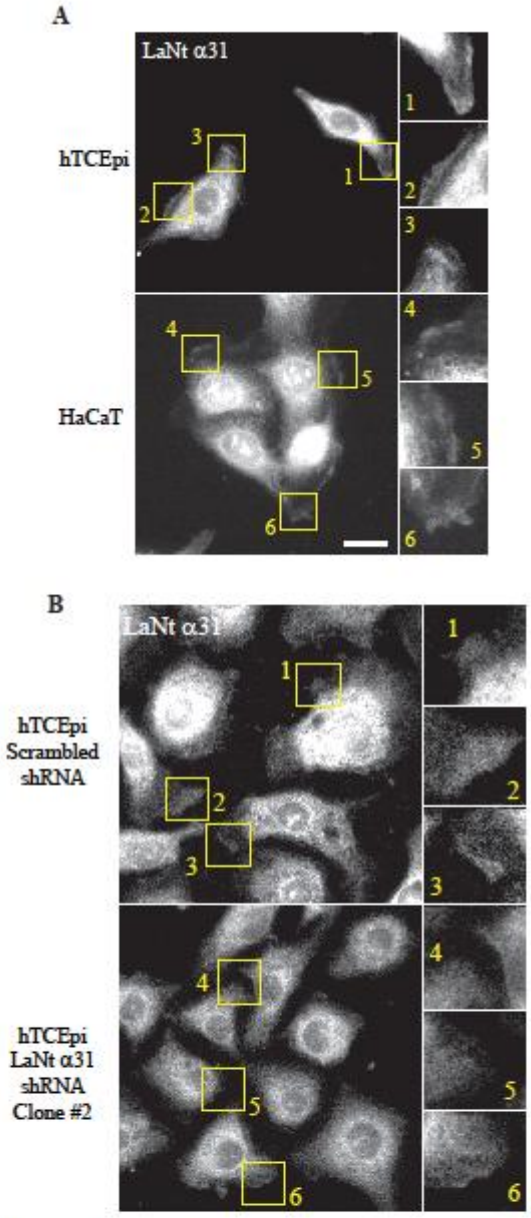

Fig. 3.3: LaNt α31 distribution in cells.
(A) hTCEpi or HaCaT cells were plated for 16h on uncoated glass coverslips, then processed for indirect immunofluorescence with antibodies against LaNt α31. Boxed regions 1-6, showing clusters/linear deposits of LaNt α31 staining, are shown at higher magnification in panels to right. (B) hTCEpi cells transduced with scrambled shRNA or LaNt α31 shRNA #2 were plated for 16h on uncoated glass coverslips, then processed for indirect immunofluorescence with antibodies against LaNt α31. Boxed regions 1-6, showing clusters/linear deposits of LaNt α31 staining, are shown at higher magnification in panels to right. Scale bars = 20 μm.

3.1 LaNt α31 distribution differs between the corneal, limbal and conjunctival epithelium

Next, we sought to determine the distribution of LaNt α31 in the anterior segment using immunohistochemistry. Interestingly, this revealed differential distribution of LaNt α31 across the surface of the eye.

In the central cornea, LaNt α31 staining was observed throughout all layers of the epithelia (Fig. 3.4A), whereas in the peripheral cornea, limbus and conjunctiva, the epithelial LaNt α31 distribution was restricted to the basal and first suprabasal layers (Fig. 3.4B; for higher magnification, compare central cornea 3.4C with limbus 3.4D and conjunctiva 3.4E). Positive immunoreactivity for LaNt α31 was also observed in blood vessels within the limbal stroma (Fig. 3.4F). Despite high similarity between the human and pig (*Sus scrofa domesticus*) LaNt α31 sequence, the precise peptide used to generate our new monoclonal antibody is not conserved between species (Fig. 3.4I). Therefore, in addition to using isotype-matched control staining, we also stained porcine anterior segments as an additional control (Fig. 3.4L).

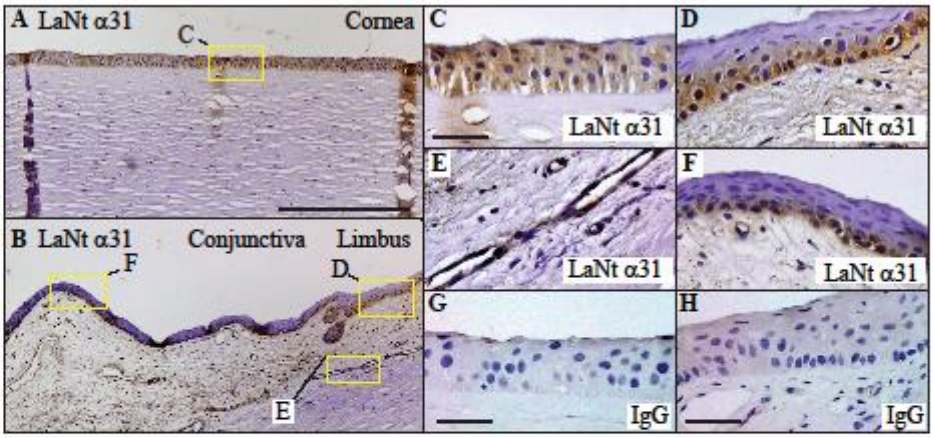

I

```
Sus Scrofa    AKGYYRPYGVPVHAPDGCIRKFHFQLDVSRL----QGSHGLNSDWLVMPFIF-LSLYMI
              ||||||||||||.|||||||||||:|....|    |.||..|.. .||.|:. ||||.|
Homo Sapiens AKGYYRPYGVPVDAPDGCIRKFHFKLVYLSLCVLPQRSHQANFG-SVMNFLHALSLQSI
```

L

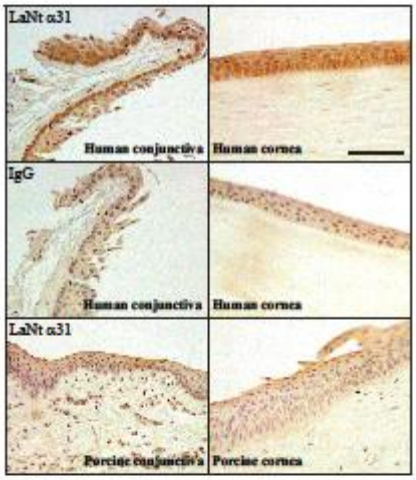

Fig. 3.4: LaNt α31 protein is differentially distributed across ocular anterior segment epithelium.

Paraffin-embedded human anterior segment sections processed for immunohistochemistry with antibodies against human LaNt α31 protein (A-F) or mouse IgG (G and H). (A) cornea, (B) conjunctiva and limbal regions. Yellow rectangles represent areas imaged at higher magnification, shown in insets (C-F). (C) central cornea, (D) limbus ,(E) vessels, (F) conjunctiva.
Scale bars = 500 μm for (A) and (B) and 50 μm for (C-H). (I) Alignment of human (Homo sapiens) and porcine (Sus Scrofa domesticus) LaNt α31 protein amino acid sequences. The peptide sequence used to generate the mouse monoclonal antibody directed against human anti-LaNt α31 protein is highlighted in red. (L) Paraffin-embedded human and porcine anterior segments sections were probed with antibodies directed against human LaNt α31 protein. In addition, human anterior segment sections were probed with mouse isotype IgG as a negative control. Scale bar =100 μm.

3.2 LaNt α31 knockdown does not affect corneal epithelial cell migration characteristics

As a first analysis of LaNt α31 function in corneal epithelial cells, Mr. Lee Troughton from our lab performed a simple scratch closure assay, comparing shRNA knockdown clones to scrambled shRNA and control hTCEpi (Fig. 3.5A). This revealed no significant difference in closure rates in hTCEpi LaNt α31 knockdown cells relative to controls (Fig. 3.5B; 85±16% closure in 16h for hTCEpi, 88%±18% for scrambled shRNA, 81±17% for LaNt α31 shRNA clone #1, 74±15% for clone #2, 82±16% for clone #3).

In addition, low-density migration assays, where the movement of individual cells were tracked over a 2h period (Fig. 3.5C), revealed that the migration speed (Fig. 3.5D) and the ratio of the linear distance migrated to total distance (processivity, Fig. 3.5E) of knockdown clones was not significantly different from controls (hTCEpi speed 0.92±0.25 μm/min; processivity 0.39±0.11; scrambled shRNA speed 0.92±0.34 μm/min, processivity 0.51±0.19; LaNt α31 shRNA clone #1 speed 1.25±0.35 μm/min, processivity 0.51±0.19; clone #2 speed 0.84±0.34 μm/min, processivity 0.41±0.15; clone #3 speed 1.22±0.35 μm/min, processivity 0.45±0.17).

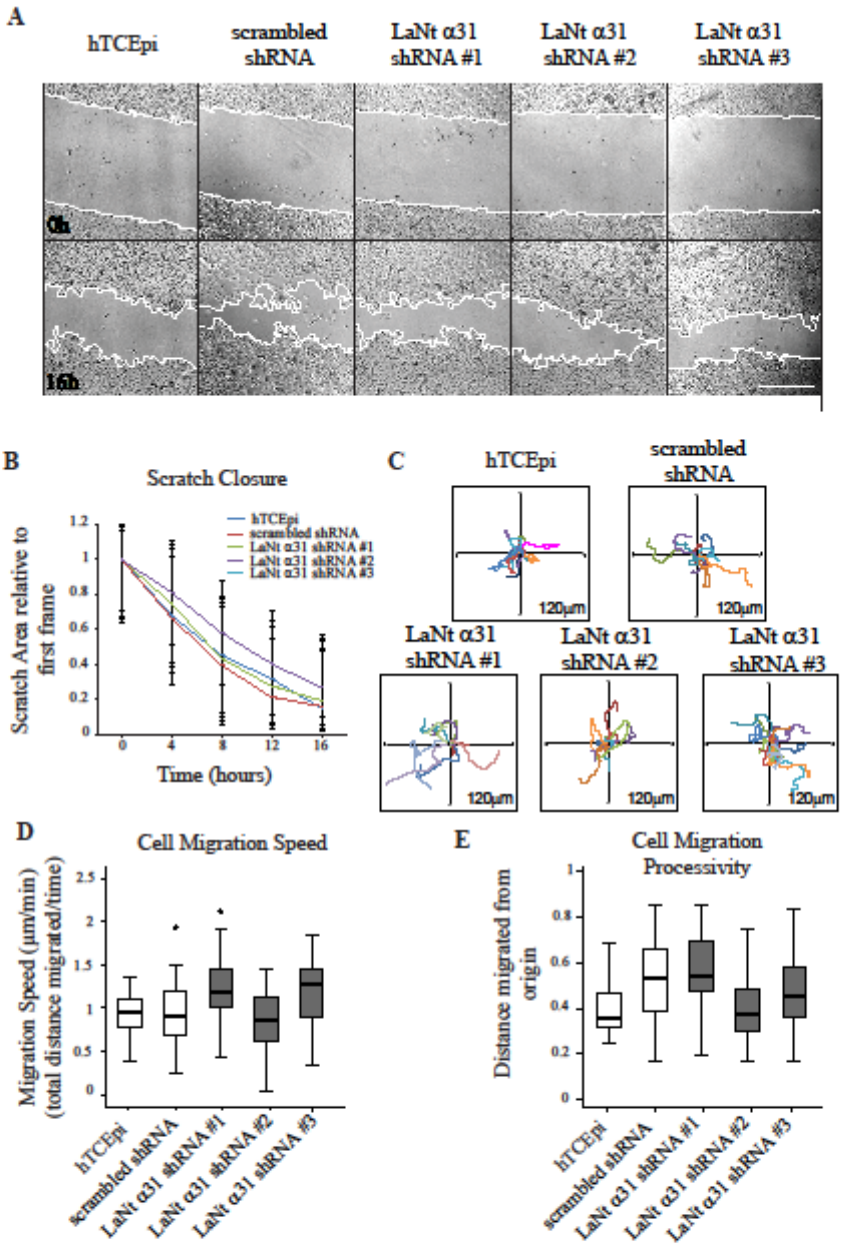

Fig. 3.5: LaNt α31 knockdown hTCEpi exhibit normal migration characteristics.
(A) and (B) hTCEpi, scrambled shRNA or LaNt α31 shRNA clones 1, 2 and 3 were grown to confluence and a scratch wound introduced and imaged during closure. (A) Representative images from immediately post scratching (T0) and after 16h of recovery (T16), white lines delineate wound margins. Scale bar =100 μm. (B) Wound area measured at 0, 4, 8, 12 and 16h post wounding plotted as mean ± SD relative to wound area at T0, n=3 independent assays. (C), (D) and (E) Cells were plated at low density and migration paths of individual cells tracked over a 2h period. (C) Vector diagrams showing representative paths of 10 individual cells with each colour representing a single cell. (D) Migration speed measured as total distance migrated over time. (E) Migration processivity measured as maximum linear distance migrated over total distance migrated. Boxes in (D) and (E) are 25th to 75th percentile, whiskers 5th and 95th 40-60 cells per type.

3.3 LaNt α31 is not incorporated into the ECM deposited by hTCEpi cells

Similar studies using HaCaTs cells were published in 2009, reporting keratinocytes as unable to close a wound *in-vitro* in the presence of LaNt α31 knockdown [461]. As the effect of LaNt α31 knockdown in hTCEpi cells does not match that published in HaCaTs, we were prompted to investigate more closely the differences in LaNt α31 distribution between HaCaTs and hTCEpi cells.

Staining coverslips where the cells were removed by NH_4OH treatment, to leave ECM extracts only, revealed that, in HaCaTs cells, LaNt α31 puncta were decorating regions of LM β3 (Fig. 3.6, lower panel). However, similar staining was not observed when hTCEpi were treated in the same manner, despite a similarly extensive LM β3 matrix (Fig. 3.6, upper panel), indicating differences between the way the two cell types organise their LaNt α31 protein. This diversity is consistent with the distribution of LaNt α31 in the central cornea, where it is expressed throughout all corneal layers.

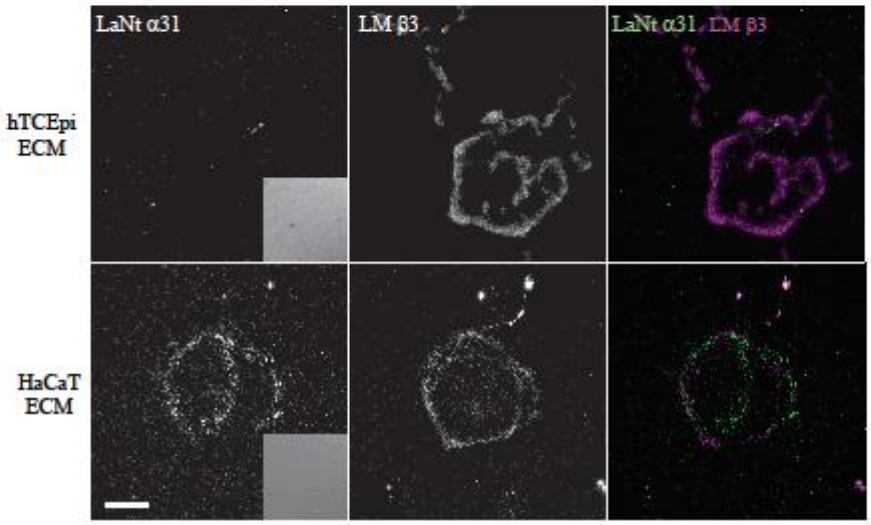

Fig. 3.6: LaNt α31 is not deposited in hTCEpi ECM.
HaCaT and hTCEpi cells were cultured overnight on uncoated glass coverslips, then cellular material removed using NH_4OH.
The exposed matrix material was processed for indirect immunofluorescence microscopy with antibodies against LaNt α31 and LM β3. Scale bar = 20 μm.

3.4 LaNt α31 overexpression leads to an extracellular protein deposition

The difference in LaNt α31 distribution between hTCEpi and HaCaTs cells may be due either to the possibility that LaNt α31 expressed by hTCEpi cells is not secreted, or to an absence of association of the secreted protein with matrix.

To analyse these aspects, and to mimic in hTCEpi cells a similar LaNt α31 deposition as in HaCaTs cells, we induced the overexpression of a full-length LaNt α31 construct containing the human cytomegalovirus (CMV) promoter, which drives high level of constitutive protein expression [494], and a C-terminal eGFP tag (Fig. 3.7A). The overexpression was induced using an adenoviral expression system [486]. hTCEpi overexpressing LaNt α31 will be indicated as +LaNt α31; hTCEpi overexpressing GFP (+GFP) or LM β3-mCherry (+LMβ3) were used as controls.

Transduction efficiency was confirmed by WB of total cell lysates from +LaNt α31 and controls +GFP or +LM β3 hTCEpi. Anti-GFP mAbs gave a band at the predicted molecular weight of ~76 kDa, together with a smaller species at around ~72 kDa, likely indicative of removal of the N-terminal secretion signal sequence (Fig. 3.7B). Interestingly, imaging of GFP fluorescence indicated that, while the distribution of the intracellular LaNt α31-GFP protein resembles the one of the antibody derived staining of untreated hTCEpi, LaNt α31-GFP signal was also present in the ECM preparations (Fig. 3.7C). This signal also appears to be very similar, though not as extensive, to the LM β3-mCherry signal observed in the ECM preparations of doubly transduced hTCEpi cells (Fig. 3.7D).

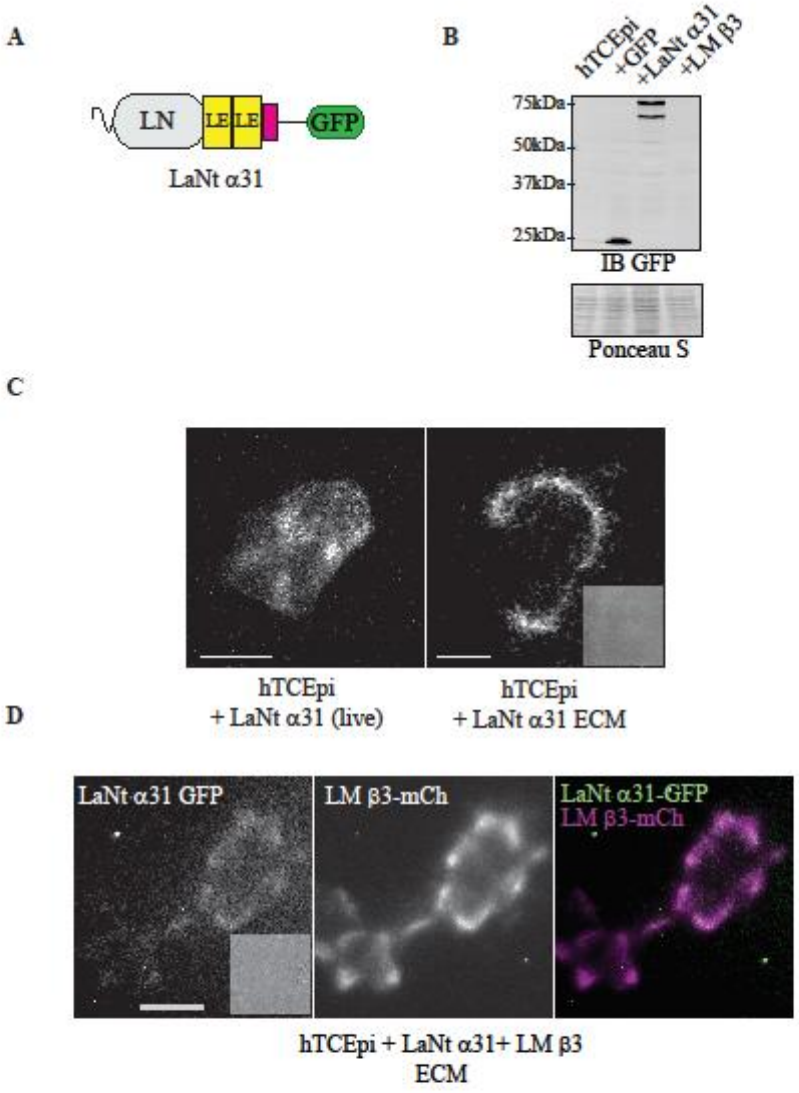

Fig. 3.7: LaNt α31 overexpression leads to LaNt α31 deposition in the ECM.
(A) Diagrammatic scheme of LaNt α31-GFP construct.(B) Total cell lysates from hTCEpi, hTCEpi transduced with GFP, LaNt α31-GFP or LM β3 mCherry were processed for WB with antibodies against GFP. Numbers indicate molecular weight markers. (C) hTCEpi cells were adenovirally transduced with LaNt α31-GFP, then plated on glass bottomed dishes for 24h prior to analysis. Left panel, GFP signal obtained from live cells; right panel, GFP obtained after removal of cellular material by NH_4OH. (D) hTCEpi were doubly transduced with LaNt α31-GFP and LM β3 mCherry constructs, plated onto glass coverslips and ECM derived as above. Insets in (C) and (D) are phase contrast images confirming cell removal. Scale bars = 20 μm.

3.5 Corneal epithelial cells overexpressing LaNt α31-GFP display decreased motility and scratch wound closure rates

LaNt α31 overexpression in hTCEpi led to a protein deposition in the ECM, therefore, we decided to exploit the opportunity to use the hTCEpi cell line and overexpression system as a tool to investigate the impact of increased LaNt α31 expression and extracellular accumulation on corneal cell behaviour. As LaNt α31 has previously been shown to influence cell migration [461], we first investigated this using a conventional scratch closure assay.

In scratch closure assays, +LaNt α31 cells displayed a dramatically reduced ability to close wound compared to controls (Fig. 3.8A,B; in 16h, 50±15% closure for +LaNt α31 compared to 98±22% closure for hTCEpi, 92±26% for +GFP and 99±36% for +LM β3, $p<0.01$).

Scratch closure assays, while useful for gaining an overall impression of motility behaviour, are unable to identify where the problem leading to delayed closure lies. We, therefore, followed up these studies with low-density motility assays, where the movement of individual cells was tracked over a 2h period of time (Fig. 3.9A,B). Assays of this type are able to distinguish fundamental differences in movement versus a failure to establish and maintain polarity. Using this assay, +LaNt α31 hTCEpi again displayed large reduction in total cell migration speed, significantly slower than controls (Fig. 3.9C, +LaNt α31 0.74±0.20 μm/min vs 1.31±0.22 μm/min for hTCEpi, 1.20±0.13 μm/min for +GFP and 1.24±0.23 μm/min for +LM β3 hTCEpi controls, $p <0.05$). However, there was no difference in processivity, measured as the maximum linear distance travelled divided by the total difference

travelled (Fig. 3.9D), indicating that the cell polarity is not specifically influenced by overexpression of LaNt α31.

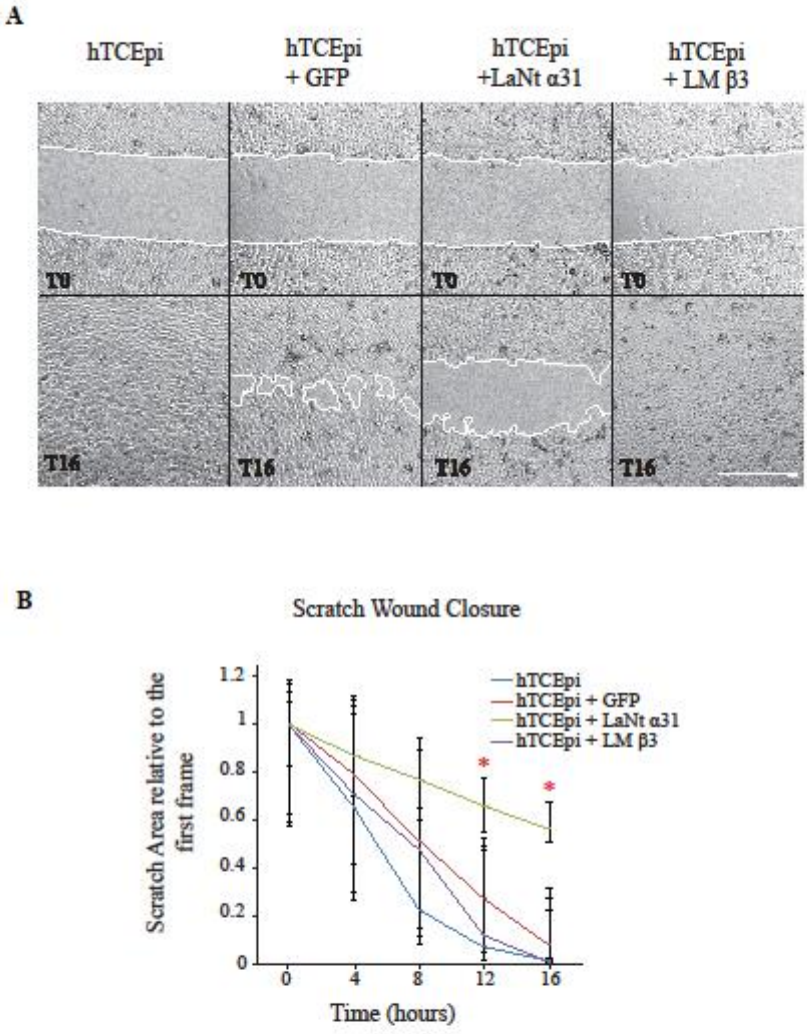

Fig. 3.8: LaNt α31 overexpression impairs hTCEpi migration.
hTCEpi, either untreated or adenovirally transduced with GFP (+GFP), LaNt α31 (+LaNt α31) or LM β3 (+LM β3), were grown to confluence and a scratch wound introduced and imaged during closure. (A) Representative images from immediately post scratching (T0) and after 16h of recovery (T16); white lines delineate wound margins. (B) Wound area measured at 0, 4, 8, 12, and 16h post wounding plotted as mean ± SD, n=3 independent assays. In (B), * denotes significant differences between means of n=3 independent assays for +LaNt α31 compared with all controls, $p<0.05$ as determined by one way ANOVA followed by Tukey's post hoc analysis.
Scale bar = 100 μm.

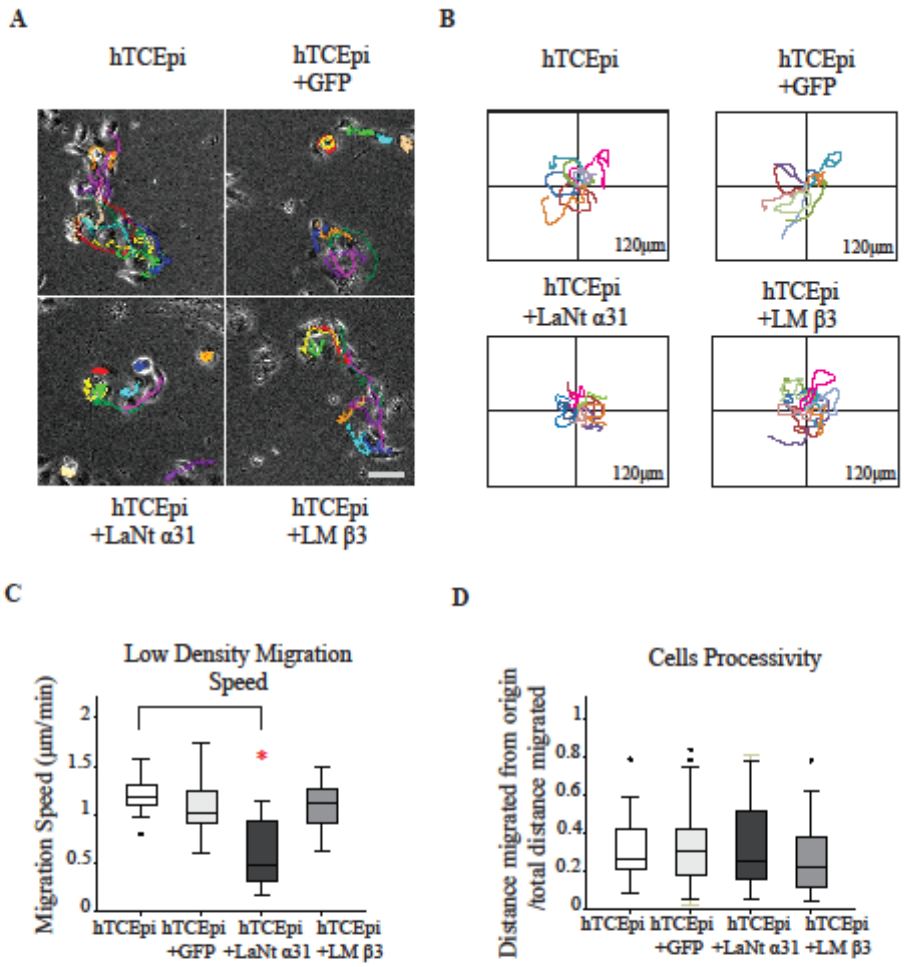

Fig. 3.9: LaNt α31 overexpression leads to a decrease in hTCEpi motility speed at times of new matrix formation.
hTCEpi, +GFP, +LaNt α31 and +LM β3 cells were plated at low density and migration paths of individual cells tracked over a 2h period.(A) Representative stills of cells showing the total distance migrated, analysed with ImageJ MTrackJ plugin. Scale bar = 20 μm. (B) Vector diagrams showing representative paths of 10 individual cells with each colour representing a single cell. (C) Migration speed measured over a 2h period of time, as total distance migrated over time. (D) Migration processivity measured as maximum linear distance migrated over total distance migrated. Boxes in (C) and (D) are 25th to 75th percentile, whiskers 5th and 95th of 40-60 cells per type. In (C), * denotes significant differences between means of n=3 independent assays for +LaNt α31 compared with all controls, $p<0.05$ as determined by one way ANOVA followed by Bonferroni post hoc analysis.

3.6 Cell-derived preformed ECM rescues the migration impairment in hTCEpi cells

To determine whether the cell motility defect of LaNt α31 overexpressing cells was caused by a cell fault or by an inadequate matrix assembly, we next investigated whether a preformed cell-derived matrix could rescue the defective phenotype observed.

Cell-derived ECMs from either hTCEpi or +LaNt α31 hTCEpi were generated 24h after plating at high density on tissue culture plastic. Onto these prepared matrixes, fresh hTCEpi or +LaNt α31 cells were plated, allowed to attach for 2h and then single cell motility behaviour analysed as above. These analyses revealed that the migration speed defect of the +LaNt α31 is rescued by provision of an extensive cell-derived matrix indicating, therefore, that +LaNt α31 cells abnormal migration is not inherent to the cells themselves (Fig. 3.10; in (B), hTCEpi on hTCEpi ECM 1.15±0.21 μm/min, +LaNt α31 on hTCEpi ECM 1.20±0.28 μm/min). Moreover, these studies revealed that the matrix deposited by +LaNt α31 cells plated at high density was indistinguishable from non-transduced hTCEpi ECM in terms of supporting cell movement (Fig. 3.10; in (B) hTCEpi on +LaNt α31 ECM 1.26±0.20 μm/min, +LaNt α31 on +LaNt α31 ECM 1.14±0.29 μm/min).

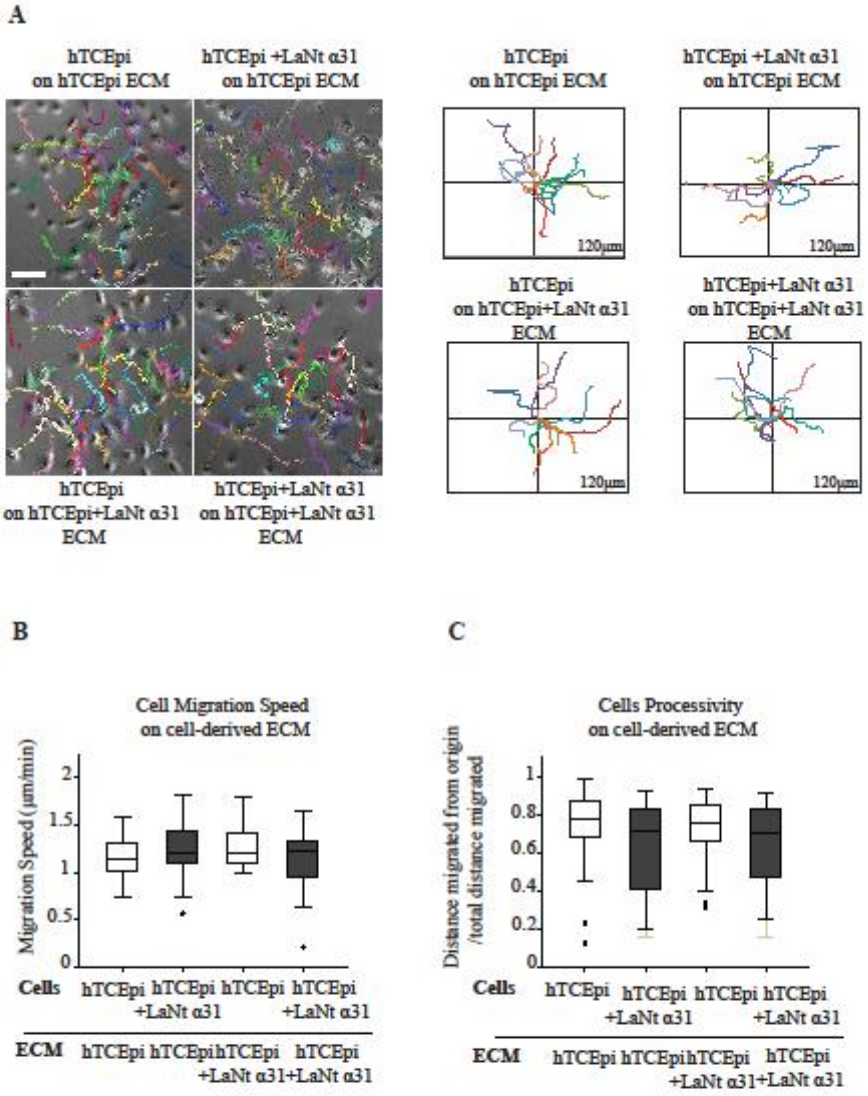

Fig. 3.10: Motility defects are rescued by a cell-derived preformed matrix. hTCEpi or +LaNt α31 hTCEpi were plated overnight at confluence and cell-derived matrixes prepared by NH_4OH removal of cellular material. Onto prepared matrixes, fresh hTCEpi or +LaNt α31 hTCEpi were seeded at low density, allowed to adhere for 2h, then migration paths of individual cells tracked over a 2h period. (A) Representative stills from motility videos and vector diagrams, scale bar = 100 μm. (B) migration speed, (C) migration processivity. Boxes in B anc C are 25th to 75th percentile, whiskers 5th and 95th of 40-60 cells per type.

3.7 LaNt α31 overexpressing cells show an increase in cell spread area

During routine work with the +LaNt α31 cells, we noted an apparent increase in cell spread area, potentially indicative of a change in the way the cells interact with their matrix (Fig. 3.11A). To analyse this further, the 2D cell area of live individual cells, plated at low density on uncoated tissue culture plastic, was analysed using Fiji32-ImageJ software (NIH). +LaNt α31 cells displayed significantly increased area compared to controls (Fig. 3.11B, +LaNt α31 2249±206 μm² vs hTCEpi 839±150 μm², +GFP 942±185 μm², +LM β3 868±200 μm², $p < 0.05$). No significant differences were observed in length/width aspect ratio, suggesting the absence of any polarity defect and consistent with motility data (Fig. 3.11C).

To determine if the spreading phenotype was a reflection of the changes in the matrix organisation induced by the LaNt α31 overexpression, we generated cell-derived ECMs from either hTCEpi or +LaNt α31 hTCEpi, 24h after being plated at high density on tissue culture plastic. Onto these prepared matrixes, fresh hTCEpi or +LaNt α31 cells were plated and cell spread area measured after 2h (Fig 3.12A).

These analyses revealed that the increased cell spread area of LaNt α31 overexpressing hTCEpi is not a direct defect of the cells themselves, but rather related to cell-matrix interactions, as it can be rescued by provision of a preformed matrix (Fig. 3.12B, +LaNt α31 on hTCEpi ECM 1303±282 μm² vs 1180±278 μm² hTCEpi on hTCEpi ECM; +LaNt α31 on +LaNt α31 ECM 1194±298 μm² vs 1266±230 μm² hTCEpi on +LaNt α31 ECM). Furthermore, LaNt α31 overexpressing hTCEpi cell polarity was not affected (Fig. 3.12C).

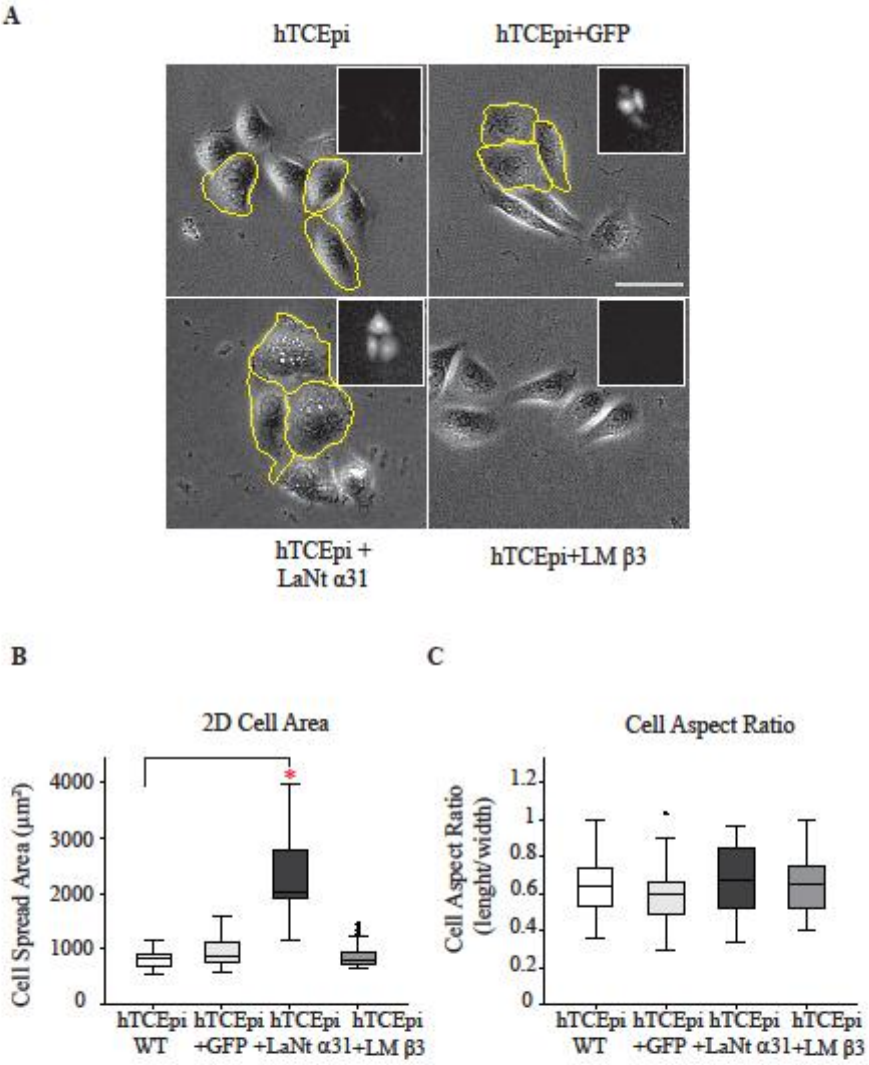

Fig. 3.11: LaNt α31 overexpressing hTCEpi display increased 2D area.
(A) Untreated, +GFP, +LaNt α31 and +LM β3 hTCEpi were seeded for 2h on uncoated tissue culture plastic and representative images were taken using a Nikon TiE epifluorescence microscope. Insets show images of the GFP signal. Yellow lines highlight increased cell area. Scale bar = 20 μm. (B) 2D cell area, (C) cell aspect ratio measured as width at widest point / length at longest point. n = 3 independent assay. In (B), * denotes significant differences between +LaNt α31 and all controls, $p<0.05$ as determined by one way ANOVA followed by Tukey's post-hoc analysis.

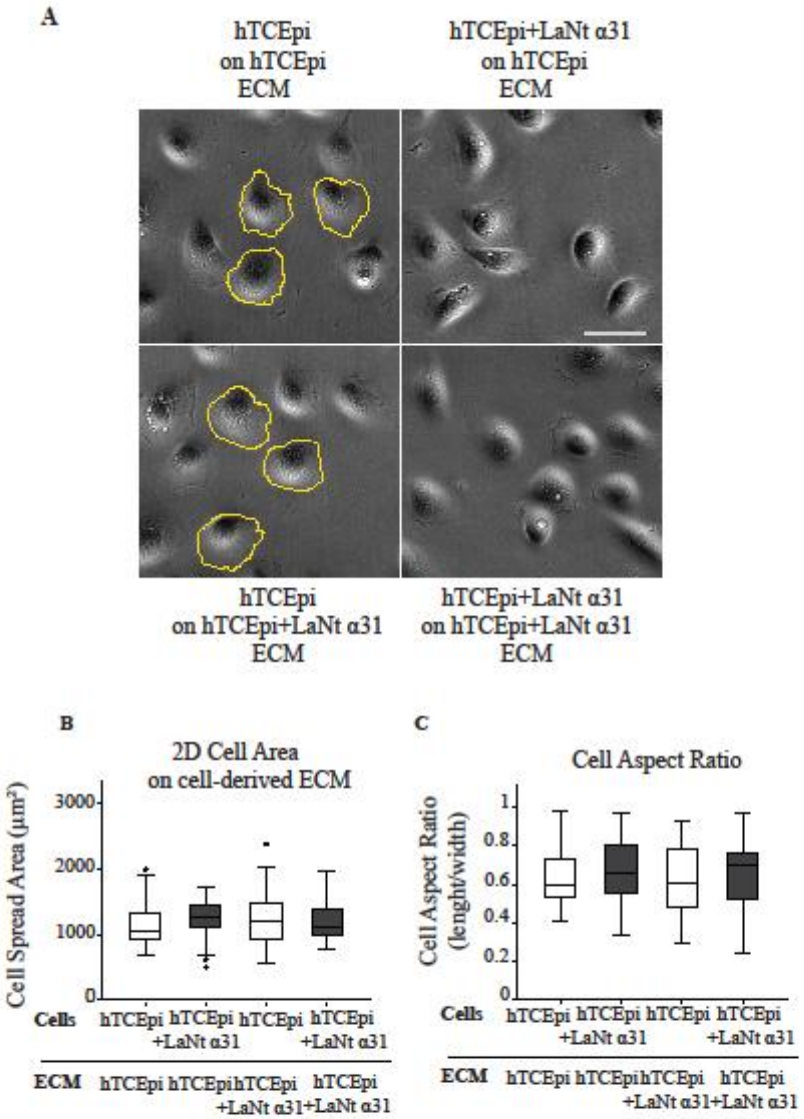

Fig. 3.12: LaNt α31 overexpressing hTCEpi increased 2D area is rescued when cells are provided with a cell-derived ECM.
(A) hTCEpi or +LaNt α31 hTCEpi were plated overnight at confluence and cell-derived matrixes prepared by NH_4OH removal of cellular material. Onto prepared matrixes, fresh hTCEpi or +LaNt α31 hTCEpi were seeded at low density, allowed to adhere for 2h, then representative images taken.
Scale bar = 20 μm. 2D cell area (B) and cell aspect ratio (C) were measured for every cell type.

3.8 hTCEpi overexpressing LaNt α31 show a decreased attachment to LM111

Having observed a change in cell motility and morphology when LaNt α31 is overexpressed in hTCEpi, we also used a rapid adhesion assay to determine if the protein LaNt α31 has an effect on the cell attachment to different ECM components [251, 495]. We performed rapid adhesion assays using hTCEpi, +LaNt α31, +GFP or +LM β3 hTCEpi attaching to plates coated with LM111, FN or Col type IV. A significant decrease in the hTCEpi cell attachment rate to the LM111 coating was observed in +LaNt α31 cells (Fig. 3.13A, 40% less attachment compared to hTCEpi, +GFP and +LM β3 cells, $p < 0.05$). Attachment to Col type IV (Fig. 3.13B) and to FN (Fig. 3.13C) was not significantly affected by the overexpression of LaNt α31, suggesting that LaNt α31 affects hTCEpi cell attachment with a LM-specific interaction.

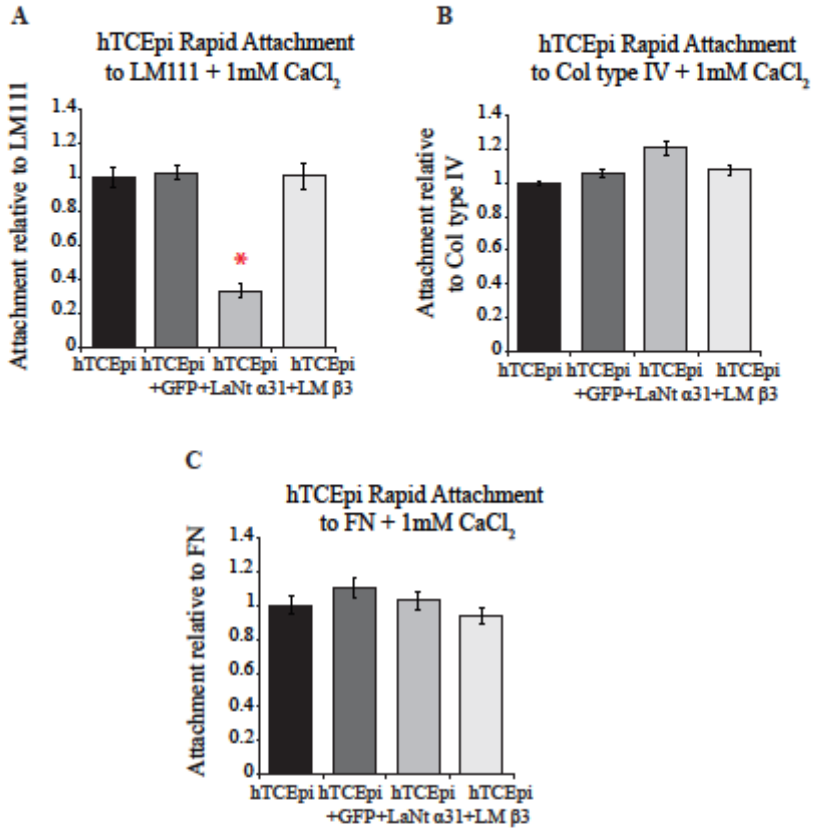

Fig. 3.13: hTCEpi rapid attachment to LM111, but not to Col type IV or FN, is decreased when LaNt α31 is overexpressed.
Cells were either untreated or adenovirally transduced with GFP, LaNt α31 and LM β3. Wells were coated with indicated proteins for 1h at 37°C. After blocking with BSA, cells were plated onto the prepared substrates and incubated at 37°C for 1h; attached cells were fixed, stained with crystal violet and absorbance read at 570 nm. In (A), (B) and (C) values were normalised to a FN 10 µg/ml coated well and plotted as mean +/- s.e.m. from 3 independent experiments, 2 replicates per condition per assay. In (A), * denotes significant difference ($p < 0.05$) as determined by one way ANOVA and Tukey's post hoc analysis.

3.9 Overexpressed LaNt α31 interacts with and modifies LM332 organisation in hTCEpi cells

The observed altered cell properties also suggested the possibility that LaNt α31 overexpression influences the organisational status of LM332 deposited by hTCEpi cells. If true, this process could in part explain the increased cell area coupled with defective cell motility and adhesion characteristics. To study this aspect, hTCEpi, +LaNt α31 or +GFP hTCEpi cells were stained for the LM α3 subunit to compare the LM matrix deposited.

When fixed 5h after seeding onto glass coverslips, control cells deposited arcs and contiguous lines of LM β3, whereas +LaNt α31 cells deposited LM β3 in tight and small clusters (Fig. 3.14A; average LM β3 cluster area for hTCEpi 236±24 pixel^2, for +GFP 234±24 pixel^2 and for +LaNt α31 79±18 pixel^2). However, when cells were plated at higher density and allowed 24h to form their matrix, there was no significant difference in LM β3 organisational status (Fig. 3.14B right panel, hTCEpi 274±44 pixel^2, +GFP 180±53 pixel^2, +LaNt α31 254±47 pixel^2).

These data point to a role for LaNt α31 at times when new matrix is being deposited; moreover, they support our cross-matrix motility findings, as they indicate that ultimately the matrix assembled by +LaNt α31 is indistinguishable from controls, at least as far as LM332 is concerned.

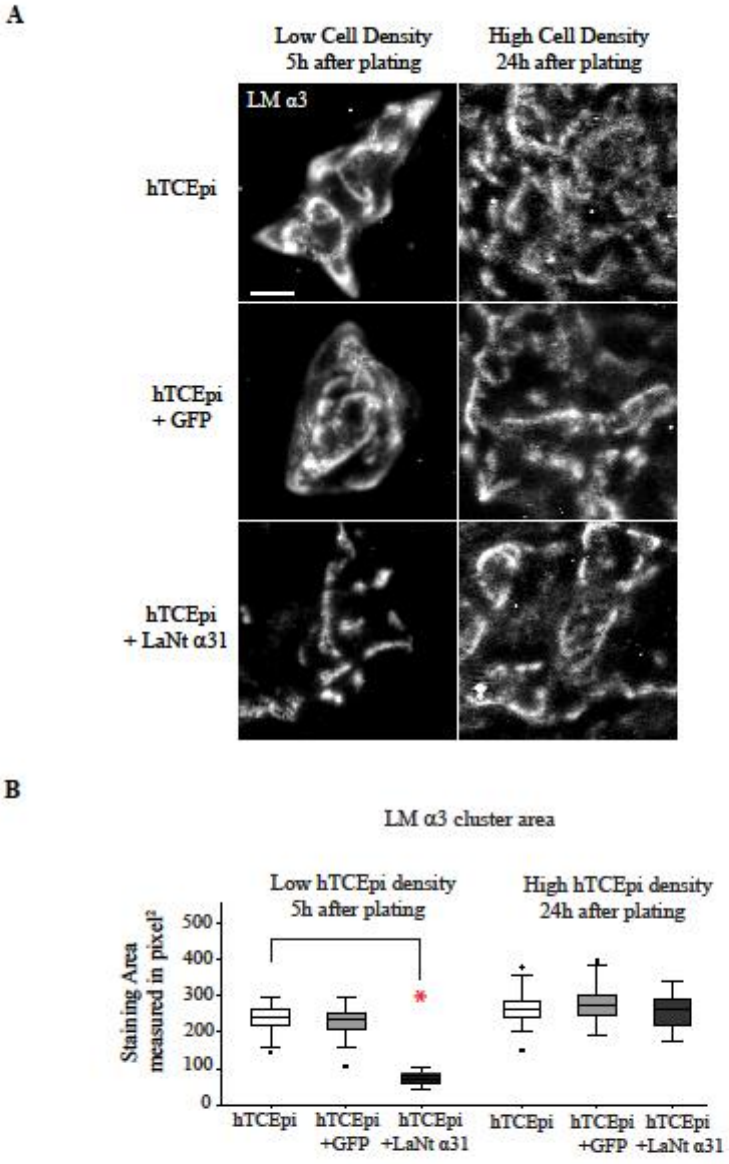

Fig. 3.14: Overexpressed LaNt α31 changes LM α3 organisation.
(A) hTCEpi, +GFP or +LaNt α31 hTCEpi were seeded at low (left panels) or high (right panels) density on uncoated glass coverslips then processed for immunofluorescence microscopy antibodies against LM α3, after 5h (left panels) or 24h (right panels). (B) LM α3 cluster area, n=50 measurements per cell type. In (B), * denotes significant differences between +LaNt α31 and all controls, $p<0.05$ as determined by one way ANOVA followed by Tukey's post-hoc analysis. Scale bar = 20 μm.

3.10 LaNt α31 overexpressing cells display mislocalised focal contacts

As described, high levels of LaNt α31 in hTCEpi cells lead to defects in cell morphology, motility and adhesion and interfere with LM organisation. A potential explanation for the observed results is the presence of differences in the cell-to-matrix attachment complexes assembled by the +LaNt α31 cells compared to controls. Epithelial cells assemble two major integrin-based cell to LM adhesive complexes; FAs and HDs [413, 496].

To analyse the effect of induced LaNt α31 expression on FAs and HDs, we first performed indirect immunofluorescence for the FA protein paxillin and the HD core component β_4 integrin, 5h after cell seeding [265, 391]. Immunostaining revealed that, while paxillin formed discrete puncta in control hTCEpi, in +LaNt α31 cells paxillin was assembled into regions of linear staining around cell margins (Fig. 3.15). The distribution of β_4 integrin revealed swirls and arcs in control cells compared to tight clusters in the +LaNt α31 cells (Fig. 3.15). These tight clusters are more reminiscent of the “cat paw” staining pattern obtained from tightly adhered cell lines, such as the 804G rat bladder epithelial line [483].

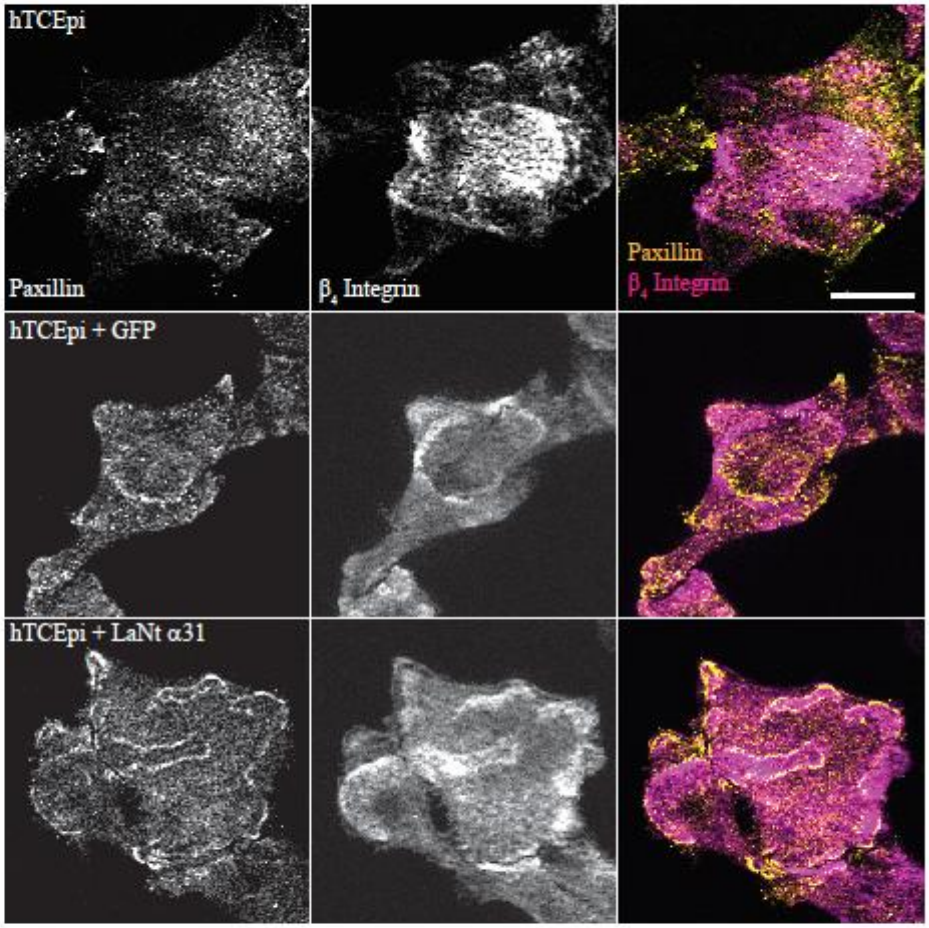

Fig. 3.15: High levels of LaNt α31 induce mislocalisation of FAs.
hTCEpi, +GFP or +LaNt α31 hTCEpi were seeded on uncoated glass coverslips and fixed after 5h, then processed for indirect immunofluorescence microscopy with antibodies against paxillin and β_4 integrin. Scale bar = 10 μm.

3.11 LaNt α31 overexpressing cells display early HD maturation

The HD-like structures assembled by cultured epithelial cells develop over time, from an initial $\alpha_6\beta_4$ integrin/plectin containing complex to more mature complexes, through recruitment of Col type XVII and BPAG1e [497]. We, therefore, investigated about the presence of changes in the maturation of HD complexes assembled by +LaNt α31 cells when cultured for a short time in a low density, conditions where differences in LM organisation had previously been observed.

Immunofluorescence analysis of the distribution of Col type XVII in relation to β_4 integrin revealed good co-localisation in +LaNt α31 cells, compared with a general lack of co-distribution in non-transduced hTCEpi or +GFP hTCEpi (Fig. 3.16, Pearson's co-localisation coefficient for hTCEpi 0.13, for +GFP 0.12, for +LaNt α31 0.57), suggesting that the HD-like complexes are more mature in +LaNt α31 cells than controls.

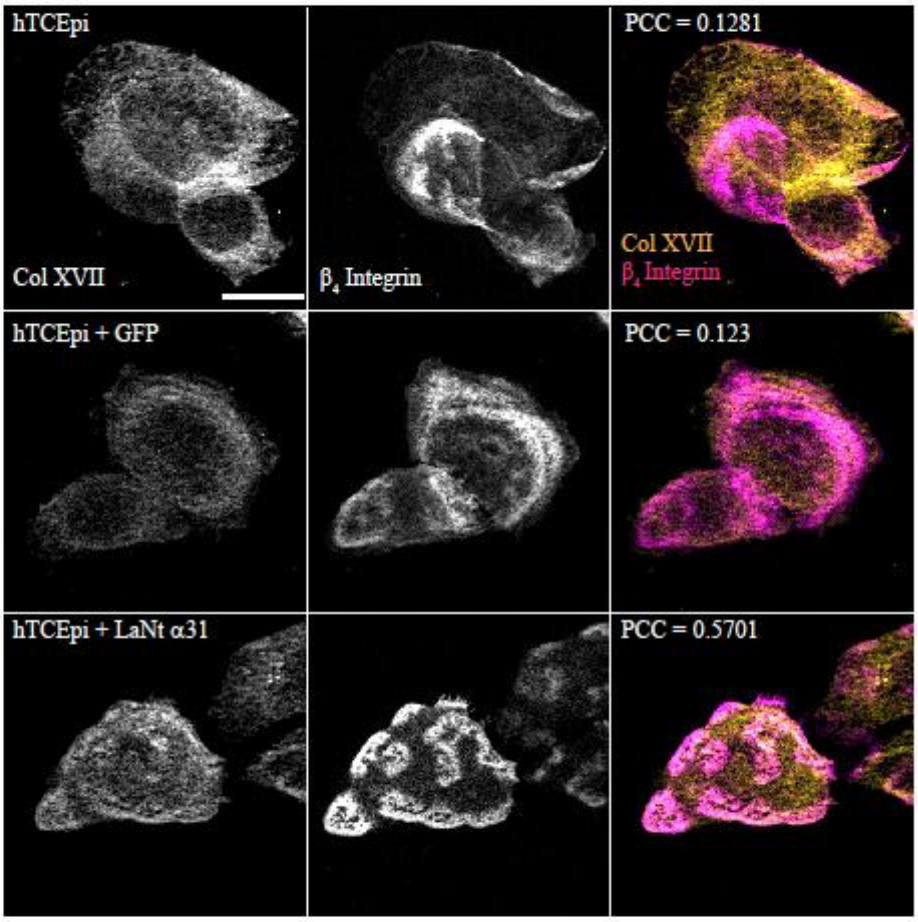

Fig. 3.16: High levels of LaNt α31 induce early maturation of HDs.
hTCEpi, +GFP or +LaNt α31 hTCEpi were seeded on uncoated glass coverslips and fixed after 5h, then processed for indirect immunofluorescence microscopy with antibodies against Col type XVII and β_4 integrin.
Numbers represent Pearson's Colocalisation Coefficient (PCC) of signals obtained in Col type XVII and β_4 integrin channels. Scale bar = 10 μm.

3.12 LaNt α31 co-distributes with LM β3 during matrix deposition

Following the data obtained from the functional assays in the presence of LaNt α31 overexpression, which point toward a role for LaNt α31 during the initial stages of matrix assembly, we next wanted to investigate LaNt α31 dynamics in relation to LMs during this period, both when new matrix is required and when cells move on a cell-derived matrix.

First, LaNt α31-GFP and LM β3-mCherry co-expressing hTCEpi cells were seeded in a cloning cylinder and imaged shortly after seeding (Fig. 3.17A, movie 1). Over the first 3h of this experiment, LM β3 and LaNt α31 were deposited in clusters toward cell peripheries (maximum intensity projection shown in Fig. 3.17B). The two proteins displayed near identical patterns and we were unable to discern any difference in timing of deposition.

Second, doubly transduced hTCEpi expressing LaNt α31-GFP and LM β3-mCherry were plated overnight at low density on uncoated glass-bottomed dishes, then imaged using confocal microscopy every 20 min over 12h. Consistent with the motility assay data, the movement patterns of individual cells was extremely restricted and did not extend beyond the extent of the LM β3 deposits already present at the start of the assay. Interestingly, throughout the time course of this experiment, rather than stable association with LM β3, the LaNt α31-GFP rapidly formed and dissociated clusters at sites of LM β3 deposits (Fig. 3.18A-movie 2, Fig. 3.19A and 3.20A). Although individually transient, the LaNt α31 and LM β3 co-distribution is strongly apparent when a maximum intensity projection of each frame of the movies is generated (Fig. 3.18B, 3.19B, 3.20B).

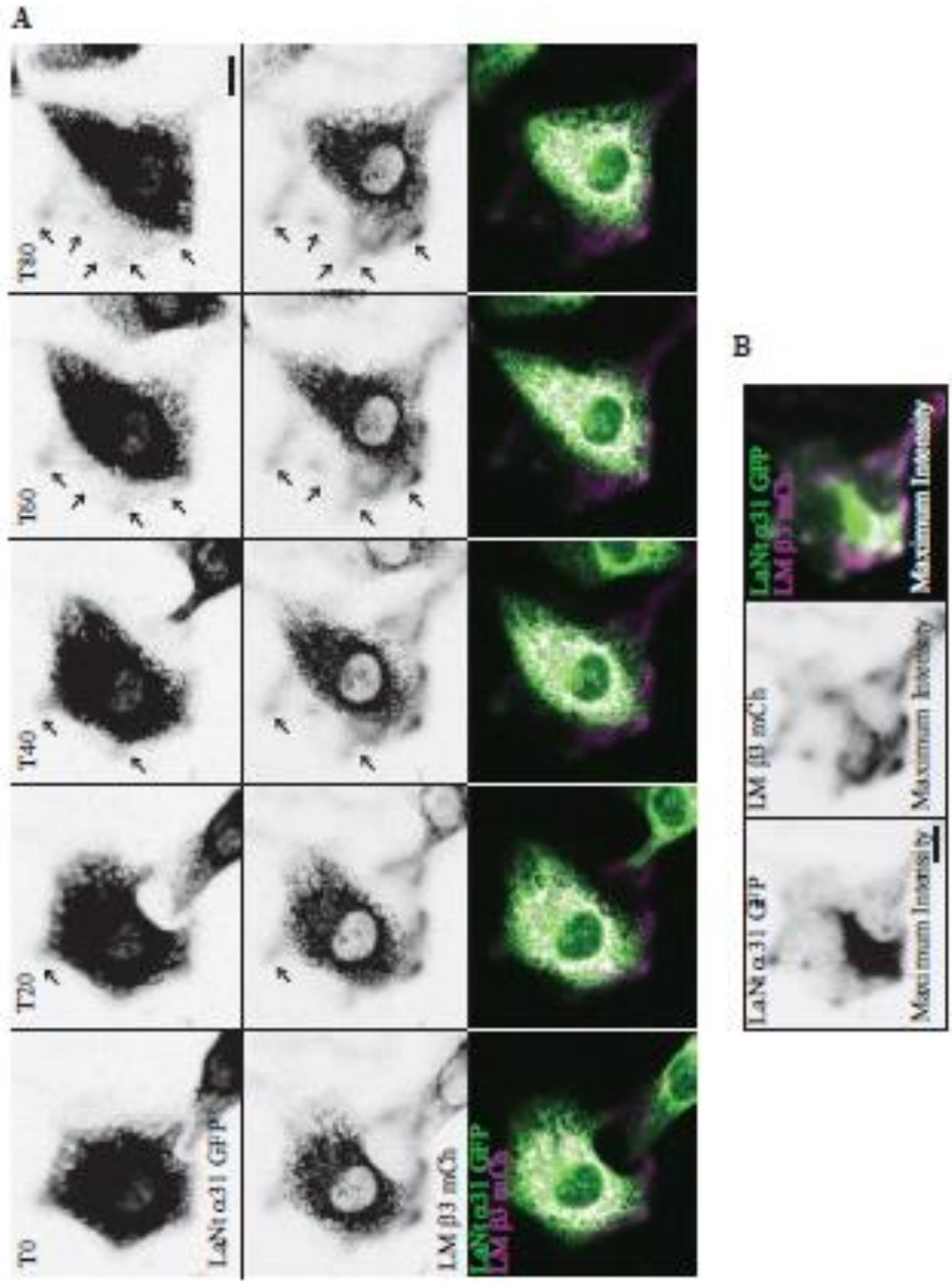

Fig. 3.17: LaNt α31 gets deposited alongside LM β3 at cell peripheries. hTCEpi doubly transduced with LaNt α31-GFP and LM β3-mCherry were plated overnight within a cloning cylinder and imaged by confocal microscopy every 20 min over 16h. (A) Representative stills from 0 to 80 min of LaNt α31-GFP (upper panels) and LM β3-mCherry (middle panels), with signals inverted. Bottom panels, merged images of LaNt α31 (pseudocoloured green) and LM β3 (pseudocoloured magenta). (B) Maximum intensity projection of entire 16h timecourse images. Scale bars = 20 μm.

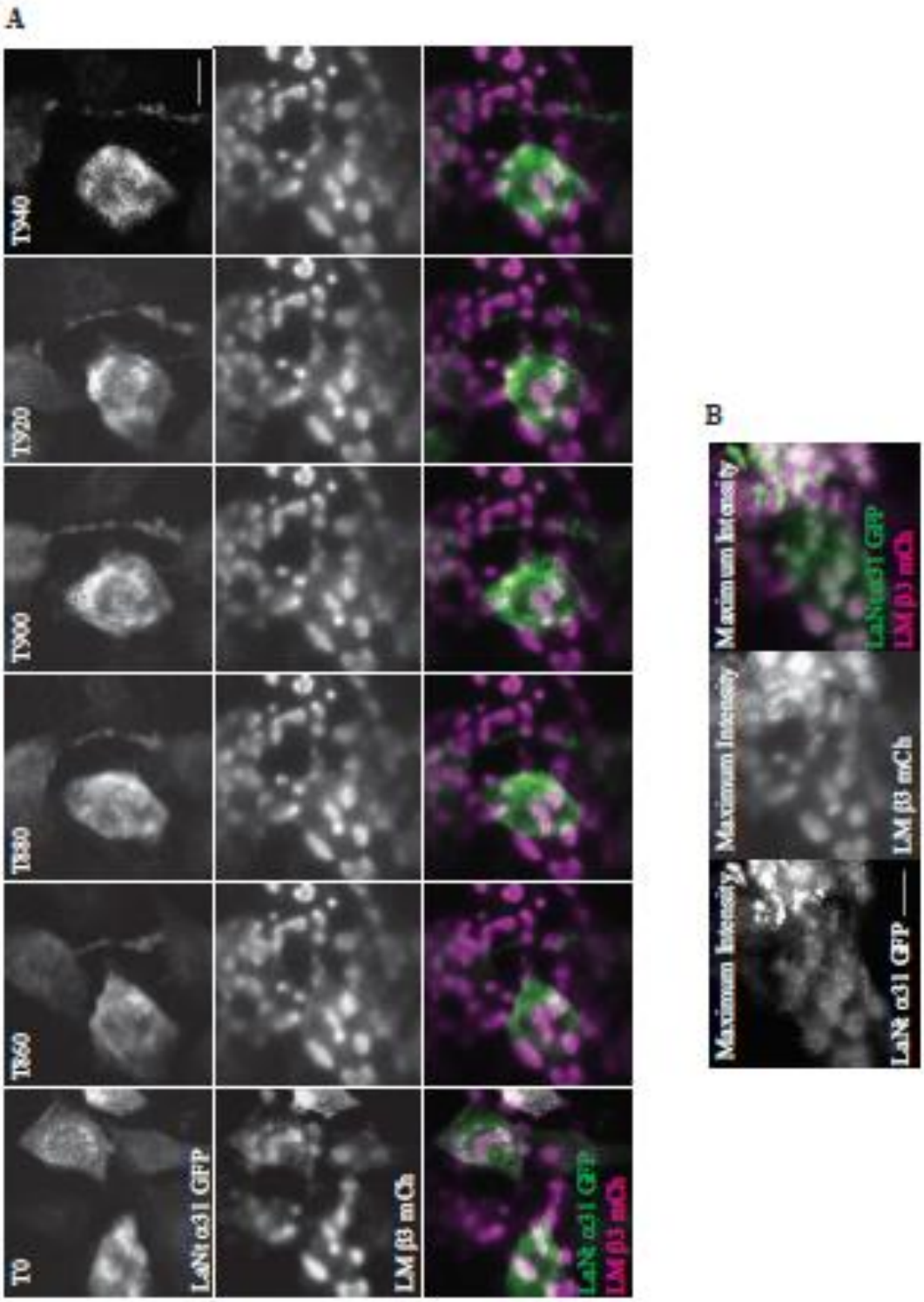

Fig. 3.18: LaNt α31 rapidly forms and disassembles clusters on top of LM β3. hTCEpi doubly transduced with LaNt α31-GFP and LM β3-mCherry were plated overnight on uncoated glass-bottomed dishes and imaged by confocal microscopy every 20 min over 16h. (A) Representative stills from 0 to 940 min of LaNt α31-GFP (upper panels) and LM β3-mCherry (bottom panels). (B) Maximum intensity projection of entire 16h timecourse images. Scale bars = 20 μm.

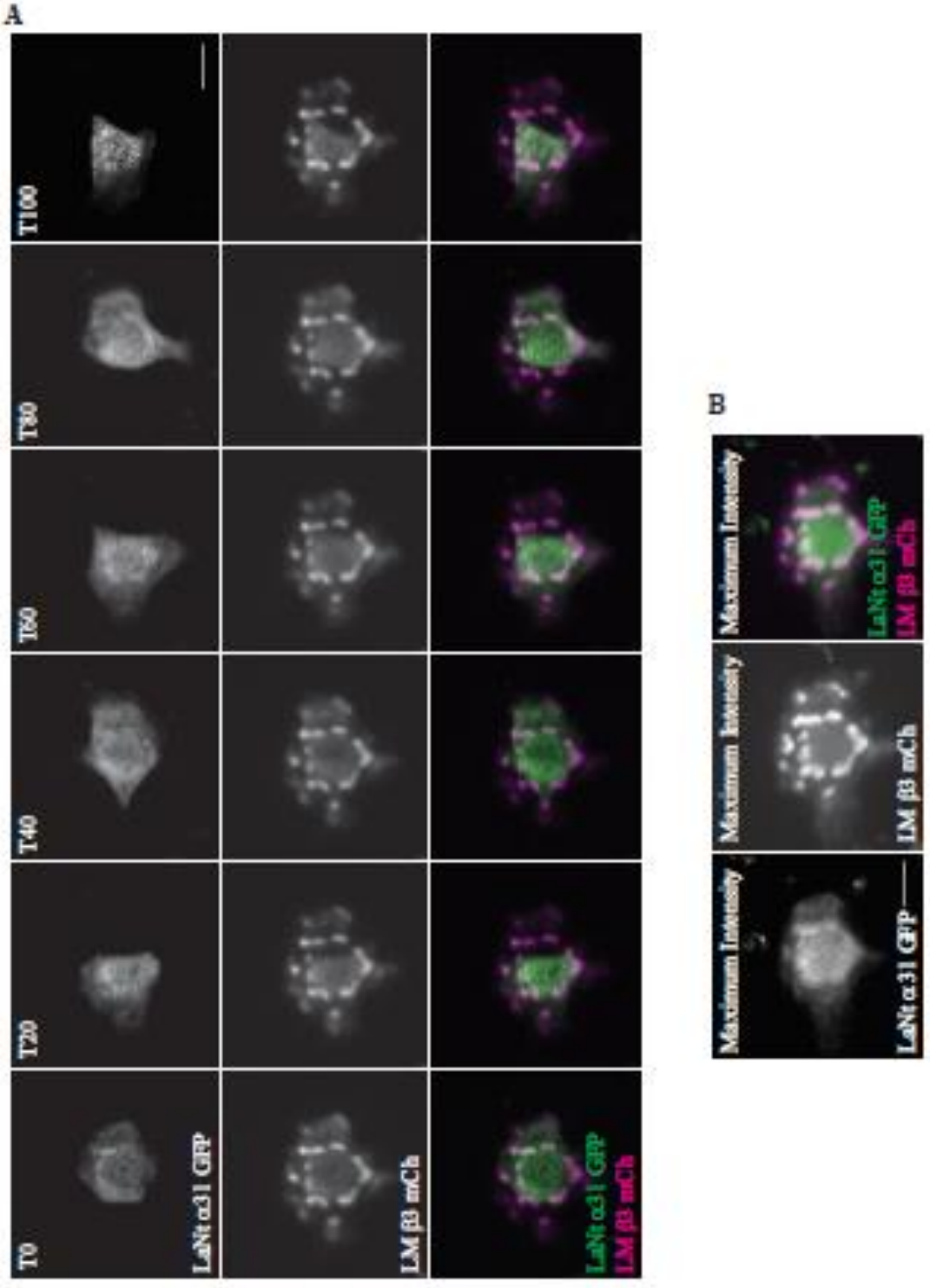

Fig. 3.19: LaNt α31 rapidly form and disassembles clusters on top of LM β3. hTCEpi doubly transduced with LaNt α31-GFP and LM β3-mCherry were plated overnight on uncoated glass-bottomed dishes and imaged by confocal microscopy every 20 min over 16h. (A) Representative stills from 0 to 100 min of LaNt α31-GFP (upper panels) and LM β3-mCherry (middle panels). Bottom panels, merged images of LaNt α31 (pseudocoloured green) and LM β3 (pseudocoloured magenta). (B) Maximum intensity projection of entire 16h timecourse images. Scale bars = 20 μm.

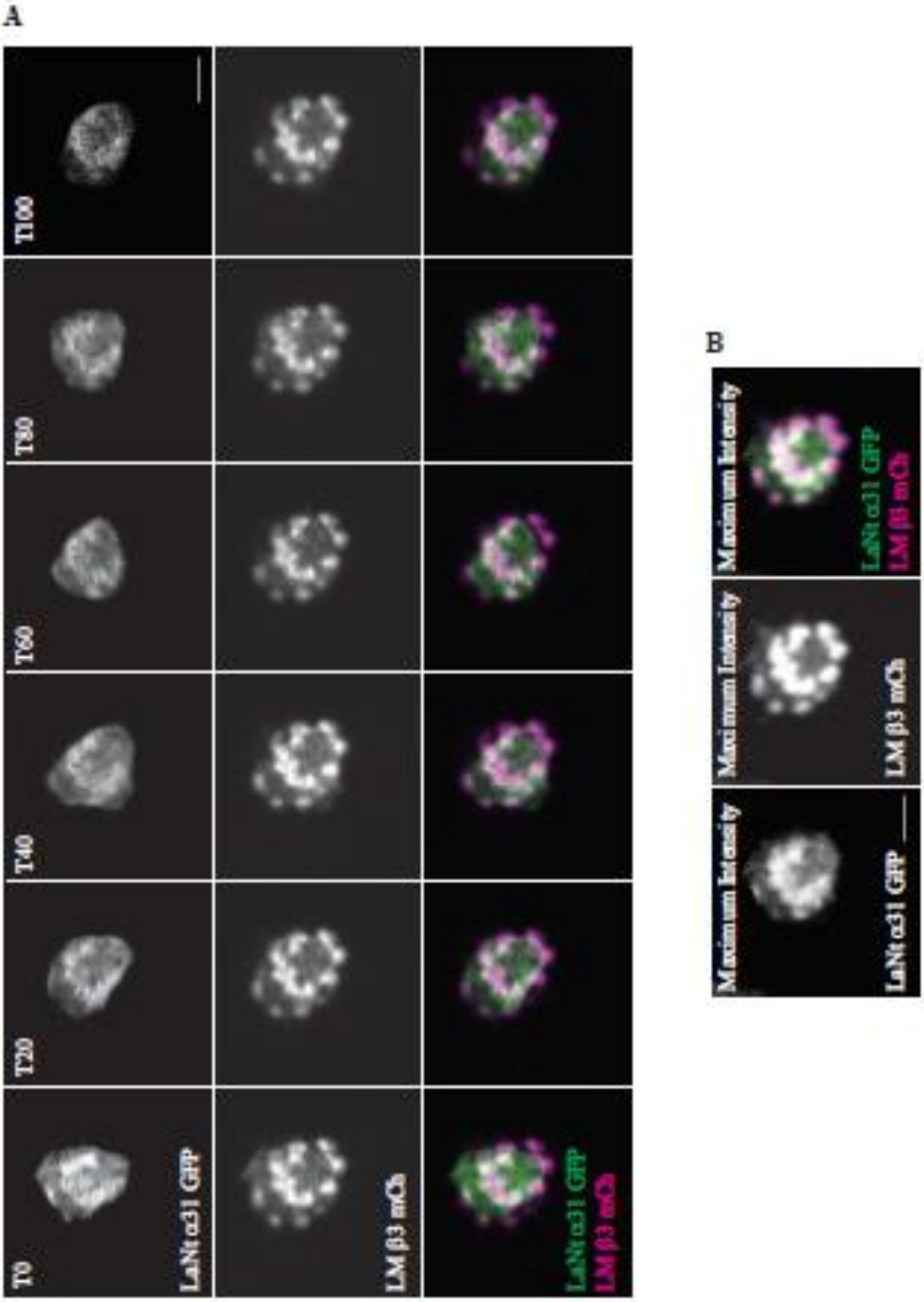

Fig. 3.20: LaNt α31 rapidly form and disassembles clusters on top of LM β3.
hTCEpi doubly transduced with LaNt α31-GFP and LM β3-mCherry were plated overnight on uncoated glass-bottomed dishes and imaged by confocal microscopy every 20 min over 16h. (A) Representative stills from 0 to 100 min of LaNt α31-GFP (upper panels) and LM β3-mCherry (middle panels). Bottom panels, merged images of LaNt α31 (pseudocoloured green) and LM β3 (pseudocoloured magenta).
(B) Maximum intensity projection of entire 16h timecourse images.
Scale bars = 20 μm.

3.13 Proximity Ligation Assay reports that LaNt α31 is spatially close to LM γ2 chain

To provide finer resolution regarding the potential co-distribution data and the LaNt α31-LM specific interaction, we next performed a Proximity Ligation Assay (PLA). PLA is a relatively recent technique with the power of detecting single protein events, such as protein-protein interactions and/or modifications in tissue and cell samples prepared for microscopy [498], with the signal visualised as an individual fluorescent dot.

hTCEpi were, first, processed for indirect immunofluorescence and probed with antibodies against LM γ2, β_4 integrin or solely the secondary rabbit-Rho or mouse-FITC conjugated secondary antibodies as controls. This analysis showed that LaNt α31 appears to co-localise with LM332 and β_4 integrin at the cell periphery (Fig. 3.21A).

hTCEpi were, then, processed for in-situ PLA and probed with antibodies against LM γ2, β_4 integrin or solely the Duolink® secondary probes as controls. The PLA showed that LaNt α31 protein is in close proximity to LM γ2 chain (Fig. 3.21B) at physiological expression levels. As the theoretical maximum distance between two target proteins for the PLA signal to be produced is 40 nm [498], this assay also gives us an idea of the LaNt α31 and LM spatial localisation in hTCEpi cells.

A

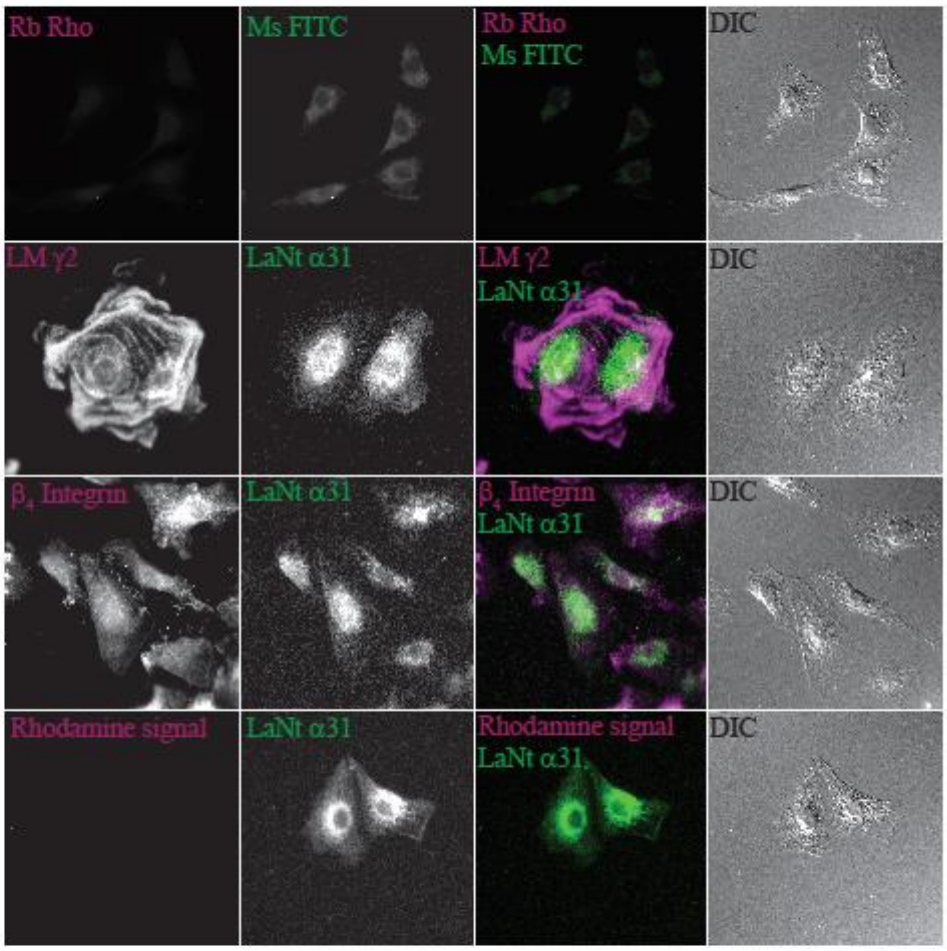
Rb Rho
Ms FITC
Rb Rho
Ms FITC
DIC
LM γ2
LaNt α31
LM γ2
LaNt α31
DIC
β4 Integrin
LaNt α31
β4 Integrin
LaNt α31
DIC
Rhodamine signal
LaNt α31
Rhodamine signal
LaNt α31
DIC

B

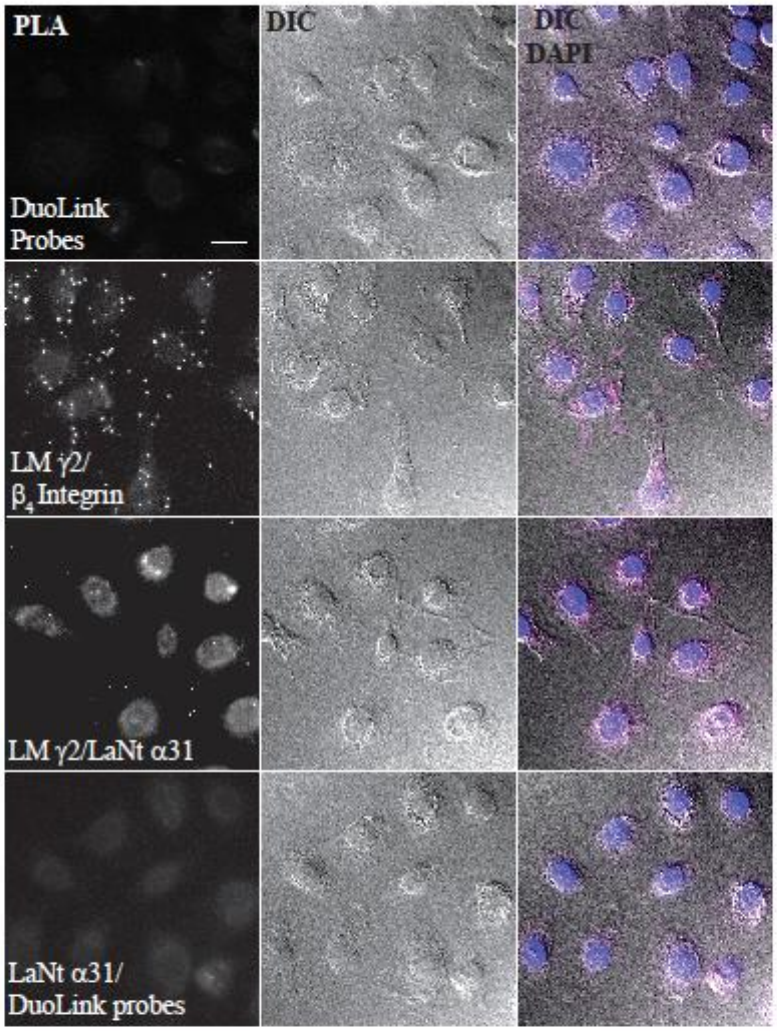

Fig. 3.21: PLA assay shows that LaNt α31 is spatially close to LM γ2 chain. (A) hTCEpi cells were cultured on glass converslips, fixed after 24h and then processed for indirect immunofluorescence microscopy using antibodies against LM γ2, LaNt α31 and β_4 integrin or Rb Rhodamine and Ms FITC-conjugated secondary antibodies. (B) hTCEpi cells were cultured on glass converslips, fixed after 24h and then processed for PLA using antibodies against LM γ2, LaNt α31 and β_4 integrin or Duolink® Orange secondary probes, following manufacturer's recommendations. LM γ2 and β_4 integrin co-staining used as positive control for co-localisation; LaNt α31 and Duolink® Orange secondary probes co-staining used as a control for secondary probes non-specific staining. Signal detected using a Zeiss ApoTome.2 fluorescence microscope. Scale bars = 20 μm.

3.14 LaNt α31 is also spatially close to actinin α4

Actinin α4 regulates skin cell migration rate via modulation of the main cell-matrix adhesion devices [499, 500]. Moreover, Col type XVII may form a complex with actinin α4 in keratinocytes, modulating actin dynamics and, therefore, cell movement [499]. Having observed an alteration in HDs and FAs when LaNt α31 is overexpressed, we decided to analyse the localisation of actinin α4 in relation to LaNt α31. Immunofluorescence showed that actinin α4 and LaNt α31 co-localise at edge of the cells (Fig. 3.22A) and PLA results revealed a close proximity between these two proteins in the same position (Fig. 3.22B). Even if these results are quite preliminary, actinin α4 co-localisation with LaNt α31 may suggest, for the latter, the function of scaffold for Col type XVII during lamellipodial formation.

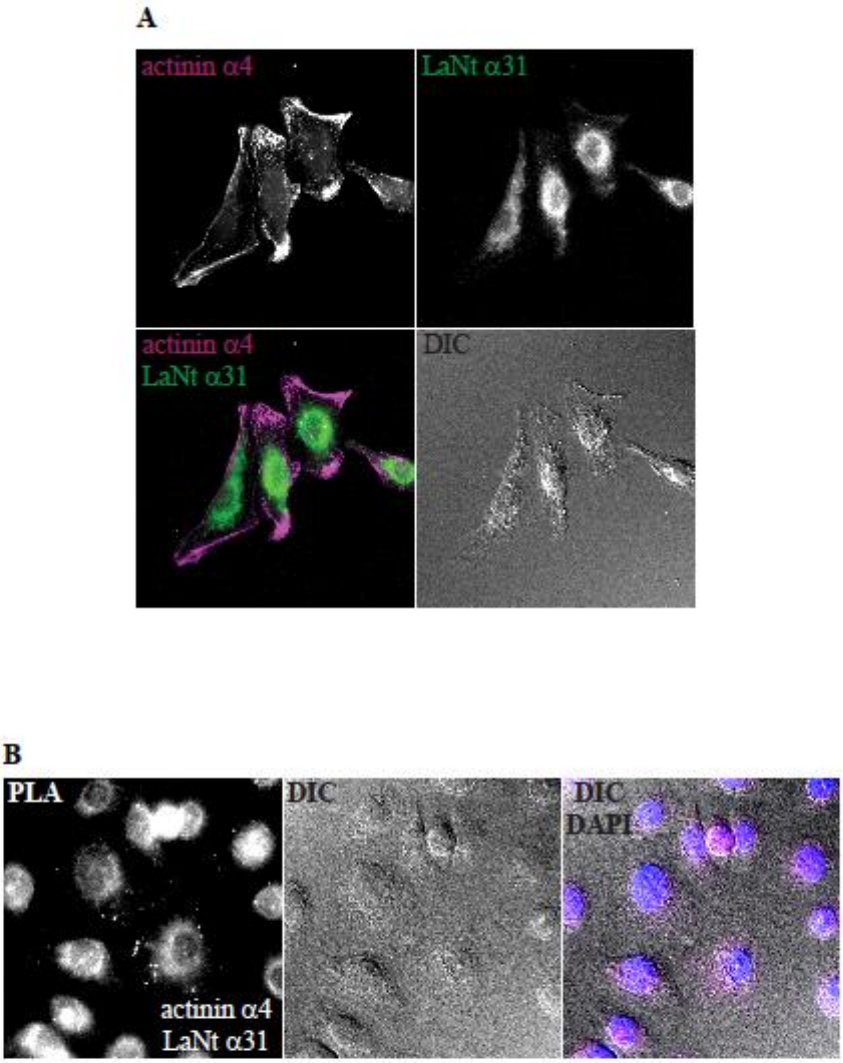

Fig. 3.22: PLA assay shows that LaNt α31 is spatially close to actinin α4. (A) hTCEpi cells were cultured on glass converslips, fixed after 24h and then processed for indirect immunofluorescence microscopy using antibodies against actinin α4 and LaNt α31. (B) hTCEpi cells were cultured on glass converslips, fixed after 24h and then processed for PLA using antibodies against actinin α4 and LaNt α31 with Duolink® Orange secondary probes, following manufacturer's recommendations. Signal detected using a Zeiss ApoTome.2 fluorescence microscope. Scale bars = 20 µm.

3.15 LM β3 precipitates along with LaNt α31

In the ECM derived from hTCEpi doubly transduced with the LaNt α31-GFP and LM β3-mCherry constructs, the GFP and mCherry signals were largely co-distributed (Fig. 3.7D), while PLA suggested co-localisation with LM γ2 (Fig 3.21B). To determine whether LaNt α31 and LM β3 associate together into a complex, we performed an IP experiment using covalently conjugated anti-GFP beads and lysates derived from +LaNt α31 and +GFP hTCEpi. We, then, blotted the immunoprecipitated proteins with antibodies against LM β3 and GFP (Fig. 3.23A), revealing that LM β3 precipitates along with LaNt α31 only, as it is not pulled down with GFP. These data indicate that LM β3 (therefore LM332) and LaNt α31 form a complex, either directly or indirectly.

3.16 LaNt α31 is observed in the LM111 polymer fraction in LM polymerisation assays

All the described data are consistent with a specific interaction between LaNt α31 and LM, possibly during early matrix assembly. As the latter starts with a LM polymerisation process, and the role of LN domains in the LM matrix assembly is well-established [151, 162, 501], we hypothesised a potential for involvement of the LaNt α31 α-LN domain during the LM polymerisation. To investigate this possibility, we used the well-established LM polymerisation assay [164] that involved incubating for 3h at 37°C LM111 from EHS tumour, along with $CaCl_2$ or EDTA as a negative control. In these experiments, polymerised LM is then pelleted by centrifugation and comparison between pellet and supernatant fractions indicates level of polymer formed. In our experiment, we added purified recombinant LaNt

α31 generated either from pSecTag plasmid (pSec) or V5 plasmid (V5) and purified by either affinity chromatography (AC) or gel filtration (GF).

Silver stain of the insoluble and polymer fractions, separated by SDS PAGE, revealed a proportion of LM111 in the pellet fraction in positive control reactions ($CaCl_2$, Fig. 3.23B). LM111 polymerisation is reported as being dependent on calcium ions [162] and, consistent with this, no band was observed in the EDTA pellet (EDTA, Fig 3.23B). Moreover, the polymer fraction appeared increased if compared to the insoluble fraction in the presence of LaNt α31, as if LaNt α31 induces higher proportion of polymer to be formed. Since the polymerisation assay was not fully optimised, we cannot assume this hypothesis to be true; nevertheless, what was very clear is the presence, within the LM polymer fraction of the +LaNt α31 lanes, of a band of ~50-60 kDa, consistent with molecular weight of LaNt α31, suggesting the latter to associate with the LM111 polymer (Fig. 3.23B).

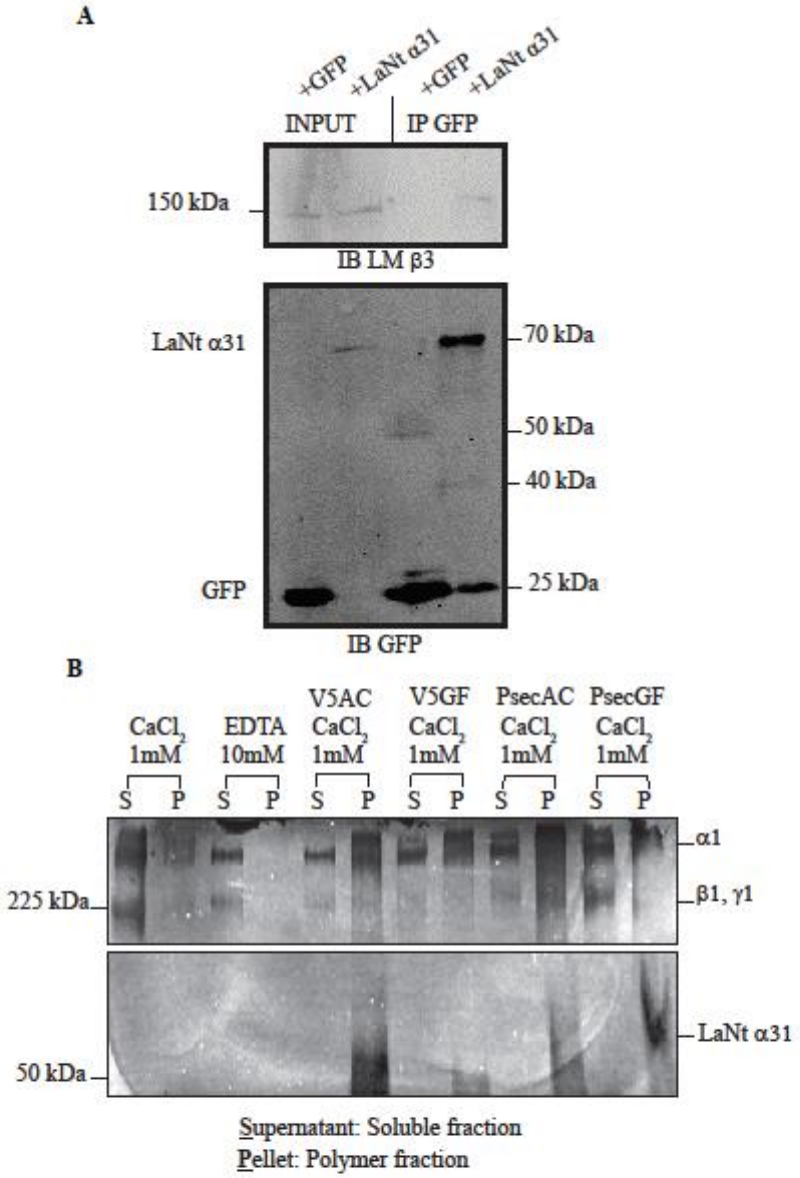

Fig. 3.23: LM β3 is precipitated along with LaNt α31 and LaNt α31 is observed in the LM111 polymer fraction.
(A) GFP and LaNt α31-GFP were immunoprecipitated from +GFP hTCEpi or +LaNt α31 hTCEpi. Input lysates equivalent to 8% of the total IP volume (left 2 lanes) and anti-GFP pull down lanes were immunoblotted with antibodies against LM β3 (upper panel) or GFP (lower panel). (B) LM111 polymerisation assay in presence of exogenous LaNt α31, either cloned into pSecTag plasmid (pSec) or V5 plasmid (V5), and purified by affinity chromatography (AC) or gel filtration (GF). Samples were centrifuged for 15 min at 11,000 rpm; supernatants and pellets were incubated overnight at 4°C with 10 mM EDTA. Soluble and polymer fractions were separated on a 7.5% polyacrilamide gel and silver stained.

3.17 Exogenously added LaNt α31 influences the ability of hTCEpi to attach to LM111

According to the polymerisation assay results, LaNt α31 protein may interact with laminin during the polymer formation steps. Laminin polymerisation is an essential process for the formation of a functional BM [502]; therefore, we wanted to determine whether hTCEpi cell adhesion to LM111 or FN was compromised in the presence of exogenously added LaNt α31. To do so, we used the rapid cell attachment assay described in section 2.1.10. LaNt α31 was added to the LM111 or collagen type IV coating solutions at either 0.02 μg/ml or 0.1 μg/ml, together with 1 mM $CaCl_2$ or EDTA, and FN was used as a positive control at a concentration of 10 μg/ml. A significant decrease in the hTCEpi cell attachment to LM111 + $CaCl_2$ coating was observed with the exogenous addition of LaNt α31 0.1 μg/ml (Fig. 3.24A, 30% less attachment, $p < 0.05$, compared to LM111 in absence of LaNt α31). Moreover, cell attachment to LM111 was reduced in the presence of EDTA (Fig. 3.24B, 20% less attachment, $p < 0.05$, compared to the presence of $CaCl_2$) but not when exogenous LaNt α31 was added to the coating solution (Fig. 3.24B). Attachment rate of cells to collagen type IV was not affected (Fig. 3.24C). These data indicate a laminin and calcium specific inhibition of cell adhesion.

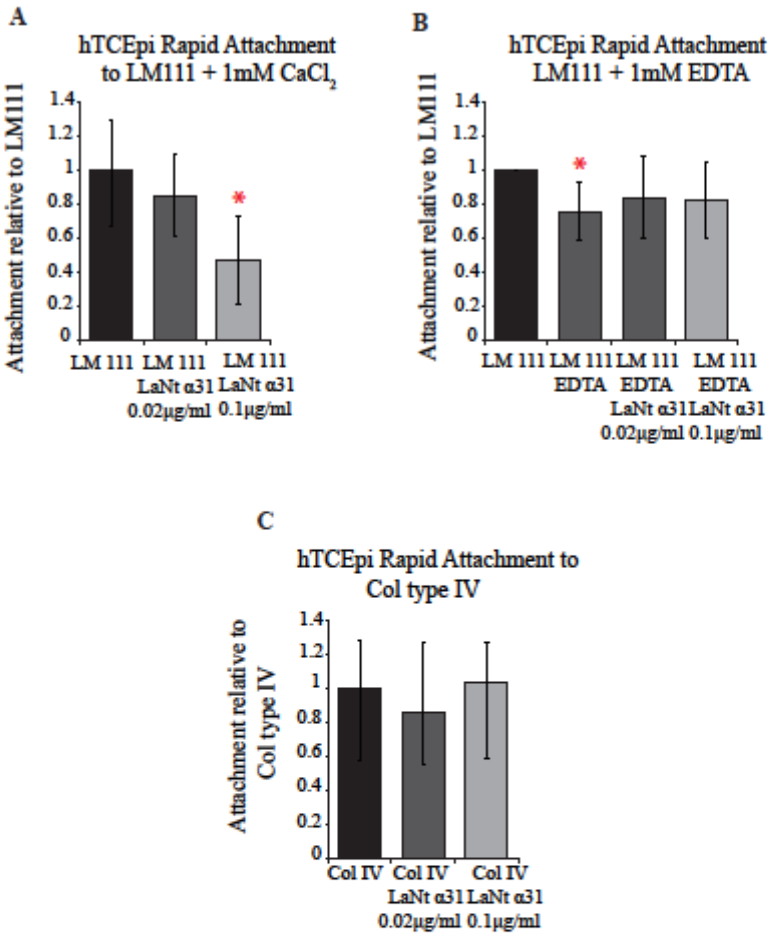

Fig. 3.24: hTCEpi rapid attachment to LM111, but not to Col type IV, is decreased in the presence of exogenously added LaNt α31.
In (A), (B) and (C) wells were coated with indicated proteins combinations for 2h at 37°C. After blocking with BSA, cells were plated onto the prepared substrates and incubated at 37°C for 1h; attached cells were fixed, stained with crystal violet and absorbance read at 570 nm. Plates values were normalised to the ECM protein alone and plotted as mean +/- s.d. from 3 independent experiments, 3 replicates per condition per assay. In (A), * denotes significant difference from LM111 alone ($p < 0.05$) as determined by one way ANOVA and Tukey's post hoc analysis.

3.18 Exogenously added netrin 1 or 4 do not affect hTCEpi attachment to LM111

The LaNt structure, characterised by a LM N-terminal domain followed by a short stretch of LM-EGF repeats, resembles that of the netrins, proteins involved in the axonal guidance cues [503]. Previously shown rapid attachment assays revealed a decrease in hTCEpi adhesion to LM111 in the presence of exogenous LaNt α31, 0.1 μg/ml. As LaNts and netrins are structurally related, we also wanted to study any possible effect on cell attachment due to interactions between ECM proteins and key netrins 1 and 4. Rapid adhesion assays were set up as previously described and revealed that hTCEpi cell attachment to LM111 is not affected by the presence of exogenously added netrin 1 or netrin 4, either 0.02 μg/ml or 0.1 μg/ml (Fig. 3.25), strengthening the already hypothesised LaNt α31-laminin specific interaction.

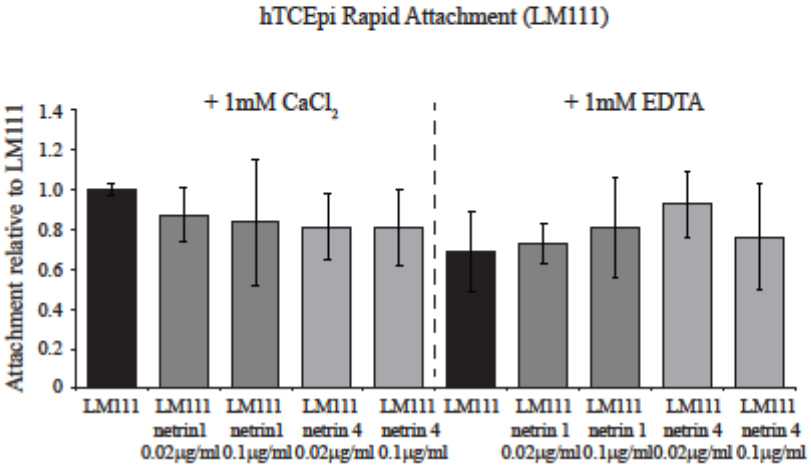

Fig. 3.25: Exogenously added netrins 1 or 4 have no effects on hTCEpi rapid attachment to LM111.
Wells were coated with indicated proteins combinations for two hours at 37°C. After blocking with BSA, cells were plated onto the prepared substrates and incubated at 37°C for 1h; attached cells were fixed, stained with crystal violet and absorbance read at 570 nm. Absorbance values are normalised to the ECM protein alone and plotted as mean +/- s.d. from 3 independent experiments, 3 replicates per condition per assay. Statistical analysis was performed using one way ANOVA and Tukey's post hoc analysis.

3.19 LaNt α31 overexpression effects on pCEC cells behaviour mirror those observed in hTCEpi

The results described so far highlight a very interesting modulatory role for LaNt α31 in corneal epithelial cell behaviour. However, all the data were obtained using an immortalised cell line. We, therefore, wanted to confirm some of our key findings in directly isolated primary corneal keratinocytes (pCEC) isolated from human limbal explants according to a slightly modified version of a previously published protocol [504].

First, isolated pCEC cells were characterised using the corneal marker Keratin 12 (Appendix, fig.4), to exclude contamination with fibroblasts or other cell types derived from the human explants [227, 505]. Next, we analysed the morphology of wild type compared to adenovirally transduced to overexpress LaNt α31 (+LaNt α31) or GFP (+GFP) pCEC cells (Fig. 3.26A). As for hTCEpi, +LaNt α31 pCECs displayed significantly increased 2D area compared to controls (Fig. 3.26B, +LaNt α31 2716±720 μm² vs pCEC 1232±377 μm² and +GFP 1277±283 μm², $p < 0.05$), whereas no difference was observed in cell aspect ratio (Fig. 3.26C).

pCEC cells were also used to perform low-density motility assays (Fig. 3.27A,B). Again, these assays showed that +LaNt α31 pCECs are characterised by a decreased migration speed compared to controls (Fig. 3.27C, +LaNt α31 0.46 ±0.14 μm/min vs pCEC 0.91±0.14 μm/min and +GFP 0.77±0.04 μm/min, average values for all the donors, $p< 0.05$) whereas no difference was observed in cell processivity (Fig. 3.27D).

Laminin organisational studies confirmed the presence of an alteration in laminin pattern deposition when cells are seeded at low density for a short period of time (Fig. 3.28A). pCEC, +LaNt α31 and +GFP pCEC cells, seeded at low density for 5h, displayed a tighter LM β3 cluster area (Fig. 3.28B, +LaNt α31 101±32 μm/min vs pCEC 233±86 μm/min and +GFP 238±133 μm/min) than when seeded at high density for 24h (Fig. 3.28B, +LaNt α31 352±132 μm/min vs pCEC 357±158 μm/min and +GFP 358±145 μm/min). Results showed no differences in pCEC cells characteristics and behaviour compared to the hTCEpi cell line. Together, these data support the reliability of our findings in hTCEpi cells as being truly reflective of limbal-derived corneal cell behaviour.

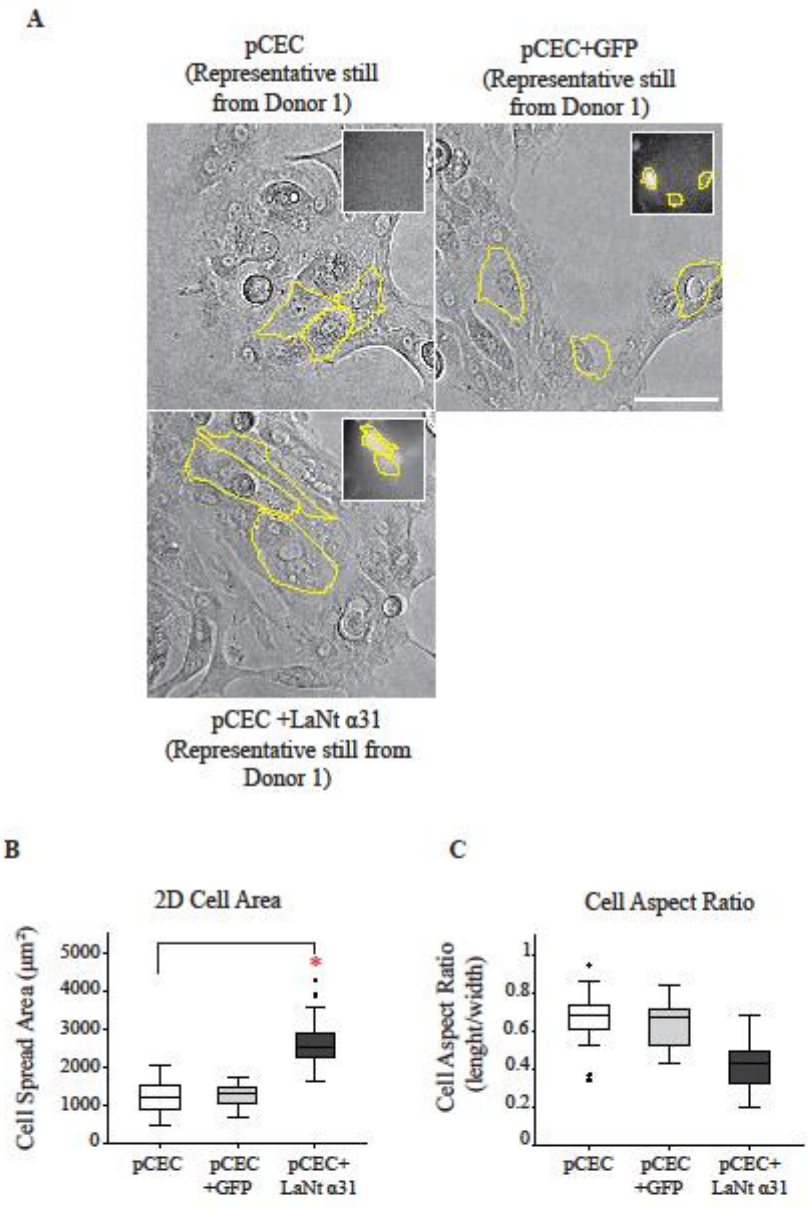

Fig. 3.26: LaNt α31 overexpressing pCECs display increased 2D area. pCEC cells were grown from limbal explants on uncoated tissue culture plastic, and either untreated or transduced with GFP (+GFP) or LaNt α31-GFP (+LaNt α31). (A) Representative images of each cell type were taken using a Nikon TiE epifluorescence microscope. Insets show images of the GFP signal. Yellow lines highlight the perimeter of cells with increased 2D area. (B) 2D cell area; (C) cell aspect ratio measured as width at widest point / length at longest point. In (B), * denotes significant
differences between +LaNt α31 and all controls, $p<0.05$ as determined by one way

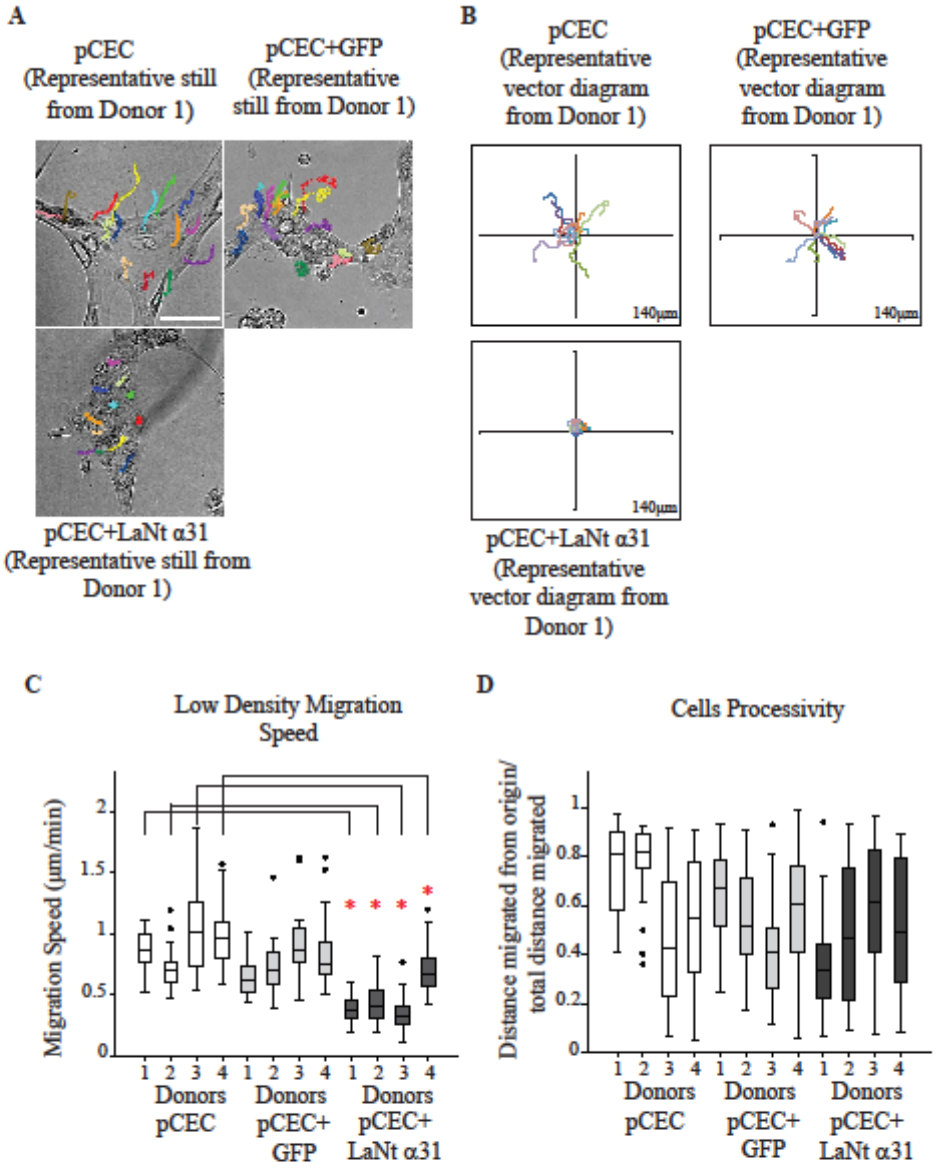

Fig. 3.27: LaNt α31 overexpression leads to a decrease in pCEC cells motility speed. pCEC, +GFP and +LaNt α31 pCECs were plated at low density and migration paths of individual cells tracked over a 2h period. (A) Representative stills of pCEC cells, isolated from Donor 1, showing the total distance migrated, analysed with ImageJ MTrackJ plugin. Scale bar = 100 μm. (B) Representative vector diagrams from Donor 1, showing motility paths of 10 individual cells with each colour representing a single cell. (C) Migration speed of individual eye donors, measured over a 2h period of time, as total distance migrated over time. (D) Migration processivity of individual eye donors, measured as maximum linear distance migrated over total distance migrated. In (C), * denotes significant differences between +LaNt α31 and all controls, $p<0.05$ as determined by one way ANOVA followed by Tukey's post-hoc analysis.

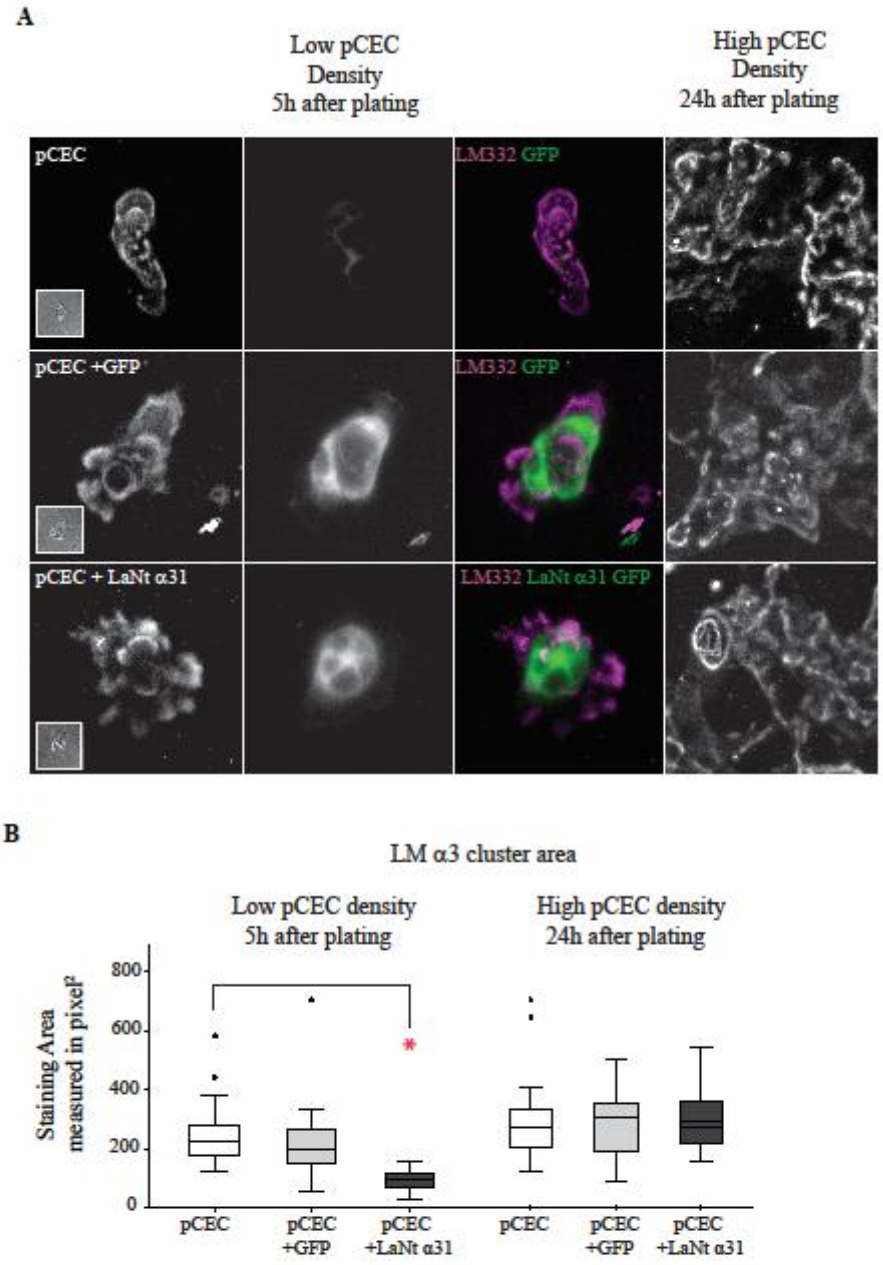

Fig. 3.28: Overexpressed LaNt α31 changes LM organisation in pCEC cells.
(A) pCEC, +GFP or +LaNt α31 pCEC cells were seeded at low (left panels) or high (right panels) density on conditioned media pre-coated glass coverslips, then processed for immunofluorescence microscopy using antibodies against LM α3, after 5h (left panels) or 24h (right panels). (B) LM α3 cluster area was measured, n=23 measurements per cell type. In (B), * denotes significant differences between +LaNt α31 and all controls, $p<0.05$ as determined by one way ANOVA followed by Tukey's post-hoc analysis.
Scale bar = 20 μm.

DISCUSSION

3a.0 hTCEpi functional assays data summary

The results presented in this chapter support a regulatory role for the laminin-derived protein LaNt α31 on corneal epithelial cell behaviour. Specifically, these data demonstrate that hTCEpi or pCEC cells overexpressing LaNt α31 show impairment in cell motility, spreading and attachment to LM111 compared to controls. Furthermore, LaNt α31 overexpressing hTCEpi are characterised by mislocalisation of focal adhesion's proteins, an early maturation of hemidesmosomes and by forming a matrix with laminin organisational changes. Live analysis of protein deposition indicate that LaNt α31 is deposited alongside LM β3; PLA results give further support to this idea, showing that they are in close proximity, and IP studies demonstrate that LaNt α31 and LM β3 are capable of associating into a complex.

There could be several interpretations of the described results, and I will address them in turn.

Interpretation 1. LaNt α31 influences LM network assembly

The major structural feature of the LaNt α31 protein, in terms of conserved domains, is the LN domain, a region well-established as being the structural domain involved in LM-to-LM interaction and LM polymerisation [162]. Our data support a model where LaNt α31 binding to LMs influences the assembly and interactions of the LMs themselves in the corneal epithelial ECM, resulting in the observed functional effects [153, 162, 164, 506].

LM polymerisation happens in a two-step process: first β and γ LN domains interact to form a relatively short-lived and unstable βγ dimer, second the α LN domain is incorporated in a slower, calcium-dependent manner to form a more stable αβγ ternary node of three LN domains [146, 507]. The presence of an α-chain LN domain in LaNt α31 could either stabilise transient βγ LN interactions or compete for binding sites where αβγ interactions are occurring, depending on when the LaNt α31 was added, which other LN domains were present and how they were assembled at that time. Therefore, LaNt α31 effects would depend on the interaction status of LMs in the matrix and on which LMs are present, in terms of how many LN domains they have.

Taking the adhesion assays to LM111 first, our data show that, when hTCEpi cells overexpressing LaNt α31 are exposed to a LM111 coating, their adhesion decreases compared to controls. In these assays, the LM111 coating was prepared in conditions that support LM polymerisation, so this result suggests that competition could exist between LaNt α31 α-LN domain and the α1 chain-LN domain in the assembled network, which would cause disruption of the formed ECM. The hypothesis of LM network status influencing cell behaviour is supported by studies using polyLM, a biomimetic polymerised LM assembled on pH acidification; rat retinal cells exhibit normal spreading and neurite outgrowth when cultured on polyLM as opposed to non-polymerised LM, which instead induced cell clustering [508].

The assays where LaNt α31 was exogenously added also displayed LM specific effects. In this case, taking the *in-vitro* polymerisation and adhesion data together, there may be a slightly different interpretation. Our data show that, when LM111 is incubated with LaNt α31, the LaNt is observed in the LM111 polymer fraction, suggesting LaNt α31 as part of the LM polymer. It should be noted that this assay is

quite crude, in that the "polymer" fraction may actually be an unstructured aggregate rather than a true polymer. Our adhesion data show decreased adhesion to the LM111 in the presence of LaNt α31, suggesting that the "polymer" formed is inferior as a substrate; again, this is in keeping with the data showing LM network assembly status influences cell behaviour.

Our data showing LaNt α31 incorporation into the LM111 polymer fraction was, actually, somewhat surprising. Previous data analysing netrin 4 in a similar experiment, demonstrated that rather than be incorporated into the polymer, the netrin 4 addition led to inhibition of LM111 polymerisation [471]. Moreover, netrin 4, due to its nanomolar binding to the LM γ1 chain, not only blocks LM polymerisation but also disrupts pre-existing LM network [474]. As LaNt α31 and netrin 4 are characterised by a very similar structure (LN domain followed by LE repeats), we might expect LaNt α31 to have the same effect as netrin 4. Beside our polymerisation assay data, the presence of exogenously added netrin 1 or 4 does not affect hTCEpi attachment to LM111, suggesting that LaNt α31 and netrins act differently.

Most of the cell work within this chapter has been carried out using hTCEpi, a limbal-derived corneal epithelial cell line. The corneal BM is characterised by a LM332-rich matrix, with small amounts of LM511 [53, 226, 231, 509, 510]. Unlike LM111, LM332 only contains a single LN domain on the β3 chain and polymerisation assay data show that LM332 does not self-polymerise or co-aggregate with LM111 [164]. Nevertheless, LM332-rich BMs function properly; perhaps, the presence of small amounts of LM α5, β1, and γ1 chains in corneal epithelia is sufficient to establish a weak interaction [226, 231] which could be, then, either stabilised or strengthened by the LaNt α31 α LN domain. It would be, at this

point, particularly interesting to study the interaction between LaNt α31 and LMs other than LM332, to better understand weather the LaNt α LN domain specifically interacts with LM332 only or can associate with different LM isoforms.

Numerous studies support the hypothesis that structural alterations of LM332 in the BM lead to defective cell adhesion and migration. It has been reported that primary keratinocytes, isolated from Herlitz JEB patients, show a significantly reduced cell-substrate adhesion and impaired migratory efficiency due to LM332 mutations [511] and a targeted disruption of LM332 in mouse keratinocytes blocks cell adhesion and inhibits migration of keratinocytes in response to EGF [512]. As with our data demonstrating rescue of the LaNt overexpressing cell phenotype by preformed matrix, it has been described that Herlitz JEB keratinocytes, which do not produce LM332, are able to adhere and migrate normally on exogenously supplied LM332 [513]. Moreover, our data demonstrate no major issues within the cellular motility machinery in overexpressing cells, supporting the premise that it is in the matrix assembly steps where the problem lies, rather than either in the cells or the matrix (at least in terms of heavily plated cells) themselves.

Specifically looking at the matrix deposited by LaNt α31 overexpressing cells, our data show that, 5h after seeding, hTCEpi cells deposit LM332 in tight clusters. Numerous studies indicate that LM deposition is modulated by cell-surface receptors, including integrins $\alpha_3\beta_1$ [417, 514] and $\alpha_6\beta_4$ [353]; the potential roles for these interactions in the observed phenotype will be described below.

Questions remain as to why the cell motility and LM organisation defects are rescued on a fully formed matrix. The answer may simply be that the relatively increased LM coverage, derived from the increased cell density, masks any organisational

difference and provides a suitably extensive network to support normal migration. Consistent with a masking effect, it has been shown in epidermal keratinocytes with different colour tagged-LMs, that when cells are presented with a preformed, cell-derived matrix they adhere to and use that matrix rather than elaborate their own [486]. The masking of organisational differences may be exacerbated by our experiments being performed on glass or tissue culture plastic, where the LM is directly adsorbed onto the substrate and, therefore, any influence on preformed LM networks is minimised. Future *in-vivo* studies and use of 3D tissue equivalent models will help to address these questions.

Interpretation 1 is summarised in the following schematic diagram:

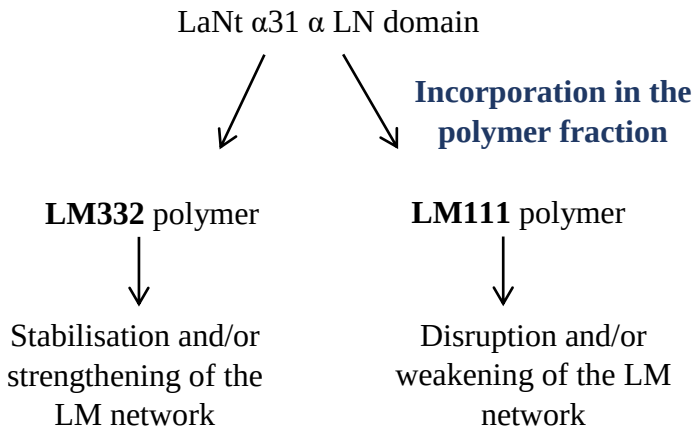

Interpretation 2. LaNt α31-cell surface receptor interactions affect matrix assembly

An alternate hypothesis that can be supported by the data is that, rather than the LaNt α31 *directly* competing for or stabilising LN-LN domain interactions, it instead *indirectly* influences these interactions by competing for LM receptor binding sites. This hypothesis is based on a number of studies that demonstrated binding to cell

surface receptors is a necessary first step for LM111 polymerisation and matrix formation in breast epithelial and ES cells, and for LM211 deposition and assembly in Schwann cells [157, 158, 515-519].

The strongest receptor binding sites in LMs are located in the LG domains [520], however cell surface receptor binding capabilities have been described for some LN domains as well, including LM α3b [148, 149, 521, 522]. In this model, when initially deposited and, therefore, at low concentration, LMs are orientated parallel to the bottom of the cell, with both the LN and LG domains interacting with surface receptors. As the LM concentration increases over time, the LG domains' superior receptor affinities outcompete the LN domains, in turn driving reorientation of the LM and tighter clustering of the receptors (Fig. 3.29), which ultimately support activities such as HD assembly. Moreover, the reorientation of the LMs would position the LN domains into close proximity, and at sufficiently high local concentration, to allow LN-LN interactions to begin.

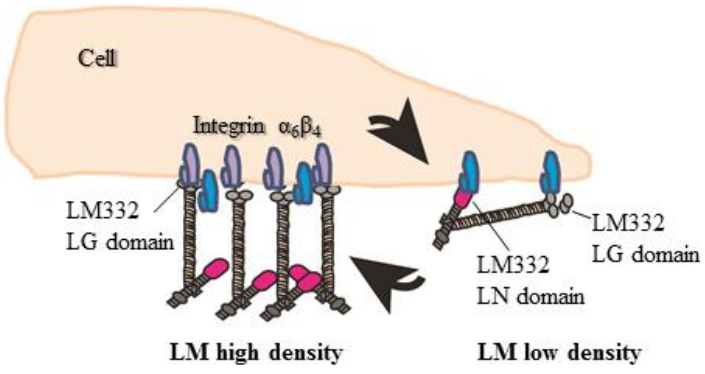

Fig. 3.29: LM LG and LN domains may compete for receptor binding sites on the base of the LM density in the ECM.

Schematic diagram showing the possible competition between LM LG domain and LM LN domain for integrin binding.

Within this model, when overexpressed in hTCEpi cells, LaNt α31 would compete with LN domain interactions for receptor binding, meaning earlier reorientation of the LM332, potentially earlier receptor and LM cluster formation and, therefore, earlier HD assembly/maturation, all of which fit our observations.

In addition, as LM332 density increases, the LG domains would outcompete the LaNt α LN domain-receptor interactions. On this basis, once sufficiently high LM332 density is reached, there would be no appreciable difference between the matrixes assembled by normal and LaNt overexpressing cells, as summarised in the following schematic diagram.

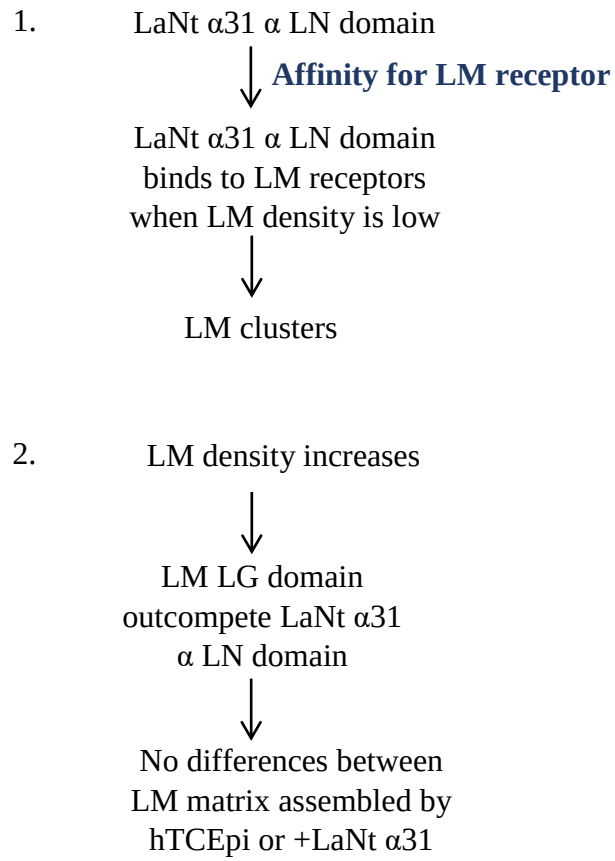

This is exactly what we observed in the high cell density, longer attachment experiments and it is consistent with the motility defects' rescue observed after supplying hTCEpi with a preformed cell-derived ECM.

It is possible that both interpretations 1 and 2 are contributing. Our live experiments demonstrate that LaNt α31 and LM β3, as far as we can resolve, are deposited together, both spatially and temporally, suggesting their initial assembly points are close together rather than the two proteins being independently secreted and subsequently organised. Moreover, the *in-vitro* polymerisation data support a direct influence of LaNt α31 on LM111 polymerisation that is not dependent on surface receptors. Determining whether LaNt α31 is exerting its effect through LN network nucleation, via a more general stabilisation of LN interactions or a combination of both mechanisms are complex questions, which will form an interesting future research direction. Specifically, it would be novel to induce the overexpression of the two proteins using a photo-switchable fluorescent probe, enabling the use of super-resolution microscopy imaging to clarify the proteins deposition time, proximity and at which point the LaNt α31 binds to and stabilises nascent LN-LN interactions.

If the LaNts bind to cell surface receptors, an important next step is to identify which receptors are involved and their relative binding affinities. Of course, if LaNt do bind to receptors, the observed phenotypic effects could be directly due to these interactions and this will be discussed in the interpretation 3.

Interpretation 3. Cell phenotypes are dependent on LaNt α31 affecting FAs and HDs assembly

We have described that hTCEpi overexpressing LaNt α31 present with mislocalisation of FAs and premature HDs maturation, in the form of early Col type XVII recruitment. Changes to FAs and HDs are intimately associated with the other aspects of the observed cellular phenotype, adhesion and migration; therefore, it is tempting to speculate that the observed cell behaviour is due to LaNt α31 effects on these two critical cell-matrix adhesive devices. These effects could be indirect, via the matrix changes described above, or direct, on components of either complexes. I will consider each of these scenarios in turn.

LaNt α31 indirect effect on HDs / FAs

The LM organisational changes, observed in the LaNt α31 overexpressing cells, could explain the differences observed in HDs maturation and FAs localisation. Previously, it has been shown that the human epidermal carcinoma line SCC12, which normally does not assemble HDs in vitro, assemble mature HDs when cultured on 804G cell-derived matrix [483]. It has also been reported that the recruitment of different FA components changes according to how cells adhere to LM111 or LM332 [452]. A very interesting study revealed that disruption, removal or inhibition of LM332 disrupts the LM332-integrin-CD151-FAK network, affecting the human ErbB2+ breast cancer cells' drug sensitivity [523]. Therefore, it would not be surprising for the altered LM pattern observed in LaNt α31 overexpressing cells to be the driving force behind both the FAs and HDs changes; put simply, if you change the LMs, you change the LM-receptor complexes.

LaNt α31 direct effect on HDs

To have a direct effect on HD assembly/localisation and maturation, LaNt α31 would need to be capable of directly binding one or more of the HD components. Although we have not extensively tested this hypothesis in the course of these studies, some of our data combined with published work suggest this could be a possibility.

As already mentioned before, it is predicted that LaNts resemble netrin proteins [461] and this similarity could lead one to believe that, in some circumstances, they also share some roles. Previously published studies revealed that netrin 1 is able to interact with $\alpha_6\beta_4$ integrin in developing pancreatic epithelium, regulating pancreatic epithelial cell adhesion and migration [466], and that netrin 4 can bind directly to β_4 integrin [469]. $\alpha_6\beta_4$ integrin is one of the core components of HDs and play a critical role for HD assembly [524]. Indeed, $\alpha_6\beta_4$ integrin-LM332 association triggers HD assembly, as has been demonstrated in several published studies [290, 302, 303, 305-307, 524, 525]. Our live imaging data of LaNt α31 distribution, which identified clustering that resembles HD-like complexes, may support this hypothesis. Considering these data, LaNt α31 may also directly bind $\alpha_6\beta_4$ integrin and nucleate HD assembly, hypothesis supported by peptides studies demonstrating that specific regions of LM α3b LN domain can support cell adhesion directly.

How could LaNt α31/β_4 integrin binding lead to early recruitment of Col type XVII? A hypothesis may be that LaNt α31, by binding to $\alpha_6\beta_4$ integrin, induces a conformational change of the latter, which, then, allows association with other HD components. In simple terms, this could purely be receptor occupancy/ligand density; the Col type XVII recruitment is *early* rather than impaired. The cytoplasmic domain of Col type XVII interacts, among other ligands, with plectin, β_4 [323, 335, 526] and

α_6 integrins [355, 486]; the early recruitment of Col type XVII observed in our study may therefore reflect the alteration of the HD assembly timing and, potentially, of the HD components localisation. It would be interesting to use live imaging to analyse HD maturation in real time.

The observed changes to HDs could explain most of the other phenotypic observations, with the exception of the cross-matrix motility assays. In cultured epithelial cells, HD maturation leads to a decrease in cell motility [237]. This study has elucidated the ability, for epithelial cells, to regulate their own behaviour via inducing changes in their own ECM; by activating an enzymatic pathway, LM332 proteolysis is triggered [237], which then causes HD nucleation and maturation [527].

Col type XVII has also been shown to regulate keratinocyte lamellipodial formation by promoting association between BPAG1e and $\alpha_6\beta_4$ integrin [355], inducing actin remodelling via Rac regulation [355, 500]. However, cells with defects in HD proteins show motility defects related to steering rather than speed, which suggest that the defects observed here are not purely down to HD-related problems.

Despite the apparently solid rationale behind this interpretation of our data one piece of evidence suggests it is unlikely to hold the answer; our PLA experiments suggest that very little, if any, LaNt α31 is close to β_4 integrin. It should be noted that these data represent a snapshot; the PLA is only effectively measured at the time point when we processed the images and our live experiments suggest that interactions, if they occur, are transient. It would, therefore, be interesting to generate a Fluorescence Resonance Energy Transfer (FRET) donor/acceptor pair and perform

live imaging to determine proximity in real time, at different stages of the HD assembly process.

LaNt α31 direct effect on FAs

In addition to HDs, FAs complexes provide additional cell to LM interaction points and are usually the first matrix attachment points to assemble. Again, the structural similarity between LaNts and netrins may be important to explain the decreased hTCEpi cell motility and the mislocalised FAs observed in our study. Netrin 1 has been shown to bind $\alpha_3\beta_1$ integrin, a key FA component on cells attached to LM332 [466], therefore LaNt α31 may be involved in defining FAs localisation/assembly through similar mechanisms as outlined for the HDs.

Many FAs and HDs components share binding sites or localisation; plectin, for instance, may mediate communication between FAs and HDs [528]. It has been shown that HD perturbation affects FA size and movement during re-epithelialisation [529], and it is now known that HDs and FAs' functions can couple and/or interfere, as shown in different types of skin diseases[260]. This means that a FAs and HDs crosstalk may be happening, masking the LaNt α31 to LM direct binding.

LaNt α31 indirect effect on FAs and HDs via actinin α4 interaction

Our PLA data indicate that LaNt α31 is in close proximity (theoretical maximum distance between epitopes = 40nm, [498]) with actinin α4, one of the four actin cross-linking protein isoforms belonging to the spectrin superfamily [425]. It has been presented that actinin α4 localises throughout the lamellipodium [447] and

regulates epithelial cell motility [499]. Furthermore, in cell-cell contacts, actinin α4 interacts with the cytoplasmic domain of Col type XVII [429] and is part of the FAs, where it interacts with β_1 integrin [530]. At FAs, actinin α4 links integrin β_1 to actin [430], but it also interacts with several FA proteins, playing a central role in both FA organisation and signalling [531-533]. If LaNt α31 interacts with actinin α4 or actinin α4 normal function is disrupted by LaNt α31 binding to integrin β_1, the FA complex or the lamellipodia assembly will be impaired, explaining the mislocalisation observed in our study and, potentially, the LM organisation and cell phenotypes.

It has been reported that, in response to binding interactions with actin-associated cytoskeletal proteins, such as α actinin or paxillin, different integrins cluster and become immobilised within FA complexes [534]. When such a clustered binding between ECM, integrins and actin happens, cell adhesion becomes locally stable [535] [536]; this may explain why, in LaNt α31 overexpressing hTCEpi cells, LM appears to be aggregated and enriched in little clumps. Further analyses on the interaction between LaNt α31 and actinin α4, perhaps using IP, label transfer or biophysical approaches like Surface Plasmon Resonance (SPR) or FRET will be extremely useful to explore this aspect.

Interpretation 3 is summarised in the following schematic diagram;

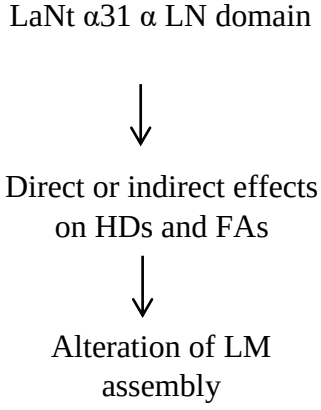

Interpretation 4. LaNt α31 overexpression induces GF release in the extracellular environment

In addition to other functions, the ECM also serves as a reservoir for GFs [537]; the matrix disruption induced by LaNt α31 overexpression could impact the "store and release" dynamics of the GFs reservoir, by altering either the ways in which GFs are stored, the amount of GFs sequestered or their release rate from the ECM. This is highly speculative, but could explain the phenotypes observed and would be a very interesting aspect to be investigated in the future.

Many GFs interact directly with ECM components, which, in turn, dictate cellular responses. For instance, GFs–ECM binding is required for FGF-2 signalling and happens via interaction with HSPGs [538]. In the lens epithelial cells, FGF-2 has been reported to bind to PLC [539, 540]; as PLC binds to LMs in the BM, a LaNt α31-induced LM network disruption could cause FGF-2 to be released. It has also been shown that lens epithelial cell proliferation and differentiation are FGF-concentration dependent processes [541], which, therefore, suggest the cell functions to be altered if GF release is not controlled.

LM disruption could also induce the release of GFs such as morphogens [542], which modulates cell adhesion via enabling traction forces between the cells and the matrix [543]. Furthermore, when these traction-activating adhesion morphogens are released in the extracellular environment, they induce a change in the stiffness and elastic properties of the matrix itself, changes that will affect cell phenotypes, well-established as influenced by the stiffness of the cell substrate [544].

Among the ECM-bound GFs, very important in our scenario is EGF and its interaction with the EGF receptor (EGFR). EGFR, in theory, could be directly bound

to LMs via their EGF-like domains, as shown for the LE domains in the γ2 LM [249]. When activated, EGFR stimulates the activation of several downstream signalling pathways, which regulate cell migration, adhesion and proliferation [545, 546]. If LaNt α31 is disrupting the LM network, more EGF may be released and, therefore, there will be less of it stored by the matrix, leading to changes in cell behaviour. Up to now, we have largely ignored the other structural feature of the LaNts, the LE repeats. This is because data from the Sasaki and Hohenester groups have shown that these regions are required to stabilise the fold of the LN domain, rather than being functional as signalling entities [146, 148]. Unpublished data from our lab show that EGFR distribution across the anterior segment almost precisely mirrors that of LaNt α31, therefore the proteins are in the appropriate location to interact and it may be possible, for the EGFR activity, to be modulated by the presence of LaNt α31 in the ECM. Again, at this point, this is only a speculation; additional experiments, such as IPs or direct binding assays as well as activity assays, are needed to further investigate the possibility of an interaction between EGFR and LaNt α31.

An additional aspect to be considered is the potential crosstalk between integrins and GF released from the ECM when LaNt α31 is overexpressed. Many of the signalling pathways activated by integrins may also be activated after GF stimulation and these molecules could, synergically, coordinate biochemical responses in multiple cell types [293, 547]. In human breast carcinoma cells [548], the association of $\alpha_6\beta_4$ and $\alpha_6\beta_1$ integrins with ErbB-2 receptor, which belongs to the EGFR family and has tyrosine kinase activity, represents one example of GF receptor - integrin crosstalk, particularly interesting for our findings.

Interpretation 4 is summarised in the following schematic diagram;

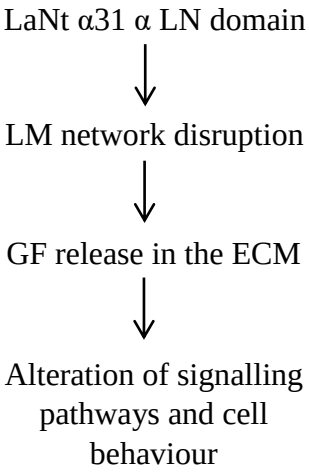

My opinion

Despite the description of multiple potential hypotheses, I believe the most likely interpretation for our data is that the observed effects are due to a LaNt α31 direct effect on LMs, which is then reflected by changes to HD and FA organisation. Supporting this interpretation, our live imaging data show that the LaNt α31 containing clusters are more transient than what described for HDs [261, 355, 495, 499]. Furthermore, we were able to rescue the LaNt α31 overexpressing hTCEpi phenotype through provision of a preformed cell-derived matrix, suggesting the increased LaNt α31 levels do not directly negatively influence cell-matrix interactions. Last but not least, the HD-like complexes assembled by LaNt α31 overexpressing cells appear more mature in terms of recruitment of collagen type XVII, suggesting assembly occurs more effectively rather than being impaired [497]. The organisational state of LM332 specifies cellular migration patterns[353, 461];

indeed, WT skin keratinocytes deposit LM332 in linear tracks and migrate normally, while JEB patient cells deposit LM332 in small circular arrays, which reflect their defective BM assembly and restricted migration [353]. This phenotype is markedly different from the tight clusters we observe in LaNt α31 overexpressing corneal cells. Overall, I think the weight of evidence in this "chicken or egg" scenario is leaning toward the matrix changes being the driving force behind all the other observed differences.

Open Questions

The functional data, although the major focus of this work, still leaves an open question; why is LaNt α31 deposited from HaCaT cells into the BM of the skin, but retained within cultured corneal epithelial cells and in tissue sections? This was interesting and surprising to discover. It is possibly that, in hTCEpi cultured cells, LaNt α31 is secreted but does not efficiently associate with the ECM, due to the lower calcium concentration in their media compared to HaCaTs (0.15 mM vs 2 mM), as calcium concentration mediates LN domain interactions. It would be interesting to deepen this aspect, perhaps by comparing hTCEpi conditioned media to that from HaCaTs and blotting for LaNt α31 to determine if secretion rates are similar. We could perform calcium switch experiments to determine if we culturing hTCEpi in high calcium conditions will increase the LaNt α31-ECM association.

It should also be noted that some proteins can localise both intracellular and extracellular, and can function in different ways on the base of their position [549]. A possible reason behind this is that the protein can coordinate the organisation and

maintenance of a global tissue function. There are data supporting the independent secretion of LM α chains only, whereas the β and γ chains cannot be secreted as monomers and remain intracellular [184]. This may, therefore, indicate ECM coordination exerted by LMs. Other examples are given by HMGB1 [550] and TTG proteins, both of which act in a different way if secreted in the cytoplasm or retained inside the cell [551]. May, therefore, be that LaNt α31 can be secreted or not secreted on the base of the function it has to play? These are open questions and will be interesting subjects for future investigations.

Chapter 4

In-vivo RESULTS

LaNt α31 OVEREXPRESSION INDUCES A LOW OFFSPRING NUMBER *IN-VIVO*

Introduction

The data obtained from our *in-vitro* work suggested a very novel and interesting role for LaNt α31 in corneal epithelium, and highlighted a specific interaction between LaNt α31 and LMs. We, therefore, decided to create a LaNt α31 overexpressing animal model to evaluate any LaNt α31-induced effect *in-vivo*.

This chapter describes the characteristics of the DNA construct injected in the mouse embryos and contains the preliminary data obtained from LaNt α31 overexpression analyses, using tissue samples collected from our animal model.

4.0 Construct features

4.0.1 Human keratin 14 and its promoter

Human Keratin 14 (hK14), encoded by the KRT14 gene, belongs to the type I acidic keratins [552] and is one of the major proteins expressed in mitotically active basal layer cells of skin, together with Keratin 5 (K5) [553]. Early studies revealed that hK14 mRNA is restricted to proliferative cells [554]; as basal cells [555] differentiate, they downregulate transcription of both K5 and K14, inducing new sets of differentiation-specific keratins [553].

The tissue specificity of hK14 is made possible by a 2.2 kb promoter segment [491], previously used to engineer mice for conditional inducible-knockout technology, driving transgene expression in the skin [556], or to gain insights into hair growth regulation [557] as hK14 promoter maintains its activity in adult skin, *in-vitro* and *in-vivo*, and is strongly active in cultured cells [558]. In addition to being highly expressed in skin, hK14 promoter has also been shown to be present in the epithelia

of tongue, mouth, forestomach, trachea, thymus and respiratory and urinary tracts [557].

During development in mouse, K14 promoter drives protein expression as early as E10 in the skin [559], with an optimal expression observed at E14 in the ocular surface epithelium [560, 561]. With regards to the eye, in the developing human cornea, hK14 promoter is highly expressed in the superficial epithelia between 8 and 10 weeks of gestation; at about 12 weeks of gestation it is extensively present in suprabasal and superficial cells [562]. At 20 weeks of gestation, the limbal epithelium was shown to express K14, which then progressively faded to be finally restricted to basal epithelia in the neonatal cornea [562].

In our study, the choice of using hK14 promoter to drive LaNt α31 overexpression *in-vivo* was based on the broad expression of this promoter in different epithelial types and, therefore, on the possibility to maximise LaNt α31 overexpression in the animal models whilst at the same time not globally expressing the transgene as this could be problematic in terms of animal viability and interpretation of obtained data.

4.0.2 Thosea asigna virus-derived 2A peptide sequence (T2A)

The Thosea Asigna virus-derived 2A peptide (T2A), with the sequence EGRGSLLTCGDVEENPGP [563], has also been included in our DNA construct. Linking a protein to T2A, or T2A-like peptide sequences, means a cellular expression of multiple proteins (in essentially equimolar quantities) derived from the same promoter [564], with a continuous translation of the proteins ensured by a ribosomal "skipping" mechanism, an alternate type of translation which prevents the

ribosome from forming a peptide bond between the C-terminal Gly of the 2A sequence and the N-terminal Pro of the downstream peptide, allowing it to continuously translate [565] [566].

4.0.3 Murine Immonoglobulin (Ig) kappa (κ) chain secretory leader sequence (IgK leader sequence)

The efficiency of protein secretion is known to be strongly affected by the signal peptide [567, 568]. In our DNA construct, we decided to include the murine IgK light-chain sequence METDTLLLWVLLLWVPGSTGDJ [569], because it is known to direct the protein fused to its N-terminus to the secretory pathway [570] allowing secretion. Therefore, the presence of the IgK leader sequence gave us a maximised chance of LaNt α31 secretion. In this model, we wanted to study the effect of LaNt α31 overexpression on BM assembly, so limiting the likelihood of having a large build-up of the overexpressed protein within expressing cells was highly desirable.

4.0.4 Myc and 6xHis tags

LaNt α31 encoding transcript cloned into the final vector used for embryonic injection was fused to different protein tags, peptide sequences usually attached to recombinant proteins to allow expression analysis or purification of the protein themselves [571]. We included the Myc tag, derived from the c-myc gene, and the 6xHis tag, consisting of six His residues. Both these protein sequences can be used to study the characteristics of the protein they are linked to, as they can be targeted

using well characterised antibodies. We included these tags to ease detection of the transgene in mouse tissue and provide flexibility for downstream applications.

4.0.5 mCherry fluorophore

mCherry is a monomeric fluorescent protein with a peak of absorption and emission at 587 nm and 610 nm respectively, used as a marker when tagged to proteins and which derives from a protein isolated from *Discosoma sp*. [572]. In our study, we decided to include mCherry in the DNA construct to ensure the possibility of protein expression analysis on embryos and tissues, as well as in live animals. Moreover, mCherry is resistant to photobleaching, is very stable and it matures quickly, allowing the signal visualisation soon after translation [573]. Here, the mCherry was added downstream of the T2A sequence, therefore the mCherry expression would indicate cells where the construct is active rather than directly tagging the protein.

4.1 LaNt α31 overexpressing mouse model construct generation

Different sequential cloning steps were performed to prepare a hK14 promoter-driven LaNt α31 overexpression DNA construct. The following table and Fig. 4.1 summarise each step.

Cloning experiment name	Plasmid obtained
Cloning Step **1**	pGEM®-5Zf(+) - LaNt α31 plasmid
Cloning Step **2**	pUBCmCherry-hK14 promoter plasmid
Cloning Step **3**	pUBCmCherry-hK14 promoter-LaNt α31 plasmid

Table 6: Summary of the DNA cloning steps performed to prepare the hK14 promoter driven-LaNt α31 overexpressing construct.

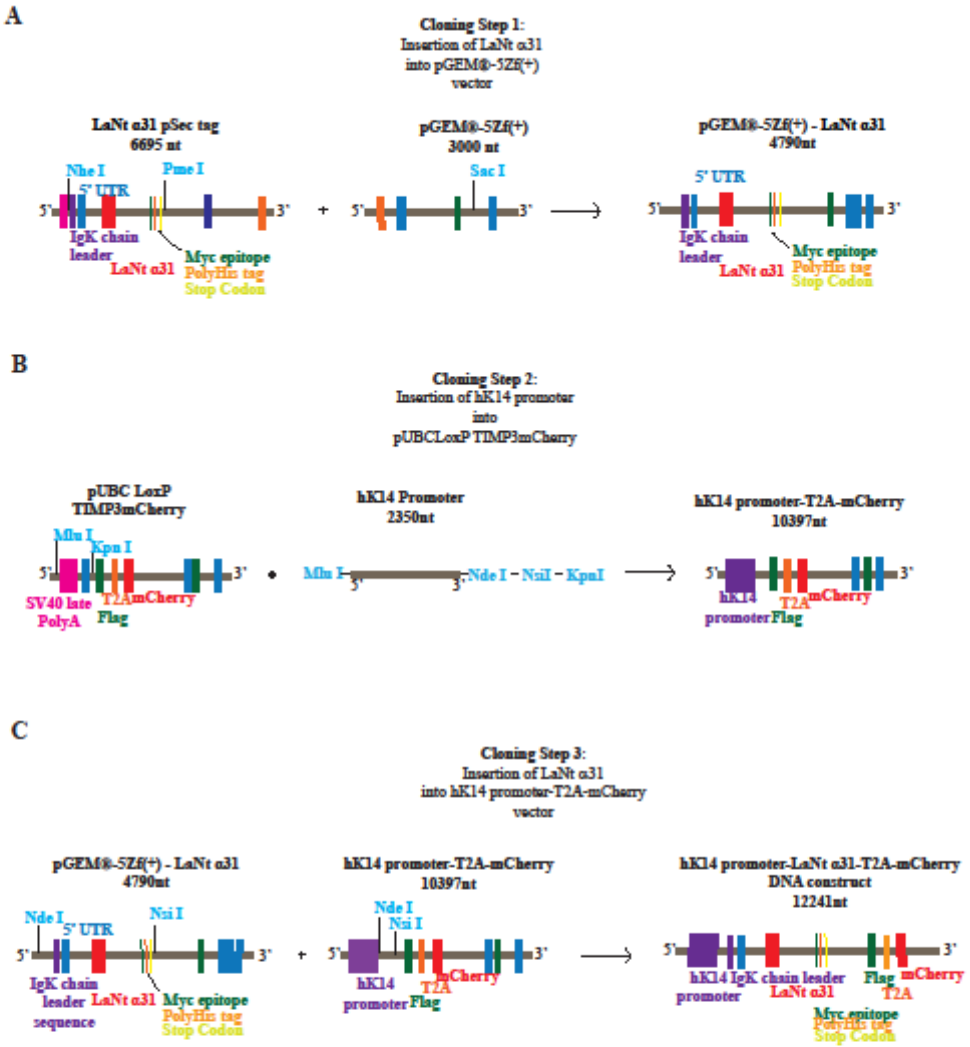

Fig. 4.1: Flow diagram of the cloning steps to produce hK14 promoter-driven LaNt α31 overexpressing DNA construct.
A) Cloning step 1; simplified plasmid maps with restriction sites used to digest DNA. LaNt α31, including the IgK, 5' UTR, Myc-His epitopes and stop codon sequences, was inserted into pGEM®-5Zf(+) vector. The arrow indicates the plasmid obtained. B) Cloning step 2; simplified plasmid maps with restriction sites used to digest DNA. hK14 promoter was amplified by PCR using modified primers to add restriction sites as indicated. pUBCLoxP TIMP3 sequence was excised from the pUBCLoxP-TIMP3mCherry vector and hK14 promoter inserted. The arrow indicates the plasmid obtained. C) Cloning step 3; simplified plasmid maps with restriction sites used to digest DNA. LaNt α31, including IgK, 5' UTR, Myc-His epitopes and stop codon, was excised from the pGEM®-5Zf(+) vector and inserted in the hK14 promoter-T2A-mCherry vector. The arrow indicates the plasmid obtained.

4.1.0 Cloning Step 1

Full-length LaNt α31 was cloned into pSecTag (Thermo Fisher Scientific) by Dr. Kevin Hamill (unpublished). This plasmid introduces sequences encoding the IgK-chain leader at the 5' end, and Myc and 6xHis epitopes at the 3' end (Fig. 4.2A). The complete construct, including 5' and 3' tags was excised with *NheI* high fidelity and *PmeI* (New England Biolabs) and cloned into pGEM®-5Zf(+) cloning vector (3000bp, Promega, Wisconsin, USA) linearised with *SacI* high fidelity (New England Biolabs) (Fig. 4.2B). Correct orientation of LaNt α31 was verified by restriction analysis of the purified DNA with *ClaI* and *NdeI* or *SalI* and *NotI*; panels C, D, E in Fig. 4.2 indicate the test and the circular map of the final plasmid.

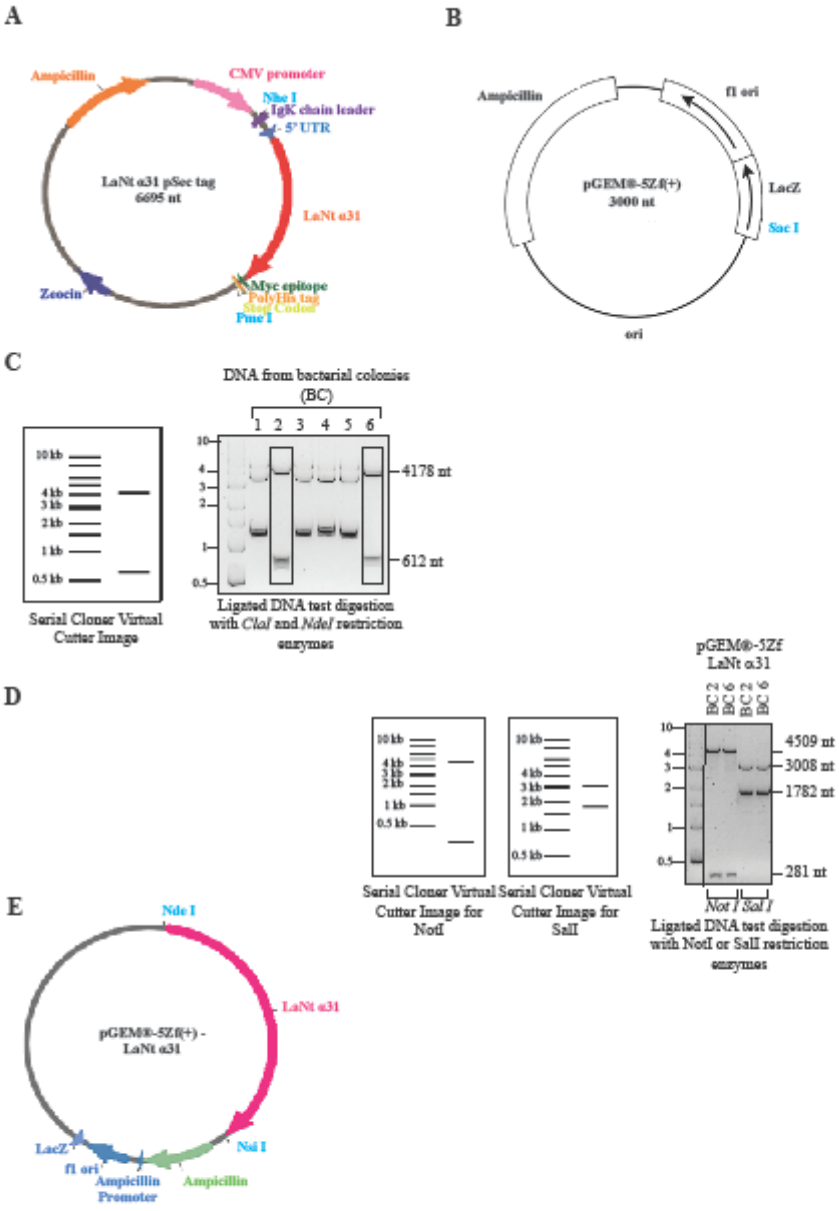

Fig. 4.2: Cloning step 1:Insertion of LaNt α31 into pGEM®-5Zf(+) vector.
(A) LaNt α31 pSecTag circular map, including *NheI* and *PmeI* restriction sites location. (B) pGEM®-5Zf (+) cloning vector circular map, including *SacI* restriction site location. (C) Virtual Cutter image, created using Serial Cloner software, compared with agarose gel electrophoresis to verify the right orientation of LaNt α31 insert in several DNA from bacterial colonies, using *ClaI* and *NdeI* restriction enzymes. (D) Successful ligation products double-tested for right orientation, using *NotI* or *SalI* restriction enzymes. Virtual Cutter image, created using Serial Cloner software, compared with agarose gel electrophoresis (E) Circular map of the pGEM®-5Zf-LaNt α31 plasmid obtained.

4.1.1 Cloning Step 2

The UBCTimp3-mCherry plasmid, encoding Timp3 followed by a T2A ribosomal entry site, was a kind gift from Prof. George Bou-Gharios. The Timp3 sequence was removed by enzymatic digestion with *MluI* and *KpnI* (Fig. 4.3A).

The sequence encoding the hK14 promoter was amplified from human genomic DNA using modified primers to incorporate one *MluI* site at the 5' end and *NdeI, NsiI* and *KpnI* sites at the 3' end (Fig. 4.3B,C). This PCR product was then digested with *MluI* and *KpnI*, gel-purified and ligated into the linearised UBCTimp3-mCherry (Fig. 4.3D). The presence and correct orientation of hK14 promoter insert into the plasmid vector was verified by restriction analysis of the purified plasmid with *MluI* and *KpnI*, *NdeI* and *NsiI* or *EcoRV* restriction enzymes (Fig. 4.3E,F). In figure 4.3G, the circular map of the final plasmid is shown.

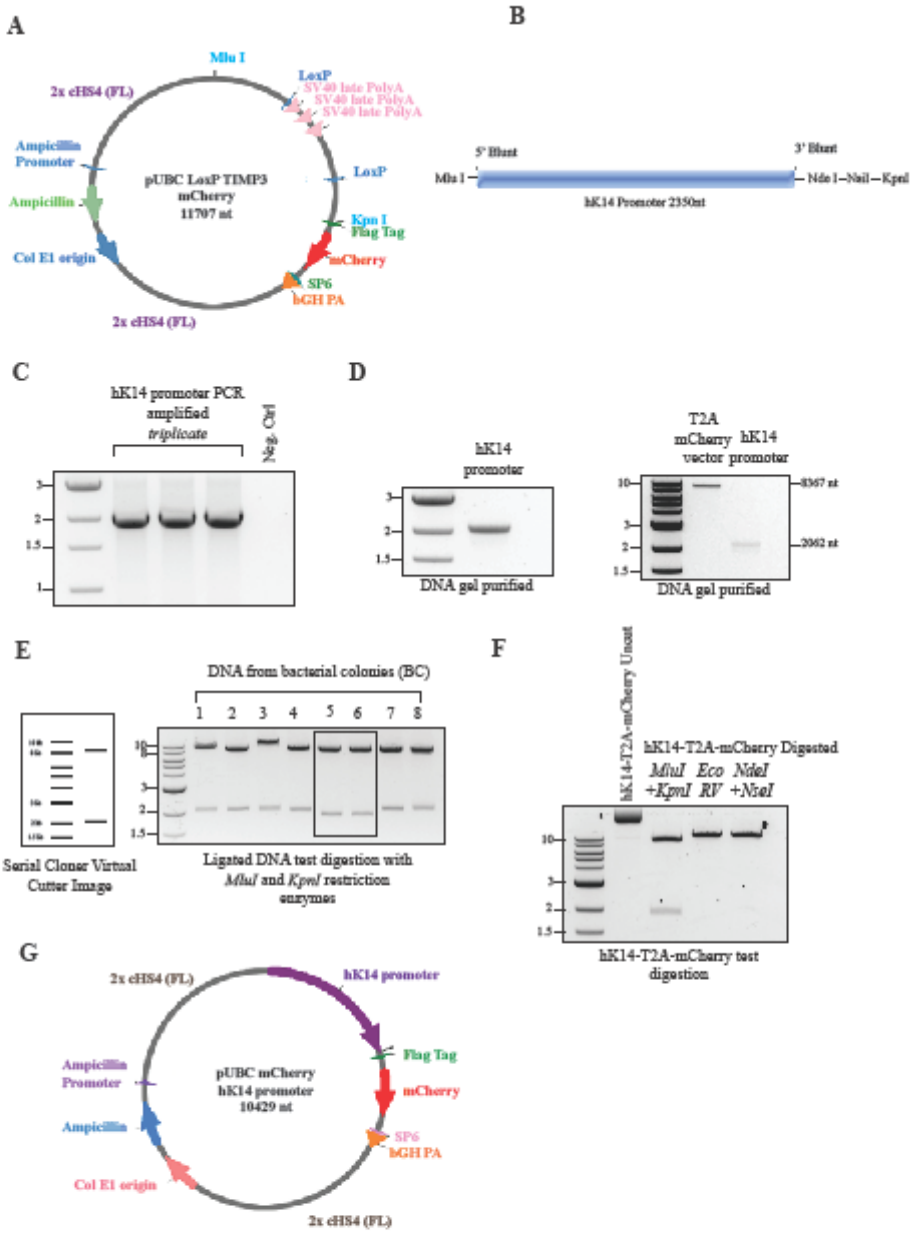

Fig. 4.3: Cloning Step 2: Insertion of hK14 promoter into pUBCLoxP-TIMP3mCherry vector. (A) Circular map of the pUBC LoxP TIMP3-mCherry plasmid, including *MluI* and *KpnI* restriction sites location. (B) Schematic representation of the modifications inserted in the hK14 promoter sequence after PCR amplification. (C) 1% Agarose gel showing hK14 promoter amplified by PCR, in triplicate, including negative control. (D) 1% agarose gel images of hK14 promoter 2Kb band (left gel) ,and T2A-mCherry backbone with hK14 insert bands (right gel) after gel purification. (E) Virtual Cutter image, created using Serial Cloner software, compared with agarose gel electrophoresis to verify the presence of hK14 promoter insert. Black box indicates successful ligation products. (F) 1% Agarose gel showing test digestion products of the T2A-mCherry plasmid. (G) Circular map of the final plasmid obtained.

4.1.2 Cloning Step 3

The pGEM®-5Zf (+)-LaNt α31 and pUBC-mCherry-hK14 promoter plasmids were enzymatically digested with *NdeI* and *NsiI* (New England Biolabs) (Fig. 4.4A), gel-purified, ligated and heat shock transformed into One-Shot TOP10 Chemically Competent *E.Coli* cells (Life Technologies). Successful integration was confirmed by digestion with *NdeI* and *NsiI* or *EcoRV and NotI* restriction enzymes (Fig. 4.4 B,C,D).

The final construct (Fig. 4.4E) was linearised, and ampicillin resistance encoding sequence removed by digestion with *ZraI* and *FspI* restriction enzymes (New England Biolabs) (Fig. 4.4 F,G).

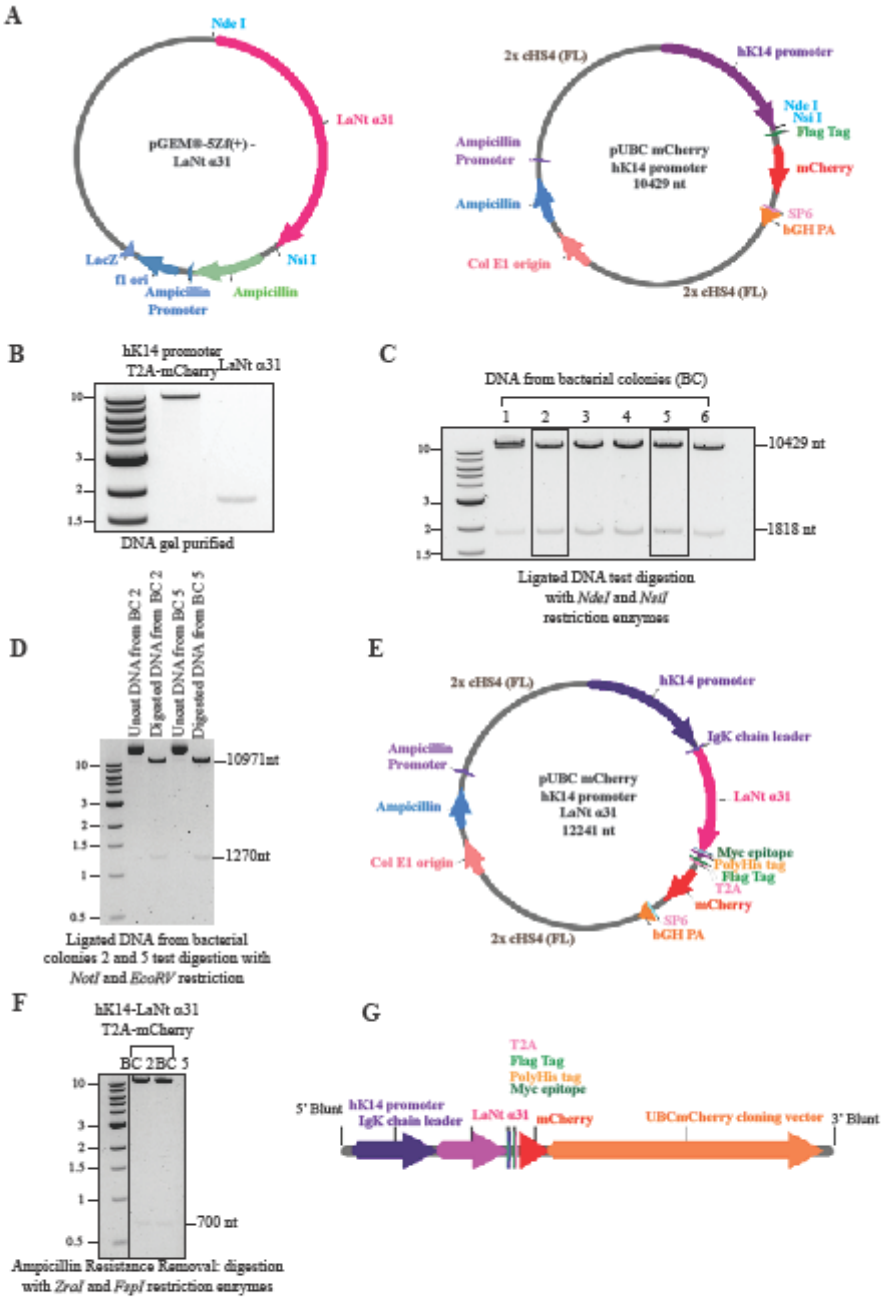

Fig. 4.4: Cloning Step 3: Insertion of LaNt α31 into hK14 promoter-T2A-mCherry vector. (A) Circular maps of pGEM®-5Zf (+)-LaNt α31 and UBC-hK14 promoter-mCherry plasmids indicating the restriction sites *NdeI* and *NseI*. (B) pUBCmCherry vector and LaNt α31 insert bands after agarose gel purification. (C) Ligation products were digested using *NdeI* and *Nse I* restriction enzymes and insert-containing DNA from BC 2 and 5 was further tested by restriction digest with *NotI* and Eco*RV* enzymes (D). (E) Circular map of the final plasmid obtained. (F) In preparation for embryonic injection, hK14-LaNt α31-T2A-mCherry plasmid was linearised using *ZraI* and *FspI* restriction enzymes. (G) Linearised map of the final DNA construct.

4.1.3 *In-vitro* tests of construct

Complete plasmids were tested by transfection into KERA-308 and HaCaT cells as follows:

Transfected DNA	Cell type
None	KERA-308 and HaCaT
UBC-hK14 promoter-mCherry plasmid	KERA-308 and HaCaT
LaNt α31-pSecTag plasmid	KERA-308 and HaCaT
UBC hK14 promoter-LaNt α31-mCherry	KERA-308 and HaCaT
UBC hK14 promoter-LaNt α31-mCherry linearised DNA	KERA-308

Table 7: DNA transfection set up to test the functionality of the hK14 promoter driven-LaNt α31 overexpressing construct *in-vitro*.

Visualisation of the T2A-driven mCherry sequence was confirmed by visualisation of the mCherry signal by fluorescence microscopy (Fig. 4.5A,B,C). Expression of hK14-driven LaNt α31 expression was confirmed by WB of total protein extracts from transfected cells with antibodies against LaNt α31 (Fig. 4.5D).

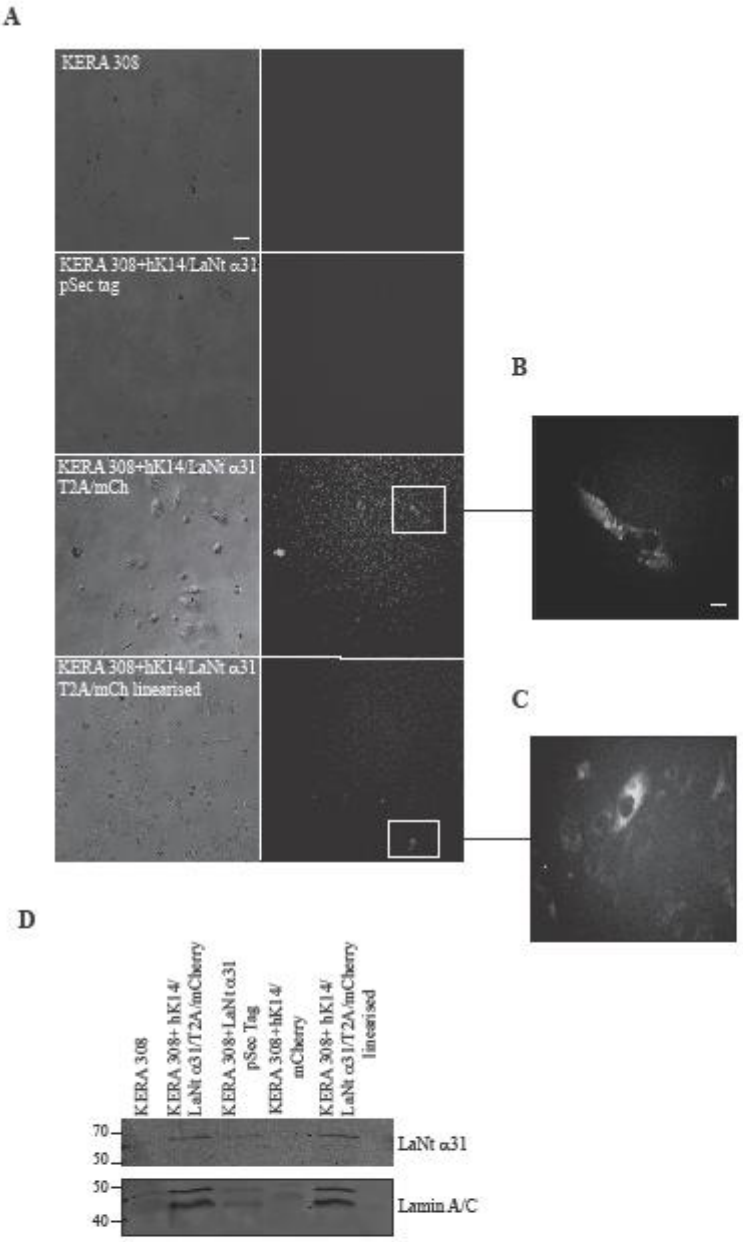

Fig. 4.5: hK14 promoter drives the expression of LaNt α31 and mCherry in-vitro. KERA-308 cells were either untreated or transfected with hK14 promoter/LaNt α31/T2A/mCherry, LaNt α31 pSec tag, hK14 promoter/mCherry or the full DNA construct in its linearised form. (A) mCherry signal was observed 24h after transfection using a 20X objective on a Nikon TiE epifluorescence microscope. In (B) and (C) mCherry expressing cells are shown at higher magnification. Scale bar = 10 μm. (D) Total protein lysates were collected from transfected samples and probed with antibodies against LaNt α31 and Lamin A/C.

4.1.4 Litters genotyping shows that only few mice carry the transgene

The hK14-LaNt α31-T2A-mCherry DNA construct (12241 nucleotides) was embryonically injected to develop LaNt α31 overexpressing animal models. A total of 140 embryos survived to the injection and were transferred into five recipient mothers. All of the recipient mothers displayed plugs the following day. Surprisingly, two of the mothers aborted and only three small litters of animals were obtained from the rest of the mothers; five mice from the first and one mouse each from the remaining two.

To determine if the construct was present in the obtained offspring's DNA, ear notches were taken 4 weeks after birth and DNA extracted. Standard PCR, using two sets of primers targeting two regions of the construct, revealed that males 1.2 and 1.3 from Litter 1 were transgenic (Fig. 4.6A).

Males 1.2 and 1.3 were mated with two and three females respectively, to obtain F1 heterozygous mice. Two litters were born from male 1.2. Respectively, three and two mice out of five showed to have the DNA construct in their genome (Fig. 4.6B). Three litters were born from male 1.3. Respectively, two, two and one mice carried the DNA construct in their genome (Fig. 4.6C).

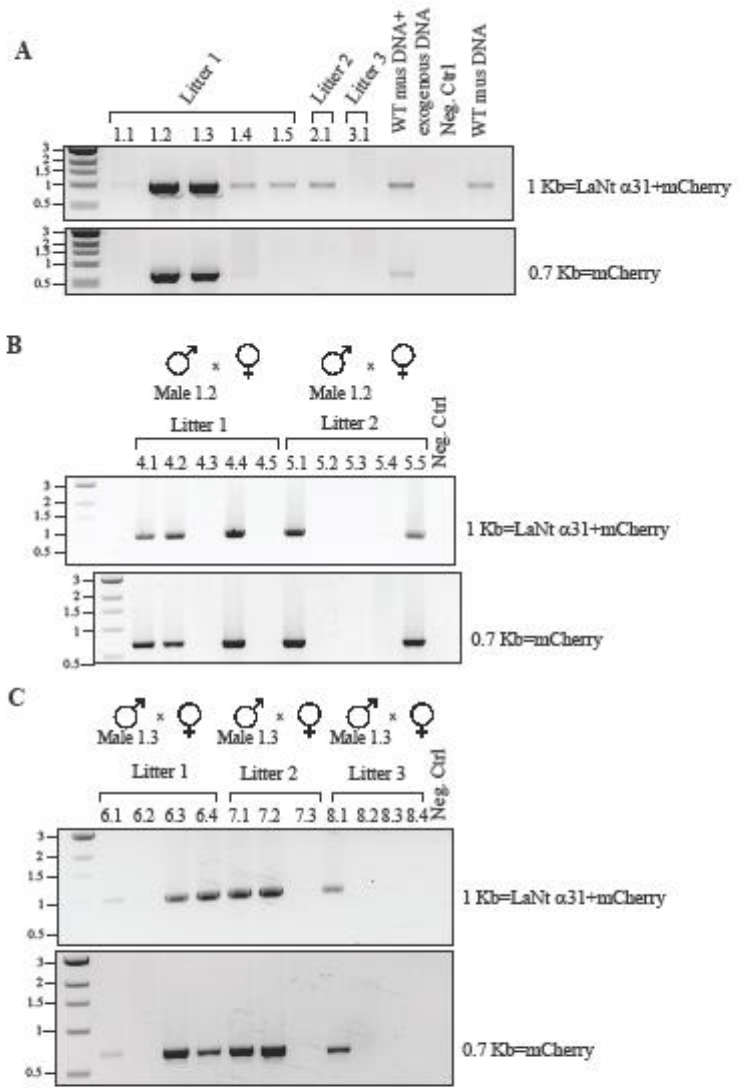

Fig. 4.6: LaNt α31 transgenic mice genotyping.
DNA from litters was obtained from ear punches and genotyping analysis was performed using a standard PCR approach and two sets of primers (LaNt α31+ mCherry or mCherry). PCR products were separated on a 1% agarose gel and imaged using a BioRad Gel Doc™ XR+ System. A) Litters born after the DNA embryonic injection. Mice 1.2 and 1.3 carried the transgene. (B) and (C) show the F1 generations born from mice 1.2 and 1.3 respectively.

4.1.5 LaNt α31 is not expressed in tissues isolated from transgenic mice

To determine whether LaNt α31 protein was expressed in the positively genotyped F1 generation's mice, we collected protein extracts from tissues known to express hK14 promoter, such as skin, eye, trachea, intestine, liver or lung, alongside non-expressing tissues like heart or kidneys [574].

Some tissues were cryopreserved as described before, to verify mCherry expression. Microscopy imaging of skin sections from mice 4.1 and 6.3 (positive to the presence of the transgene) and from control mouse 4.3 (negative to the presence of the transgene) revealed only signal auto-fluorescence (Fig. 4.7A), mainly due to the presence of hairs, which naturally fluoresce [575]. Some other tissues were, instead, homogenised in preparation for WB, performed to verify LaNt α31 protein expression; protein extract from LaNt α31 pSecTag-transfected 293A cells was used as a positive control and LaNt α31 band was detected only in the positive control sample (Fig. 4.7B). From these analyses, the transgene-containing animals showed no LaNt α31 protein expression.

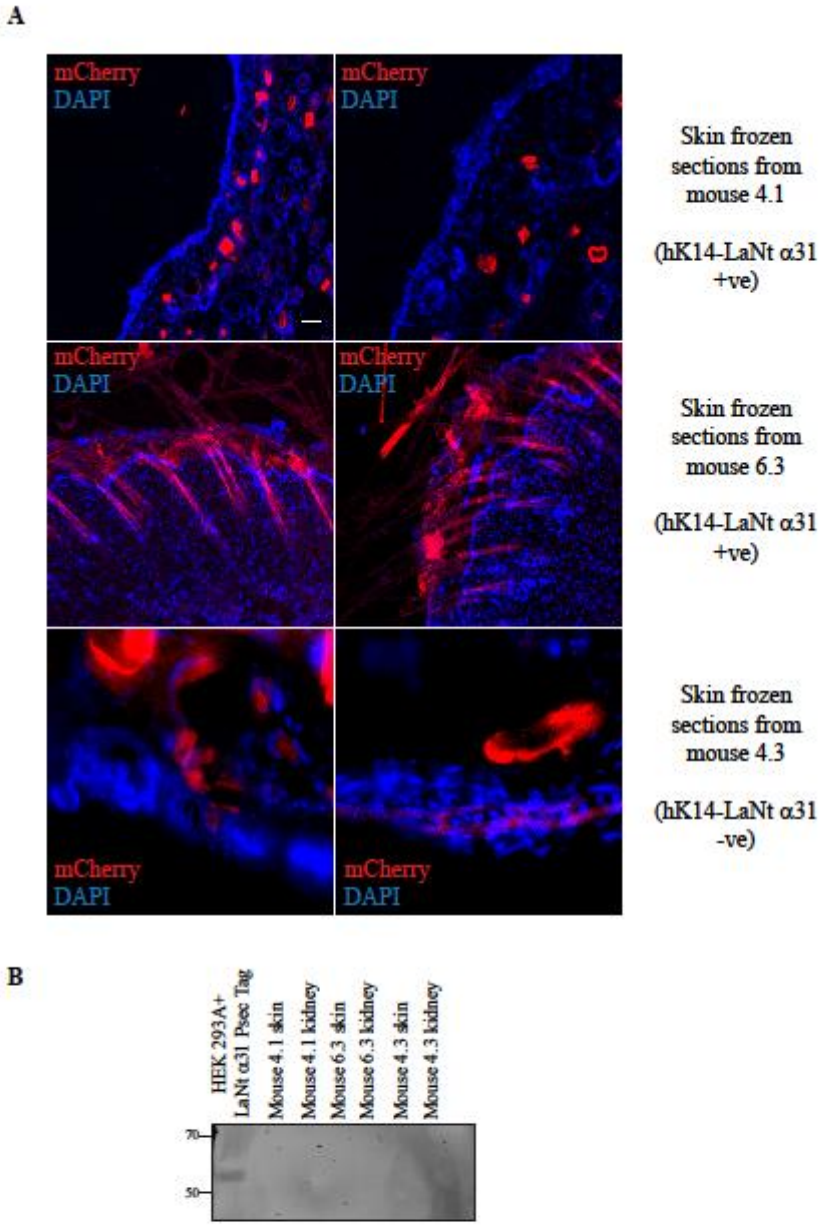

Fig. 4.7: LaNt α31 is not expressed in tissues collected from transgene positive mice 4.1 and 6.3.
(A) Skin frozen sections collected from mice 4.1, 6.3 (positive to the presence of hK14-LaNt α31/T2A/mCherry in their genome) and 4.3 (negative to the presence of hK14-LaNt α31/T2A/mCherry in its genome). O.C.T. frozen blocks were processed with Leica Cryostat CM3050 and sections of 10 µm cut. Sections were mounted with Fluoroshield DAPI mounting medium. DAPI and mCherry signals were analysed using a 10X objective on the Zeiss Apotome.2. (B) Total protein lysates were prepared homogenising tissue samples collected from mice 4.1, 6.3 and 4.3. WB was performed using antibodies against 6XHis tag. Scale bar = 100 µm.

4.1.6 Early pregnancy interruption after transgenic mice timed-mating shows incredibly low offspring and absence of LaNt α31 overexpression

The surprisingly low number of offspring obtained, the detection of the transgene in only two mice, but which was not associated with the protein expression, and the absence of specific mCherry signal in the skin, prompted us to hypothesise LaNt α31 overexpression associated lethality. For this reason, we decided to prematurely stop the pregnancy at E15.5, to collect the embryos and to analyse the protein expression during development.

Transgenic males 1.2 and 1.3 were timing-mated and two pregnant females were sacrificed at E15.5, by which time hK14 promoter has been shown to be already expressed [559, 560]. Intriguingly, only one foetus was found and genotyping analysis revealed the absence of the hK14-LaNt α31-T2A-mCherry DNA construct in the genome (Fig. 4.8 A,B).

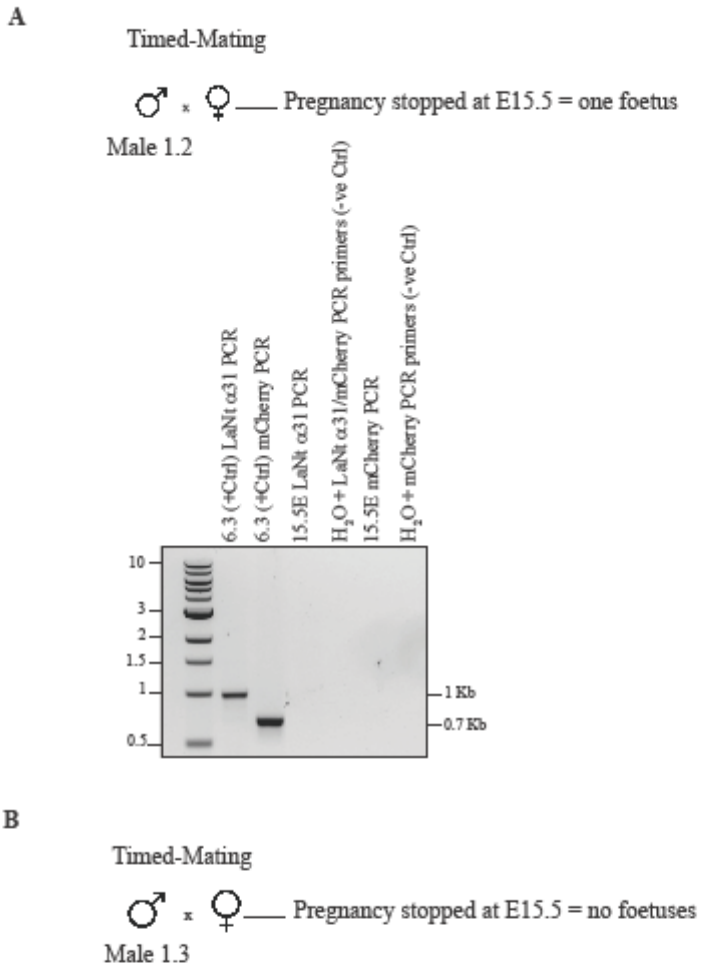

Fig. 4.8: Early pregnancy interruption of hK14-LaNt α31 DNA costruct carrying mice.
In (A) and (B), mouse 1.2 and 1.3 respectively were timed-mated. The single foetus collected at E15.5 was genotyped using a standard PCR approach and two sets of primers (LaNt α31+ mCherry or mCherry). PCR products were separated on a 1% agarose gel and imaged using a BioRad Gel Doc™ XR+ System. DNA from transgenic male 6.3 used as a positive control.

DISCUSSION

4a.0 LaNt α31 Overexpressing Animal Model data summary

The results presented in this chapter indicate that, after DNA embryonic injection, LaNt α31 overexpression could not be detected in adult mouse tissues, despite the DNA construct being present. Moreover, when the pregnancy was interrupted at E15.5, we only found one foetus which did not show LaNt α31 overexpression.

There are, at least, four possible reasons behind our observations, which are described below.

Interpretation 1. The inserted DNA does not express

Although only few animals composed the litters obtained in our study, we detected the presence of our DNA construct in some of them, therefore indicating that they carried the transgene even though they were not expressing the related protein. The first, most obvious, interpretation to the absence of LaNt α31 overexpression in the live offspring, is that the exogenous DNA may have been integrated in a region of the host genome where is not transcribed or translated. As the integration site is completely random, the exogenous DNA sequence could have been incorporated in the so-called non-coding DNA, DNA regions that form more than 85% of mice and humans' genome [576] and do not encode protein sequences. The DNA construct injected in the mouse embryos could have been integrated into different non-coding DNA portions, such as cys- or trans- regulatory elements, introns, transposons or telomeres, ending up in regions that have different roles (genes transcription regulation, proteins binding, etc.) but are definitely not accessible to the transcription/translation machinery [577].

When integrated in the host genome, exogenous DNA can also multimerise at the integration's site, leading to the integration of multiple number of copies of the transgene [578]. In transgenic animals, a high copy number may result in a decreased gene expression [579], which could be plausible in our scenario. Moreover, the sequence composition (e.g. the presence of enhancer or silencer sequences and the type of promoter used), the molecule's size and the physical form of the vector carrying the transgene, as well as the injection site, are all factors that affect the efficiency of DNA-mediated transformation [580]. Our construct is bigger than 10 Kb and it includes two identical silencer sequences, characteristics that could potentially affect the success of the DNA integration [580]. We relied on numbers of animals generated to counteract the random integration issues; however, we could have performed fluorescence *in situ* hybridization (FISH), looking for the transgenic material on our non-expressing tissue/cells to determine integration sites.

Interpretation 2. The exogenous DNA and/or the host genome is altered following microinjection

Rather than purely a lack of expression of the transgenic material, the failure to detect protein expression may reflect a more general issue with the host cell genome. After a transgenic manipulation such as the embryonic microinjection, many processes can occur to the DNA and to the host genome before the exogenous DNA get integrated. For instance, if the exogenous DNA is multimerising at the site of integration, as described above, the high number of tandem repeating elements can trigger deletion, breakage or translocation episodes [581, 582]. There are data related to the interruption of coding sequences due to the integration mechanism [583], and

evidences of extensive physical rearrangements at the site of integration after microinjection in mice [584-586]. Also, studies have highlighted the possibility that linear DNA molecules, as the construct we have used in this work, after being microinjected can be rearranged in concatemers, which are long continuous molecules containing multiple copies of the same DNA construct linked in series [587].

One more reason behind the absence of protein expression after microinjection, which can be applied to our work, is given by the possible disruption of the recipient genomic loci's natural organisation following the foreign DNA integration [588], inducing instability of the site. Indeed, it has been reported that the foreign DNA can be integrated into pericentromeric satellite DNA, essential core centromere-building sequences with fundamental roles in stabilising interactions between DNA-binding proteins and driving chromosomal segregation during mitosis [589], making the locus unstable [590]. As our work is the first attempt to create an animal model with a LaNt α31 overexpression, any of these mechanisms could be happening.

Interpretation 3. The injected DNA is not integrated into the host genome

Despite the fact that DNA microinjection in mouse embryos is now a common technique of genetic transformation, and there are previously published data showing that transferred DNA sequences can be transmitted to succeeding litter in mice [591] [592], it is not unusual that foreign DNA is not integrated in the host genome [578, 593, 594]. When Gordon et al, in their study, injected an isolated gene into a one-cell embryo, they only succeeded in obtaining 2 transgenic mice out of 78 [591]. One

explanation for such a low efficiency is that the cells carrying a large amount of additional genetic material, as in our LaNt α31 overexpressing animal model where the final construct was larger than 10Kb, would not survive through development, with a resulting preferential survival of uninjected cells [591]. Interestingly, after transformation, cells can maintain the exogenous DNA independent of the host DNA, in structures called transgenomes [595]. Scangos et al demonstrated that about 10% of the transformed cells lose these transgenic sequences if maintained under nonselective conditions [596]; if this mechanism also happens *in-vivo*, it may explain our results, since we have analysed the mice tissues only 6 weeks after birth and, therefore, the amplified product in our PCR screen may be coming from a transgenome rather than integrated DNA. In this study, we could have tested for our DNA construct integration using techniques such as a gel-purification assay, in which integrated DNA can be separated from free vector using pulsed-field gel electrophoresis (PFGE) on the base of the molecular weight [597], or a RAIC-PCR assay, capable of detecting even rare integration events *in-vivo* [598].

Interpretation 4. The injected DNA is lethal during development

Although scenarios 1, 2 and 3 are all individually plausible for the lack of LaNt α31 expression observed in the low number of transgenics produced, they still do not explain why our yield, in terms of transgenics produced, was lower than expected. If, on one side, this could be explained by poor technique, poor breeding stock or inferior quality materials however, on the other side the LaNt α31 transgenic production was carried out by a very experienced technician who routinely produces

similar animals, and was performed over multiple independent microinjection events, in parallel with other ongoing projects that did give rise to the expected numbers of transgenics. Therefore, we should consider an explanation where overexpression of the LaNt α31 protein is deleterious/embryonic lethal. This situation would explain both the low number of offspring obtained and that all the animals obtained carrying the transgene did not display expression of the protein.

Our *in-vitro* data demonstrate that many of the hTCEpi cell behaviours are impaired when LaNt α31 is overexpressed. As already described, there are multiple examples of diseases caused by defects of various kinds in the LM network formation and stability, such as Pierson Syndrome, JEB, the LM α2-Deficient Congenital Muscular Dystrophy or Nephrotic Syndrome [91, 96, 97, 599]. It is, therefore, not difficult to hypothesise that tissue formation will be affected if the LM network is disrupted, supporting the possibility of lethality during development. Many losses can occur during the pregnancy [493] and, since we analysed the outcome of our DNA construct integration only 6 weeks after birth, there is also the possibility that any initial events, if they exist, were missed, highlighting the necessity to study the foetal development in the early stages.

In addition to the possible LaNt α31 effects described in chapter 3, the mouse BM/ECM contains numerous other interactions that we have not considered in our 2D cell culture system. For example, the HD/LM332 complex is stabilised by collagen type VII anchoring fibrils, so a further explanation is that LaNt α31 could be competing for Col type VII binding sites. As collagen type VII binding is involved in determining where HDs form and is required for tissue integrity [269, 327], if collagen type VII binding to laminin was disturbed by the presence of LaNt α31, the animals may present with a form of epithelial fragility similar to that

observed in dystrophic epidermolysis bullosa. A previously published study using a collagen type XVII knockout mouse model showed that more than 90% of the newborns die after few days, as they develop blisters and detachment of the epidermis [600]. As a further support to the hypothesis that a LaNt α31-induced LM network disruption is lethal *in-vivo*, there are data reporting that the LM332 knockout mouse model, generated with a pathogenic LAMB3 genetic variant, showed pronounced blistering of the entire skin surface and died within 24h [601], while the α3 knockout mice died within the first days of life due to severe blistering [512].

In connection with the similarity between LaNt α31 and netrins, *in-vivo* negative effects have been observed in the presence of an overexpression of netrin 4. When netrin 4 was expressed in mouse skin under control of the hK14 promoter, as our construct, such an overexpression increased the lymphatic permeability and downregulating tight junction proteins [602], which could suggest a potential double effect of LaNt α31 on the ECM; LaNt α31 may be disrupting the LM network **AND** weakening the tight junctions, inducing a premature death of the offspring.

Final conclusions and future directions

Irrespective of which, among the described hypotheses, underlie our results, all the findings described in this thesis strongly indicate that, in corneal epithelial cells, LaNt α31 can be considered as a key regulator of the cell to LM adhesive complex assembly and maturation. Furthermore, being LaNt α31 differentially distributed throughout the anterior segment, we can claim that this protein has context-specific functions.

Previous studies on LaNts transcripts indicate extensive distribution of LaNt family members [461], suggesting that these relatively unstudied proteins may have widespread roles in multiple tissues and different developmental contexts. This points to a potential role for the LaNt proteins in regulating any of the processes where BM remodelling is required, including wound repair, tissue morphogenesis, differentiation, angiogenesis or pathogenic situations involving defective BM function, such as tumour cell invasion and metastasis.

I think that our *in-vivo* study gave us strong hints, although very preliminary, about the importance of LaNts proteins and their association with LMs. It would have been very interesting for me to repeat the functional assays using different LM isoforms, to understand the LM-LaNts specificity of interaction. There is still an open question on the LM-LaNt α31 time and order of deposition, two aspects that could be resolved applying live microscopy to the proteins of interest tagged with inducible fluorescence, or imaging techniques such as FRET and atomic-force microscopy (ATM). Furthermore, a ligand-binding assay or a receptor-blocking experiment could be extremely useful to have an insight into the LaNt α31 receptor binding activity.

Particularly compelling is also the study of LaNt α31 overexpression on disease's tissues. The Eye and Vision Science Department in Liverpool has a large archive of wax-embedded eye tissues, collected from patients affected by a variety of pathologies; analysing the protein localisation in these tissues could possibly uncover novel aspects of the same projects. On the other side, many questions raised from the *in-vivo* study, which only exposed a narrow part of a big picture. Believing that an overexpression of LaNt α31 is lethal during the development, the next step would definitely be to change the DNA cloning approach to create an inducible DNA construct. This would allow the pregnancy to complete normally and the protein overexpression to be induced only after birth, giving us the possibility to study the LaNt α31 overexpression effects on a live animal. All these aspects establish very interesting future research directions, which will lead to innovative and interdisciplinary outcomes.

Appendix

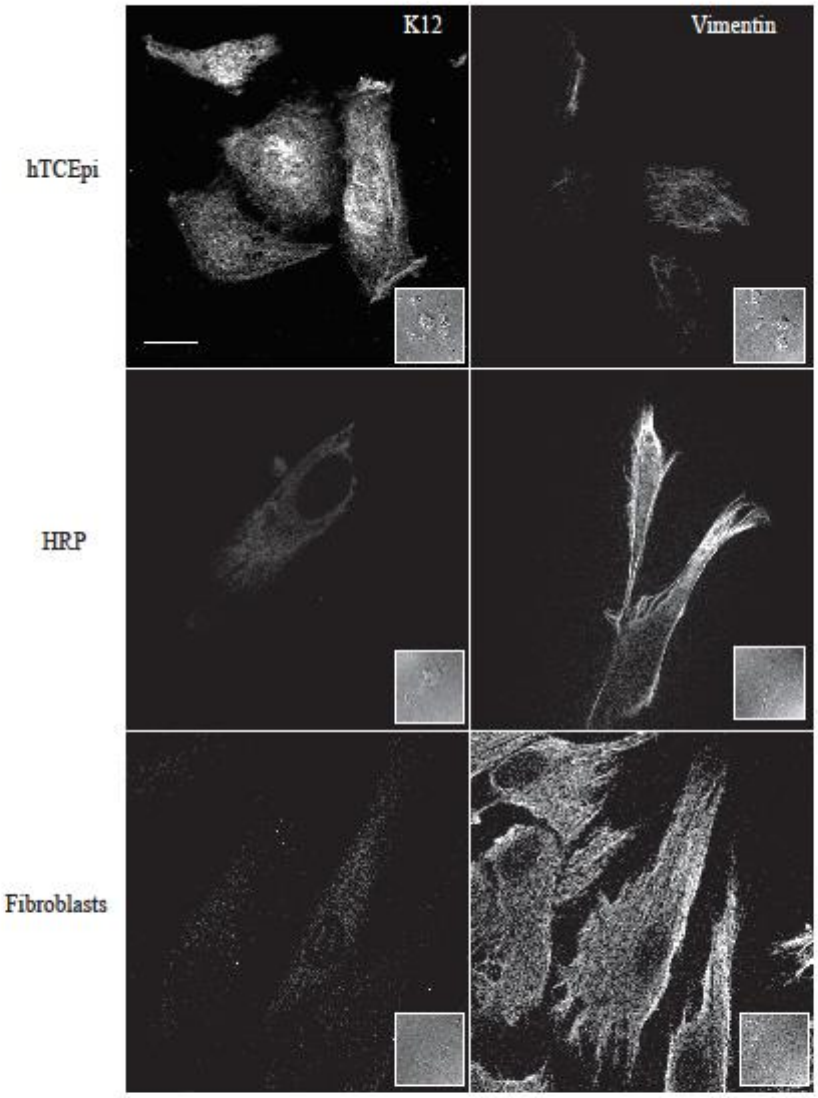

Fig.1: Characterisation of telomerase-immortalised human corneal epithelial cells (hTCEpi).
hTCEpi, HRP and Fibroblasts were seeded on glass coverslips. After 24h, cells were fixed and processed for indirect immunofluorescence microscopy with antibodies against K12 and Vimentin. Images were taken using a 40X objective on a Zeiss Apotome.2. Insets show DIC images. Scale bar = 20 μm.

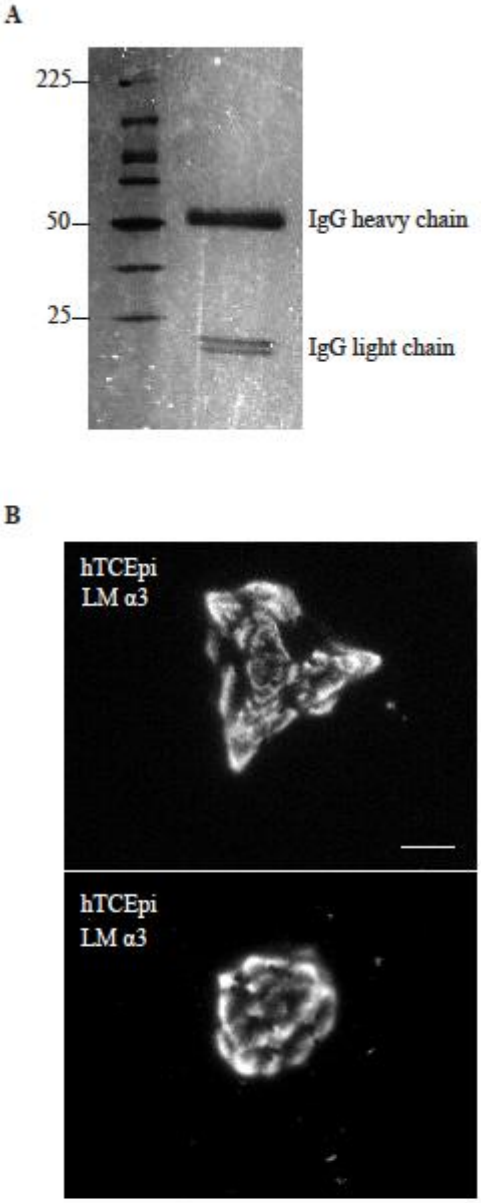

Fig. 2: RG13 mAb test for purity and functionality.
(A) 12.5% polyacrylamide gel silver stained; RG13 mAb containing-conditioned media was purified by affinity chromatography and concentrated with ammonium sulphate precipitation. Samples were prepared with 500 ng of purified RG13 mAb, 1X sample buffer and 10% β-mercaptoethanol. (B) hTCEpi cells were seeded on glass coverslips overnight, acetone-fixed and stained for LM α3 using the purified RG13 mAb. Images acquired using a 100X objective on a Nikon TiE epifluorescence microscope. Scale bar = 20 μm.

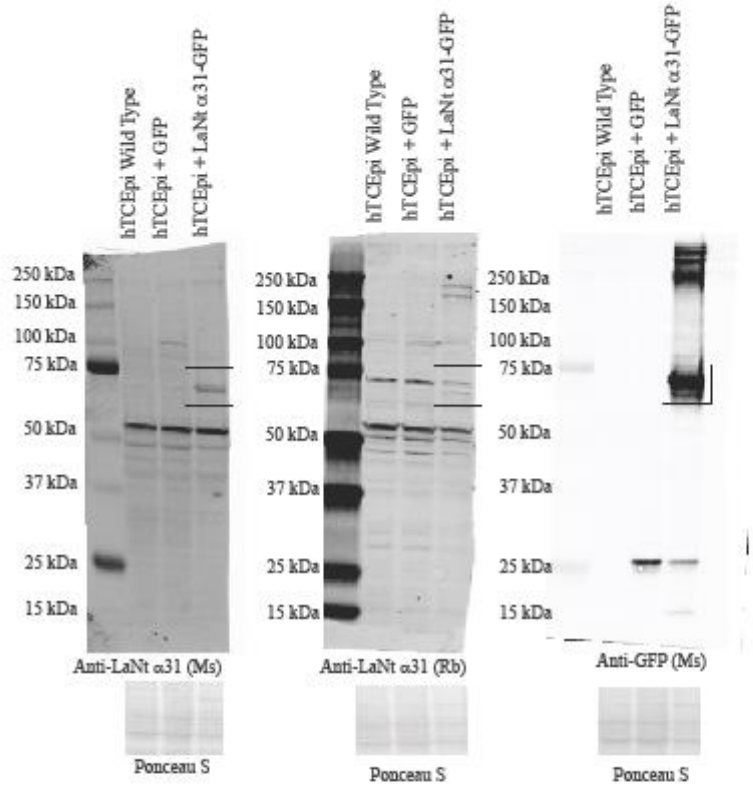

Fig.3: Rabbit polyclonal anti-LaNt α31 antibody characterisation in hTCEpi cell lysates.

hTCEpi, +GFP and +LaNt α31 cell lysates were probed with mouse anti-LaNt α31, rabbit anti-LaNt α31 and mouse anti-GFP Abs. The black rectangle indicates LaNt α31 protein recognised by all the Abs used.

WBs courtesy of Mr. Lee David Troughton.

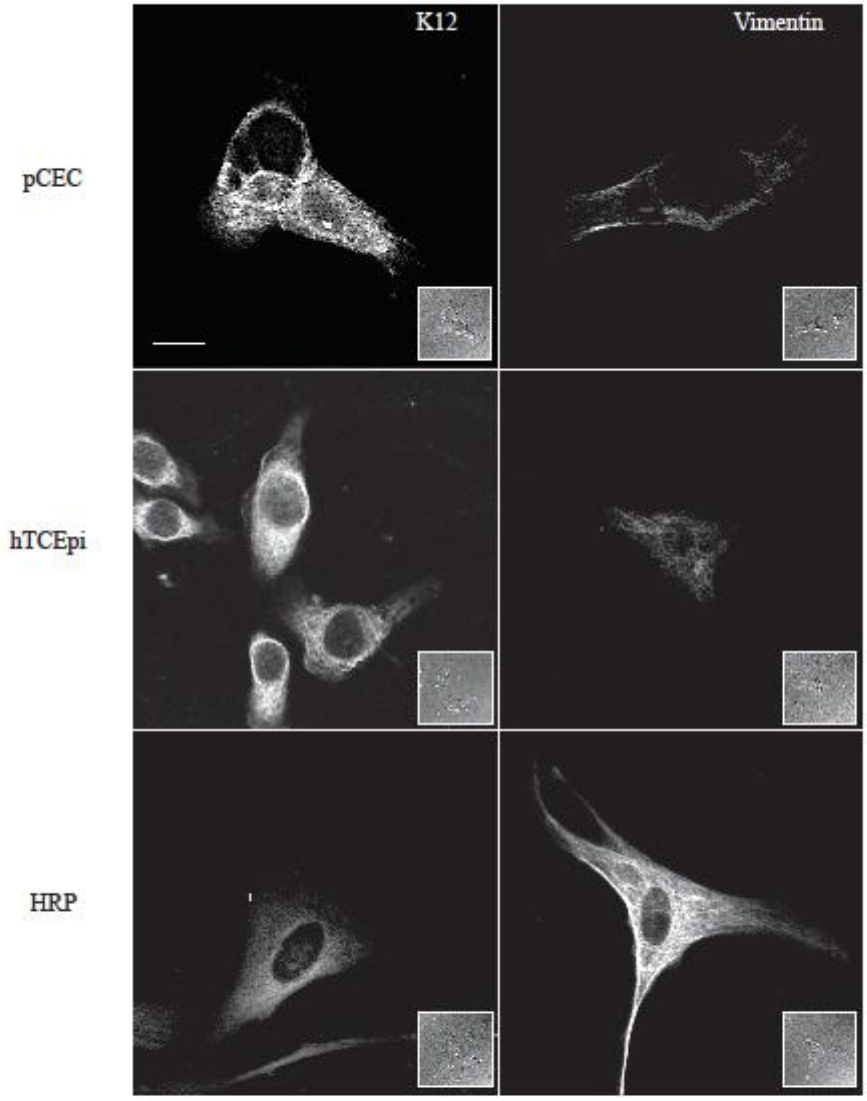

Fig. 4: Characterisation of human corneal primary cells (pCEC).
pCEC, hTCEpi and HRP were seeded on glass coverslips, pre-coated with conditioned media for pCEC cells only. After 24h, cells were fixed and processed for indirect immunofluorescence microscopy with antibodies against K12 and Vimentin. Images were taken using a 40X objective on a Zeiss Apotome.2. Insets show DIC images. Scale bar = 20µm.

Bibliography

1. Yang, D.-H., et al., *Renal collecting system growth and function depend upon embryonic γ1 laminin expression.* Development, 2011. **138**(20): p. 4535-4544.

2. Halfter, W., et al., *Protein composition and biomechanical properties of in vivo-derived basement membranes*. 2013

3. Tucker, G.C., et al., *Cell-adhesion and substrate-adhesion molecules: their instructive roles in neural crest cell migration.* Development (Cambridge, England), 1988. **103 Suppl**: p. 81-94.

4. Kalluri, R., *Basement membranes: Structure, assembly and role in tumour angiogenesis.* Nature Reviews Cancer, 2003. **3**(6): p. 422-433.

5. Liotta, L.A., et al., *Metastatic potential correlates with enzymatic degradation of basement membrane collagen.* Nature, 1980. **284**(5751): p. 67-68.

6. Vaccaro, C.A. and J.S. Brody, *Structural Features of Alveolar Wall Basement Membrane in the Adult Rat Lung*. 1981, Rockefeller University Press. p. 427.

7. Tanjore, H. and R. Kalluri, *The role of type IV collagen and basement membranes in cancer progression and metastasis.* Am J Pathol, 2006. **168**(3): p. 715-7.

8. Yurchenco, P.D., *Basement Membranes: Cell Scaffoldings and Signaling Platforms*. 2011.

9. Vukicevic, S., et al., *Identification of multiple active growth factors in basement membrane Matrigel suggests caution in interpretation of cellular activity related to extracellular matrix components.* Exp Cell Res, 1992. **202**(1): p. 1-8.

10. Spirin, K.S., et al., *Basement membrane and growth factor gene expression in normal and diabetic human retinas.* Current Eye Research, 1999. **18**(6): p. 490-499.

11. Démarchez, M., *The dermal-epidermal junction.* Biologie de la Peau, 2011.

12. Leblond, C.P. and S. Inoue, *Structure, composition, and assembly of basement membrane.* 1989(0002-9106 (Print)).

13. Martin, G.R. and R. Timpl, *Laminin and other basement membrane components.* 1987(0743-4634 (Print)).

14. Li, S., et al., *Laminin-sulfatide binding initiates basement membrane assembly and enables receptor signaling in Schwann cells and fibroblasts.* 2005(0021-9525 (Print)).

15. Haralson, M.A., *Book review: Extracellular matrix; a practical approach. Edited by M. A. Haralson and J. R. Hassell, 404 pp. 1995. IRL/Oxford University Press, Oxford PB £29.50.* General Pharmacology, 1995. **28**: p. 167.

16. Mao, M., et al., *Type IV Collagens and Basement Membrane Diseases: Cell Biology and Pathogenic Mechanisms.* 2015(1063-5823 (Print)).

17. Di Lullo, G.A., et al., *Mapping the ligand-binding sites and disease-associated mutations on the most abundant protein in the human, type I collagen.* 2002 (0021-9258 (Print).

18. Sweeney, S.M., et al., *Candidate cell and matrix interaction domains on the collagen fibril, the predominant protein of vertebrates.* 2008(0021-9258 (Print)).

19. Perumal, S., J.P.R.O. Antipova O Fau - Orgel, and J.P. Orgel, *Collagen fibril architecture, domain organization, and triple-helical conformation govern its proteolysis.* 2008(1091-6490 (Electronic)).

20. Shoulders, M.D. and R.T. Raines, *Collagen structure and stability.* 2009(1545-4509 (Electronic)).

21. Boutaud, A., et al., *Type IV collagen of the glomerular basement membrane. Evidence that the chain specificity of network assembly is encoded by the noncollagenous NC1 domains.* J Biol Chem, 2000. **275**(39): p. 30716-24.

22. Paulsson, M., *Basement membrane proteins: structure, assembly, and cellular interactions.* Crit Rev Biochem Mol Biol, 1992. **27**(1-2): p. 93-127.

23. Yurchenco, P.D. and J.J. O'Rear, *Basement membrane assembly.* Methods Enzymol, 1994. **245**: p. 489-518.

24. Ancsin, J.B. and R. Kisilevsky, *Laminin interactions important for basement membrane assembly are promoted by zinc and implicate laminin zinc finger-like sequences.* J Biol Chem, 1996. **271**(12): p. 6845-51.

25. Charonis, A.S., et al., *Binding of laminin to type IV collagen: a morphological study.* J Cell Biol, 1985. **100**(6): p. 1848-53.

26. Aumailley, M., et al., *Binding of nidogen and the laminin-nidogen complex to basement membrane collagen type IV.* Eur J Biochem, 1989. **184**(1): p. 241-8.

27. Fox, J.W., et al., *Recombinant nidogen consists of three globular domains and mediates binding of laminin to collagen type IV.* Embo j, 1991. **10**(11): p. 3137-46.

28. Esko, J.D., K. Kimata, and U. Lindahl, *Proteoglycans and Sulfated Glycosaminoglycans*, in *Essentials of Glycobiology*, A. Varki, et al., Editors. 2009, Cold Spring Harbor Laboratory Press

The Consortium of Glycobiology Editors, La Jolla, California.: Cold Spring Harbor (NY).

29. Sarrazin, S., W.C. Lamanna, and J.D. Esko, *Heparan sulfate proteoglycans.* Cold Spring Harb Perspect Biol, 2011. **3**(7).

30. Lin, X., *Functions of heparan sulfate proteoglycans in cell signaling during development.* Development, 2004. **131**(24): p. 6009-21.

31. Park, P.W., O. Reizes, and M. Bernfield, *Cell Surface Heparan Sulfate Proteoglycans: Selective Regulators of Ligand-Receptor Encounters.* Journal of Biological Chemistry, 2000. **275**(39): p. 29923-29926.

32. Bernfield, M., et al., *Functions of cell surface heparan sulfate proteoglycans.* Annu Rev Biochem, 1999. **68**: p. 729-77.

33. Smith, E.M., et al., *PDGF-A interactions with fibronectin reveal a critical role for heparan sulfate in directed cell migration during Xenopus gastrulation.* Proceedings of the National Academy of Sciences, 2009. **106**(51): p. 21683-21688.

34. Miner, J.H., *Renal basement membrane components.* Kidney Int, 1999. **56**(6): p. 2016-24.

35. Nurcombe, V. and S.M. Cool, *Heparan sulfate control of proliferation and differentiation in the stem cell niche.* Crit Rev Eukaryot Gene Expr, 2007. **17**(2): p. 159-71.

36. Kallunki, P., et al., *Cloning of human heparan sulfate proteoglycan core protein, assignment of the gene (HSPG2) to 1p36.1----p35 and identification of a BamHI restriction fragment length polymorphism.* Genomics, 1991. **11**(2): p. 389-96.

37. Ohji, M., et al., *Basement membrane synthesis by human corneal epithelial cells in vitro.* Invest Ophthalmol Vis Sci, 1994. **35**(2): p. 479-85.

38. Murdoch, A.D., et al., *Widespread expression of perlecan proteoglycan in basement membranes and extracellular matrices of human tissues as detected by a novel monoclonal antibody against domain III and by in situ hybridization.* J Histochem Cytochem, 1994. **42**(2): p. 239-49.

39. Melrose, J., et al., *The structure, location, and function of perlecan, a prominent pericellular proteoglycan of fetal, postnatal, and mature hyaline cartilages.* J Biol Chem, 2006. **281**(48): p. 36905-14.

40. Farach-Carson, M.C. and D.D. Carson, *Perlecan--a multifunctional extracellular proteoglycan scaffold.* Glycobiology, 2007. **17**(9): p. 897-905.

41. Iozzo, R.V., et al., *The biology of perlecan: the multifaceted heparan sulphate proteoglycan of basement membranes and pericellular matrices.* Biochem J, 1994. **302 (Pt 3)**: p. 625-39.

42. Handler, M., P.D. Yurchenco, and R.V. Iozzo, *Developmental expression of perlecan during murine embryogenesis.* Dev Dyn, 1997. **210**(2): p. 130-45.

43. Hopf, M., et al., *Crystal structure and mutational analysis of a perlecan-binding fragment of nidogen-1.* Nat Struct Biol, 2001. **8**(7): p. 634-40.

44. Ettner, N., et al., *The N-terminal globular domain of the laminin alpha1 chain binds to alpha1beta1 and alpha2beta1 integrins and to the heparan sulfate-containing domains of perlecan.* FEBS Lett, 1998. **430**(3): p. 217-21.

45. Inomata, T., et al., *Perlecan-deficient mutation impairs corneal epithelial structure.* Invest Ophthalmol Vis Sci, 2012. **53**(3): p. 1277-84.

46. Tsen, G., et al., *Agrin is a heparan sulfate proteoglycan.* J Biol Chem, 1995. **270**(7): p. 3392-9.

47. Patthy, L. and K. Nikolics, *Functions of agrin and agrin-related proteins.* Trends Neurosci, 1993. **16**(2): p. 76-81.

48. Magill-Solc, C. and U.J. McMahan, *Synthesis and transport of agrin-like molecules in motor neurons.* J Exp Biol, 1990. **153**: p. 1-10.

49. Kroger, S. and J.E. Schroder, *Agrin in the developing CNS: new roles for a synapse organizer.* News Physiol Sci, 2002. **17**: p. 207-12.

50. Khan, A.A., et al., *Physiological regulation of the immunological synapse by agrin.* Science, 2001. **292**(5522): p. 1681-6.

51. Melching, L.I., et al., *The cleavage of biglycan by aggrecanases.* Osteoarthritis Cartilage, 2006. **14**(11): p. 1147-54.

52. Shin, J.E., et al., *Transcriptional Regulation of Proteoglycans and Glycosaminoglycan Chain-synthesizing Glycosyltransferases by UV Irradiation in Cultured Human Dermal Fibroblasts.* J Korean Med Sci, 2011. **26**(3): p. 417-24.

53. Torricelli Aé, A.M., *The Corneal Epithelial Basement Membrane: Structure, Function, and Disease.* 2013. **54**(9): p. 6390-400.

54. García, B., et al., *Differential Expression of Proteoglycans by Corneal Stromal Cells in KeratoconusProteoglycan Expression in Keratoconus Corneal Stroma.* Investigative Ophthalmology & Visual Science, 2016. **57**(6): p. 2618-2628.

55. Fuerst, P.G., S.M. Rauch, and R.W. Burgess, *Defects in eye development in transgenic mice overexpressing the heparan sulfate proteoglycan agrin.* Dev Biol, 2007. **303**(1): p. 165-80.

56. Dong, L., et al., *Neurologic defects and selective disruption of basement membranes in mice lacking entactin-1/nidogen-1.* Lab Invest, 2002. **82**(12): p. 1617-30.

57. Cohen, M., F. Moody-Corbett, and E. Godfrey, *Neuritic deposition of agrin on culture substrate: implications for nerve-muscle synaptogenesis.* Journal of Neuroscience, 1994. **14**(5): p. 3293-3303.

58. Burkin, D.J., et al., *Laminin and alpha7beta1 integrin regulate agrin-induced clustering of acetylcholine receptors.* Journal of Cell Science, 2000. **113**(16): p. 2877-2886.

59. Sugiyama, J., D.C. Bowen, and Z.W. Hall, *Dystroglycan binds nerve and muscle agrin.* Neuron, 1994. **13**(1): p. 103-15.

60. Kammerer, R.A., et al., *Interaction of agrin with laminin requires a coiled-coil conformation of the agrin-binding site within the laminin gamma1 chain.* Embo j, 1999. **18**(23): p. 6762-70.

61. Denzer, A.J., et al., *Agrin binds to the nerve-muscle basal lamina via laminin.* J Cell Biol, 1997. **137**(3): p. 671-83.

62. Mascarenhas, J.B., et al., *Mapping of the laminin-binding site of the N-terminal agrin domain (NtA).* Embo j, 2003. **22**(3): p. 529-36.

63. Chung, A.E. and M.E. Durkin, *Entactin: structure and function.* Am J Respir Cell Mol Biol, 1990. **3**(4): p. 275-82.

64. Miosge, N., et al., *Nidogen-1 and nidogen-2 are found in basement membranes during human embryonic development.* Histochem J, 2001. **33**(9-10): p. 523-30.

65. Gersdorff, N., et al., *Laminin γ3 Chain Binds to Nidogen and Is Located in Murine Basement Membranes.* Journal of Biological Chemistry, 2005. **280**(23): p. 22146-22153.

66. Lossl, P., et al., *Analysis of nidogen-1/laminin gamma1 interaction by cross-linking, mass spectrometry, and computational modeling reveals multiple binding modes.* PLoS One, 2014. **9**(11): p. e112886.

67. Murshed, M., et al., *The absence of nidogen 1 does not affect murine basement membrane formation.* Mol Cell Biol, 2000. **20**(18): p. 7007-12.

68. Schymeinsky, J., et al., *Gene structure and functional analysis of the mouse nidogen-2 gene: nidogen-2 is not essential for basement membrane formation in mice.* Mol Cell Biol, 2002. **22**(19): p. 6820-30.

69. Bader, B.L., et al., *Compound genetic ablation of nidogen 1 and 2 causes basement membrane defects and perinatal lethality in mice.* Mol Cell Biol, 2005. **25**(15): p. 6846-56.

70. Bose, K., et al., *Loss of nidogen-1 and -2 results in syndactyly and changes in limb development.* J Biol Chem, 2006. **281**(51): p. 39620-9.

71. Mayer, U., et al., *Sites of nidogen cleavage by proteases involved in tissue homeostasis and remodelling.* Eur J Biochem, 1993. **217**(3): p. 877-84.

72. Argraves, W.S., et al., *Fibulins: physiological and disease perspectives.* EMBO Rep, 2003. **4**(12): p. 1127-31.

73. Timpl, R., et al., *Fibulins: a versatile family of extracellular matrix proteins.* Nat Rev Mol Cell Biol, 2003. **4**(6): p. 479-89.

74. Yanagisawa, H., et al., *Fibulin-5 is an elastin-binding protein essential for elastic fibre development in vivo.* Nature, 2002. **415**(6868): p. 168-171.

75. Nakamura, T., et al., *Fibulin-5/DANCE is essential for elastogenesis in vivo.* Nature, 2002. **415**(6868): p. 171-175.

76. Chapman, S.L., et al., *Fibulin-2 and fibulin-5 cooperatively function to form the internal elastic lamina and protect from vascular injury.* Arterioscler Thromb Vasc Biol, 2010. **30**(1): p. 68-74.

77. Weigell-Weber, M., et al., *Genomewide homozygosity mapping and molecular analysis of a candidate gene located on 22q13 (fibulin-1) in a previously undescribed vitreoretinal dystrophy.* Arch Ophthalmol, 2003. **121**(8): p. 1184-8.

78. Kennan, A., et al., *Identification of an IMPDH1 mutation in autosomal dominant retinitis pigmentosa (RP10) revealed following comparative microarray analysis of transcripts derived from retinas of wild-type and Rho(-/-) mice.* Hum Mol Genet, 2002. **11**(5): p. 547-57.

79. Utani, A., M. Nomizu, and Y. Yamada, *Fibulin-2 binds to the short arms of laminin-5 and laminin-1 via conserved amino acid sequences.* J Biol Chem, 1997. **272**(5): p. 2814-20.

80. George, E.L., et al., *Defects in mesoderm, neural tube and vascular development in mouse embryos lacking fibronectin.* Development, 1993. **119**(4): p. 1079-91.

81. Pankov, R. and K.M. Yamada, *Fibronectin at a glance.* Journal of Cell Science, 2002. **115**(20): p. 3861-3863.

82. ffrench-Constant, C., *Alternative splicing of fibronectin--many different proteins but few different functions.* Exp Cell Res, 1995. **221**(2): p. 261-71.

83. Kosmehl, H., A. Berndt, and D. Katenkamp, *Molecular variants of fibronectin and laminin: structure, physiological occurrence and histopathological aspects.* Virchows Arch, 1996. **429**(6): p. 311-22.

84. Mao, Y. and J.E. Schwarzbauer, *Fibronectin fibrillogenesis, a cell-mediated matrix assembly process.* Matrix Biol, 2005. **24**(6): p. 389-99.

85. Darribere, T. and J.E. Schwarzbauer, *Fibronectin matrix composition and organization can regulate cell migration during amphibian development.* Mech Dev, 2000. **92**(2): p. 239-50.

86. Grinnell, F., *Fibronectin and wound healing.* J Cell Biochem, 1984. **26**(2): p. 107-16.

87. Hasty, D.L. and W.A. Simpson, *Effects of fibronectin and other salivary macromolecules on the adherence of Escherichia coli to buccal epithelial cells.* Infect Immun, 1987. **55**(9): p. 2103-9.

88. Larjava H, K.L., Häkkinen L., *Interactions with Fibronectin during Wound Healing.* . Madame Curie Bioscience Database, 2013.

89. Miner, J.H., et al., *Compositional and structural requirements for laminin and basement membranes during mouse embryo implantation and gastrulation.* Development, 2004. **131**(10): p. 2247-56.

90. Ferrigno, O., et al., *Murine Laminin α3A and α3B Isoform Chains Are Generated by Usage of Two Promoters and Alternative Splicing.* Journal of Biological Chemistry, 1997. **272**(33): p. 20502-20507.

91. McLean, W.H., et al., *An unusual N-terminal deletion of the laminin alpha3a isoform leads to the chronic granulation tissue disorder laryngo-onycho-cutaneous syndrome.* Hum Mol Genet, 2003. **12**(18): p. 2395-409.

92. Ryan, M.C., et al., *Cloning of the LamA3 gene encoding the alpha 3 chain of the adhesive ligand epiligrin. Expression in wound repair.* J Biol Chem, 1994. **269**(36): p. 22779-87.

93. Aumailley, M., et al., *A simplified laminin nomenclature.* Matrix Biol, 2005. **24**(5): p. 326-32.

94. Timpl, R., et al., *Laminin - A glycoprotein from basement membranes.* Journal of Biological Chemistry, 1979. **254**(19): p. 9933-9937.

95. Burgeson, R.E., et al., *A new nomenclature for the laminins.* Matrix Biol, 1994. **14**(3): p. 209-11.

96. Scheele, S., et al., *Laminin isoforms in development and disease.* J Mol Med (Berl), 2007. **85**(8): p. 825-36.

97. McGowan, K.A. and M.P. Marinkovich, *Laminins and human disease.* Microsc Res Tech, 2000. **51**(3): p. 262-79.

98. Avila, J.L., et al., *Antibodies to basement membrane proteins nidogen and laminin in sera from streptococcal-related diseases and juvenile rheumatoid arthritis patients.* Clin Exp Immunol, 1987. **70**(3): p. 555-61.

99. Lazarova, Z., et al., *Comparative analysis of methods for detection of anti-laminin 5 autoantibodies in patients with anti-epiligrin cicatricial pemphigoid.* J Am Acad Dermatol, 2004. **51**(6): p. 886-92.

100. Dainichi, T., et al., *From anti-p200 pemphigoid to anti-laminin gamma1 pemphigoid.* J Dermatol, 2010. **37**(3): p. 231-8.

101. Vafia, K., et al., *Pathogenicity of Autoantibodies in Anti-p200 Pemphigoid.* PLoS One, 2012. **7**(7).

102. Florea, F., et al., *Autoimmunity against laminins.* Clin Immunol, 2016. **170**: p. 39-52.

103. Florea, F., et al., *Ex vivo pathogenicity of anti-laminin gamma1 autoantibodies.* Am J Pathol, 2014. **184**(2): p. 494-506.

104. Domloge-Hultsch, N., et al., *Epiligrin, the major human keratinocyte integrin ligand, is a target in both an acquired autoimmune and an inherited subepidermal blistering skin disease.* J Clin Invest, 1992. **90**(4): p. 1628-33.

105. Yancey, K.B. and C.A. Egan, *Pemphigoid: clinical, histologic, immunopathologic, and therapeutic considerations.* Jama, 2000. **284**(3): p. 350-6.

106. Izumi, R., et al., *Bullous pemphigoid positive for anti-BP180 and anti-laminin 5 antibodies in a patient with graft-vs-host disease.* J Am Acad Dermatol, 2007. **56**(5 Suppl): p. S94-7.

107. Takahara, M., et al., *Mucous membrane pemphigoid with antibodies to the beta(3) subunit of Laminin 332 in a patient with acute myeloblastic leukemia and graft-versus-host disease.* Dermatology, 2009. **219**(4): p. 361-4.

108. Chan, L.S., et al., *Bullous systemic lupus erythematosus with autoantibodies recognizing multiple skin basement membrane components, bullous pemphigoid antigen 1, laminin-5, laminin-6, and type vii collagen.* Archives of Dermatology, 1999. **135**(5): p. 569-573.

109. Umemoto, N., et al., *A case of nonscarring subepidermal blistering disease associated with autoantibodies reactive with both type VII collagen and laminin 5.* Dermatology, 2003. **207**(1): p. 61-4.

110. Mitate, E., et al., *Concurrence of autoantibodies to both laminin gamma1 and gamma2 subunits in a patient with kidney rejection response.* Acta Derm Venereol, 2013. **93**(1): p. 114-5.

111. Lazarova, Z., et al., *Passive transfer of anti-laminin 5 antibodies induces subepidermal blisters in neonatal mice.* J Clin Invest, 1996. **98**(7): p. 1509-18.

112. Lazarova, Z., et al., *Human Anti-Laminin 5 Autoantibodies Induce Subepidermal Blisters in an Experimental Human Skin Graft Model.* Journal of Investigative Dermatology, 2000. **114**(1): p. 178-184.

113. Vecchi, M.L., et al., *Anti-laminin auto antibodies in ANCA-associated vasculitis.* Nephrol Dial Transplant, 2000. **15**(10): p. 1600-3.

114. Cohen, D.E., et al., *Anti-laminin autoantibodies in collagen vascular diseases: the use of adequate controls in studies of autoimmune responses to laminin.* Ann Rheum Dis, 1994. **53**(3): p. 191-3.

115. Caproni, M., et al., *Antilaminin-1 antibodies in cutaneous lupus erythematosus patients.* Lupus, 2009. **18**(9): p. 858.

116. Hershko, A.Y., et al., *Extracorporeal immunoadsorption of antibodies against the VRT-101 laminin epitope in systemic lupus erythematosus: a feasibility evaluation study.* Immunol Res, 2013. **56**(2-3): p. 376-81.

117. Bubier, J.A., et al., *A mouse model of generalized non-Herlitz junctional epidermolysis bullosa.* J Invest Dermatol, 2010. **130**(7): p. 1819-28.

118. Fine, J.-D., *Epidermolysis Bullosa.* International Journal of Dermatology, 1986. **25**(3): p. 143-157.

119. Nakano, A., et al., *Laminin 5 mutations in junctional epidermolysis bullosa: molecular basis of Herlitz vs. non-Herlitz phenotypes.* Hum Genet, 2002. **110**(1): p. 41-51.

120. Muhle, C., et al., *Novel and recurrent mutations in the laminin-5 genes causing lethal junctional epidermolysis bullosa: molecular basis and clinical course of Herlitz disease.* Hum Genet, 2005. **116**(1-2): p. 33-42.

121. Castori, M., et al., *Herlitz junctional epidermolysis bullosa: laminin-5 mutational profile and carrier frequency in the Italian population.* Br J Dermatol, 2008. **158**(1): p. 38-44.

122. Varki, R., et al., *Epidermolysis bullosa. I. Molecular genetics of the junctional and hemidesmosomal variants.* Journal of Medical Genetics, 2006. **43**(8): p. 641-652.

123. Fine, J.D., et al., *Cause-specific risks of childhood death in inherited epidermolysis bullosa.* J Pediatr, 2008. **152**(2): p. 276-80.

124. Pulkkinen, L. and J. Uitto, *Mutation analysis and molecular genetics of epidermolysis bullosa.* Matrix Biol, 1999. **18**(1): p. 29-42.

125. Fine, J.D., et al., *Revised classification system for inherited epidermolysis bullosa: Report of the Second International Consensus Meeting on diagnosis and classification of epidermolysis bullosa.* J Am Acad Dermatol, 2000. **42**(6): p. 1051-66.

126. Ida, J.B., et al., *Upper airway complications of junctional epidermolysis bullosa.* J Pediatr, 2012. **160**(4): p. 657-661.e1.

127. Fine, J.D., et al., *Eye involvement in inherited epidermolysis bullosa: experience of the National Epidermolysis Bullosa Registry.* Am J Ophthalmol, 2004. **138**(2): p. 254-62.

128. Wallerstein, R., et al., *Epidermolysis bullosa, pyloric atresia, and obstructive uropathy: a report of two case reports with molecular correlation and clinical management.* Pediatr Dermatol, 2000. **17**(4): p. 286-9.

129. Pfendner EG, L.A., *Junctional Epidermolysis Bullosa.* Pagon RA, Adam MP, Ardinger HH, et al., editors, 2014.

130. Kunz, M., et al., *Mutation reports: epidermolysis bullosa simplex associated with severe mucous membrane involvement and novel mutations in the plectin gene.* J Invest Dermatol, 2000. **114**(2): p. 376-80.

131. Pasmooij, A.M., et al., *Features of epidermolysis bullosa simplex due to mutations in the ectodomain of type XVII collagen.* Br J Dermatol, 2004. **151**(3): p. 669-74.

132. Pasmooij, A.M., et al., *Revertant mosaicism in junctional epidermolysis bullosa due to multiple correcting second-site mutations in LAMB3.* J Clin Invest, 2007. **117**(5): p. 1240-8.

133. Bauer, J.W. and C. Lanschuetzer, *Type XVII collagen gene mutations in junctional epidermolysis bullosa and prospects for gene therapy.* Clin Exp Dermatol, 2003. **28**(1): p. 53-60.

134. Mellerio, J.E., et al., *E210K mutation in the gene encoding the beta3 chain of laminin-5 (LAMB3) is predictive of a phenotype of generalized atrophic benign epidermolysis bullosa.* Br J Dermatol, 1998. **139**(2): p. 325-31.

135. Hammersen, J., et al., *A New Mouse Model of Junctional Epidermolysis Bullosa: The LAMB3 628G>A Knockin Mouse.* Journal of Investigative Dermatology, 2015. **135**(3): p. 921-924.

136. Zenker, M., et al., *Congenital nephrosis, mesangial sclerosis, and distinct eye abnormalities with microcoria: an autosomal recessive syndrome.* Am J Med Genet A, 2004. **130a**(2): p. 138-45.

137. Chen, Y.M., Y. Kikkawa, and J.H. Miner, *A missense LAMB2 mutation causes congenital nephrotic syndrome by impairing laminin secretion.* J Am Soc Nephrol, 2011. **22**(5): p. 849-58.

138. Aydin, B., et al., *A novel mutation of laminin beta-2 gene in Pierson syndrome manifested with nephrotic syndrome in the early neonatal period.* Genet Couns, 2013. **24**(2): p. 141-7.

139. Matejas, V., et al., *Mutations in the human laminin beta2 (LAMB2) gene and the associated phenotypic spectrum.* Hum Mutat, 2010. **31**(9): p. 992-1002.

140. Carafoli, F., S.A. Hussain, and E. Hohenester, *Crystal Structures of the Network-Forming Short-Arm Tips of the Laminin β1 and γ1 Chains.* PLoS One, 2012. **7**(7).

141. Allamand, V. and P. Guicheney, *Merosin-deficient congenital muscular dystrophy, autosomal recessive (MDC1A, MIM#156225, LAMA2 gene coding for alpha2 chain of laminin).* Eur J Hum Genet, 2002. **10**(2): p. 91-4.

142. Sparks SE, Q.-R.S., Harper A, et al. , *Congenital Muscular Dystrophy Overview.* Pagon RA, Adam MP, Ardinger HH, et al., editors., 2001.

143. Ehrig, K., et al., *Merosin, a tissue-specific basement membrane protein, is a laminin-like protein.* Proc Natl Acad Sci U S A, 1990. **87**(9): p. 3264-8.

144. Sanz, L., et al., *A novel cell binding site in the coiled-coil domain of laminin involved in capillary morphogenesis.* The EMBO Journal, 2003. **22**(7): p. 1508-1517.

145. Timpl, R., et al., *Structure and function of laminin LG modules.* Matrix Biol, 2000. **19**(4): p. 309-17.

146. Hussain, S.-A., F. Carafoli, and E. Hohenester, *Determinants of laminin polymerization revealed by the structure of the alpha 5 chain amino-terminal region.* Embo Reports, 2011. **12**(3): p. 276-282.

147. Beck, K., I. Hunter, and J. Engel, *Structure and function of laminin: anatomy of a multidomain glycoprotein.* The FASEB Journal, 1990. **4**(2): p. 148-60.

148. Garbe, J.H., et al., *Complete sequence, recombinant analysis and binding to laminins and sulphated ligands of the N-terminal domains of laminin alpha3B and alpha5 chains.* Biochem J, 2002. **362**(Pt 1): p. 213-21.

149. Nielsen, P.K. and Y. Yamada, *Identification of Cell-binding Sites on the Laminin α5 N-terminal Domain by Site-directed Mutagenesis.* Journal of Biological Chemistry, 2001. **276**(14): p. 10906-10912.

150. Nomizu, M., et al., *Identification of homologous biologically active sites on the N-terminal domain of laminin alpha chains.* Biochemistry, 2001. **40**(50): p. 15310-7.

151. Odenthal, U., et al., *Molecular analysis of laminin N-terminal domains mediating self-interactions.* Journal of Biological Chemistry, 2004. **279**(43): p. 44504-44512.

152. Woodley, D.T., et al., *Interactions of basement membrane components.* Biochim Biophys Acta, 1983. **761**(3): p. 278-83.

153. Yurchenco, P.D., et al., *LAMININ POLYMERIZATION INVITRO - EVIDENCE FOR A 2-STEP ASSEMBLY WITH DOMAIN SPECIFICITY.* Journal of Biological Chemistry, 1985. **260**(12): p. 7636-7644.

154. Suzuki, N., F. Yokoyama, and M. Nomizu, *Functional sites in the laminin alpha chains.* Connect Tissue Res, 2005. **46**(3): p. 142-52.

155. Yurchenco, P.D., et al., *Models for the self-assembly of basement membrane.* J Histochem Cytochem, 1986. **34**(1): p. 93-102.

156. Yurchenco, P.D. and W.G. Wadsworth, *Assembly and tissue functions of early embryonic laminins and netrins.* Curr Opin Cell Biol, 2004. **16**(5): p. 572-9.

157. Cohen, M.W., et al., *Laminin-induced clustering of dystroglycan on embryonic muscle cells: comparison with agrin-induced clustering.* J Cell Biol, 1997. **136**(5): p. 1047-58.

158. Colognato, H., D.A. Winkelmann, and P.D. Yurchenco, *Laminin polymerization induces a receptor-cytoskeleton network.* Journal of Cell Biology, 1999. **145**(3): p. 619-631.

159. Sanders, C.R. and J.K. Nagy, *Misfolding of membrane proteins in health and disease: the lady or the tiger?* Current opinion in structural biology, 2000. **10**(4): p. 438-442.

160. Xu, H., et al., *Murine muscular dystrophy caused by a mutation in the laminin [alpha]2 (Lama2) gene.* Nat Genet, 1994. **8**(3): p. 297-302.

161. Patton, B.L., et al., *A single point mutation in the LN domain of LAMA2 causes muscular dystrophy and peripheral amyelination.* J Cell Sci, 2008. **121**(Pt 10): p. 1593-604.

162. Yurchenco, P.D. and Y.S. Cheng, *Self-assembly and calcium-binding sites in laminin. A three-arm interaction model.* J Biol Chem, 1993. **268**(23): p. 17286-99.

163. Schittny, J.C. and P.D. Yurchenco, *Terminal short arm domains of basement membrane laminin are critical for its self-assembly.* J Cell Biol, 1990. **110**(3): p. 825-32.

164. Cheng, Y.S., et al., *Self-assembly of laminin isoforms.* Journal of Biological Chemistry, 1997. **272**(50): p. 31525-31532.

165. Champliaud, M.F., et al., *Human amnion contains a novel laminin variant, laminin 7, which like laminin 6, covalently associates with laminin 5 to promote stable epithelial-stromal attachment.* The Journal of Cell Biology, 1996. **132**(6): p. 1189-1198.

166. McKee, K.K., S. Capizzi, and P.D. Yurchenco, *Scaffold-forming and Adhesive Contributions of Synthetic Laminin-binding Proteins to Basement Membrane Assembly.* Journal of Biological Chemistry, 2009. **284**(13): p. 8984-8994.

167. Bork, P., et al., *Structure and distribution of modules in extracellular proteins.* Q Rev Biophys, 1996. **29**(2): p. 119-67.

168. Aumailley, M., *The laminin family.* Cell Adhesion and Migration, 2013. **7**(1): p. 48-55.

169. Stetefeld, J., et al., *Crystal structure of three consecutive laminin-type epidermal growth factor-like (LE) modules of laminin gamma1 chain harboring the nidogen binding site.* J Mol Biol, 1996. **257**(3): p. 644-57.

170. Hohenester, E. and J. Engel, *Domain structure and organisation in extracellular matrix proteins.* Matrix Biol, 2002. **21**(2): p. 115-28.

171. Okamoto, O., et al., *Normal Human Keratinocytes Bind to the α3LG4/5 Domain of Unprocessed Laminin-5 through the Receptor Syndecan-1.* Journal of Biological Chemistry, 2003. **278**(45): p. 44168-44177.

172. Ogawa, T., et al., *The short arm of laminin γ2 chain of laminin-5 (laminin-332) binds syndecan-1 and regulates cellular adhesion and migration by suppressing phosphorylation of integrin β4 chain.* Molecular biology of the cell, 2007. **18**(5): p. 1621-1633.

173. Baumgartner, R., et al., *Structure of the nidogen binding LE module of the laminin gamma1 chain in solution.* J Mol Biol, 1996. **257**(3): p. 658-68.

174. Giannelli, G., et al., *Induction of cell migration by matrix metalloprotease-2 cleavage of laminin-5.* Science, 1997. **277**(5323): p. 225-8.

175. Sasaki, M., et al., *Laminin, a multidomain protein. The A chain has a unique globular domain and homology with the basement membrane proteoglycan and the laminin B chains.* Journal of Biological Chemistry, 1988. **263**(32): p. 16536-44.

176. Hohenester, E., et al., *The crystal structure of a laminin G-like module reveals the molecular basis of alpha-dystroglycan binding to laminins, perlecan, and agrin.* Mol Cell, 1999. **4**(5): p. 783-92.

177. Carafoli, F., N.J. Clout, and E. Hohenester, *Crystal Structure of the LG1-3 Region of the Laminin α2 Chain.* Journal of Biological Chemistry, 2009. **284**(34): p. 22786-22792.

178. Aumailley, M. and T. Krieg, *Laminins: A Family of Diverse Multifunctional Molecules of Basement Membranes.* Journal of Investigative Dermatology, 1996. **106**(2): p. 209-214.

179. Aumailley, M., R. Timpl, and A. Sonnenberg, *Antibody to integrin alpha 6 subunit specifically inhibits cell-binding to laminin fragment 8.* Exp Cell Res, 1990. **188**(1): p. 55-60.

180. Nishiuchi, R., et al., *Ligand-binding specificities of laminin-binding integrins: a comprehensive survey of laminin-integrin interactions using recombinant alpha3beta1, alpha6beta1, alpha7beta1 and alpha6beta4 integrins.* Matrix Biol, 2006. **25**(3): p. 189-97.

181. Ott, U., et al., *Protease resistance and conformation of laminin.* Eur J Biochem, 1982. **123**(1): p. 63-72.

182. Taraboletti, G., et al., *Sulfatide-binding domain of the laminin A chain.* Journal of Biological Chemistry, 1990. **265**(21): p. 12253-8.

183. Kalb, E. and J. Engel, *Binding and calcium-induced aggregation of laminin onto lipid bilayers.* Journal of Biological Chemistry, 1991. **266**(28): p. 19047-19052.

184. Yurchenco, P.D., et al., *The α chain of laminin-1 is independently secreted and drives secretion of its β- and γ-chain partners.* Proc Natl Acad Sci U S A, 1997. **94**(19): p. 10189-94.

185. Kunneken, K., et al., *Recombinant human laminin-5 domains. Effects of heterotrimerization, proteolytic processing, and N-glycosylation on alpha3beta1 integrin binding.* J Biol Chem, 2004. **279**(7): p. 5184-93.

186. Denzer, A.J., et al., *Electron microscopic structure of agrin and mapping of its binding site in laminin-1.* Embo j, 1998. **17**(2): p. 335-43.

187. Costell, M., et al., *Structural characterization of recombinant domain II of the basement membrane proteoglycan perlecan.* FEBS Letters, 1996. **396**(2): p. 127-131.

188. Schulze, B., et al., *Structural and functional analysis of the globular domain IVa of the laminin α1 chain and its impact on an adjacent RGD site.* Biochemical Journal, 1996. **314**(3): p. 847-851.

189. Allamand, V., et al., *Mild congenital muscular dystrophy in two patients with an internally deleted laminin alpha2-chain.* Hum Mol Genet, 1997. **6**(5): p. 747-52.

190. Fahey, B. and B.M. Degnan, *Origin and evolution of laminin gene family diversity.* Mol Biol Evol, 2012. **29**(7): p. 1823-36.

191. Nomizu, M., et al., *Mechanism of laminin chain assembly into a triple-stranded coiled-coil structure.* Biochemistry, 1996. **35**(9): p. 2885-93.

192. Sasaki, M., et al., *Sequence of the cDNA encoding the laminin B1 chain reveals a multidomain protein containing cysteine-rich repeats.* Proc Natl Acad Sci U S A, 1987. **84**(4): p. 935-9.

193. Utani, A., et al., *Laminin chain assembly. Specific sequences at the C terminus of the long arm are required for the formation of specific double- and triple-stranded coiled-coil structures.* Journal of Biological Chemistry, 1994. **269**(29): p. 19167-19175.

194. Engvall, E., *Laminin variants: why, where and when?* Kidney Int, 1993. **43**(1): p. 2-6.

195. Bieglmayer, C., A. Feiks, and R. Rudelstorfer, *Laminin in pregnancy.* Gynecol Obstet Invest, 1986. **22**(1): p. 7-11.

196. Nguyen, N.M., et al., *Laminin alpha-chain expression and basement membrane formation by MLE-15 respiratory epithelial cells.* Am J Physiol Lung Cell Mol Physiol, 2002. **282**(5): p. L1004-11.

197. Klein, G., et al., *Role of laminin A chain in the development of epithelial cell polarity.* Cell, 1988. **55**(2): p. 331-41.

198. Miner, J.H. and C. Li, *Defective glomerulogenesis in the absence of laminin α5 demonstrates a developmental role for the kidney glomerular basement membrane.* Developmental biology, 2000. **217**(2): p. 278-289.

199. Patton, B.L., *Laminins of the neuromuscular system.* Microsc Res Tech, 2000. **51**(3): p. 247-61.

200. Miner, J.H., J. Cunningham, and J.R. Sanes, *Roles for Laminin in Embryogenesis: Exencephaly, Syndactyly, and Placentopathy in Mice Lacking the Laminin α5 Chain.* J Cell Biol, 1998. **143**(6): p. 1713-23.

201. Koch, M., et al., *Characterization and expression of the laminin gamma3 chain: a novel, non-basement membrane-associated, laminin chain.* J Cell Biol, 1999. **145**(3): p. 605-18.

202. Yin, Y., et al., *Expression of laminin chains by central neurons: analysis with gene and protein trapping techniques.* Genesis, 2003. **36**(2): p. 114-27.

203. Dickson, B.J., *Molecular Mechanisms of Axon Guidance.* Science, 2002. **298**(5600): p. 1959-1964.

204. Lin, J.C., et al., *The netrin-G1 ligand NGL-1 promotes the outgrowth of thalamocortical axons.* Nat Neurosci, 2003. **6**(12): p. 1270-1276.

205. Miner, J.H., et al., *The Laminin α Chains: Expression, Developmental Transitions, and Chromosomal Locations of α1-5, Identification of Heterotrimeric Laminins 8–11, and Cloning of a Novel α3 Isoform.* J Cell Biol, 1997. **137**(3): p. 685-701.

206. Hallmann, R., et al., *Expression and function of laminins in the embryonic and mature vasculature.* Physiol Rev, 2005. **85**(3): p. 979-1000.

207. Aumailley, M. and N. Smyth, *The role of laminins in basement membrane function.* J Anat, 1998. **193 (Pt 1)**: p. 1-21.

208. Pouliot, N. and N. Kusuma, *Laminin-511: a multi-functional adhesion protein regulating cell migration, tumor invasion and metastasis.* Cell Adh Migr, 2013. **7**(1): p. 142-9.

209. Goldfinger, L., et al., *The alpha3 laminin subunit, alpha6beta4 and alpha3beta1 integrin coordinately regulate wound healing in cultured epithelial cells and in the skin.* Journal of Cell Science, 1999. **112**(16): p. 2615-2629.

210. Zhang, K. and R.H. Kramer, *Laminin 5 Deposition Promotes Keratinocyte Motility.* Experimental Cell Research, 1996. **227**(2): p. 309-322.

211. Kainulainen, T., et al., *Laminin-5 expression is independent of the injury and the microenvironment during reepithelialization of wounds.* J Histochem Cytochem, 1998. **46**(3): p. 353-60.

212. Nguyen, B.P., S.G. Gil, and W.G. Carter, *Deposition of laminin 5 by keratinocytes regulates integrin adhesion and signaling.* J Biol Chem, 2000. **275**(41): p. 31896-907.

213. Sato, N., et al., *Abnormal deposition of laminin and type IV collagen at corneal epithelial basement membrane during wound healing in diabetic rats.* Jpn J Ophthalmol, 1999. **43**(5): p. 343-7.

214. Ljubimov, A.V., et al., *Human corneal epithelial basement membrane and integrin alterations in diabetes and diabetic retinopathy.* J Histochem Cytochem, 1998. **46**(9): p. 1033-41.

215. Thyboll, J., et al., *Deletion of the laminin alpha4 chain leads to impaired microvessel maturation.* Mol Cell Biol, 2002. **22**(4): p. 1194-202.

216. Jakobsson, L., et al., *Laminin deposition is dispensable for vasculogenesis but regulates blood vessel diameter independent of flow.* Faseb j, 2008. **22**(5): p. 1530-9.

217. Kortesmaa, J., P. Yurchenco, and K. Tryggvason, *Recombinant laminin-8 (alpha(4)beta(1)gamma(1)). Production, purification,and interactions with integrins.* J Biol Chem, 2000. **275**(20): p. 14853-9.

218. Legeais, J.M., et al., *Influence of ePTFE polymer implant permeability on the rate and density of corneal extracellular matrix synthesis.* J Biomed Mater Res, 1997. **36**(1): p. 49-54.

219. Patel, S., et al., *Corneal sensitivity and some properties of the tear film after laser in situ keratomileusis.* J Refract Surg, 2001. **17**(1): p. 17-24.

220. Reinstein, D.Z., T.J. Archer, and M. Gobbe, *Corneal epithelial thickness profile in the diagnosis of keratoconus.* J Refract Surg, 2009. **25**(7): p. 604-10.

221. Bron, A.M., et al., *Falsely elevated intraocular pressure due to increased central corneal thickness.* Graefes Arch Clin Exp Ophthalmol, 1999. **237**(3): p. 220-4.

222. Ruberti, J.W., A.S. Roy, and C.J. Roberts, *Corneal biomechanics and biomaterials.* Annu Rev Biomed Eng, 2011. **13**: p. 269-95.

223. Kruse, F.E., *Stem cells and corneal epithelial regeneration.* Eye (Lond), 1994. **8 (Pt 2)**: p. 170-83.

224. Thoft, R.A. and J. Friend, *The X, Y, Z hypothesis of corneal epithelial maintenance.* Invest Ophthalmol Vis Sci, 1983. **24**(10): p. 1442-3.

225. Stepp, M.A. and J.D. Zieske, *The corneal epithelial stem cell niche.* Ocul Surf, 2005. **3**(1): p. 15-26.

226. Kabosova, A., et al., *Compositional differences between infant and adult human corneal basement membranes.* Invest Ophthalmol Vis Sci, 2007. **48**(11): p. 4989-99.

227. Schermer, A., S. Galvin, and T.T. Sun, *Differentiation-related expression of a major 64K corneal keratin in vivo and in culture suggests limbal location of corneal epithelial stem cells.* J Cell Biol, 1986. **103**(1): p. 49-62.

228. Streilein, J.W., et al., *Functional Dichotomy between Langerhans Cells that Present Antigen to Naive and to Memory/Effector T Lymphocytes.* Immunological Reviews, 1990. **117**(1): p. 159-183.

229. Robertson, D.M., et al., *Characterization of growth and differentiation in a telomerase-immortalized human corneal epithelial cell line.* Investigative Ophthalmology & Visual Science, 2005. **46**(2): p. 470-478.

230. Filenius, S., et al., *Laminin Synthesis and the Adhesion Characteristics of Immortalized Human Corneal Epithelial Cells to Laminin Isoforms.* Experimental Eye Research, 2001. **72**(1): p. 93-103.

231. Ljubimov, A.V., et al., *Human corneal basement membrane heterogeneity: Topographical differences in the expression of type IV collagen and laminin isoforms.* Laboratory Investigation, 1995. **72**(4): p. 461-473.

232. Kariya, Y., et al., *Characterization of laminin 5B and NH2-terminal proteolytic fragment of its alpha3B chain: promotion of cellular adhesion, migration, and proliferation.* J Biol Chem, 2004. **279**(23): p. 24774-84.

233. Sugawara, K., et al., *Laminin-332 and -511 in skin.* Experimental Dermatology, 2008. **17**(6): p. 473-480.

234. Rousselle, P., et al., *Kalinin: an epithelium-specific basement membrane adhesion molecule that is a component of anchoring filaments.* J Cell Biol, 1991. **114**(3): p. 567-76.

235. Rousselle, P., et al., *Laminin 5 binds the NC-1 domain of type VII collagen.* J Cell Biol, 1997. **138**(3): p. 719-28.

236. Marinkovich, M.P., G.P. Lunstrum, and R.E. Burgeson, *The anchoring filament protein kalinin is synthesized and secreted as a high molecular weight precursor.* J Biol Chem, 1992. **267**(25): p. 17900-6.

237. Goldfinger, L.E., M.S. Stack, and J.C. Jones, *Processing of laminin-5 and its functional consequences: role of plasmin and tissue-type plasminogen activator.* J Cell Biol, 1998. **141**(1): p. 255-65.

238. Tsubota, Y., et al., *Regulation of biological activity and matrix assembly of laminin-5 by COOH-terminal, LG4-5 domain of alpha3 chain.* J Biol Chem, 2005. **280**(15): p. 14370-7.

239. Matsui, C., et al., *The Assembly of Laminin-5 Subunits.* Journal of Biological Chemistry, 1995. **270**(40): p. 23496-23503.

240. Chen, Z.L. and S. Strickland, *Neuronal death in the hippocampus is promoted by plasmin-catalyzed degradation of laminin.* Cell, 1997. **91**(7): p. 917-25.

241. Amano, S., et al., *Bone morphogenetic protein 1 is an extracellular processing enzyme of the laminin 5 gamma 2 chain.* J Biol Chem, 2000. **275**(30): p. 22728-35.

242. Tsubota, Y., et al., *Isolation and Activity of Proteolytic Fragment of Laminin-5 α3 Chain.* Biochemical and Biophysical Research Communications, 2000. **278**(3): p. 614-620.

243. Décline, F., et al., *Keratinocyte motility induced by TGF-β1 is accompanied by dramatic changes in cellular interactions with laminin 5.* Cell Motility and the Cytoskeleton, 2003. **54**(1): p. 64-80.

244. Sigle, R.O., et al., *Globular domains 4/5 of the laminin α3 chain mediate deposition of precursor laminin 5.* Journal of Cell Science, 2004. **117**(19): p. 4481-4494.

245. Veitch, D.P., et al., *Mammalian tolloid metalloproteinase, and not matrix metalloprotease 2 or membrane type 1 metalloprotease, processes laminin-5 in keratinocytes and skin.* J Biol Chem, 2003. **278**(18): p. 15661-8.

246. Hirosaki, T., et al., *Laminin-6 Is Activated by Proteolytic Processing and Regulates Cellular Adhesion and Migration Differently from Laminin-5.* Journal of Biological Chemistry, 2002. **277**(51): p. 49287-49295.

247. Utani, A., et al., *A unique sequence of the laminin alpha 3 G domain binds to heparin and promotes cell adhesion through syndecan-2 and -4.* J Biol Chem, 2001. **276**(31): p. 28779-88.

248. Kato, K., et al., *Identification of neurite outgrowth promoting sites on the laminin alpha 3 chain G domain.* Biochemistry, 2002. **41**(35): p. 10747-53.

249. Schenk, S., et al., *Binding to EGF receptor of a laminin-5 EGF-like fragment liberated during MMP-dependent mammary gland involution.* J Cell Biol, 2003. **161**(1): p. 197-209.

250. Hirosaki, T., et al., *Structural requirement of carboxyl-terminal globular domains of laminin alpha 3 chain for promotion of rapid cell adhesion and migration by laminin-5.* J Biol Chem, 2000. **275**(29): p. 22495-502.

251. Gagnoux-Palacios, L., et al., *The Short Arm of the Laminin γ2 Chain Plays a Pivotal Role in the Incorporation of Laminin 5 into the Extracellular Matrix and in Cell Adhesion.* The Journal of Cell Biology, 2001. **153**(4): p. 835-850.

252. Aumailley, M., et al., *Laminin 5 processing and its integration into the ECM.* Matrix Biol, 2003. **22**(1): p. 49-54.

253. van Balkom, I.D. and R.C. Hennekam, *Dermal eccrine cylindromatosis.* J Med Genet, 1994. **31**(4): p. 321-4.

254. Tunggal, L., et al., *Defective Laminin 5 Processing in Cylindroma Cells.* Am J Pathol, 2002. **160**(2): p. 459-68.

255. Geiger, B., J.P. Spatz, and A.D. Bershadsky, *Environmental sensing through focal adhesions.* Nat Rev Mol Cell Biol, 2009. **10**(1): p. 21-33.

256. Huang, S. and D.E. Ingber, *The structural and mechanical complexity of cell-growth control.* Nat Cell Biol, 1999. **1**(5): p. E131-8.

257. Lock, J.G., B. Wehrle-Haller, and S. Strömblad, *Cell–matrix adhesion complexes: Master control machinery of cell migration.* Seminars in Cancer Biology, 2008. **18**(1): p. 65-76.

258. Weiss, P. and W. Ferris, *ELECTRON-MICROSCOPIC STUDY OF THE TEXTURE OF THE BASEMENT MEMBRANE OF LARVAL AMPHIBIAN SKIN.* Proc Natl Acad Sci U S A, 1954. **40**(6): p. 528-40.

259. Green, K.J. and J.C. Jones, *Desmosomes and hemidesmosomes: structure and function of molecular components.* Faseb j, 1996. **10**(8): p. 871-81.

260. Tsuruta, D., et al., *Hemidesmosomes and focal contact proteins: functions and cross-talk in keratinocytes, bullous diseases and wound healing.* J Dermatol Sci, 2011. **62**(1): p. 1-7.

261. Tsuruta, D., S.B. Hopkinson, and J.C.R. Jones, *Hemidesmosome protein dynamics in live epithelial cells.* Cell Motility and the Cytoskeleton, 2003. **54**(2): p. 122-134.

262. Borradori, L. and A. Sonnenberg, *Structure and function of hemidesmosomes: more than simple adhesion complexes.* J Invest Dermatol, 1999. **112**(4): p. 411-8.

263. Tidman, M.J. and R.A. Eady, *Ultrastructural morphometry of normal human dermal-epidermal junction. The influence of age, sex, and body region on laminar and nonlaminar components.* J Invest Dermatol, 1984. **83**(6): p. 448-53.

264. Tidman, M.J. and R.A.J. Eady, *Hemidesmosome Heterogeneity in Junctional Epidermolysis Bullosa Revealed by Morphometric Analysis.* Journal of Investigative Dermatology, 1986. **86**(1): p. 51-56.

265. Litjens, S.H., J.M. de Pereda, and A. Sonnenberg, *Current insights into the formation and breakdown of hemidesmosomes.* Trends Cell Biol, 2006. **16**(7): p. 376-83.

266. Burgeson, R.E. and A.M. Christiano, *The dermal-epidermal junction.* Curr Opin Cell Biol, 1997. **9**(5): p. 651-8.

267. Wiche, G., *Role of plectin in cytoskeleton organization and dynamics.* Journal of Cell Science, 1998. **111**(17): p. 2477-2486.

268. Hopkinson, S.B. and J.C. Jones, *The N terminus of the transmembrane protein BP180 interacts with the N-terminal domain of BP230, thereby mediating keratin cytoskeleton anchorage to the cell surface at the site of the hemidesmosome.* Mol Biol Cell, 2000. **11**(1): p. 277-86.

269. Jones, J.C., S.B. Hopkinson, and L.E. Goldfinger, *Structure and assembly of hemidesmosomes.* Bioessays, 1998. **20**(6): p. 488-94.

270. Sterk, L.M., et al., *The tetraspan molecule CD151, a novel constituent of hemidesmosomes, associates with the integrin alpha6beta4 and may regulate the spatial organization of hemidesmosomes.* J Cell Biol, 2000. **149**(4): p. 969-82.

271. Masunaga, T., et al., *Localization of laminin-5 in the epidermal basement membrane.* J Histochem Cytochem, 1996. **44**(11): p. 1223-30.

272. Masunaga, T., et al., *The Extracellular Domain of BPAG2 Localizes to Anchoring Filaments and its Carboxyl Terminus Extends to the Lamina Densa of Normal Human Epidermal Basement Membrane.* Journal of Investigative Dermatology, 1997. **109**(2): p. 200-206.

273. Nievers, M.G., R.Q.J. Schaapveld, and A. Sonnenberg, *Biology and function of hemidesmosomes.* Matrix Biology, 1999. **18**(1): p. 5-17.

274. Uematsu, J., et al., *Demonstration of type II hemidesmosomes in a mammary gland epithelial cell line, BMGE-H.* J Biochem, 1994. **115**(3): p. 469-76.

275. Fontao, L., et al., *Polarized expression of HD1: relationship with the cytoskeleton in cultured human colonic carcinoma cells.* Exp Cell Res, 1997. **231**(2): p. 319-27.

276. Wiche, G., et al., *Cloning and sequencing of rat plectin indicates a 466-kD polypeptide chain with a three-domain structure based on a central alpha-helical coiled coil.* J Cell Biol, 1991. **114**(1): p. 83-99.

277. Smith, F.J., et al., *Plectin deficiency results in muscular dystrophy with epidermolysis bullosa.* Nat Genet, 1996. **13**(4): p. 450-7.

278. Stanley, J.R., et al., *Isolation of complementary DNA for bullous pemphigoid antigen by use of patients' autoantibodies.* J Clin Invest, 1988. **82**(6): p. 1864-70.

279. Sawamura, D., et al., *Human bullous pemphigoid antigen (BPAG1). Amino acid sequences deduced from cloned cDNAs predict biologically important peptide segments and protein domains.* J Biol Chem, 1991. **266**(27): p. 17784-90.

280. Tanaka, T., et al., *Comparison of molecularly cloned bullous pemphigoid antigen to desmoplakin I confirms that they define a new family of cell adhesion junction plaque proteins.* J Biol Chem, 1991. **266**(19): p. 12555-9.

281. Elliott, C.E., et al., *Plectin transcript diversity: identification and tissue distribution of variants with distinct first coding exons and rodless isoforms.* Genomics, 1997. **42**(1): p. 115-25.

282. Wiche, G. and L. Winter, *Plectin isoforms as organizers of intermediate filament cytoarchitecture.* Bioarchitecture, 2011. **1**(1): p. 14-20.

283. Niessen, C.M., et al., *A minimal region on the integrin beta4 subunit that is critical to its localization in hemidesmosomes regulates the distribution of HD1/plectin in COS-7 cells.* J Cell Sci, 1997. **110 (Pt 15)**: p. 1705-16.

284. McLean, W.H., et al., *Loss of plectin causes epidermolysis bullosa with muscular dystrophy: cDNA cloning and genomic organization.* Genes Dev, 1996. **10**(14): p. 1724-35.

285. Zillikens, D., *Acquired skin disease of hemidesmosomes.* J Dermatol Sci, 1999. **20**(2): p. 134-54.

286. Borradori, L., et al., *Role of the bullous pemphigoid antigen 180 (BP180) in the assembly of hemidesmosomes and cell adhesion--reexpression of BP180 in generalized atrophic benign epidermolysis bullosa keratinocytes.* Exp Cell Res, 1998. **239**(2): p. 463-76.

287. McMillan, J.R., M. Akiyama, and H. Shimizu, *Epidermal basement membrane zone components: ultrastructural distribution and molecular interactions.* J Dermatol Sci, 2003. **31**(3): p. 169-77.

288. Guo, L., et al., *Gene targeting of BPAG1: abnormalities in mechanical strength and cell migration in stratified epithelia and neurologic degeneration.* Cell, 1995. **81**(2): p. 233-43.

289. McGrath, J.A., *Recently Identified Forms of Epidermolysis Bullosa.* Ann Dermatol, 2015. **27**(6): p. 658-66.

290. Kurpakus, M.A. and J.C. Jones, *A novel hemidesmosomal plaque component: tissue distribution and incorporation into assembling hemidesmosomes in an in vitro model.* Exp Cell Res, 1991. **194**(1): p. 139-46.

291. Springer, T.A. and J.H. Wang, *The three-dimensional structure of integrins and their ligands, and conformational regulation of cell adhesion.* Adv Protein Chem, 2004. **68**: p. 29-63.

292. Arnaout, M.A., B. Mahalingam, and J.P. Xiong, *Integrin structure, allostery, and bidirectional signaling.* Annu Rev Cell Dev Biol, 2005. **21**: p. 381-410.

293. Clark, E.A. and J.S. Brugge, *Integrins and signal transduction pathways: the road taken.* Science, 1995. **268**(5208): p. 233-9.

294. Calderwood, D.A., S.J. Shattil, and M.H. Ginsberg, *Integrins and actin filaments: reciprocal regulation of cell adhesion and signaling.* J Biol Chem, 2000. **275**(30): p. 22607-10.

295. Jones, J.C., et al., *Hemidesmosomes: extracellular matrix/intermediate filament connectors.* Exp Cell Res, 1994. **213**(1): p. 1-11.

296. Takada, Y. and M.E. Hemler, *The primary structure of the VLA-2/collagen receptor alpha 2 subunit (platelet GPIa): homology to other integrins and the presence of a possible collagen-binding domain.* J Cell Biol, 1989. **109**(1): p. 397-407.

297. Giancotti, F.G., et al., *Proteolytic processing of endogenous and recombinant beta 4 integrin subunit.* J Cell Biol, 1992. **118**(4): p. 951-9.

298. Tamura, R.N., et al., *Epithelial integrin alpha 6 beta 4: complete primary structure of alpha 6 and variant forms of beta 4.* J Cell Biol, 1990. **111**(4): p. 1593-604.

299. Nievers, M.G., et al., *Formation of hemidesmosome-like structures in the absence of ligand binding by the (alpha)6(beta)4 integrin requires binding of HD1/plectin to the cytoplasmic domain of the (beta)4 integrin subunit.* J Cell Sci, 2000. **113 (Pt 6)**: p. 963-73.

300. Mercurio, A.M., I. Rabinovitz, and L.M. Shaw, *The alpha 6 beta 4 integrin and epithelial cell migration.* Curr Opin Cell Biol, 2001. **13**(5): p. 541-5.

301. Kurpakus, M.A., V. Quaranta, and J.C. Jones, *Surface relocation of alpha 6 beta 4 integrins and assembly of hemidesmosomes in an in vitro model of wound healing.* J Cell Biol, 1991. **115**(6): p. 1737-50.

302. Vidal, F., et al., *Integrin [beta]4 mutations associated with junctional epidermolysis bullosa with pyloric atresia.* Nat Genet, 1995. **10**(2): p. 229-234.

303. Ruzzi, L., et al., *A homozygous mutation in the integrin alpha6 gene in junctional epidermolysis bullosa with pyloric atresia.* J Clin Invest, 1997. **99**(12): p. 2826-31.

304. Pulkkinen, L., et al., *Homozygous α6 integrin mutation in junctional epidermolysis bullosa with congenital duodenal atresia.* Human molecular genetics, 1997. **6**(5): p. 669-674.

305. Dowling, J., Q.C. Yu, and E. Fuchs, *Beta4 integrin is required for hemidesmosome formation, cell adhesion and cell survival.* J Cell Biol, 1996. **134**(2): p. 559-72.

306. Georges-Labouesse, E., et al., *Absence of integrin alpha 6 leads to epidermolysis bullosa and neonatal death in mice.* Nat Genet, 1996. **13**(3): p. 370-3.

307. van der Neut, R., et al., *Epithelial detachment due to absence of hemidesmosomes in integrin beta 4 null mice.* Nat Genet, 1996. **13**(3): p. 366-9.

308. Sincock, P.M., G. Mayrhofer, and L.K. Ashman, *Localization of the transmembrane 4 superfamily (TM4SF) member PETA-3 (CD151) in normal human tissues: comparison with CD9, CD63, and alpha5beta1 integrin.* J Histochem Cytochem, 1997. **45**(4): p. 515-25.

309. Kazarov, A.R., et al., *An extracellular site on tetraspanin CD151 determines α3 and α6 integrin–dependent cellular morphology.* J Cell Biol, 2002. **158**(7): p. 1299-309.

310. Yauch, R.L., et al., *Highly stoichiometric, stable, and specific association of integrin alpha3beta1 with CD151 provides a major link to phosphatidylinositol 4-kinase, and may regulate cell migration.* Mol Biol Cell, 1998. **9**(10): p. 2751-65.

311. Yauch, R.L., et al., *Direct extracellular contact between integrin alpha(3)beta(1) and TM4SF protein CD151.* J Biol Chem, 2000. **275**(13): p. 9230-8.

312. Sterk, L.M., et al., *Association of the tetraspanin CD151 with the laminin-binding integrins alpha3beta1, alpha6beta1, alpha6beta4 and alpha7beta1 in cells in culture and in vivo.* J Cell Sci, 2002. **115**(Pt 6): p. 1161-73.

313. Hasegawa, H., et al., *SFA-1/PETA-3 (CD151), a Member of the Transmembrane 4 Superfamily, Associates Preferentially with α₅β₁ Integrin and Regulates Adhesion of Human T Cell Leukemia Virus Type 1-Infected T Cells to Fibronectin.* The Journal of Immunology, 1998. **161**(6): p. 3087-3095.

314. Berditchevski, F. and E. Odintsova, *Characterization of Integrin–Tetraspanin Adhesion Complexes: Role of Tetraspanins in Integrin Signaling.* J Cell Biol, 1999. **146**(2): p. 477-92.

315. Sincock, P.M., et al., *PETA-3/CD151, a member of the transmembrane 4 superfamily, is localised to the plasma membrane and endocytic system of endothelial cells, associates with multiple integrins and modulates cell function.* J Cell Sci, 1999. **112 (Pt 6)**: p. 833-44.

316. Wright, M.D., et al., *Characterization of mice lacking the tetraspanin superfamily member CD151.* Mol Cell Biol, 2004. **24**(13): p. 5978-88.

317. Sachs, N., et al., *Kidney failure in mice lacking the tetraspanin CD151.* The Journal of Cell Biology, 2006. **175**(1): p. 33-39.

318. Franzke, C.W., et al., *Collagenous transmembrane proteins: collagen XVII as a prototype.* Matrix Biol, 2003. **22**(4): p. 299-309.

319. Giudice, G.J., D.J. Emery, and L.A. Diaz, *Cloning and primary structural analysis of the bullous pemphigoid autoantigen BP180.* J Invest Dermatol, 1992. **99**(3): p. 243-50.

320. Hirako, Y., et al., *Demonstration of the molecular shape of BP180, a 180-kDa bullous pemphigoid antigen and its potential for trimer formation.* J Biol Chem, 1996. **271**(23): p. 13739-45.

321. Hirako, Y., et al., *Cleavage of BP180, a 180-kDa Bullous Pemphigoid Antigen, Yields a 120-kDa Collagenous Extracellular Polypeptide.* Journal of Biological Chemistry, 1998. **273**(16): p. 9711-9717.

322. Loffek, S., et al., *Transmembrane collagen XVII modulates integrin dependent keratinocyte migration via PI3K/Rac1 signaling.* PLoS One, 2014. **9**(2): p. e87263.

323. Nishie, W., et al., *Dynamic interactions of epidermal collagen XVII with the extracellular matrix: laminin 332 as a major binding partner.* Am J Pathol, 2011. **179**(2): p. 829-37.

324. Jonkman, M.F., et al., *Inflammatory variant of epidermolysis bullosa acquisita with igg autoantibodies against type vii collagen and laminin α3.* Archives of Dermatology, 2000. **136**(2): p. 227-231.

325. Krawczyk, W.S. and G.F. Wilgram, *Hemidesmosome and desmosome morphogenesis during epidermal wound healing.* J Ultrastruct Res, 1973. **45**(1): p. 93-101.

326. Gipson, I.K., J. Friend, and S.J. Spurr, *Transplant of corneal epithelium to rabbit corneal wounds in vivo.* Invest Ophthalmol Vis Sci, 1985. **26**(4): p. 425-33.

327. Gipson, I.K., et al., *Hemidesmosome formation in vitro.* J Cell Biol, 1983. **97**(3): p. 849-57.

328. Geerts, D., et al., *Binding of integrin alpha6beta4 to plectin prevents plectin association with F-actin but does not interfere with intermediate filament binding.* J Cell Biol, 1999. **147**(2): p. 417-34.

329. Koster, J., et al., *Two different mutations in the cytoplasmic domain of the integrin beta 4 subunit in nonlethal forms of epidermolysis bullosa prevent interaction of beta 4 with plectin.* J Invest Dermatol, 2001. **117**(6): p. 1405-11.

330. Nakano, A., et al., *Epidermolysis Bullosa with Congenital Pyloric Atresia: Novel Mutations in the [bgr]4 Integrin Gene (ITGB4) and Genotype/Phenotype Correlations.* Pediatr Res, 2001. **49**(5): p. 618-626.

331. Andra, K., et al., *Targeted inactivation of plectin reveals essential function in maintaining the integrity of skin, muscle, and heart cytoarchitecture.* Genes Dev, 1997. **11**(23): p. 3143-56.

332. Wickstrom, S.A., K. Radovanac, and R. Fassler, *Genetic analyses of integrin signaling.* Cold Spring Harb Perspect Biol, 2011. **3**(2).

333. Koster, J., et al., *Role of Binding of Plectin to the Integrin β4 Subunit in the Assembly of Hemidesmosomes.* Mol Biol Cell, 2004. **15**(3): p. 1211-23.

334. Rezniczek Gü, A., et al., *Linking Integrin α(6)β(4)-based Cell Adhesion to the Intermediate Filament Cytoskeleton: Direct Interaction between the β(4) Subunit and Plectin at Multiple Molecular Sites.* J Cell Biol, 1998. **141**(1): p. 209-25.

335. Schaapveld, R.Q., et al., *Hemidesmosome formation is initiated by the beta4 integrin subunit, requires complex formation of beta4 and HD1/plectin, and involves a direct interaction between beta4 and the bullous pemphigoid antigen 180.* J Cell Biol, 1998. **142**(1): p. 271-84.

336. Gipson, I.K., et al., *Redistribution of the hemidesmosome components alpha 6 beta 4 integrin and bullous pemphigoid antigens during epithelial wound healing.* Exp Cell Res, 1993. **207**(1): p. 86-98.

337. Janes, S.M. and F.M. Watt, *New roles for integrins in squamous-cell carcinoma.* Nat Rev Cancer, 2006. **6**(3): p. 175-183.

338. Wilhelmsen, K., S.H.M. Litjens, and A. Sonnenberg, *Multiple Functions of the Integrin α6β4 in Epidermal Homeostasis and Tumorigenesis.* Molecular and Cellular Biology, 2006. **26**(8): p. 2877-2886.

339. Hopkinson, S.B., et al., *Focal Contact and Hemidesmosomal Proteins in Keratinocyte Migration and Wound Repair.* Adv Wound Care (New Rochelle), 2014. **3**(3): p. 247-63.

340. Margadant, C., et al., *Regulation of hemidesmosome disassembly by growth factor receptors.* Curr Opin Cell Biol, 2008. **20**(5): p. 589-96.

341. Dans, M., et al., *Tyrosine phosphorylation of the beta 4 integrin cytoplasmic domain mediates Shc signaling to extracellular signal-regulated kinase and antagonizes formation of hemidesmosomes.* J Biol Chem, 2001. **276**(2): p. 1494-502.

342. Merdek, K.D., et al., *Intrinsic signaling functions of the beta4 integrin intracellular domain.* J Biol Chem, 2007. **282**(41): p. 30322-30.

343. Nikolopoulos, S.N., et al., *Targeted Deletion of the Integrin β4 Signaling Domain Suppresses Laminin-5-Dependent Nuclear Entry of Mitogen-Activated Protein Kinases and NF-κB, Causing Defects in Epidermal Growth and Migration.* Molecular and Cellular Biology, 2005. **25**(14): p. 6090-6102.

344. Rabinovitz, I., L. Tsomo, and A.M. Mercurio, *Protein Kinase C-α Phosphorylation of Specific Serines in the Connecting Segment of the β4 Integrin Regulates the Dynamics of Type II Hemidesmosomes.* Molecular and Cellular Biology, 2004. **24**(10): p. 4351-4360.

345. Wilhelmsen, K., et al., *Serine Phosphorylation of the Integrin β4 Subunit Is Necessary for Epidermal Growth Factor Receptor–induced Hemidesmosome Disruption.* Molecular Biology of the Cell, 2007. **18**(9): p. 3512-3522.

346. Alt, A., et al., *Protein kinase Cdelta-mediated phosphorylation of alpha6beta4 is associated with reduced integrin localization to the hemidesmosome and decreased keratinocyte attachment.* Cancer Res, 2001. **61**(11): p. 4591-8.

347. Walko, G., M.J. Castañón, and G. Wiche, *Molecular architecture and function of the hemidesmosome.* Cell Tissue Res, 2015. **360**(2): p. 363-78.

348. Carroll, D.K., et al., *p63 regulates an adhesion programme and cell survival in epithelial cells.* Nat Cell Biol, 2006. **8**(6): p. 551-561.

349. Mulder, K.W., et al., *Diverse epigenetic strategies interact to control epidermal differentiation.* Nat Cell Biol, 2012. **14**(7): p. 753-63.

350. Blanpain, C., et al., *Canonical notch signaling functions as a commitment switch in the epidermal lineage.* Genes Dev, 2006. **20**(21): p. 3022-35.

351. Restivo, G., et al., *IRF6 is a mediator of Notch pro-differentiation and tumour suppressive function in keratinocytes.* Embo j, 2011. **30**(22): p. 4571-85.

352. Watt, F.M., S. Estrach, and C.A. Ambler, *Epidermal Notch signalling: differentiation, cancer and adhesion.* Curr Opin Cell Biol, 2008. **20**(2): p. 171-9.

353. Sehgal, B.U., et al., *Integrin beta4 regulates migratory behavior of keratinocytes by determining laminin-332 organization.* J Biol Chem, 2006. **281**(46): p. 35487-98.

354. Sheppard, D., *In vivo functions of integrins: lessons from null mutations in mice.* Matrix Biology, 2000. **19**(3): p. 203-209.

355. Hamill, K.J., et al., *Type XVII collagen regulates lamellipod stability, cell motility, and signaling to Rac1 by targeting bullous pemphigoid antigen 1e to alpha6beta4 integrin.* J Biol Chem, 2011. **286**(30): p. 26768-80.

356. Frank, D.E. and W.G. Carter, *Laminin 5 deposition regulates keratinocyte polarization and persistent migration.* J Cell Sci, 2004. **117**(Pt 8): p. 1351-63.

357. Baudoin, C., L. Fantin, and G. Meneguzzi, *Proteolytic Processing of the Laminin α3 G Domain Mediates Assembly of Hemidesmosomes but Has No Role on Keratinocyte Migration.* Journal of Investigative Dermatology, 2005. **125**(5): p. 883-888.

358. Seltmann, K., et al., *Keratins mediate localization of hemidesmosomes and repress cell motility.* J Invest Dermatol, 2013. **133**(1): p. 181-90.

359. Chen, C.S., et al., *Cell shape provides global control of focal adhesion assembly.* Biochem Biophys Res Commun, 2003. **307**(2): p. 355-61.

360. Wu, C., *Focal Adhesion: A Focal Point in Current Cell Biology and Molecular Medicine.* Cell Adh Migr, 2007. **1**(1): p. 13-8.

361. Sastry, S.K. and K. Burridge, *Focal adhesions: a nexus for intracellular signaling and cytoskeletal dynamics.* Exp Cell Res, 2000. **261**(1): p. 25-36.

362. Winkler, J., H. Lunsdorf, and B.M. Jockusch, *Energy-filtered electron microscopy reveals that talin is a highly flexible protein composed of a series of globular domains.* Eur J Biochem, 1997. **243**(1-2): p. 430-6.

363. Critchley, D.R. and A.R. Gingras, *Talin at a glance.* J Cell Sci, 2008. **121**(Pt 9): p. 1345-7.

364. Chishti, A.H., et al., *The FERM domain: a unique module involved in the linkage of cytoplasmic proteins to the membrane.* Trends in Biochemical Sciences. **23**(8): p. 281-282.

365. Mitra, S.K., D.A. Hanson, and D.D. Schlaepfer, *Focal adhesion kinase: in command and control of cell motility.* Nat Rev Mol Cell Biol, 2005. **6**(1): p. 56-68.

366. Critchley, D.R., *Focal adhesions - the cytoskeletal connection.* Curr Opin Cell Biol, 2000. **12**(1): p. 133-9.

367. Goldmann, W.H., et al., *Native talin is a dumbbell-shaped homodimer when it interacts with actin.* J Struct Biol, 1994. **112**(1): p. 3-10.

368. Tremuth, L., et al., *A fluorescence cell biology approach to map the second integrin-binding site of talin to a 130-amino acid sequence within the rod domain.* J Biol Chem, 2004. **279**(21): p. 22258-66.

369. Bass, M.D., et al., *Talin contains three similar vinculin-binding sites predicted to form an amphipathic helix.* Biochem J, 1999. **341 (Pt 2)**: p. 257-63.

370. Nuckolls, G.H., L.H. Romer, and K. Burridge, *Microinjection of antibodies against talin inhibits the spreading and migration of fibroblasts.* Journal of Cell Science, 1992. **102**(4): p. 753-762.

371. Albiges-Rizo, C., P. Frachet, and M.R. Block, *Down regulation of talin alters cell adhesion and the processing of the alpha 5 beta 1 integrin.* J Cell Sci, 1995. **108 (Pt 10)**: p. 3317-29.

372. Priddle, H., et al., *Disruption of the talin gene compromises focal adhesion assembly in undifferentiated but not differentiated embryonic stem cells.* J Cell Biol, 1998. **142**(4): p. 1121-33.

373. Monkley, S.J., et al., *Disruption of the talin gene arrests mouse development at the gastrulation stage.* Dev Dyn, 2000. **219**(4): p. 560-74.

374. Goldmann, W.H., *Correlation between the interaction of the vinculin tail domain with lipid membranes, its phosphorylation and cell mechanical behaviour.* Cell Biol Int, 2010. **34**(4): p. 339-42.

375. Peng, X., et al., *New Insights into Vinculin Function and Regulation.* Int Rev Cell Mol Biol, 2011. **287**: p. 191-231.

376. Ezzell, R.M., et al., *Vinculin promotes cell spreading by mechanically coupling integrins to the cytoskeleton.* Exp Cell Res, 1997. **231**(1): p. 14-26.

377. Xu, W., H. Baribault, and E.D. Adamson, *Vinculin knockout results in heart and brain defects during embryonic development.* Development, 1998. **125**(2): p. 327-37.

378. Chen, H., et al., *Spatial distribution and functional significance of activated vinculin in living cells.* J Cell Biol, 2005. **169**(3): p. 459-70.

379. Ziegler, W.H., R.C. Liddington, and D.R. Critchley, *The structure and regulation of vinculin.* Trends Cell Biol, 2006. **16**(9): p. 453-60.

380. Fillingham, I., et al., *A vinculin binding domain from the talin rod unfolds to form a complex with the vinculin head.* Structure, 2005. **13**(1): p. 65-74.

381. Wachsstock, D.H., J.A. Wilkins, and S. Lin, *Specific interaction of vinculin with α-actinin.* Biochemical and Biophysical Research Communications, 1987. **146**(2): p. 554-560.

382. Brindle, N.P., et al., *The focal-adhesion vasodilator-stimulated phosphoprotein (VASP) binds to the proline-rich domain in vinculin.* Biochem J, 1996. **318 (Pt 3)**: p. 753-7.

383. DeMali, K.A., C.A. Barlow, and K. Burridge, *Recruitment of the Arp2/3 complex to vinculin: coupling membrane protrusion to matrix adhesion.* J Cell Biol, 2002. **159**(5): p. 881-91.

384. Wood, C.K., et al., *Characterisation of the paxillin-binding site and the C-terminal focal adhesion targeting sequence in vinculin.* Journal of Cell Science, 1994. **107**(2): p. 709-717.

385. Menkel, A.R., et al., *Characterization of an F-actin-binding domain in the cytoskeletal protein vinculin.* J Cell Biol, 1994. **126**(5): p. 1231-40.

386. Bellin, R.M., et al., *Synemin may function to directly link muscle cell intermediate filaments to both myofibrillar Z-lines and costameres.* J Biol Chem, 2001. **276**(34): p. 32330-7.

387. Serrano, K. and D.V. Devine, *Vinculin is proteolyzed by calpain during platelet aggregation: 95 kDa cleavage fragment associates with the platelet cytoskeleton.* Cell Motil Cytoskeleton, 2004. **58**(4): p. 242-52.

388. Geng, L., et al., *Modification of the composition of polycystin-1 multiprotein complexes by calcium and tyrosine phosphorylation.* Biochim Biophys Acta, 2000. **1535**(1): p. 21-35.

389. Johnson, R.P., et al., *A conserved motif in the tail domain of vinculin mediates association with and insertion into acidic phospholipid bilayers.* Biochemistry, 1998. **37**(28): p. 10211-22.

390. Zaidel-Bar, R., et al., *A paxillin tyrosine phosphorylation switch regulates the assembly and form of cell-matrix adhesions.* J Cell Sci, 2007. **120**(Pt 1): p. 137-48.

391. Turner, C.E., J.R. Glenney, Jr., and K. Burridge, *Paxillin: a new vinculin-binding protein present in focal adhesions.* J Cell Biol, 1990. **111**(3): p. 1059-68.

392. Turner, C.E. and J.T. Miller, *Primary sequence of paxillin contains putative SH2 and SH3 domain binding motifs and multiple LIM domains: identification of a vinculin and pp125Fak-binding region.* Journal of Cell Science, 1994. **107**(6): p. 1583-1591.

393. Dawid, I.B., J.J. Breen, and R. Toyama, *LIM domains: multiple roles as adapters and functional modifiers in protein interactions.* Trends Genet, 1998. **14**(4): p. 156-62.

394. Brown, M.C. and C.E. Turner, *Paxillin: adapting to change.* Physiological reviews, 2004. **84**(4): p. 1315-1339.

395. Liu, S., et al., *Binding of paxillin to [alpha]4 integrins modifies integrin-dependent biological responses.* Nature, 1999. **402**(6762): p. 676-681.

396. Hagel, M., et al., *The adaptor protein paxillin is essential for normal development in the mouse and is a critical transducer of fibronectin signaling.* Mol Cell Biol, 2002. **22**(3): p. 901-15.

397. Andre, E. and M. Beckerandre, *Expression of an N-Terminally Truncated Form of Human Focal Adhesion Kinase in Brain.* Biochemical and Biophysical Research Communications, 1993. **190**(1): p. 140-147.

398. Hildebrand, J.D., M.D. Schaller, and J.T. Parsons, *Identification of sequences required for the efficient localization of the focal adhesion kinase, pp125FAK, to cellular focal adhesions.* J Cell Biol, 1993. **123**(4): p. 993-1005.

399. Schaller, M.D., et al., *Focal adhesion kinase and paxillin bind to peptides mimicking beta integrin cytoplasmic domains.* J Cell Biol, 1995. **130**(5): p. 1181-7.

400. Golubovskaya, V.M., *Focal Adhesion Kinase as a Cancer Therapy Target.* Anticancer Agents Med Chem, 2010. **10**(10): p. 735-41.

401. Kweh, F., et al., *Neurofibromin physically interacts with the N-terminal domain of Focal Adhesion Kinase.* Mol Carcinog, 2009. **48**(11): p. 1005-17.

402. Calalb, M.B., T.R. Polte, and S.K. Hanks, *Tyrosine phosphorylation of focal adhesion kinase at sites in the catalytic domain regulates kinase activity: a role for Src family kinases.* Mol Cell Biol, 1995. **15**(2): p. 954-63.

403. Taylor, J.M., et al., *Characterization of Graf, the GTPase-activating Protein for Rho Associated with Focal Adhesion Kinase: PHOSPHORYLATION AND POSSIBLE REGULATION BY MITOGEN-ACTIVATED PROTEIN KINASE.* Journal of Biological Chemistry, 1998. **273**(14): p. 8063-8070.

404. McLean, G.W., et al., *The role of focal-adhesion kinase in cancer - a new therapeutic opportunity.* Nat Rev Cancer, 2005. **5**(7): p. 505-15.

405. Ilic, D., et al., *Reduced cell motility and enhanced focal adhesion contact formation in cells from FAK-deficient mice.* Nature, 1995. **377**(6549): p. 539-44.

406. Owen, J.D., et al., *Induced focal adhesion kinase (FAK) expression in FAK-null cells enhances cell spreading and migration requiring both auto- and activation loop phosphorylation sites and inhibits adhesion-dependent tyrosine phosphorylation of Pyk2.* Mol Cell Biol, 1999. **19**(7): p. 4806-18.

407. Sieg, D.J., et al., *FAK integrates growth-factor and integrin signals to promote cell migration.* Nat Cell Biol, 2000. **2**(5): p. 249-56.

408. Wang, J.G., et al., *Uniaxial Cyclic Stretch Induces Focal Adhesion Kinase (FAK) Tyrosine Phosphorylation Followed by Mitogen-Activated Protein Kinase (MAPK) Activation.* Biochemical and Biophysical Research Communications, 2001. **288**(2): p. 356-361.

409. Cary, L.A., J.F. Chang, and J.L. Guan, *Stimulation of cell migration by overexpression of focal adhesion kinase and its association with Src and Fyn.* J Cell Sci, 1996. **109 (Pt 7)**: p. 1787-94.

410. Owens, L.V., et al., *Overexpression of the focal adhesion kinase (p125FAK) in invasive human tumors.* Cancer Res, 1995. **55**(13): p. 2752-5.

411. Slack, J.K., et al., *Alterations in the focal adhesion kinase/Src signal transduction pathway correlate with increased migratory capacity of prostate carcinoma cells.* Oncogene, 2001. **20**(10): p. 1152-63.

412. Wang, D., et al., *p125 focal adhesion kinase promotes malignant astrocytoma cell proliferation in vivo.* J Cell Sci, 2000. **113 Pt 23**: p. 4221-30.

413. Carter, W.G., et al., *The role of integrins alpha 2 beta 1 and alpha 3 beta 1 in cell-cell and cell-substrate adhesion of human epidermal cells.* J Cell Biol, 1990. **110**(4): p. 1387-404.

414. Winograd-Katz, S.E., et al., *The integrin adhesome: from genes and proteins to human disease.* Nat Rev Mol Cell Biol, 2014. **15**(4): p. 273-88.

415. Carter, W.G., M.C. Ryan, and P.J. Gahr, *Epiligrin, a new cell adhesion ligand for integrin alpha 3 beta 1 in epithelial basement membranes.* Cell, 1991. **65**(4): p. 599-610.

416. Kikkawa, Y., N. Sanzen, and K. Sekiguchi, *Isolation and Characterization of Laminin-10/11 Secreted by Human Lung Carcinoma Cells: LAMININ-10/11 MEDIATES CELL ADHESION THROUGH INTEGRIN α3β1.* Journal of Biological Chemistry, 1998. **273**(25): p. 15854-15859.

417. deHart, G.W., K.E. Healy, and J.C. Jones, *The role of alpha3beta1 integrin in determining the supramolecular organization of laminin-5 in the extracellular matrix of keratinocytes.* Exp Cell Res, 2003. **283**(1): p. 67-79.

418. Korhonen, M., et al., *Distribution of the alpha 1-alpha 6 integrin subunits in human developing and term placenta.* Lab Invest, 1991. **65**(3): p. 347-56.

419. Mette, S.A., et al., *Distribution of integrin cell adhesion receptors on normal bronchial epithelial cells and lung cancer cells in vitro and in vivo.* Am J Respir Cell Mol Biol, 1993. **8**(5): p. 562-72.

420. Hertle, M.D., J.C. Adams, and F.M. Watt, *Integrin expression during human epidermal development in vivo and in vitro.* Development, 1991. **112**(1): p. 193-206.

421. Kreidberg, J.A., *Functions of α3β1 integrin.* Current Opinion in Cell Biology, 2000. **12**(5): p. 548-553.

422. Lampe, P.D., et al., *Cellular interaction of integrin alpha3beta1 with laminin 5 promotes gap junctional communication.* J Cell Biol, 1998. **143**(6): p. 1735-47.

423. Masaki, T., M. Endo, and S. Ebashi, *Localization of 6S component of a alpha-actinin at Z-band.* J Biochem, 1967. **62**(5): p. 630-2.

424. Blanchard, A., V. Ohanian, and D. Critchley, *The structure and function of alpha-actinin.* J Muscle Res Cell Motil, 1989. **10**(4): p. 280-9.

425. Honda, K., et al., *Actinin-4, a novel actin-bundling protein associated with cell motility and cancer invasion.* J Cell Biol, 1998. **140**(6): p. 1383-93.

426. Djinovic-Carugo, K., et al., *Structure of the alpha-actinin rod: molecular basis for cross-linking of actin filaments.* Cell, 1999. **98**(4): p. 537-46.

427. Belkin, A.M. and V.E. Koteliansky, *Interaction of iodinated vinculin, metavinculin and α-actinin with cytoskeletal proteins.* FEBS Letters, 1987. **220**(2): p. 291-294.

428. Greene, D.K., et al., *Syndecan-4 associates with α-actinin.* Journal of Biological Chemistry, 2003. **278**(9): p. 7617-7623.

429. Gonzalez, A.M., et al., *Interactions of a hemidesmosome component and actinin family members.* Journal of Cell Science, 2001. **114**(23): p. 4197-4206.

430. Pavalko, F.M. and K. Burridge, *Disruption of the actin cytoskeleton after microinjection of proteolytic fragments of alpha-actinin.* J Cell Biol, 1991. **114**(3): p. 481-91.

431. Otey, C.A., et al., *Mapping of the alpha-actinin binding site within the beta 1 integrin cytoplasmic domain.* J Biol Chem, 1993. **268**(28): p. 21193-7.

432. Rajfur, Z., et al., *Dissecting the link between stress fibres and focal adhesions by CALI with EGFP fusion proteins.* Nat Cell Biol, 2002. **4**(4): p. 286-93.

433. Fukami, K., et al., *Identification of a Phosphatidylinositol 4,5-Bisphosphate-binding Site in Chicken Skeletal Muscle α-Actinin.* Journal of Biological Chemistry, 1996. **271**(5): p. 2646-2650.

434. Wozniak, M.A., et al., *Focal adhesion regulation of cell behavior.* Biochimica et Biophysica Acta (BBA)-Molecular Cell Research, 2004. **1692**(2): p. 103-119.

435. Kong, F., et al., *Demonstration of catch bonds between an integrin and its ligand.* The Journal of Cell Biology, 2009. **185**(7): p. 1275-1284.

436. Dembo, M., et al., *The reaction-limited kinetics of membrane-to-surface adhesion and detachment.* Proc R Soc Lond B Biol Sci, 1988. **234**(1274): p. 55-83.

437. Zamir, E. and B. Geiger, *Molecular complexity and dynamics of cell-matrix adhesions.* J Cell Sci, 2001. **114**(Pt 20): p. 3583-90.

438. Kamm, R.D. and M.R. Kaazempur-Mofrad, *On the molecular basis for mechanotransduction.* Mech Chem Biosyst, 2004. **1**(3): p. 201-9.

439. Shi, Q. and D. Boettiger, *A Novel Mode for Integrin-mediated Signaling: Tethering Is Required for Phosphorylation of FAK Y397.* Mol Biol Cell, 2003. **14**(10): p. 4306-15.

440. Margadant, F., et al., *Mechanotransduction in vivo by repeated talin stretch-relaxation events depends upon vinculin.* PLoS Biol, 2011. **9**(12): p. e1001223.

441. del Rio, A., et al., *Stretching single talin rod molecules activates vinculin binding.* Science, 2009. **323**(5914): p. 638-41.

442. Nayal, A., et al., *Paxillin phosphorylation at Ser273 localizes a GIT1-PIX-PAK complex and regulates adhesion and protrusion dynamics.* J Cell Biol, 2006. **173**(4): p. 587-9.

443. Zaidel-Bar, R., et al., *Hierarchical assembly of cell-matrix adhesion complexes.* Biochem Soc Trans, 2004. **32**(Pt3): p. 416-20.

444. Stricker, J., et al., *Spatiotemporal Constraints on the Force-Dependent Growth of Focal Adhesions.* Biophysical Journal, 2011. **100**(12): p. 2883-2893.

445. Yoshigi, M., et al., *Mechanical force mobilizes zyxin from focal adhesions to actin filaments and regulates cytoskeletal reinforcement.* J Cell Biol, 2005. **171**(2): p. 209-15.

446. Crowley, E. and A.F. Horwitz, *Tyrosine phosphorylation and cytoskeletal tension regulate the release of fibroblast adhesions.* J Cell Biol, 1995. **131**(2): p. 525-37.

447. Small, J.V., et al., *The lamellipodium: where motility begins.* Trends Cell Biol, 2002. **12**(3): p. 112-20.

448. Franco, S.J. and A. Huttenlocher, *Regulating cell migration: calpains make the cut.* Journal of Cell Science, 2005. **118**(17): p. 3829-3838.

449. Digman, M.A., et al., *Stoichiometry of molecular complexes at adhesions in living cells.* Proceedings of the National Academy of Sciences, 2009. **106**(7): p. 2170-2175.

450. Laukaitis, C.M., et al., *Differential dynamics of alpha 5 integrin, paxillin, and alpha-actinin during formation and disassembly of adhesions in migrating cells.* J Cell Biol, 2001. **153**(7): p. 1427-40.

451. White, D.P., P.T. Caswell, and J.C. Norman, *αvβ3 and α5β1 integrin recycling pathways dictate downstream Rho kinase signaling to regulate persistent cell migration.* J Cell Biol, 2007. **177**(3): p. 515-25.

452. Dogic, D., P. Rousselle, and M. Aumailley, *Cell adhesion to laminin 1 or 5 induces isoform-specific clustering of integrins and other focal adhesion components.* J Cell Sci, 1998. **111 (Pt 6)**: p. 793-802.

453. Hamill, K.J., et al., *Laminin deposition in the extracellular matrix: a complex picture emerges.* Journal Of Cell Science, 2009. **122**(Pt 24): p. 4409-4417.

454. Modrek, B. and C.J. Lee, *Alternative splicing in the human, mouse and rat genomes is associated with an increased frequency of exon creation and/or loss.* Nat Genet, 2003. **34**(2): p. 177-80.

455. Pan, Q., et al., *Deep surveying of alternative splicing complexity in the human transcriptome by high-throughput sequencing.* Nat Genet, 2008. **40**(12): p. 1413-5.

456. Hayashi, Y., et al., *Identification and recombinant production of human laminin alpha4 subunit splice variants.* Biochem Biophys Res Commun, 2002. **299**(3): p. 498-504.

457. Hao, J., et al., *Cell line-specific translation of two laminin 5 beta3 chain isoforms.* Gene, 2002. **283**(1-2): p. 237-44.

458. Talts, J.F., et al., *Structural analysis and proteolytic processing of recombinant G domain of mouse laminin alpha2 chain.* FEBS Lett, 1998. **426**(1): p. 71-6.

459. Lee, G., et al., *Alternative transcriptional initiation and splicing of mouse Lamc2 message.* Mol Cells, 2001. **12**(3): p. 380-90.

460. Sammeth, M., S. Foissac, and R. Guigo, *A general definition and nomenclature for alternative splicing events.* PLoS Comput Biol, 2008. **4**(8): p. e1000147.

461. Hamill, K.J., et al., *Identification of a novel family of laminin N-terminal alternate splice isoforms: structural and functional characterization.* The Journal Of Biological Chemistry, 2009. **284**(51): p. 35588-35596.

462. Sugawara, K., et al., *Spatial and temporal control of laminin-332 (5) and -511 (10) expression during induction of anagen hair growth.* J Histochem Cytochem, 2007. **55**(1): p. 43-55.

463. Moore, S.W., M. Tessier-Lavigne, and T.E. Kennedy, *Netrins and their receptors.* Adv Exp Med Biol, 2007. **621**: p. 17-31.

464. Rajasekharan, S. and T.E. Kennedy, *The netrin protein family.* Genome Biol, 2009. **10**(9): p. 239.

465. Kappler, J., et al., *Glycosaminoglycan-Binding Properties and Secondary Structure of the C-Terminus of Netrin-1.* Biochemical and Biophysical Research Communications, 2000. **271**(2): p. 287-291.

466. Yebra, M., et al., *Recognition of the neural chemoattractant Netrin-1 by integrins alpha6beta4 and alpha3beta1 regulates epithelial cell adhesion and migration.* Dev Cell, 2003. **5**(5): p. 695-707.

467. Shekarabi, M. and T.E. Kennedy, *The netrin-1 receptor DCC promotes filopodia formation and cell spreading by activating Cdc42 and Rac1.* Mol Cell Neurosci, 2002. **19**(1): p. 1-17.

468. Picard, M., et al., *Spatial and temporal activation of the small GTPases RhoA and Rac1 by the netrin-1 receptor UNC5a during neurite outgrowth.* Cell Signal, 2009. **21**(12): p. 1961-73.

469. Hu, Y., et al., *Netrin-4 Promotes Glioblastoma Cell Proliferation through Integrin β4 Signaling.* Neoplasia, 2012. **14**(3): p. 219-IN23.

470. Shipp, E.L. and L.C. Hsieh-Wilson, *Profiling the sulfation specificities of glycosaminoglycan interactions with growth factors and chemotactic proteins using microarrays.* Chem Biol, 2007. **14**(2): p. 195-208.

471. Schneiders, F.I., et al., *Binding of netrin-4 to laminin short arms regulates basement membrane assembly.* J Biol Chem, 2007. **282**(33): p. 23750-8.

472. Koch, M., et al., *A novel member of the netrin family, beta-netrin, shares homology with the beta chain of laminin: identification, expression, and functional characterization.* J Cell Biol, 2000. **151**(2): p. 221-34.

473. Liu, Y., et al., *Novel Role for Netrins in Regulating Epithelial Behavior during Lung Branching Morphogenesis.* Current Biology, 2004. **14**(10): p. 897-905.

474. Reuten, R., et al., *Structural decoding of netrin-4 reveals a regulatory function towards mature basement membranes.* Nature Communications, 2016. **7**: p. 13515.

475. Staquicini, F.I., et al., *Discovery of a functional protein complex of netrin-4, laminin gamma1 chain, and integrin alpha6beta1 in mouse neural stem cells.* Proc Natl Acad Sci U S A, 2009. **106**(8): p. 2903-8.

476. Han, Y., et al., *Netrin-1 simultaneously suppresses corneal inflammation and neovascularization.* Invest Ophthalmol Vis Sci, 2012. **53**(3): p. 1285-95.

477. Han, Y., et al., *Therapeutic effects of topical netrin-4 in a corneal acute inflammatory model.* Int J Ophthalmol, 2015. **8**(2): p. 228-33.

478. Maier, A.B., et al., *Netrin-4 Mediates Corneal Hemangiogenesis but Not Lymphangiogenesis in the Mouse-Model of Suture-Induced Neovascularization.* Invest Ophthalmol Vis Sci, 2017. **58**(3): p. 1387-1396.

479. Boukamp, P., et al., *Normal keratinization in a spontaneously immortalized aneuploid human keratinocyte cell line.* Journal of Cell Biology, 1988. **106**(3): p. 761-771.

480. Yuspa, S.H. and C.C. Harris, *Altered differentiation of mouse epidermal cells treated with retinyl acetate in vitro.* Exp Cell Res, 1974. **86**(1): p. 95-105.

481. De Falco, E., et al., *A standardized laboratory and surgical method for in vitro culture isolation and expansion of primary human Tenon's fibroblasts.* Cell Tissue Bank, 2013. **14**(2): p. 277-87.

482. Hopkinson, S.B., K.S. Riddelle, and J.C. Jones, *Cytoplasmic domain of the 180-kD bullous pemphigoid antigen, a hemidesmosomal component: molecular and cell biologic characterization.* J Invest Dermatol, 1992. **99**(3): p. 264-70.

483. Langhofer, M., S.B. Hopkinson, and J.C. Jones, *The matrix secreted by 804G cells contains laminin-related components that participate in hemidesmosome assembly in vitro.* J Cell Sci, 1993. **105 (Pt 3)**: p. 753-64.

484. Galfre, G. and C. Milstein, *Preparation of monoclonal antibodies: strategies and procedures.* Methods Enzymol, 1981. **73**(Pt B): p. 3-46.

485. Gonzales, M., et al., *A cell signal pathway involving laminin-5, alpha3beta1 integrin, and mitogen-activated protein kinase can regulate epithelial cell proliferation.* Mol Biol Cell, 1999. **10**(2): p. 259-70.

486. Hopkinson, S.B., et al., *Fluorescently tagged laminin subunits facilitate analyses of the properties, assembly and processing of laminins in live and fixed lung epithelial cells and keratinocytes.* Matrix Biol, 2008. **27**(7): p. 640-7.

487. Naldini, L., et al., *Efficient transfer, integration, and sustained long-term expression of the transgene in adult rat brains injected with a lentiviral vector.* Proc Natl Acad Sci U S A, 1996. **93**(21): p. 11382-8.

488. Howard, C., et al., *Human retinal pigment epithelial SPARC expression and age: an immunohistochemical study.* Histol Histopathol, 2010. **25**(9): p. 1163-9.

489. Jacobsen, H., H. Klenow, and K. Overgaard-Hansen, *The N-terminal amino-acid sequences of DNA polymerase I from Escherichia coli and of the large and the small fragments obtained by a limited proteolysis.* Eur J Biochem, 1974. **45**(2): p. 623-7.

490. Wang, F.J. and L.S. Ripley, *DNA sequence effects on single base deletions arising during DNA polymerization in vitro by Escherichia coli Klenow fragment polymerase.* Genetics, 1994. **136**(3): p. 709-19.

491. Staggers, W.R., A.J. Paterson, and J.E. Kudlow, *Sequence of the functional human keratin K14 promoter.* Gene, 1995. **153**(2): p. 297-8.

492. B. Hogan, F.C.a.E.L., *Manipulating the mouse embryo: A laboratory manual.* Cold Spring Harbor Laboratory, 1986.

493. Pinkert, C.A., *Transgenic Animal Technology*. Elsevier, 2014.

494. Xia, W., et al., *High levels of protein expression using different mammalian CMV promoters in several cell lines.* Protein Expression and Purification, 2006. **45**(1): p. 115-124.

495. Hamill, K.J., et al., *Fibronectin Expression Determines Skin Cell Motile Behavior.* Journal of Investigative Dermatology, 2012. **132**(2): p. 448-457.

496. DiPersio, C.M., S. Shah, and R.O. Hynes, *alpha 3A beta 1 integrin localizes to focal contacts in response to diverse extracellular matrix proteins.* J Cell Sci, 1995. **108 (Pt 6)**: p. 2321-36.

497. Hopkinson, S.B., et al., *Interaction of BP180 (type XVII collagen) and alpha6 integrin is necessary for stabilization of hemidesmosome structure.* J Invest Dermatol, 1998. **111**(6): p. 1015-22.

498. Fredriksson, S., et al., *Protein detection using proximity-dependent DNA ligation assays.* Nat Biotechnol, 2002. **20**(5): p. 473-7.

499. Hamill, K.J., et al., *Actinin-4 in keratinocytes regulates motility via an effect on lamellipodia stability and matrix adhesions.* Faseb j, 2013. **27**(2): p. 546-56.

500. Hiroyasu, S., Z.T. Colburn, and J.C. Jones, *A hemidesmosomal protein regulates actin dynamics and traction forces in motile keratinocytes.* Faseb j, 2016. **30**(6): p. 2298-310.

501. Hohenester, E. and P.D. Yurchenco, *Laminins in basement membrane assembly.* Cell Adh Migr, 2013. **7**(1): p. 56-63.

502. Yurchenco, P.D., Y.S. Cheng, and H. Colognato, *Laminin forms an independent network in basement membranes.* J Cell Biol, 1992. **117**(5): p. 1119-33.

503. Serafini, T., et al., *The netrins define a family of axon outgrowth-promoting proteins homologous to C. elegans UNC-6.* Cell, 1994. **78**(3): p. 409-24.

504. Sobrin, L., et al., *Regulation of MMP-9 activity in human tear fluid and corneal epithelial culture supernatant.* Invest Ophthalmol Vis Sci, 2000. **41**(7): p. 1703-9.

505. Chaloin-Dufau, C., T.T. Sun, and D. Dhouailly, *Appearance of the keratin pair K3/K12 during embryonic and adult corneal epithelial differentiation in the chick and in the rabbit.* Cell Differ Dev, 1990. **32**(2): p. 97-108.

506. Colognato, H. and P.D. Yurchenco, *Form and function: The laminin family of heterotrimers.* Developmental Dynamics, 2000. **218**(2): p. 213-234.

507. Purvis, A. and E. Hohenester, *Laminin network formation studied by reconstitution of ternary nodes in solution.* J Biol Chem, 2012. **287**(53): p. 44270-7.

508. Hochman-Mendez, C., et al., *A fractal nature for polymerized laminin.* PLoS One, 2014. **9**(10): p. e109388.

509. Tuori, A., et al., *The immunohistochemical composition of the human corneal basement membrane.* Cornea, 1996. **15**(3): p. 286-94.

510. Schlotzer-Schrehardt, U., et al., *Characterization of extracellular matrix components in the limbal epithelial stem cell compartment.* Exp Eye Res, 2007. **85**(6): p. 845-60.

511. Hartwig, B., et al., *Laminin-5-deficient human keratinocytes: defective adhesion results in a saltatory and inefficient mode of migration.* Exp Cell Res, 2007. **313**(8): p. 1575-87.

512. Ryan, M.C., et al., *Targeted Disruption of the LAMA3 Gene in Mice Reveals Abnormalities in Survival and Late Stage Differentiation of Epithelial Cells.* J Cell Biol, 1999. **145**(6): p. 1309-24.

513. Verrando, P., et al., *Keratinocytes from junctional epidermolysis bullosa do adhere and migrate on the basement membrane protein nicein through alpha 3 beta 1 integrin.* Lab Invest, 1994. **71**(4): p. 567-74.

514. Hamelers, I.H.L., et al., *The Rac activator Tiam1 is required for α3β1-mediated laminin-5 deposition, cell spreading, and cell migration.* The Journal of Cell Biology, 2005. **171**(5): p. 871-881.

515. Henry, M.D. and K.P. Campbell, *A role for dystroglycan in basement membrane assembly.* Cell, 1998. **95**(6): p. 859-70.

516. Henry, M.D., et al., *Distinct roles for dystroglycan, beta1 integrin and perlecan in cell surface laminin organization.* J Cell Sci, 2001. **114**(Pt 6): p. 1137-44.

517. Montanaro, F., M. Lindenbaum, and S. Carbonetto, *alpha-Dystroglycan is a laminin receptor involved in extracellular matrix assembly on myotubes and muscle cell viability.* J Cell Biol, 1999. **145**(6): p. 1325-40.

518. Tsiper, M.V. and P.D. Yurchenco, *Laminin assembles into separate basement membrane and fibrillar matrices in Schwann cells.* J Cell Sci, 2002. **115**(Pt 5): p. 1005-15.

519. Weir, M.L., et al., *Dystroglycan loss disrupts polarity and beta-casein induction in mammary epithelial cells by perturbing laminin anchoring.* J Cell Sci, 2006. **119**(Pt 19): p. 4047-58.

520. Shang, M., et al., *The LG3 module of laminin-5 harbors a binding site for integrin alpha3beta1 that promotes cell adhesion, spreading, and migration.* J Biol Chem, 2001. **276**(35): p. 33045-53.

521. Colognato-Pyke, H., et al., *Mapping of network-forming, heparin-binding, and alpha 1 beta 1 integrin-recognition sites within the alpha-chain short arm of laminin-1.* J Biol Chem, 1995. **270**(16): p. 9398-406.

522. Colognato, H., et al., *The laminin alpha2-chain short arm mediates cell adhesion through both the alpha1beta1 and alpha2beta1 integrins.* J Biol Chem, 1997. **272**(46): p. 29330-6.

523. Yang, X.H., et al., *Disruption of laminin-integrin-CD151-focal adhesion kinase axis sensitizes breast cancer cells to ErbB2 antagonists.* Cancer Res, 2010. **70**(6): p. 2256-63.

524. Jones, J.C., et al., *A function for the integrin alpha 6 beta 4 in the hemidesmosome.* Cell Regul, 1991. **2**(6): p. 427-38.

525. Spinardi, L., et al., *A recombinant tail-less integrin beta 4 subunit disrupts hemidesmosomes, but does not suppress alpha 6 beta 4-mediated cell adhesion to laminins.* The Journal of Cell Biology, 1995. **129**(2): p. 473-487.

526. Koster, J., et al., *Analysis of the interactions between BP180, BP230, plectin and the integrin alpha6beta4 important for hemidesmosome assembly.* J Cell Sci, 2003. **116**(Pt 2): p. 387-99.

527. Baker, S.E., et al., *Laminin-5 and hemidesmosomes: role of the alpha 3 chain subunit in hemidesmosome stability and assembly.* J Cell Sci, 1996. **109 (Pt 10)**: p. 2509-20.

528. Kitajima, Y., *Cross-Talk between Hemidesmosomes and Focal Contacts: Understanding Subepidermal Blistering Diseases.* Journal of Investigative Dermatology, 2010. **130**(6): p. 1493-1496.

529. Ozawa, T., et al., *Dynamic Relationship of Focal Contacts and Hemidesmosome Protein Complexes in Live Cells.* J Invest Dermatol, 2010. **130**(6): p. 1624-35.

530. Otey, C.A., F.M. Pavalko, and K. Burridge, *An interaction between alpha-actinin and the beta 1 integrin subunit in vitro.* J Cell Biol, 1990. **111**(2): p. 721-9.

531. Crawford, A.W., J.W. Michelsen, and M.C. Beckerle, *An interaction between zyxin and alpha-actinin.* J Cell Biol, 1992. **116**(6): p. 1381-93.

532. Pomies, P., H.A. Louis, and M.C. Beckerle, *CRP1, a LIM domain protein implicated in muscle differentiation, interacts with alpha-actinin.* J Cell Biol, 1997. **139**(1): p. 157-68.

533. Otey, C.A. and O. Carpen, *Alpha-actinin revisited: a fresh look at an old player.* Cell Motil Cytoskeleton, 2004. **58**(2): p. 104-11.

534. Burridge, K., et al., *Focal adhesions: transmembrane junctions between the extracellular matrix and the cytoskeleton.* Annu Rev Cell Biol, 1988. **4**: p. 487-525.

535. Ingber, D., *Integrins as mechanochemical transducers.* Current Opinion in Cell Biology, 1991. **3**(5): p. 841-848.

536. Wang, N., J.P. Butler, and D.E. Ingber, *Mechanotransduction across the cell surface and through the cytoskeleton.* Science, 1993. **260**(5111): p. 1124-7.

537. Kim, S.-H., J. Turnbull, and S. Guimond, *Extracellular matrix and cell signalling: the dynamic cooperation of integrin, proteoglycan and growth factor receptor.* Journal of Endocrinology, 2011. **209**(2): p. 139-151.

538. Schlessinger, J., *Cell signaling by receptor tyrosine kinases.* Cell, 2000. **103**(2): p. 211-25.

539. Iozzo, R.V., *Matrix proteoglycans: from molecular design to cellular function.* Annu Rev Biochem, 1998. **67**: p. 609-52.

540. Tholozan, F.M., et al., *FGF-2 release from the lens capsule by MMP-2 maintains lens epithelial cell viability.* Mol Biol Cell, 2007. **18**(11): p. 4222-31.

541. McAvoy, J.W. and C.G. Chamberlain, *Fibroblast growth factor (FGF) induces different responses in lens epithelial cells depending on its concentration.* Development, 1989. **107**(2): p. 221-8.

542. Tabata, T. and Y. Takei, *Morphogens, their identification and regulation.* Development, 2004. **131**(4): p. 703-712.

543. Discher, D.E., P. Janmey, and Y.L. Wang, *Tissue cells feel and respond to the stiffness of their substrate.* Science, 2005. **310**(5751): p. 1139-43.

544. Wells, R.G., *The role of matrix stiffness in regulating cell behavior.* Hepatology, 2008. **47**(4): p. 1394-400.

545. Oda, K., et al., *A comprehensive pathway map of epidermal growth factor receptor signaling.* Mol Syst Biol, 2005. **1**: p. 2005.0010.

546. Richter, P., et al., *Analysis of activated EGFR signalling pathways and their relation to laminin-5 gamma2 chain expression in oral squamous cell carcinoma (OSCC).* Histochem Cell Biol, 2005. **124**(2): p. 151-60.

547. Schwartz, M.A. and M.H. Ginsberg, *Networks and crosstalk: integrin signalling spreads.* Nat Cell Biol, 2002. **4**(4): p. E65-E68.

548. Falcioni, R., et al., *α6β4 and α6β1 Integrins Associate with ErbB-2 in Human Carcinoma Cell Lines.* Experimental Cell Research, 1997. **236**(1): p. 76-85.

549. Radisky, D.C., et al., *Single proteins might have dual but related functions in intracellular and extracellular microenvironments.* Nat Rev Mol Cell Biol, 2009. **10**(3): p. 228-34.

550. Muller, S., et al., *New EMBO members' review: the double life of HMGB1 chromatin protein: architectural factor and extracellular signal.* Embo j, 2001. **20**(16): p. 4337-40.

551. Milakovic, T., et al., *Intracellular localization and activity state of tissue transglutaminase differentially impacts cell death.* J Biol Chem, 2004. **279**(10): p. 8715-22.

552. Moll, R., et al., *The catalog of human cytokeratins: patterns of expression in normal epithelia, tumors and cultured cells.* Cell, 1982. **31**(1): p. 11-24.

553. Fuchs, E. and H. Green, *Changes in keratin gene expression during terminal differentiation of the keratinocyte.* Cell, 1980. **19**(4): p. 1033-42.

554. Nelson WG, S.T., *The 50- and 58-kdalton keratin classes as molecular markers for stratified squamous epithelia: cell culture studies.* J Cell Biol, 1983. **97**(1): p. 244-51.

555. Byrne, C., M. Tainsky, and E. Fuchs, *Programming gene expression in developing epidermis.* Development, 1994. **120**(9): p. 2369-83.

556. Vasioukhin, V., et al., *The magical touch: genome targeting in epidermal stem cells induced by tamoxifen application to mouse skin.* Proc Natl Acad Sci U S A, 1999. **96**(15): p. 8551-6.

557. Coulombe, P.A., R. Kopan, and E. Fuchs, *Expression of keratin K14 in the epidermis and hair follicle: insights into complex programs of differentiation.* J Cell Biol, 1989. **109**(5): p. 2295-312.

558. Wang, X., et al., *Transgenic studies with a keratin promoter-driven growth hormone transgene: prospects for gene therapy.* Proc Natl Acad Sci U S A, 1997. **94**(1): p. 219-26.

559. Shirley, S.H., et al., *The skinny on Slug.* Mol Carcinog, 2010. **49**(10): p. 851-61.

560. Sun, P., et al., *Cytokeratin expression during mouse embryonic and early postnatal mammary gland development.* Histochem Cell Biol, 2010. **133**(2): p. 213-21.

561. Kurpakus, M.A., M.T. Maniaci, and M. Esco, *Expression of keratins K12, K4 and K14 during development of ocular surface epithelium.* Curr Eye Res, 1994. **13**(11): p. 805-14.

562. Eghtedari, Y., et al., *Keratin 14 Expression in Epithelial Progenitor Cells of the Developing Human Cornea.* Stem Cells Dev, 2016. **25**(9): p. 699-711.

563. Ryan, M.D., A.M. King, and G.P. Thomas, *Cleavage of foot-and-mouth disease virus polyprotein is mediated by residues located within a 19 amino acid sequence.* J Gen Virol, 1991. **72 (Pt 11)**: p. 2727-32.

564. de Felipe, P., et al., *E unum pluribus: multiple proteins from a self-processing polyprotein.* Trends in Biotechnology, 2006. **24**(2): p. 68-75.

565. Donnelly, M.L., et al., *The 'cleavage' activities of foot-and-mouth disease virus 2A site-directed mutants and naturally occurring '2A-like' sequences.* J Gen Virol, 2001. **82**(Pt 5): p. 1027-41.

566. Daniels, R.W., et al., *Expression of multiple transgenes from a single construct using viral 2A peptides in Drosophila.* PLoS One, 2014. **9**(6): p. e100637.

567. Knappskog, S., et al., *The level of synthesis and secretion of Gaussia princeps luciferase in transfected CHO cells is heavily dependent on the choice of signal peptide.* J Biotechnol, 2007. **128**(4): p. 705-15.

568. Klatt, S. and Z. Konthur, *Secretory signal peptide modification for optimized antibody-fragment expression-secretion in Leishmania tarentolae.* Microb Cell Fact, 2012. **11**: p. 97.

569. Hengartner, H., T. Meo, and E. Muller, *Assignment of genes for immunoglobulin kappa and heavy chains to chromosomes 6 and 12 in mouse.* Proc Natl Acad Sci U S A, 1978. **75**(9): p. 4494-8.

570. Coloma, M.J., et al., *Novel vectors for the expression of antibody molecules using variable regions generated by polymerase chain reaction.* J Immunol Methods, 1992. **152**(1): p. 89-104.

571. Munro, S. and H.R. Pelham, *Use of peptide tagging to detect proteins expressed from cloned genes: deletion mapping functional domains of Drosophila hsp 70.* Embo j, 1984. **3**(13): p. 3087-93.

572. Baird, G.S., D.A. Zacharias, and R.Y. Tsien, *Biochemistry, mutagenesis, and oligomerization of DsRed, a red fluorescent protein from coral.* Proceedings of the National Academy of Sciences, 2000. **97**(22): p. 11984-11989.

573. Shaner, N.C., et al., *Improved monomeric red, orange and yellow fluorescent proteins derived from Discosoma sp. red fluorescent protein.* Nat Biotechnol, 2004. **22**(12): p. 1567-72.

574. Vassar, R., et al., *Tissue-specific and differentiation-specific expression of a human K14 keratin gene in transgenic mice.* Proc Natl Acad Sci U S A, 1989. **86**(5): p. 1563-7.

575. Monici, M., *Cell and tissue autofluorescence research and diagnostic applications.* Biotechnol Annu Rev, 2005. **11**: p. 227-56.

576. Elgar, G. and T. Vavouri, *Tuning in to the signals: noncoding sequence conservation in vertebrate genomes.* Trends Genet, 2008. **24**(7): p. 344-52.

577. Taft, R.J., M. Pheasant, and J.S. Mattick, *The relationship between non-protein-coding DNA and eukaryotic complexity.* BioEssays, 2007. **29**(3): p. 288-299.

578. Palmiter, R.D., et al., *Dramatic growth of mice that develop from eggs microinjected with metallothionein-growth hormone fusion genes.* Nature, 1982. **300**(5893): p. 611-5.

579. Bieberich, C. and G. Scangos, *Transgenic mice in the study of immunology.* BioEssays, 1986. **4**(6): p. 245-248.

580. Brinster, R.L., et al., *Factors affecting the efficiency of introducing foreign DNA into mice by microinjecting eggs.* Proc Natl Acad Sci U S A, 1985. **82**(13): p. 4438-42.

581. Covarrubias, L., Y. Nishida, and B. Mintz, *Early postimplantation embryo lethality due to DNA rearrangements in a transgenic mouse strain.* Proc Natl Acad Sci U S A, 1986. **83**(16): p. 6020-4.

582. Mahon, K.A., P.A. Overbeek, and H. Westphal, *Prenatal lethality in a transgenic mouse line is the result of a chromosomal translocation.* Proc Natl Acad Sci U S A, 1988. **85**(4): p. 1165-8.

583. Rijkers, T., A. Peetz, and U. Rüther, *Insertional mutagenesis in transgenic mice.* Transgenic Research, 1994. **3**(4): p. 203-215.

584. Wilkie, T.M. and R.D. Palmiter, *Analysis of the integrant in MyK-103 transgenic mice in which males fail to transmit the integrant.* Mol Cell Biol, 1987. **7**(5): p. 1646-55.

585. Hamada, T., et al., *Mechanism of chromosomal integration of transgenes in microinjected mouse eggs: sequence analysis of genome-transgene and transgene-transgene junctions at two loci.* Gene, 1993. **128**(2): p. 197-202.

586. Mark, W.H., et al., *Genomic structure of the locus associated with an insertional mutation in line 4 transgenic mice.* Genomics, 1992. **13**(1): p. 159-166.

587. Burdon, T.G. and R.J. Wall, *Fate of microinjected genes in preimplantation mouse embryos.* Molecular Reproduction and Development, 1992. **33**(4): p. 436-442.

588. Wurtele, H., K.C.E. Little, and P. Chartrand, *Illegitimate DNA integration in mammalian cells.* Gene Ther, 2003. **10**(21): p. 1791-1799.

589. Bierhoff, H., A. Postepska-Igielska, and I. Grummt, *Noisy silence: Non-coding RNA and heterochromatin formation at repetitive elements.* Epigenetics, 2014. **9**(1): p. 53-61.

590. Butner, K. and C.W. Lo, *Modulation of tk expression in mouse pericentromeric heterochromatin.* Mol Cell Biol, 1986. **6**(12): p. 4440-9.

591. Gordon, J.W., et al., *Genetic transformation of mouse embryos by microinjection of purified DNA.* Proceedings of the National Academy of Sciences, 1980. **77**(12): p. 7380-7384.

592. Costantini, F. and E. Lacy, *Introduction of a rabbit beta-globin gene into the mouse germ line.* Nature, 1981. **294**(5836): p. 92-4.

593. Brinster, R.L., et al., *Somatic Expression of Herpes Thymidine Kinase in Mice following Injection of a Fusion Gene into Eggs.* Cell, 1981. **27**(1 Pt 2): p. 223-31.

594. Lacy, E., et al., *A foreign beta-globin gene in transgenic mice: integration at abnormal chromosomal positions and expression in inappropriate tissues.* Cell, 1983. **34**(2): p. 343-58.

595. Xu, W., *Genetic analysis of transgenome structure and size of chromosome-mediated gene transfer lines.* Cell Res, 1992. **2**(1): p. 15-23.

596. Scangos, G. and F.H. Ruddle, *Mechanisms and applications of DNA-mediated gene transfer in mammalian cells - a review.* Gene, 1981. **14**(1-2): p. 1-10.

597. Ledwith, B.J., et al., *Plasmid DNA vaccines: assay for integration into host genomic DNA.* Dev Biol (Basel), 2000. **104**: p. 33-43.

598. Wang, Z., et al., *Detection of integration of plasmid DNA into host genomic DNA following intramuscular injection and electroporation.* Gene Ther, 2004. **11**(8): p. 711-21.

599. Yurchenco, P.D. and B.L. Patton, *Developmental and pathogenic mechanisms of basement membrane assembly.* Curr Pharm Des, 2009. **15**(12): p. 1277-94.

600. Hurskainen, T., et al., *Transmembrane collagen XVII is a novel component of the glomerular filtration barrier.* Cell Tissue Res, 2012. **348**(3): p. 579-88.

601. Kuster, J.E., et al., *IAP insertion in the murine LamB3 gene results in junctional epidermolysis bullosa.* Mamm Genome, 1997. **8**(9): p. 673-81.

602. Larrieu-Lahargue, F., et al., *Netrin-4 induces lymphangiogenesis in vivo.* Blood, 2010. **115**(26): p. 5418-26.